U. S. NAVAL OCEANOGRAPHIC OFFICE

MARINE GEOPHYSICAL SURVEY PROGRAM GEOFF
WESTERN NORTH PACIFIC OCEAN
AND SOUTH CHINA SEA

AREA 5 VOLUME 2

SUMMARY REPORT OF GEOPHYSICAL INFORMATION

ALPINE GEOPHYSICAL ASSOCIATES, INC.
OAK STREET NORWOOD, NEW JERSEY

U. S. NAVAL OCEANOGRAPHIC OFFICE CONTRACT N62306-2020

Code 4800 Wash, D.C. 20390

MARINE GEOPHYSICAL SURVEY PROGRAM 65-67 WESTERN NORTH PACIFIC OCEAN AND SOUTH CHINA SEA

AREA ST, VOLUME 2

SUMMARY REPORT OF GEOPHYSICAL INFORMATION

Approved for distribution: W. T. McGuinness, Project Manager
C. B. Officer, Scientific Director

August 1968

ALPINE GEOPHYSICAL ASSOCIATES, INC.

OAK STREET NORWOOD, NEW JERSEY

LIST OF VOLUMES FOR AREA ST

Vol. 1 - Summary report of acoustic information (conf.)

- Part I. Summary report and bottom reflection loss
- Part II. Summary tables of acoustic station results
- Part III. Underway 3.5 kHz normal incidence reflection loss

Vol. 2 - Summary report of geophysical information

- Part I. Bathymetry and subbottom profiling
- Part II. Magnetics
- Part III. Core data
- Part IV. Sound velocity profiles
- Part V. Hydrographic station data

Vol. 3 - Catalog of data

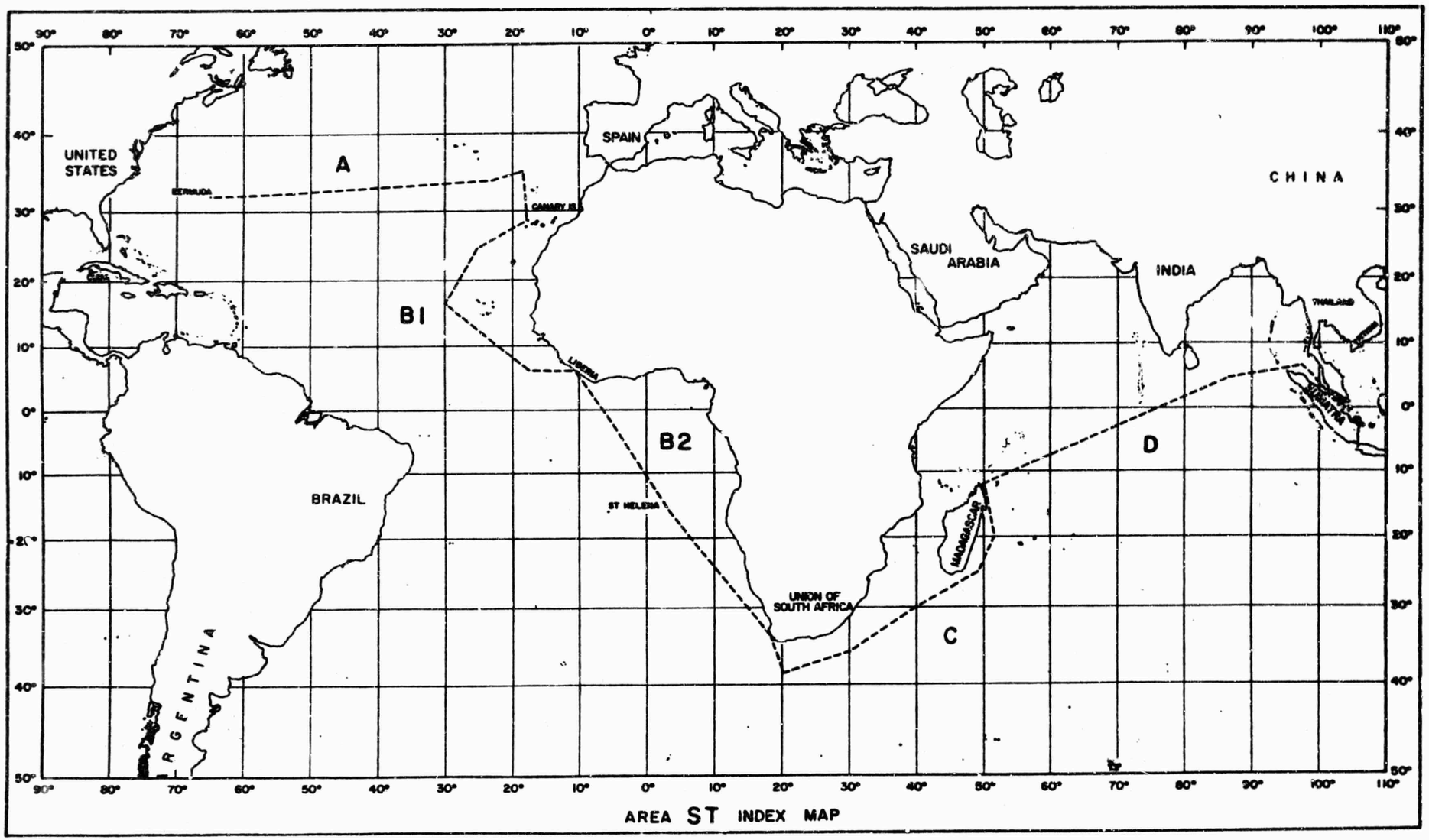

AREA ST INDEX MAP

PART I

Bathymetry and Subbottom Profiling

by

James A. Henry

PART II

Magnetics

by

D. L. Halpin

PART III

Core Data

by

C. Lair and P. Sanko

PART IV

Sound Velocity Profiles

by

Eleanor Weininger, E. T. Miller, and R. A. Wehnau

PART V

Hydrographic Station Data

by

M. H. Rodriguez, Jr.

PART I

AREA ST VOLUME 2

Bathymetry and Subbottom Profiling

by

James A. Henry

VOLUME 2, PART I

TABLE OF CONTENTS

TABLE OF CONTENTS (cont'd)

LIST OF FIGURES

LIST OF FIGURES (cont'd)

I INTRODUCTION

Area ST is a survey in transit conducted by the Alpine ships R/V RUTH ANN AND R/V SANTA MARIA. Approximately 30,000 nautical miles of cruise track data were obtained by the two ships departing Bermuda and arriving Singapore via Las Palmas, Monrovia, Capetown, and Diego-Suarez.

Continuous bathymetric and subbottom profiles were taken throughout with a 12 kHz precision echo sounder recorder and a 20,000 joule arcer.

Physiographic province boundaries enccuntered are imposed on cruise track Figures 1-5. These boundaries are determined by gradient change and/or topographic roughness.

Previously established province names are adhered to when available. Unnamed features are designated by association with adjacent provinces.

The term "microcontinental" is used in the Indian Ocean where continental is inapplicable due to many microcontinents found therein.

The following text is a summary description touching each physiographic province and noteworthy feature encountered from Bermuda to Singapore. Supplementary Figures 6-37 display correlations and examples of submarine features. Approximate vertical exaggeration of Figures 6-37 is 1:20.

Descriptions in the text appear in the same order in which the provinces were encountered.

II PHYSIOGRAPHIC PROVINCE DESCRIPTION

Bermuda Pedestal and Rise

North and east of Bermuda, the island shelf break occurs in less than 50 meters of water. The slope deepens quickly to the pedestal base between 4250 and 4325 meters. The average apparent gradient from the shelf break to the slope base is 1:75.

Deepening from the pedestal base, the Bermuda Rise appears relatively smooth. Nearing the Sohm Abyssal Plain the rise gradually becomes more rugged. Occasional relief to 500 meters is noted as scarps to 800 meters and a seamount to 1700 meters relief appear. Subbottom reflectors diverge from the bottom surface and occur more frequently eastward. The Bermuda Rise is penetrated by a north-northwest striking finger of the Sohm Abyssal Plain.

Sohm Abyssal Plain

The Sohm Abyssal Plain, bordered westerly by the Bermuda Rise and on the east by abyssal hills, maintains a characteristic smooth flat bottom surface at 5500 meters, deepening overall by a few meters eastward. Isolated abyssal hills appear scattered along the plain boundaries. An abyssal hill cluster of 50 to 300 meters relief appears 30 nautical miles north-northeast of station T-1. Subbottom reflectors to 200 meters conform to the smooth bottom surface. The eastern boundary is defined where the smooth flat bottom is interrupted by abyssal hills. A bordering jagged trough and a 5550-meter abyssal plain strike northeast along this eastern boundary.

Abyssal Hills

An abyssal hill province extends from the Sohm Abyssal Plain east to the lower step base of the Mid-Atlantic Ridge (Heezen, et al., 1959).

The average depth of 5250 meters increases to the west. Topcgraphic relief ranges to 800 meters and subbottom reflectors appear to 400 meters beneath the bottom surface. A maximum depth axis strikes and deepens to the northeast from 5625 to 5725 meters.

Mid-Atlantic Ridge

The Mid-Atlantic Ridge traversed in the vicinity of 34° north latitude, is composed of the lower, middle, and upper steps, high fractured plateaus, rift mountains, and a rift valley (Heezen, et al., 1959). The ridge and its flanks appear to be cut several times by large faults striking slightly south of east (103° to 116°) (Figures 1 and 7).

The western (lower, middle and upper) steps of the Mid-Atlantic Ridge are bordered on the west by abyssal hills and on the east by the high fractured plateau. The lower step trends northeast and parallels the rift valley. Westward facing 750-meter escarpments form the eastern and western limits of the lower step. Overall depth increases to the west. Relief to 1000 meters is displayed as well as subbottom reflectors to 500 meters appearing between hills.

The middle step, trending northeast, is bordered east and west by the 750-meter escarpments of the lower and upper steps. The overall depth of 4000 to 4250 meters increases slightly toward the ridge. Relief to 300 meters is interrupted by relatively smooth flat areas. Subbottom reflectors to 300 meters appear between hills.

The upper step, striking northeast, is bordered by the escarpments of the middle step and the high fractured plateau. Deepening to the west, the average depth of 3500-3750 meters is broken by rough, 1000-meter topography. Subbottom reflectors to 700 meters appear between hills.

The western high fractured plateau trending northeast is bordered to the east by the rift mountains and west by the upper step escarpments. Jagged 600-meter relief topography deepens to the west from 2500-3500 meters. Local subbottom reflectors to 500 meters appear in valleys defining sediment pockets.

The rift mountains are bordered east and west by the high fractured plateaus. These mountain areas parallel either side of the northeast trending rift valley. The valley, deepening southwest from 2600 to 3200 meters, is better defined on the southerly traverse. Subbottom reflectors are absent in both the valley and mountain provinces.

The eastern high fractured plateau which trends northeast, is bordered to the west by the rift mountains, and to the east by the upper step escarpment. The northern traverse appears broken by a fault displacing the rift valley 75 nautical miles. This is perhaps a transform fault (Wilson, 1965).

The eastern upper step, bordered on the west by the high fractured plateau, and to the east by the middle step, appears very broad (555 nautical miles) and includes faults and seamounts. Relief to 350 meters decreases eastward as subbottom reflectors to 900 meters increase in frequency. Several faults apparently strike slightly south of east through the province, one of which displaces a low north-south trending ridge approximately 45 nautical miles.

Two branches of the seamount group incorporating Atlantis, Plato, Cruiser and Great Meteor Seamounts appear on the eastern limits of the upper step. The western branch trends northwest while the eastern branch trends north-northeast. Seamount depths range from 1600 to 4000 meters.

The area between the two branches appears shallower than the adjacent upper step depth. Displaying little relief, this region deepens slightly to the northwest. Subbottom reflectors to 700 meters both conform to the bottom surface and define local irregular buried topography.

The middle step trending north-south incorporates a low ridge and broken terrace. The lower and upper step escarpments border the middle step on the east and west. Subbottom reflectors to 500 meters appear between local highs conforming to the bottom surface and defining irregular buried topography.

Trending slightly east of north, the lower step is limited east and west by escarpments to 750 meters relief. Composed of jagged 500-meter relief topography, the step deepens overall towards the east. Local subbottom reflectors to 200 meters appear between peaks.

Madeira Abyssal Plain/Hills Interchange

East of the lower step escarpment and west of Horseshoe Rise appears a province, seemingly the intersection of the northerly encroaching Madeira Abyssal Plain with the abyssal hills. The bottom surface appears flat, but is frequently interrupted by abyssal hills of relief to 250 meters. Scattered subbottom reflectors to 400 meters generally conform, but locally appear unconformable to the ocean bottom surface.

Horseshoe Rise, Seamount and Abyssal Plain.

Horseshoe Rise, containing Horseshoe Seamount borders northwest at the Madeira Abyssal Plain/Hills Interchange and southeast at Madeira Rise (Figure 9). Horseshoe Seamount is distinctly asymmetric in cross-sectional profile with the steep smooth southwest flank (10:1) facing the Madeira Rise. The seamount rises to within 2000 meters of sea level with local relief to 100 meters on the more gently sloping northwest flank (40:1).

Subbottom reflectors indicate sediment accumulation on the top and northwest flank. A small rise is located at the base of the southeast flank. The Horseshoe Rise shallows from the northwest boundary to the Madeira Rise. Topographic relief to 200 meters is noted on the rise. Shallow subbottom reflectors conform to the bottom surface while the deeper reflectors, ranging to 500 meters, display buried topography.

Madeira Rise and Pedestal

The Madeira Rise incorporating the Madeira Pedestal extends northwest to Horseshoe Rise and small abyssal plain, and southeast to the Madeira Abyssal Plain. This province generally displays relief to 100 meters. The pedestal rises to within 75 meters of sea level. Adjacent to the pedestal, an up-raised area to 500 meters relief drops off to the smoother rise. Shallow subbottom reflectors to 100 meters conform to the bottom surface whereas deeper reflectors to 300 meters show jagged buried topography. Reflectors diverge from the bottom as the rise deepens southward toward the Madeira Abyssal Plain.

Madeira Abyssal Plain

The Madeira Abyssal Plain trending northeast is bordered by the Madeira Rise and Salvage Island Rise. A small calculated gradient of 4400:1 is noted to the southwest (Figures 9 and 10). Maximum depth of 4350 to 4375 meters exists near the northwestern boundary. The bottom surface is smooth with an apparent gradient of 1000:1 to the northwest. Subbottom reflectors to 50 meters basically conform to the bottom surface.

Continental Rise in the Vicinity of the Canary and Cape Verde Islands

The lower and upper continental rise encountered in this area are divided into the more easily defined Salvage Island Rise, Canary Island

Rise (with seamounts), terraces, and the Cape Verde Rise. As each particular rise has its own characteristics, they are separated for discussion purposes in the following text.

Salvage Island Rise is a broad swell trending northeast, lying between the Madeira Abyssal Plain (north) and the Canaries Abyssal Plain (south) (Figure 10). Topographic relief is varied, ranging from smooth surfaces to 150 meters of relief in irregular hills. The latter are predominantly associated with the crest of the rise. Subbottom reflectors to 450 meters appear distorted with respect to the crest topography. Reflectors to 250 meters are subparallel leaving the rise crest. Within the province, depths fall from 3350 meters at the crest to 4350 meters at the base.

The Canaries Abyssal Plain is bounded north by the Salvage Island Rise and south by the Canary Island Rise and deepens 50 to 75 meters to the northwest (Figure 10). This 3600 to 3650 meter abyssal plain fills a depression that was perhaps the upper continental or Canary Island Rise. Subbottom reflectors to 200 meters appear locally in conformity with the bottom surface while deeper reflectors to 300 meters diverge from the limits toward the central axis of the plain.

The Canary Island Rise borders the Canaries Abyssal Plain to the northwest and the island slope base to the southwest. The bottom surface displays 50-meter relief and deepens to the northwest. Local subbottom reflectors to 150 meters appear to conform to the bottom surface.

The Canary Island slope reaching to a depth of 3000 to 3250 meters is defined by gradient. Irregular topography may be due to cruise track orientation with respect to the slope.

The Canary Rise is limited to the northeast by the island slope and is joined southwest by the Cape Verde Rise (Figure 11). A terrace appears southwest of the Canary Islands at 3750 meters. A relationship between the small abyssal plain north of the Canaries and this terrace may exist as both are bordered by a broad swell at their seaward margin and have similar depths. Two seamounts appear ridge-like, trending east-west on the Canary Island Rise. These seamounts seem to be sediment barriers as the bottom deepens from north to south by 75 to 100 meters. The upper portion of the rise is very smooth displaying 50 to 500 meter subbottom reflectors generally conforming to the bottom surface but diverging locally with increased bottom depth. The lower portion of the rise, approaching Station T-4, is also very smooth with subbottom reflectors to 300 meters. The shallow reflectors conform with the bottom surface whereas deeper ones indicate a more irregular buried profile.

The Cape Verde Rise encountered southwest of Station T-4, to T-5, and southeast to the Gambia Abyssal Plain continues from the Canary Rise as part of the continental rise. This rise incorporates a southeast trending fracture zone and Krilof Seamount near 17°15'N/29°15'W (Figures 11 and 12). The Cape Verde Rise from Station T-4 southwest to the fracture zone displays relief to 150 meters with local hills showing 50-400 meters of relief. This rise deepens and smooths to the northeast from the fracture zone. Southeast, between the fracture zone and Gambia Abyssal Plain, the rise deepens to 5200 meters, shallows to 4800 meters and deepens again. Overall relief amounts to 150 meters with local hills showing relief to 500 meters. Shallow subbottom reflectors to 100 meters conform with the bottom . Deep reflectors to 500 meters define irregular buried topography.

The fracture zone displays relief to 700 meters and subbottom reflectors to 300 meters. Krilof Seamount rises to within 1540 meters of sea level showing 3350 meters of relief. Faults are noted trending southeast across the rise in rugged steps and scarps.

Gambia Abyssal Plain

The Gambia Abyssal Plain is bounded northwest by the Cape Verde Rise and southeast by the Sierra Leone Rise. A tongue of abyssal hills, trending east-southeast, protrudes into the province at approximately 11°N (Figure 13). The average abyssal plain depth is 5100 to 5150 meters. The smooth bottom is broken by isolated hills to 350 meters. Shallow subbottom reflectors to 100 meters generally conform to the smooth bottom surface but marginal areas exhibit some distortion. Deeper reflectors to 350 meters appear more rugged.

Sierra Leone Rise and Guinea Fracture Zone

The Sierra Leone Rise is bordered northwest by the Gambia Abyssal Plain and southeast by the Sierra Leone Abyssal Plain. The Guinea Fracture Zone and two seamounts surmount the rise (Figure 13). The rise ascends from abyssal depths to 3700 meters on the fracture zone. Relief to 200 meters appears in local hills and scarps interrupted by an 800-meter hill with surrounding smooth areas of no observed relief. Two seamounts appear south of the fracture zone on the rise. The Guinea Fracture Zone drops 1300 meters to the northwest in a series of steps and scarps (Krause, 1964). Subbottom reflectors range to 500 meters, the shallower conforming to the bottom and the deeper identifying buried topography.

Sierra Leone Abyssal Plain

The Sierra Leone Abyssal Plain is bordered northwest by the Sierra Leone Rise and east by the continental rise (Figure 13). The abyssal plain deepens slightly southwest to a depth of 4925 meters near Station T-6.

Subbottom reflectors to 250 meters conform to the bottom surface, converging slightly toward the margins. Reflectors to 300 meters depict unconforming beds.

Continental Rise, Slope, and Shelf to Monrovia

The continental rise west of Monrovia is bordered west by the Sierra Leone Abyssal Plain and east by the continental slope base arbitrarily defined at the 400 meter isobath. It ascends from abyssal depths to the slope base and appears generally smooth with local relief to 25 meters. Shallow reflectors to 50 meters conform to the bottom whereas deeper reflectors to 200 meters fluctuate, diverging with increasing depth. Reflectors to 300 meters display rugged buried topography.

The continental slope extends from the shelf break near Monrovia to the slope/rise boundary at 4000 meters. Since the ships, arriving and departing Monrovia, traversed the continental slope at very slight angles, the boundary is not displayed clearly by gradient or topography The ships, however, traversed almost normal to an unusual canyon system, cutting the shelf and slope (Figure 14). Good correlations are noted. Subbottom reflectors to 150 meters are eroded by many canyons existing in the area. Continuous deeper reflectors ranging down to 400 meters appear to conform with the bottom prior to erosion.

The continental rise south of Monrovia is bounded northwest by the 4000 meter slope base and southeast by the Guinea Abyssal Plain at 5100 meters (Figure 15). Ascending 1100 meters from the abyssal depths to the slope base, the rise appears very smooth with occasional 50-meter relief. This smooth surface is broken by one small seamount and few isolated hills ranging up to 700 meters in relief. Subbottom reflectors to 150 meters conform to the smooth bottom surface. Deeper reflectors to 500 meters display buried features.

Guinea Abyssal Plain

The Guinea Abyssal Plain is bordered northwest by the continental rise and southeast by the emerging Guinea Rise (Figure 15). The overall depth of 5100 to 5110 meters deepens very slightly to the southwest. The smooth bottom is pierced by occasional abyssal hills to 600 meters relief. Subbottom reflectors to 700 meters are generally parallel or subparallel to the bottom. Discordant deep reflectors indicate buried topography.

Guinea Rise

The Guinea Rise is bordered northwest by the Guinea Abyssal Plain and southeast by the Angola Abyssal Plain. The rise is composed of alternating rugged and smooth topography (Figure 16). Scattered seamounts, atop the rise, range up to 3500 meters. No ridge-like feature is present. A seamount (Figures 3 and 17) rising within 200 meters of sea level, appears in the Cameroon Line. Northeast trending troughs are noted on both flanks of the rise with negative relief to 1500 meters. Subbottom reflectors to 450 meters define irregular buried topography whereas shallower reflectors to 300 meters conform to the smooth bottom in local areas between seamounts.

Angola Abyssal Plain

The Angola Abyssal Plain is bordered northwest by the Guinea Rise and southeast by the continental (Walvis) rise (Figure 17). Bottom depth increases west-southwest from 5500 meters to 5525 meters. Here, the smooth bottom is pierced by occasional abyssal hills to 425 meters in relief. An abyssal hill appears at 17°40'S/04°20'E with associated reflectors to 250 meters. Subbottom reflectors to 100 meters conform to the bottom while deeper reflectors to 350 meters fluctuate. Subbottom reflectors to 250 meters converge toward the southeast boundary. A 50-meter reflector appears as an outcrop.

Continental (Walvis) Rise

The continental (Walvis) rise is bordered northwest by the Angola Abyssal Plain and southeast by Walvis Ridge (Figure 18). Displaying relief to 25 meters, the rise deepens smoothly from the ridge base into a moat-like northeast trending wide valley, swells slightly, then drops gently into the Angola Abyssal Plain. Two abyssal hills and a seamount interrupt the smooth rise. Subbottom reflectors to 100 meters conform to the bottom in local areas whereas reflectors to 400 meters display unconforming buried topography.

Walvis Ridge

Walvis Ridge is bordered northwest by the continental (Walvis) rise and southeast by the South African continental rise. The ridge incorporates an abyssal plain and marginal ridge. The southeast boundary is not well recorded and is assumed with respect to magnetic anomalies (Heirtzler, 1968) (Figure 18). Walvis Ridge ascends gently from the bordering rise, drops abruptly to an abyssal plain, and emerges again as a marginal ridge paralleling the major ridge trend. The ridge displays general relief to 200 meters with local bordering escarpments to 1600 meters relief. Shallow subbottom reflectors to 100 meters in the abyssal plain area conform to the bottom while deeper reflectors to 300 meters diverge toward its central axis. In other smooth areas reflectors to 450 meters define buried topography.

Continental Rise, Slope and Shelf (West, South and East of Capetown)

The southwest African continental rise ascends gradually from the Walvis Ridge in a series of terraces to the arbitrary 3250-meter-isobath rise/slope boundary (Figure 18). The angular approach to the rise and slope is such that a gradient change and/or topographic boundary cannot be determined accurately. The rise is generally smooth with local relief to

50 meters. Shallow 50-meter subbottom relfectors conform to the bottom while reflectors to 450 meters display subparallel beds. Isolated reflectors to 450 meters define rugged buried topography.

The continental slope west of Capetown is bordered northwest by the continental rise and east by the continental shelf. The Orange River Canyon appears near 30°50'S/15°05'E at 1400-1500 meters (Figure 19). Subbottom reflectors to 20 meters appear to conform to the bottom whereas reflectors from 50 to 500 meters diverge down slope with increasing depth. Reflectors ranging from 50 to 200 meters in isolated areas identify filled channels and other buried features.

The continental shelf west and south of Capetown is bordered south and west by the slope and incorporates a southerly trending canyon (Figure 20). The shelf displays local relief to 25 meters with the exception of canyon relief ranging to 150 meters. Subbottom reflectors to 450 meters generally diverge seaward.

The continental slope west and south of Capetown is bordered landward at the 500-meter shelf break and seaward by the continental rise. It incorporates canyons, benches, and escarpments (Figure 21). Three canyons appear high on the slope, displaying relief to 250 meters. Near the slope/rise boundary, two asymmetric features appear with 750 to 1200 meter relief. The first of these deepens along its southerly trending crest from 2250 to 2850 meters and the second southwest trending feature deepens from 3350 to 3900 meters along its crest. Two bench-like features appear midway on the continental slope, the first of which deepens southeast from 2000 to 2575 meters, and the second, paralleling the first, deepens from 3000 to 3255 meters. Generally, the continental slope displays relief to 150 meters, but where asymmetric features and canyons appear, relief increases.

Subbottom reflectors to 50 meters conform to the bottom whereas isolated reflectors up to 250 meters define buried topography.

South of Capetown, the continental rise extends from the slope and escarpment base east to the Agulhas Plateau and scarp zone (Figure 23). A 3000-meter relief seamount of the Mallory Group exists on the rise (Figure 22). The rise appears as a wide valley and deepens southwest to 5400 meters. Relief to 400 meters gradually decreases eastward toward the scarp zone. Local subbottom reflectors to 100 meters conform to the bottom. Subbottom reflectors to 300 meters diverge west from the scarp zone and display buried features.

Agulhas Plateau and Associated Scarp Zones

The Agulhas Plateau is bordered on the east and west by scarp zones which are in turn bordered east by the Transkei Abyssal Plain and west by the microcontinental rise (Figure 23). The Agulhas Plateau, with the exception of the bordering scarp zones, is a raised tabular feature widening and deepening to the south. The plateau displays relief to 750 meters. The eastern scarp zone deepens to the Transkei Abyssal Plain with relief to 500 meters while the western scarp zone deepens toward the microcontinental rise with relief to 700 meters, Local subbottom reflectors to 50 meters conform to the bottom whereas reflectors to 400 meters define buried topography.

Transkei Abyssal Plain

The Transkei Abyssal Plain borders the Agulhas scarp zone and microcontinental rise (Figure 24). The abyssal plain which deepens slightly to the southeast, is interrupted by two hills of 200 and 350 meters relief and their surrounding depression.

Continuous subbottom reflectors to 50 meters conform to the bottom and are underlaid by subparallel reflectors to 200 meters which converge slightly towards the margins. Subbottom reflectors to 200 meters display related buried features in the vicinity of the abyssal hills piercing the abyssal plain.

Microcontinental Rise to Mozambique Ridge

The western microcontinental rise of the Mozambique Ridge is bordered on the southwest by the Transkei Abyssal Plain and on the northeast by the Mozambique Ridge. The southern traverse of the microcontinental rise appears smooth to the 4400-meter isobath. Relief of 50 meters continues to the ridge base. Subbottom reflectors to 100 meters conform to the bottom; deeper reflectors to 200 meters are subparallel and display buried features. The northern traverse, in part nearly parallel to the ridge, displays a smooth rise with local relief to 50 meters. Subbottom reflectors to 200 meters indicate unconforming beds, buried troughs, and hills. Overall, the 50 to 250 meter subbottom reflectors conform to the smooth bottom with local divergence.

Mozambique Ridge and Fracture Zone

The Mozambique Ridge and north-south striking Mozambique Fracture Zone are bordered west by the microcontinental rise and east by the Natal Basin (Figure 25). This submerged microcontinent trends and narrows to the north. The northwestern boundary is not obvious due to ship-track orientation and is therefore defined topographically. The Mozambique Fracture Zone appears as tabular steps and escarpments on the eastern ridge and slope (Figure 25). A 2000-meter escarpment appears on the eastern ridge boundary of the northern crossing. Deepening north, the ridge top

appears plateau-like with 50 to 400 meter relief. The southern crossing displays a depression of 800 meters negative relief. Local subbottom reflectors to 400 meters do not conform to the bottom.

Abyssal Plain/Hills (Natal Basin)

A north-south trending 5010-meter abyssal plain is bordered west by the Mozambique Ridge and south and east by abyssal hills which in turn border east on the Mozambique Abyssal Plain (Figure 25). Subbottom reflectors to 100 meters conform to the abyssal plain bottom, but diverge at the eastern boundary. Subbottom reflectors to 50 meters in the hilly province conform locally whereas deeper reflectors to 150 meters define rugged buried topography. An 800-meter hill appears in the abyssal hills province probably in association with the nearby fracture zone. A 300-meter reflector midway between the scarp and slope base diverges both east and west.

Mozambique Abyssal Plain

The Mozambique Abyssal Plain borders west and southwest at the abyssal hills province and east at the Zambezi Cone (Figures 25 and 26). This plain, at a maximum depth of 4960 meters, is very smooth with the exception of 25-meter relief at its boundaries. Subbottom reflectors to 200 meters conform to the smooth bottom. Locally, reflectors to 250 meters diverge and define buried irregular topography.

Zambezi Cone (Natal Basin)

The north-south trending Zambezi Cone which was traversed at its southern tip, is bordered west by the Mozambique Abyssal Plain and east by an abyssal plain of the Natal Basin (Figure 26). Distributaries of the Zambezi Canyons appear to trend normal to the deepening isobaths. The topography is generally smooth between the channels. Discontinuous and undulating reflectors to 175 meters occasionally conform to the bottom surface.

Subbottom reflectors to 250 meters display filled and buried channels. Reflectors to 350 meters beneath the depositional area appear to converge northwest. What may be a turbidity current terminus is noted at 30°30'S/ 39°35'E.

Abyssal Plain (Natal Basin)

An abyssal plain trending slightly west of south borders the Zambezi Cone to the west and the microcontinental rise of the Madagascar Ridge to the east (Figure 26). The plain is very smooth, deepening slightly to the southwest. Subbottom reflectors to 100 meters conform to the bottom.

East and West Microcontinental Rise to Madagascar Ridge and Madagascar

The microcontinental rise borders west at the abyssal plain and east at the Madagascar Ridge (Figure 27). Descending from the ridge to the abyssal plain, the rise appears generally smooth and undulating with relief to 25 meters. A shallow 50-meter reflector conforms to the bottom. Deeper reflectors to 150 meters conform locally and define pocketed sediment.

The microcontinental rise south and east of Madagascar projects between the Madagascar Ridge and a scarp extension of that ridge (Figures 27 and 28). Deepening slightly to the east, away from the microcontinent, the relatively smooth topography of 100 meters is interrupted by isolated hills to 450 meters relief. Local subbottom reflectors to 50 meters conform to the bottom in smooth areas whereas reflectors to 250 meters display unconforming beds and buried topography.

The next province of the microcontinental rise borders the scarp extension to the south and the Madagascar slope near Diego-Suarez to the west and north. Sloping eastward and seaward from the microcontinent, the rise is interrupted by the Malagasy Abyssal Plain (Figures 28 and 29). The microcontinental rise appears generally smooth with local hills to 350 meters

relief. Subbottom reflectors to 100 meters conform with local bottom topography as reflectors to 300 meters conform locally, but generally display divergence and rugged buried topography.

Madagascar Ridge and Fracture Zone

The Madagascar Ridge trending south from Madagascar, borders east and west on the microcontinental rise (Figure 27). This plateau-like ridge has an average depth of 1500 to 2000 meters, deepening to the southeast. Topographic relief to 250 meters is evident. What seems to be the Prince Edward Fracture Zone appears as a normally faulted area on the western slope of the ridge. Subbottom reflectors to 600 meters further define this feature. Local 50-meter reflectors conform to bottom topography whereas deeper reflectors to 475 meters show unconforming beds and buried topography. A normal fault appearing at 26°35'S/45°30'E indicates a nearly vertical displacement of 100 meters.

Scarp Extension of the Madagascar Ridge

A small ridge extends northeast from the Madagascar Ridge onto the seaward sloping microcontinental rise. This extension is bordered north and south by the microcontinental rise (Figure 28). The rugged topography indicated by 1250-meter relief becomes smoother and deepens towards the north. A northeast striking fault forms the southern boundary and displays smooth southeasterly facing scarps with a conformable 500-meter reflector. Local subbottom reflectors to 50 meters conform to the bottom in smooth areas. Reflectors to 300 meters define unconforming and rugged topography.

Malagasy Abyssal Plain

The western edge of the Malagasy Abyssal Plain encountered at 4920 meters and again at 4880 meters interrupts the microcontinental rise with very smooth, flat topography. Subbottom reflectors to 250 meters appear in

the first crossing, diverging southward and defining irregular buried topography. No reflectors were noted in the second encounter.

Microcontinental Slope and Rise (Northeast of Madagascar)

The microcontinental slope east of Madagascar, traversed nearly parallel to the regional isobaths, appears rugged with relief to 500 meters. Erosional channels and possible faulting are apparent. Local subbottom reflectors to 50 meters conform to the bottom as deeper reflectors to 350 meters define unconforming beds and irregluar buried topography. The microcontinental slope northeast of Diego-Suarez deepens from the 100-meter shelf break to 2500 meters (Figure 28). The slope appears to steepen, continuing to the slope/rise boundary at depths of 3200 to 3450 meters. The north-northwest trending slope base seems to display faulting northeast of Diego-Suarez as suggested by Heezen (1965). Local subbottom reflectors to 50 meters conform to the bottom and deeper reflectors to 250 meters define irregular buried topography.

The microcontinental rise appears eastward from the slope/rise boundary into the Mascarene Basin (Figure 29). Overall topography is smooth with local relief to 125 meters. Subbottom reflectors to 50 meters conform to the smooth bottom whereas reflectors to 250 meters define unconforming beds and local rugged buried topography. A seamount, appearing on the rise, displays 2265-meter relief.

Mascarene Basin (Abyssal Hills, Scarp Zones, and Amirante Trench)

The Mascarene Basin incorporates east and west limiting scarp zones as well as the Amirante Trench.

The western scarp zone topography of 450-meter relief deepens east from 4225 to 4800 meters at the scarp zone base. A seamount with 1050-meter relief is located at 11°30'S/51°05'E. Subbottom reflectors to 100 meters conform basically with bottom topography but are locally unconformable.

The eastern scarp topography to 400 meters of relief deepens into the Amirante Trench to the east and is bordered by abyssal hills to the west. Shallow reflectors to 50 meters conform with the bottom topography; the deeper local reflectors to 300 meters diverge and display rugged buried features.

Abyssal hills are present within the basin displaying an average depth of 4500 to 4750 meters. This province has relief to 400 meters. Subbottom reflectors to 100 meters locally conform to bottom topography, whereas deeper local reflectors to 200 meters diverge and define buried topography.

The Amirante Trench, trending southeast is bordered to the southwest by a 425-meter relief scarp, and northeast by the Mascarene Plateau. Deepening northwest from 4650 to 4825 meters, the trench bottom displays relief to 100 meters with subbottom reflectors to 100 meters.

Mascarene Plateau (Upper and Lower Rises)

The Mascarene Plateau is bordered northeast by the Mascarene Upper Rise and southwest by the Amirante Trench. The small rise from the trench to the base of the Mascarene Plateau displays relief to 100 meters; subbottom reflectors to 300 meters define rugged buried topography.

A U-shaped northern portion of the Mascarene Plateau partially encloses seamounts, ridges, terraces, faults and rise areas.

A southwestern ridge incorporates a faulted intermountain area which is relatively flat on both sides of the median 125-meter scarp. Local relief to the west of the scarp is negligible but increases to 25 meters to the east. The ridge top at 2250 meters deepens to 4300 meters in the intermountain area. Subbottom reflectors to 100 meters conform to the smooth

undulating bottom; reflectors to 350 meters display rugged buried topography.

The crest of the north-south trending ridge, centrally located on the rise, deepens north from 1700 to 2650 meters.

The rise, located west of the north-south trending ridge, deepens to the southwest and displays a northeast trending 200-meter escarpment. Shallow subbottom reflectors to 100 meters locally conform to the bottom, and reflectors to 500 meters display apparent faulting.

The eastern rise ascending from the above ridge is bordered northeast by the eastern Mascarene Plateau. Sloping to the southwest, undulating topography displays relief to 250 meters; shallow subbottom reflectors conform locally but deeper reflectors to 400 meters define unconformable topography.

The northeast portion of the Mascarene Plateau borders southeast on the north-south trending ridge and northeast at the Mascarene Upper Rise (Figure 30). A flat-topped pedestal situated atop the plateau rises to within 650 meters of sea level. Subbottom reflectors to 500 meters are subparallel to the bottom, outcropping on the top and flanks of the plateau. A 1000-meter scarp at the northwestern flank parallels the regional trend of the plateau.

The Mascarene Rise descends northeast from the Mascarene Plateau to the Madingley Abyssal Plain (Figure 30). The rise is divided by an escarpment into an upper and lower zone. Shallow subbottom reflectors to 50 meters generally conform to the bottom; reflectors to 250 meters display irregular buried topography.

Madingley Abyssal Plain

The Madingley Abyssal Plain west of the Mascarene Rise, extends northeast into the Madingley Rise at 4000 meters. Subbottom reflectors to

150 meters conform to the smooth bottom; local unconforming reflectors to 225 meters display irregular buried topography.

Madingley Rise

The Madingley Rise borders southwest on the Madingley Abyssal Plain and northeast on the western flank of the Mid-Indian Ocean Ridge. The rise deepens approximately 250 meters toward the Mid-Indian Ocean Ridge. Rugged topography to 500-meter relief increases to 1125-meter relief in the central rise area. Subbottom reflectors to 200 meters locally conform to the flat bottom topography in valley areas; unconforming reflectors to 250 meters display buried topography.

Mid-Indian Ocean Ridge

The Mid-Indian Ocean Ridge, composed of east and west flanks, rift mountains and a rift valley, appears trending slightly east of north.

The west flank of the ridge is bordered west by the Madingley Rise and east by the rift mountain. Rugged topography to 1500 meters relief appears as scarps, hills, seamounts, and intermountain valleys. Peaks have average depths of 3250 meters; valley depths average 4250 meters. Smooth escarpments exist within the western flank dropping into flat floored valleys. Subbottom reflectors to 150 meters locally conform to the bottom whereas reflectors to 200 meters display irregular buried features.

The east flank of the Mid-Indian Ocean Ridge is bordered east by abyssal hills and west by the rift mountains. Rugged topography to 1250 meters relief appears as scarps, hills, seamounts, and parallel trending intermountain valleys. A flat-floored intermountain valley appears trending and deepening slightly east of north. Subbottom reflectors to 200 meters locally conform to the bottom; discontinuous irregular reflectors to 600 meters define buried features.

The rift mountains and valley separate the east and west flanks (Figure 31). The rift mountain peak depth deepens toward the flanks. Subparallel valleys are oriented north-south alongside the rift valley. Subbottom reflectors are not present within the province. The rift valley axis strikes north-south and deepens to the south from 4000 to 4125 meters. The valley, bordered east and west by the rift mountains, displays relief to 2300 meters.

Abyssal Hills

An abyssal hills province borders west at the eastern Mid-Indian Ocean Ridge flank and east on the microcontinental rise of the Chagos Laccadive. The southern traverse displays rugged topography to 650 meters relief whereas on the northern traverse topography of only 400 meters relief is noted. In cross-sectional profile, some of the abyssal hills are asymmetric. The province is interrupted by a north-northeast deepening and trending valley. Local subbottom reflectors to 200 meters appear conformable in pockets and define buried topography.

Chagos Laccadive (Maldive, Rise and Trench)

The Chagos Laccadive, (Heezen, 1966) trending slightly east of north, is an eastward tilting tabular feature of 1500 meters relief (Figure 32). Topography of 150 meters relief atop this feature is interrupted by a flat-topped, 1000-meter relief Maldive. A 750-meter negative relief depression appears on the western margin. The average depth increases eastward from 2500 to 3000 meters. East and west bordering escarpments descend into Chagos Trench and microcontinental rise, respectively. The rise descends west into the limiting abyssal hills. Relief to 300 meters is interrupted by a parallel north-south trending scarp and trough system. Subbottom reflectors to 200 meters conform to the bottom with local reflectors defining rugged buried topography.

Subbottom reflectors to 200 meters associated with the Laccadive conform to the bottom; reflectors to 525 meters appear irregular and indicate deeper buried rugged topography.

The Chagos Trench parallels and limits the Chagos Laccadive to the west. A north-northeast striking fracture zone bounds the trench to the east (Figures 32 and 33). The trench deepens from north to south along its central axis. Undulating topography to 200 meters relief appears in the trench with unconforming subbottom reflectors to 225 meters.

NNE/SSW Fracture Zone

The north-northeast striking fracture zone borders the Chagos Trench to the west and the Ceylon Abyssal Plain to the east (Figure 33). Correlating fault blocks and scarps appear to deepen to the south-southwest. Subbottom reflectors to 200 meters generally conform to the bottom, but are locally discordant.

Ceylon Abyssal Plain

The northern portion of the Ceylon Abyssal Plain borders west on the fracture zone and east on the continental rise extending south from India (Figure 33). Deepening slightly southwest, the abyssal plain is very smooth. Two isolated abyssal hills of 150 and 200 meters relief interrupt the smooth surface. Local subbottom reflectors to 150 meters conform to the smooth bottom. Deeper reflectors to 275 meters, undulating and parallel to each other, are discordant with the bottom. These reflectors appear to diverge from the margins, displaying irregular buried features.

Continental Rise (Scarp)

The continental rise extends southeast from India separating the Ceylon Abyssal Plain and the Ganges Cone. Deepening to the south and southwest, the 25-meter relief undulating topography is interrupted by a

575-meter relief hill. Subbottom reflectors to 50 meters conform to the bottom; deeper reflectors to 250 meters appear unconformable.

Ganges Cone

The Ganges Cone trending and deepening slightly west of south, borders west on the continental rise of India and east on the micro-continental rise of the Ninety-East Ridge. The cone displays overall smooth topography with intermittent submarine troughs, isolated seamounts, hills and faulting. A sharp southwest trending trough displays 30 to 75 meter negative relief. The trough shallows as the cone deepens to the south. A large hill or seamount displays 650 to 800 meter relief supplemented by a 600-meter subbottom reflector defining its buried portions (Figure 34). Terraced troughs with depths of 150 meters appear on the cone (Figure 35). Subbottom reflectors to 150 meters conform to the smooth cone surface, and local shallow and deeper reflectors to 300 meters diverge, undulate and outline unconforming zones. Local areas of buried topography are indicated by the deeper reflectors.

Ninety-East Ridge

Ninety-East Ridge trending north-south (Heezen, 1964), ascends gently from the western rise. Irregular topography and escarpments mark the boundary with the eastern rise (Figure 36). The average depth of the ridge deepens to the south. Its 200-meter relief is interrupted by two seamounts. Local reflectors to 250 meters conform to the bottom; deeper diverging reflectors do not conform to the bottom but display rugged buried topography.

The western microcontinental rise to the Ninety-East Ridge deepens 100 meters towards the Ganges Cone, displaying relief to 25 meters. Undulating subbottom reflectors to 300 meters display buried topography.

The eastern microcontinental rise deepens 725 meters into the Foredeep (Weeks et al., 1967) (Figure 37). The rise displays relief to 25 meters with generally conforming and locally diverging subbottom reflectors to 100 meters. Deeper reflectors to 450 meters diverge with increased depth and appear to display faulting whereas undulating reflectors to 600 meters define irregular buried topography.

Foredeep

The Foredeep, (Weeks, 1967; Peter, 1966; and Alexander, 1961), an extension of the Java Trench, is bordered east by the Indonesian Arc's Frontal Thrust Masses and west by the Ninety-East Ridge's microcontinental rise (Figure 37). The maximum depth axis deepens southeast from 4300 meters to 4350 meters. Topography is smooth whereas subbottom reflectors to 250 meters diverge toward maximum depth.

Indonesian Arc

The Indonesian Arc trending north-northwest, is composed of Frontal Thrust Masses, an Outer Island Arc, the Interdeep, and the Inner Volcanic Arcs. Bounded west by the Foredeep, the arc borders the Backdeep to the east (Weeks, 1967; Peter, 1966; and Alexander, 1961) (Figure 37).

The Frontal Thrust Masses rise abruptly out of the Foredeep to an average peak depth of 1000 to 1250 meters and deepen east into a limiting valley. Rugged 1000-meter relief topography appears with conforming subbottom reflectors to 100 meters displayed in troughs. Deeper unconforming reflectors to 600 meters are noted.

The Outer Island Arc rises west from the valley, separating the Frontal Thrust Masses from the Interdeep. Deepening markedly south-southeast, the arc increases in depth from 600 meters to 1175 meters along its crest. One isolated 50-meter subbottom reflector is noted which conforms to the bottom between hills.

The Interdeep deepens slightly south-southwest from 2650 to 2700 meters along a smooth flat bottom. Conforming subbottom reflectors to 300 meters appear; reflectors to 350 meters define the buried valley walls and display unconforming beds.

A tabular feature increases relief (700 to 950 meters) eastward from the Interdeep. Its smooth surface dips west from 1500 to 2000 meters. To the east, the feature is limited by a valley which separates it from the Inner Volcanic Arc. Subbottom reflectors to 150 meters conform to the bottom whereas local reflectors to 150 meters define buried topography.

The Inner Volcanic Arc, trending from 150 to 425 meters, descends east into the Backdeep and west into a bordering valley. The arc displays sharp, rugged topography to 1300 meters of relief. The western bordering deep increases in depth north-northwest from 1250 to 1950 meters, with topography to 175 meters in relief. Local subbottom reflectors to 50 meters conform to the bottom; deeper reflectors to 300 meters define rugged buried topography.

Backdeep (Ridge, Rise and Terrace)

The Backdeep, east of the Indonesian Arc, incorporates the continental rise, a terminating ridge and a smooth terrace, (Weeks, 1967; Peter, 1966; and Alexander, 1961) (Figure 37).

Ascending east from the Inner Volcanic Arc base, the rise terminates against a nearly buried ridge and displays a smooth, undulating surface. Subbottom reflectors to 300 meters conform to the undulating bottom whereas local reflectors to 350 meters diverge and undulate out of phase with the bottom.

A nearly buried ridge, bordered on the west by the rise, and east by a terrace trends and deepens southwest from 850 to 1300 meters. With local

200-meter relief, the ridge displays isolated reflectors to 50 meters which conform to the smooth bottom; deeper reflectors to 700 meters undulate.

The terrace, bordered southeast by the rise and northwest by the ridge appears very smooth. Subbottom reflectors to 100 meters conform to the smooth bottom whereas deeper reflectors to 400 meters are discordant.

The rise, bordered by the terrace and slope appears very smooth to the north. Reflectors from 50 to 250 meters generally conform to the bottom. The southern traverse displays 50 to 200 meter relief with one isolated subbottom reflector which conforms to the bottom. Deeper reflectors up to 450 meters appear to display faulting and rugged buried topography.

Continental Slope and Shelf

The relatively smooth continental slope separates the continental rise and shelf (Figure 37). Subbottom reflectors to 300 meters appear to converge toward the continental shelf.

The continental shelf encountered west of the shelf break in the Malacca Straits, is generally smooth but displays isolated 50 to 100 meter relief (Figure 37). The continental shelf shallows from the shelf break to Singapore.

III REFERENCES

Alexander, J.B. 1961. A short outline of the geology of Malaya with special reference to Mesozoic Orogeny. 10th Pacific Congress, Honolulu, Hawaii.

Halpin, D. (Part 2 this volume) (in press) Area ST, Volume 2, Magnetics. Prepared by Alpine Geophysical Associates, Inc. U.S. Naval Oceanographic Office, SP-97-ST-2.

Heezen, B.C. and Tharp, M. 1966. Physiography of the Indian Ocean. Phil. Trans. Roy. Soc. London, A, 259: 137-149.

Heezen, B.C. and Tharp, M. 1965. A symposium on Continental Drift VIII, tectonic fabric of the Atlantic and Indian Oceans and Continental Drift. Phil. Trans. Roy. Soc. London, A, 258: 90-106.

Heezen, B.C. and Tharp, M. 1964. Physiographic diagram of the Indian Ocean, the Red Sea, the South China Sea, the Sulu Sea, and the Celebes Sea. Geol. Soc. Am. New York.

Heezen, B.C. and Tharp, M. 1961. Physiographic diagram of the South Atlantic Ocean. the Caribbean Sea, the Scotia Sea, and the eastern margin of the South Pacific Ocean. Geol. Soc. Am. New York.

Heezen, B.C. and Tharp, M. 1957. Physiographic diagram - Atlantic Ocean, IV, The Floors of the Oceans, I, the North Atlantic. Geol. Soc. Am. Spec. Papers, 65: 122 pp.

Heezen, B.C., Tharp, M. and Ewing, M. 1959. The Floors of the Oceans,I, The North Atlantic. Geol. Soc. Am. Spec. Papers, 65: 122 pp.

Krause, D.C. 1964. Guinea Fracture Zone in the Equatorial Atlantic. Science, 146: 57-59.

Peter, G., Weeks, L. and Burnes, R.E. 1966. A reconnaissance geophysical survey in the Andaman Sea and across the Andaman-Nicobar Arc. J. Geophys. Res., 71(2): 495-509.

Pike, T.M. 1966. Area I, Volume 5, Bathymetry and subbottom profiling. Prepared by Alpine Geophysical Associates, Inc. U.S. Naval Oceanographic Office, SP-96-I-5.

Weeks, L.A.,Harbison, R.N. and Peter, G. 1967. Island Arc System in the Andaman Sea. Bull. Am. Assoc. Petrol. Geologists, 51(9): 1803-1815.

Wilson, J.T. 1965. A new class of faults and their bearing on Continental Drift. Nature, 207: 343-347.

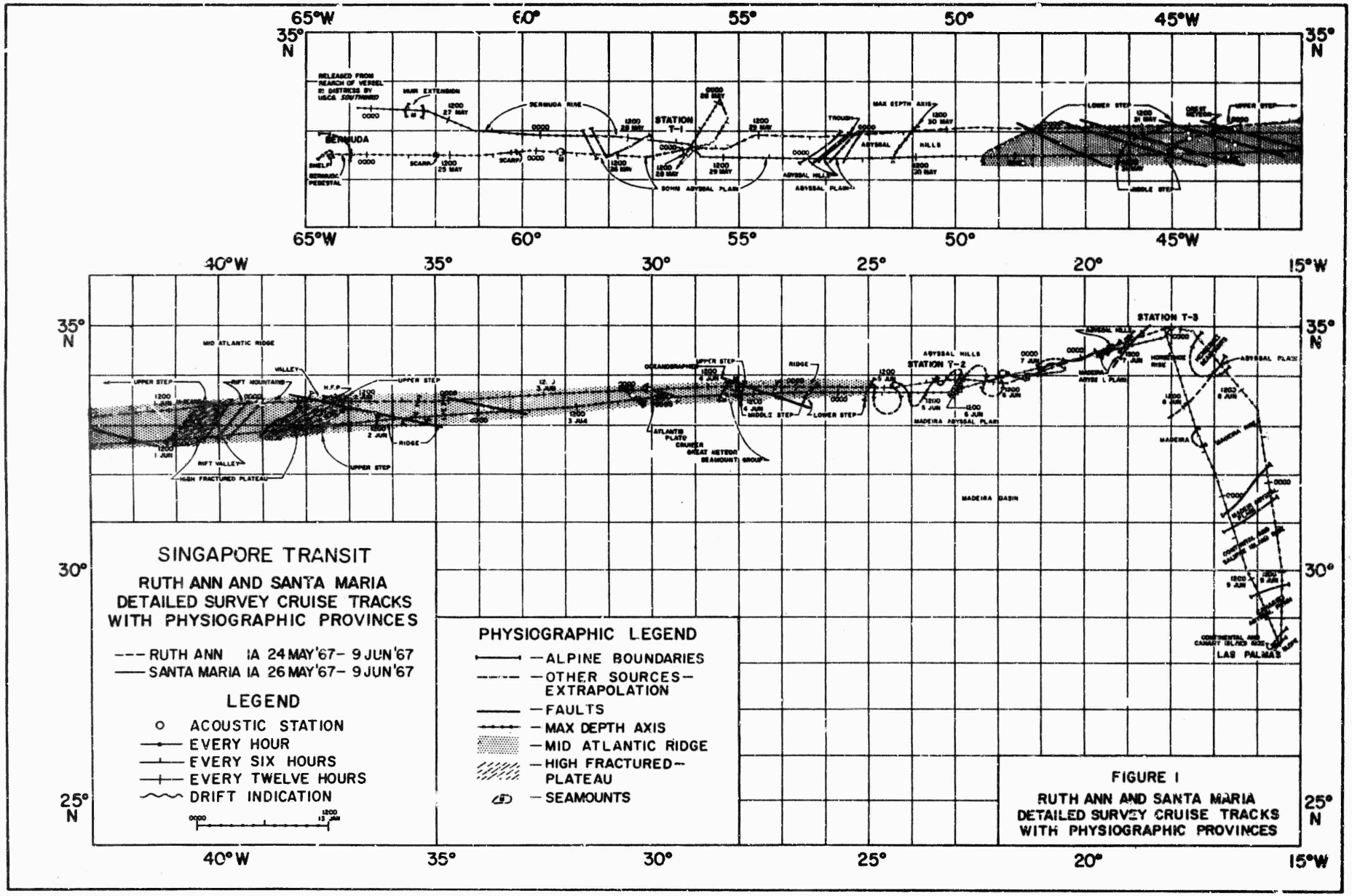
65°W
60°
55°
50°
45°W
35° N
40°W
35°
30°
25°
20°
15°W
30°
25° N
STATION T-1
STATION T-2
STATION T-3
BERMUDA
MID ATLANTIC RIDGE
MADEIRA BASIN
LAS PALMAS
SINGAPORE TRANSIT
RUTH ANN AND SANTA MARIA
DETAILED SURVEY CRUISE TRACKS
WITH PHYSIOGRAPHIC PROVINCES
--- RUTH ANN IA 24 MAY'67 - 9 JUN'67
—— SANTA MARIA IA 26 MAY'67 - 9 JUN'67
LEGEND
ACOUSTIC STATION
EVERY HOUR
EVERY SIX HOURS
EVERY TWELVE HOURS
DRIFT INDICATION
PHYSIOGRAPHIC LEGEND
— ALPINE BOUNDARIES
— OTHER SOURCES — EXTRAPOLATION
— FAULTS
— MAX DEPTH AXIS
— MID ATLANTIC RIDGE
— HIGH FRACTURED — PLATEAU
— SEAMOUNTS
FIGURE I
RUTH ANN AND SANTA MARIA
DETAILED SURVEY CRUISE TRACKS
WITH PHYSIOGRAPHIC PROVINCES

FIGURE I

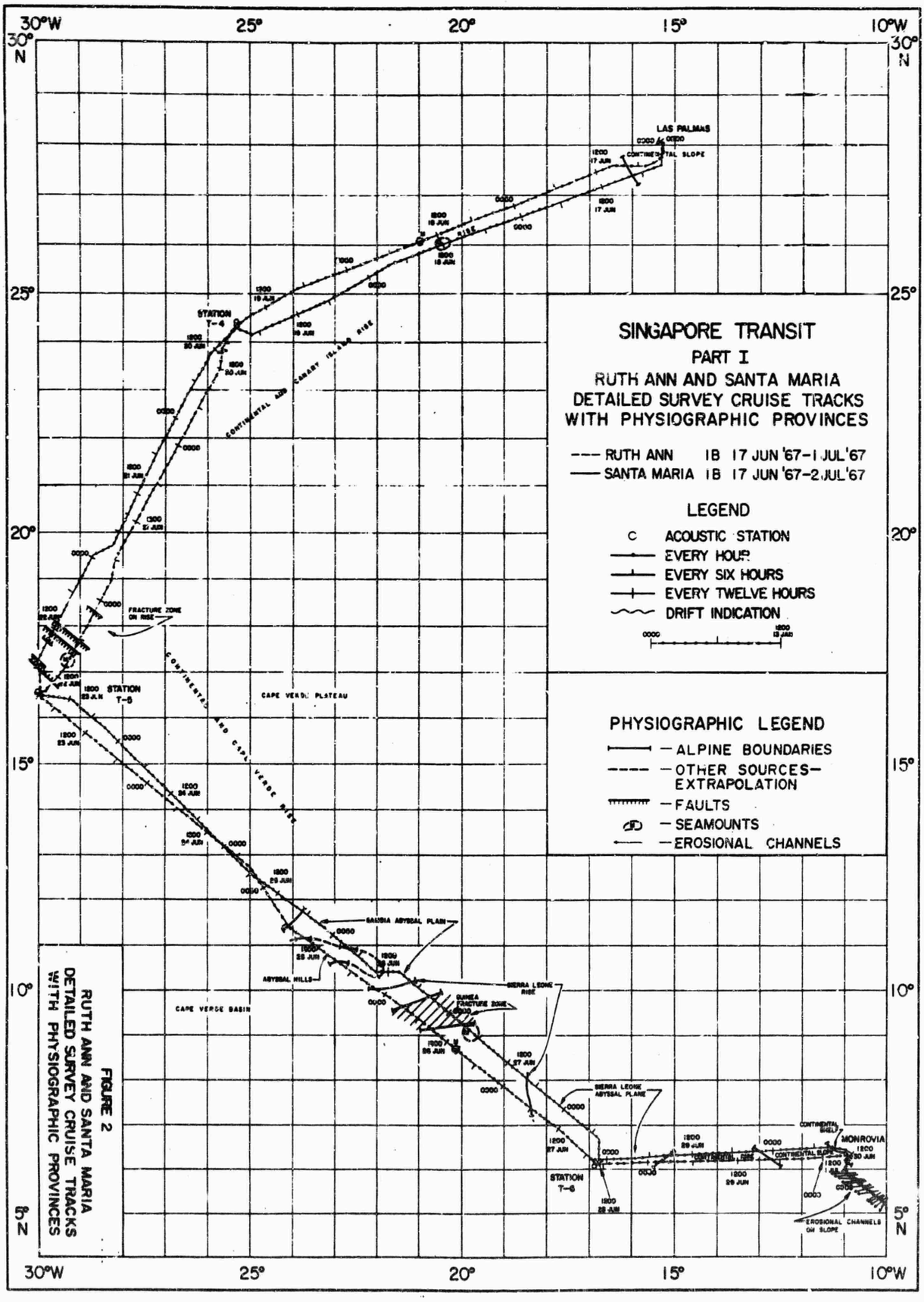
30°W
25°
20°
15°
10°W
30° N
25°
20°
15°
10°
5° N
LAS PALMAS
CONTINENTAL SLOPE
CANARY ISLANDS RISE
CONTINENTAL AND
STATION T-4
STATION T-5
STATION T-6
FRACTURE ZONE ON RISE
CONTINENTAL AND CAPE VERDE RISE
CAPE VERDE PLATEAU
SAUDIA ABYSSAL PLAIN
ABYSSAL HILLS
CAPE VERDE BASIN
GUINEA FRACTURE ZONE
SIERRA LEONE RISE
SIERRA LEONE ABYSSAL PLAIN
CONTINENTAL SHELF
MONROVIA
EROSIONAL CHANNELS ON SLOPE
SINGAPORE TRANSIT
PART I
RUTH ANN AND SANTA MARIA
DETAILED SURVEY CRUISE TRACKS
WITH PHYSIOGRAPHIC PROVINCES
--- RUTH ANN IB 17 JUN '67-1 JUL '67
—— SANTA MARIA IB 17 JUN '67-2 JUL '67
LEGEND
C ACOUSTIC STATION
EVERY HOUR
EVERY SIX HOURS
EVERY TWELVE HOURS
DRIFT INDICATION
PHYSIOGRAPHIC LEGEND
— ALPINE BOUNDARIES
— OTHER SOURCES— EXTRAPOLATION
— FAULTS
— SEAMOUNTS
— EROSIONAL CHANNELS
FIGURE 2
RUTH ANN AND SANTA MARIA
DETAILED SURVEY CRUISE TRACKS
WITH PHYSIOGRAPHIC PROVINCES

FIGURE 2

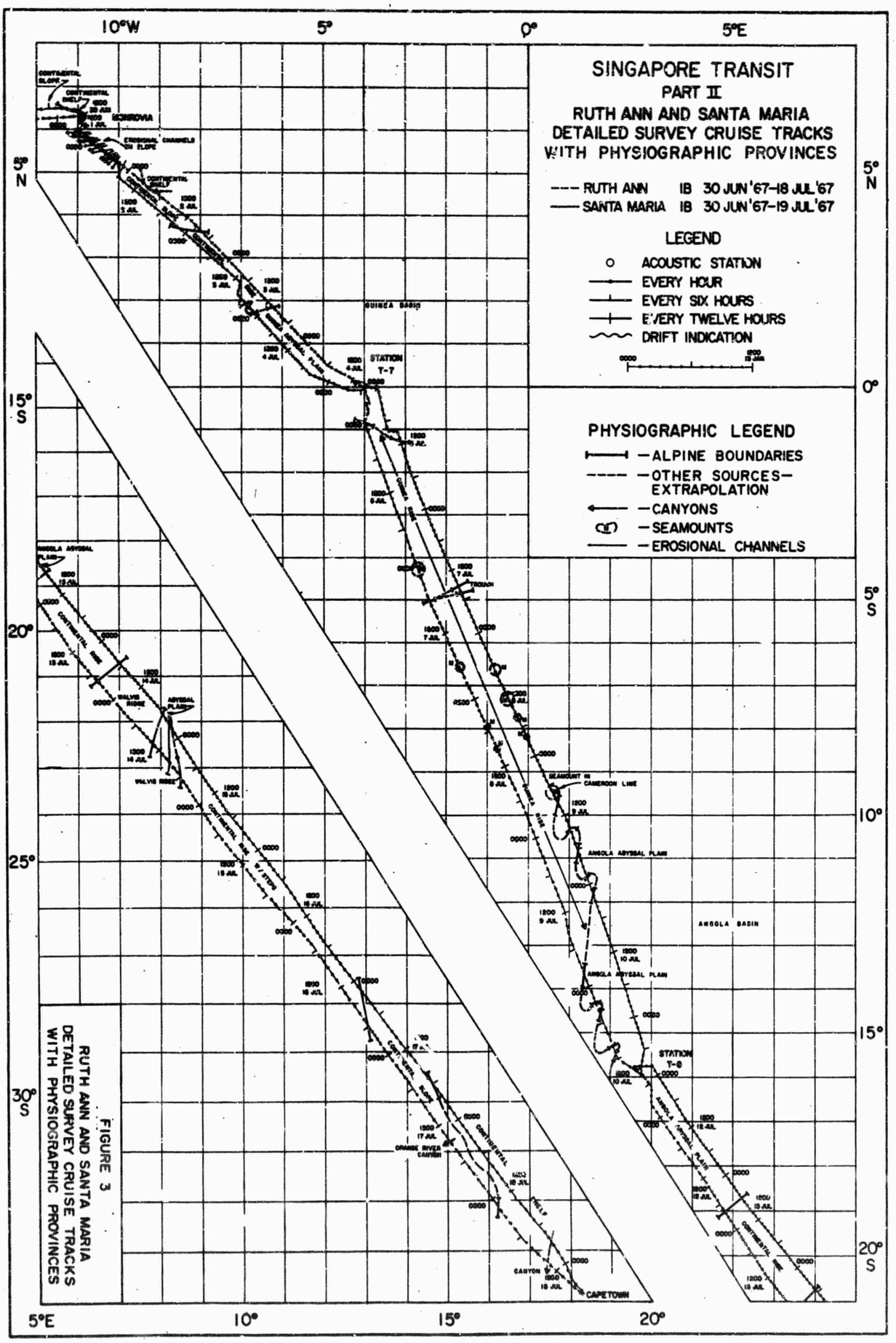
SINGAPORE TRANSIT
PART II
RUTH ANN AND SANTA MARIA
DETAILED SURVEY CRUISE TRACKS
WITH PHYSIOGRAPHIC PROVINCES
--- RUTH ANN IB 30 JUN '67–18 JUL '67
—— SANTA MARIA IB 30 JUN '67–19 JUL '67
LEGEND
ACOUSTIC STATION
EVERY HOUR
EVERY SIX HOURS
EVERY TWELVE HOURS
DRIFT INDICATION
PHYSIOGRAPHIC LEGEND
—ALPINE BOUNDARIES
—OTHER SOURCES— EXTRAPOLATION
—CANYONS
—SEAMOUNTS
—EROSIONAL CHANNELS
10°W
5°
0°
5°E
5° N
15° S
20°
25°
30° S
5° S
10°
15°
20° S
MONROVIA
GUINEA BASIN
STATION T-7
STATION T-8
ANGOLA BASIN
ANGOLA ABYSSAL PLAIN
CAPE TOWN
FIGURE 3
RUTH ANN AND SANTA MARIA
DETAILED SURVEY CRUISE TRACKS
WITH PHYSIOGRAPHIC PROVINCES

FIGURE 3

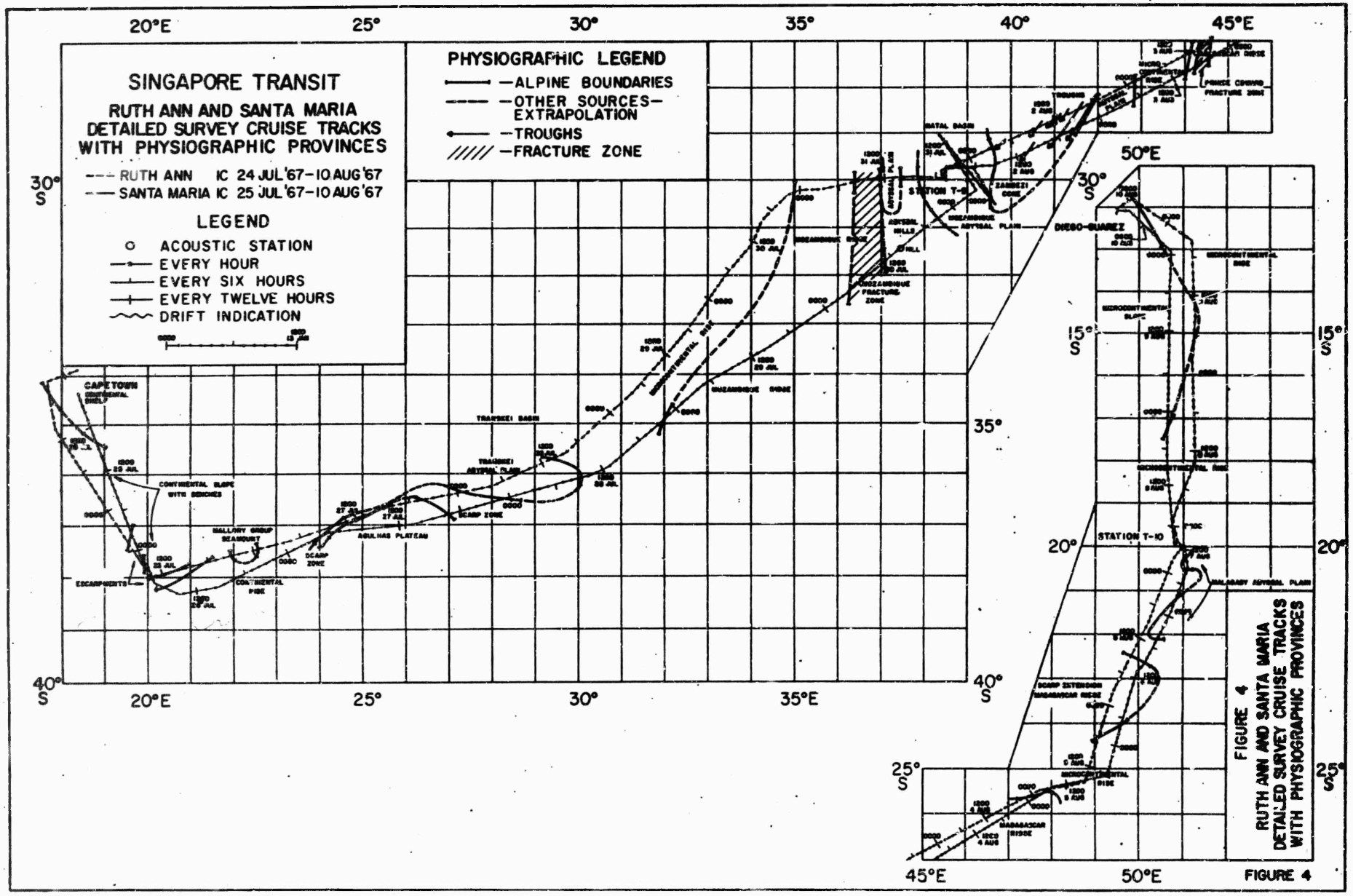
SINGAPORE TRANSIT
RUTH ANN AND SANTA MARIA
DETAILED SURVEY CRUISE TRACKS
WITH PHYSIOGRAPHIC PROVINCES
--- RUTH ANN IC 24 JUL '67 – 10 AUG '67
—— SANTA MARIA IC 25 JUL '67 – 10 AUG '67
LEGEND
ACOUSTIC STATION
EVERY HOUR
EVERY SIX HOURS
EVERY TWELVE HOURS
DRIFT INDICATION
PHYSIOGRAPHIC LEGEND
—ALPINE BOUNDARIES
— —OTHER SOURCES— EXTRAPOLATION
—TROUGHS
////—FRACTURE ZONE
20°E
25°
30°
35°
40°
45°E
50°E
30° S
40° S
15° S
20° S
25° S
35°
CAPE TOWN
CONTINENTAL SLOPE WITH SEACHES
ESCARPMENTS
MALLORY GROUP SEAMOUNT
CONTINENTAL RISE
SCARP ZONE
AGULHAS PLATEAU
TRANSKEI BASIN
TRANSKEI ABYSSAL PLAIN
MOZAMBIQUE RIDGE
MOZAMBIQUE FRACTURE ZONE
ABYSSAL HILLS
NATAL BASIN
ZAMBEZI CONE
MOZAMBIQUE ABYSSAL PLAIN
STATION T-9
DIEGO-SUAREZ
MICROCONTINENTAL RISE
MICROCONTINENTAL SLOPE
STATION T-10
SCARP EXTENSION MADAGASCAR RIDGE
MADAGASCAR RIDGE
MADAGASCAR ABYSSAL PLAIN
PRINCE EDWARD FRACTURE ZONE
FIGURE 4
RUTH ANN AND SANTA MARIA
DETAILED SURVEY CRUISE TRACKS
WITH PHYSIOGRAPHIC PROVINCES

FIGURE 4

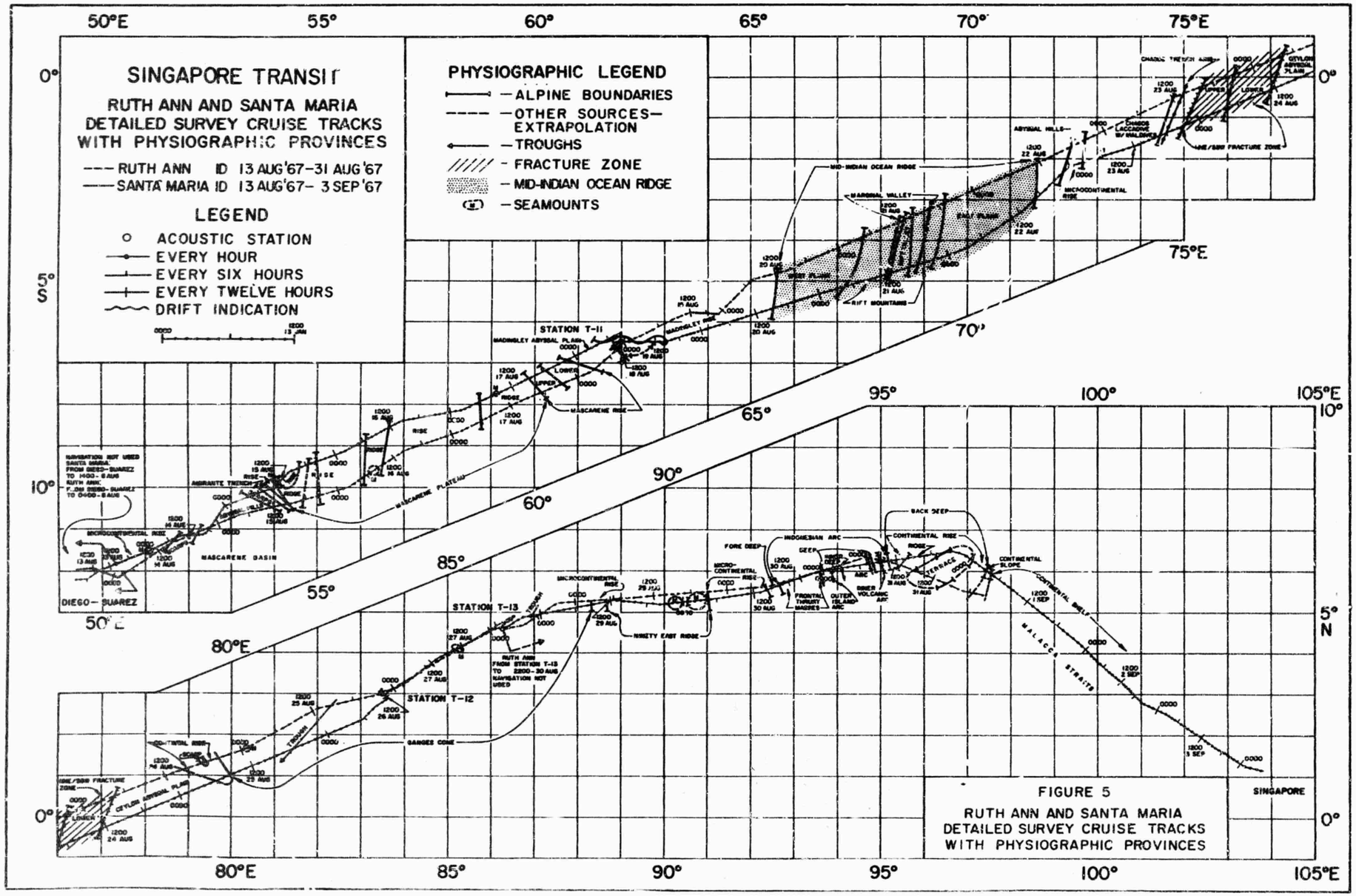
SINGAPORE TRANSIT
RUTH ANN AND SANTA MARIA
DETAILED SURVEY CRUISE TRACKS
WITH PHYSIOGRAPHIC PROVINCES
--- RUTH ANN ID 13 AUG'67-31 AUG'67
—— SANTA MARIA ID 13 AUG'67- 3 SEP'67
LEGEND
ACOUSTIC STATION
EVERY HOUR
EVERY SIX HOURS
EVERY TWELVE HOURS
DRIFT INDICATION
PHYSIOGRAPHIC LEGEND
—ALPINE BOUNDARIES
—OTHER SOURCES— EXTRAPOLATION
—TROUGHS
- FRACTURE ZONE
—MID-INDIAN OCEAN RIDGE
—SEAMOUNTS
50°E
55°
60°
65°
70°
75°E
80°E
85°
90°
95°
100°
105°E
0°
5° S
10°
5° N
STATION T-11
STATION T-12
STATION T-13
MID-INDIAN OCEAN RIDGE
MARGINAL VALLEY
RIFT MOUNTAINS
ABYSSAL HILLS
MICROCONTINENTAL RIDGE
MADINGLEY RISE
MASCARENE PLATEAU
MASCARENE BASIN
AMIRANTE TRENCH
DIEGO-SUAREZ
GANGES CONE
NINETY EAST RIDGE
FORE DEEP
INDONESIAN ARC
BACK DEEP
CONTINENTAL RISE
CONTINENTAL SLOPE
CONTINENTAL SHELF
MALACCA STRAITS
SINGAPORE
FIGURE 5
RUTH ANN AND SANTA MARIA
DETAILED SURVEY CRUISE TRACKS
WITH PHYSIOGRAPHIC PROVINCES

FIGURE 5

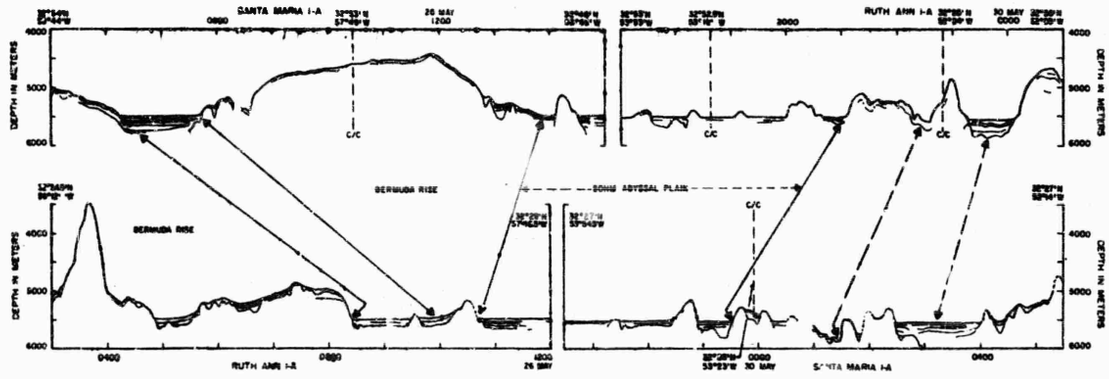

FIG.6 BATHYMETRIC PROFILES – SOHM ABYSSAL PLAIN

FIGURE 6

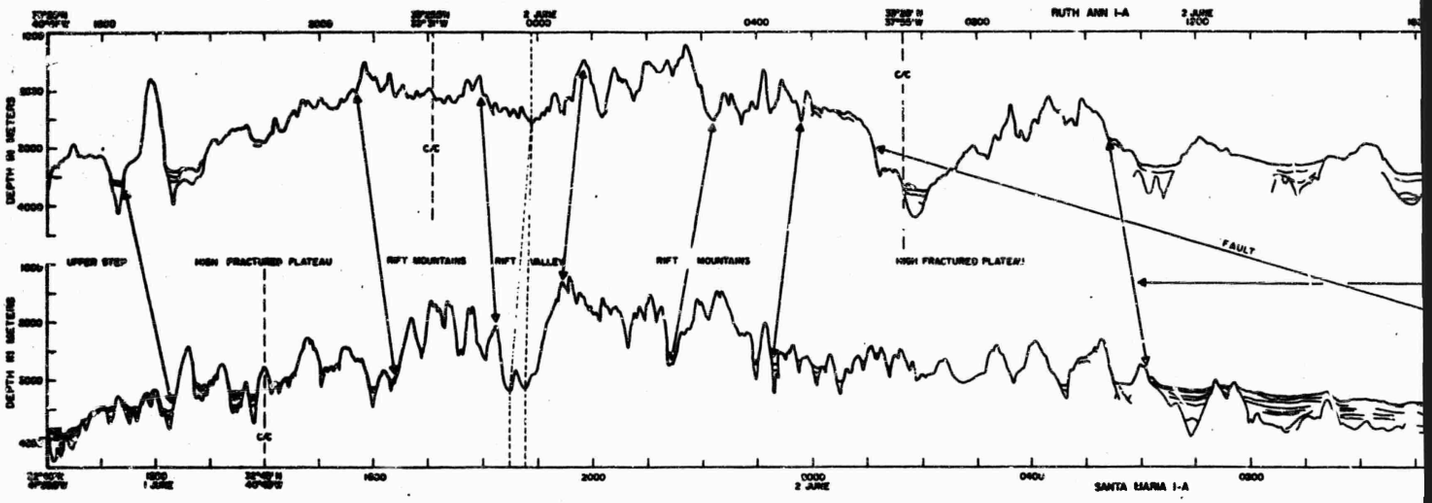

FIG.7 BATHYMETRIC PROFILES — MID-ATLANTIC RIDGE

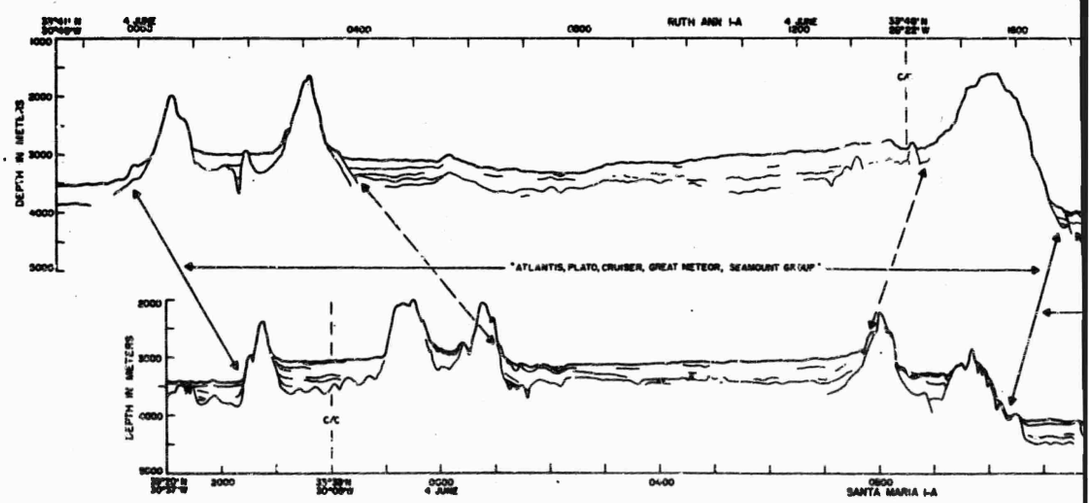

FIG. 8 BATHYMETRIC PROFILES — ATLANTIS, PLATO, CRUISER, GREAT METEOR, SEAMOUNT GRO

A

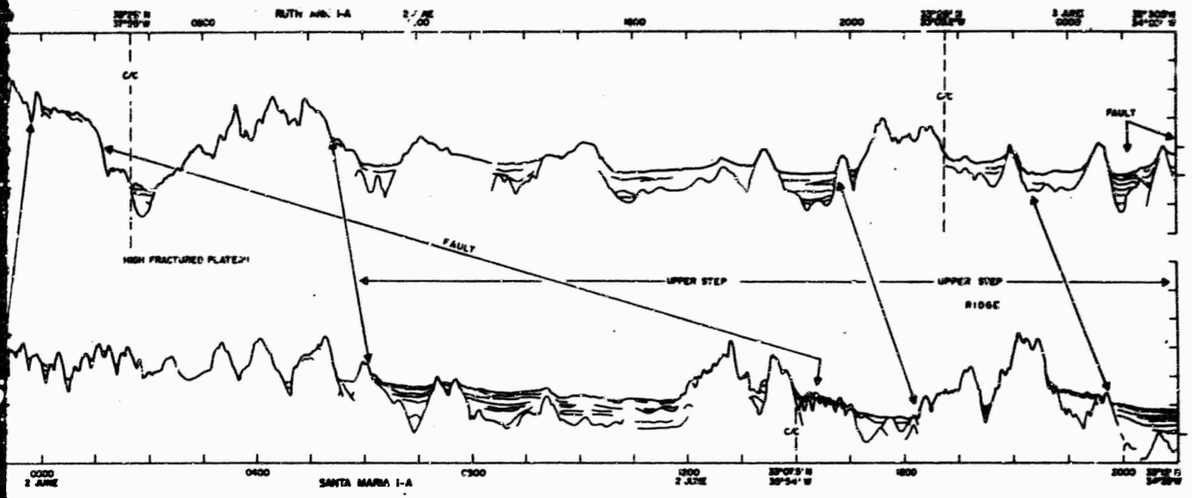

FIG.7 BATHYMETRIC PROFILES — MID-ATLANTIC RIDGE

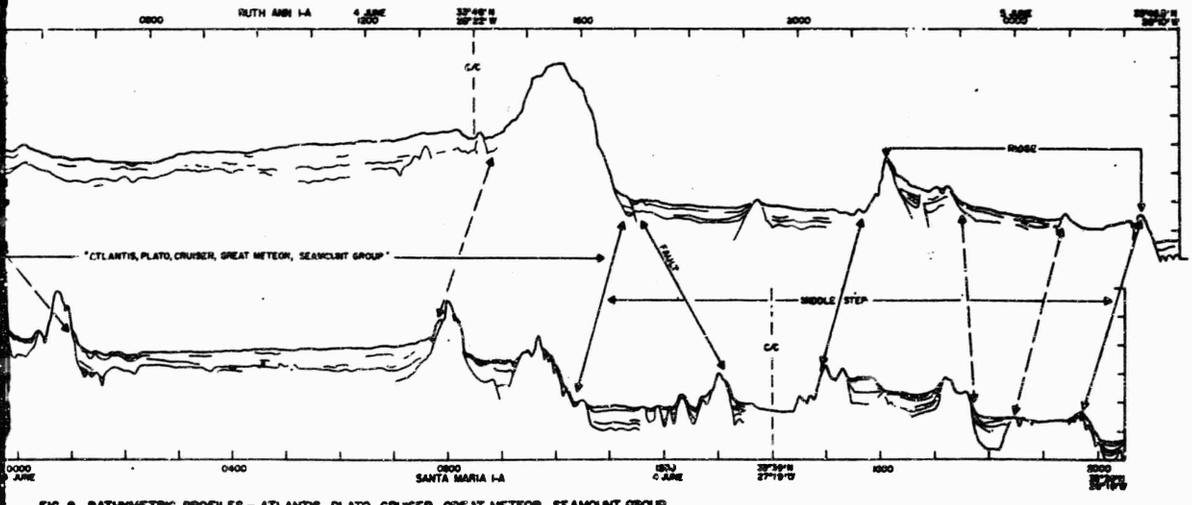

FIG. 8 BATHYMETRIC PROFILES — ATLANTIS, PLATO, CRUISER, GREAT METEOR, SEAMOUNT GROUP

B

FIGURE 7
FIGURE 8

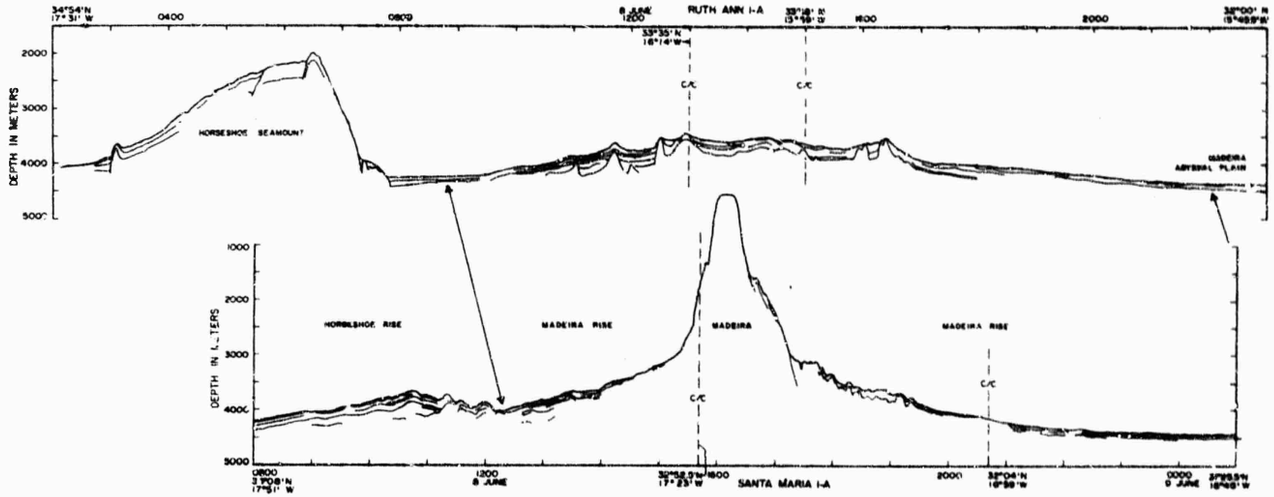

FIG. 9 BATHYMETRIC PROFILES – HORSESHOE SEAMOUNT AND MADEIRA

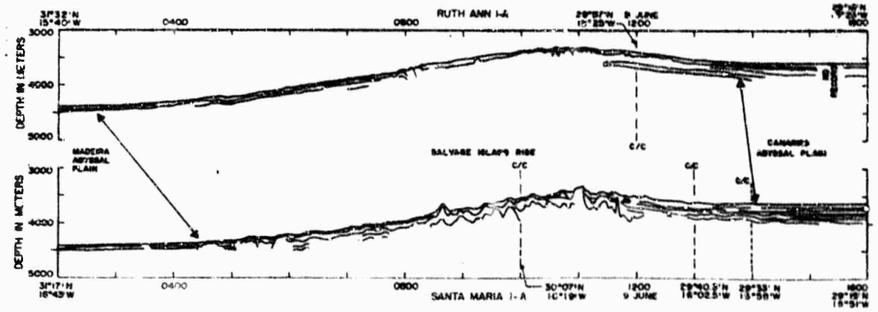

FIG. 10 BATHYMETRIC PROFILES – SALVAGE ISLAND RISE

FIGURE 9
FIGURE 10

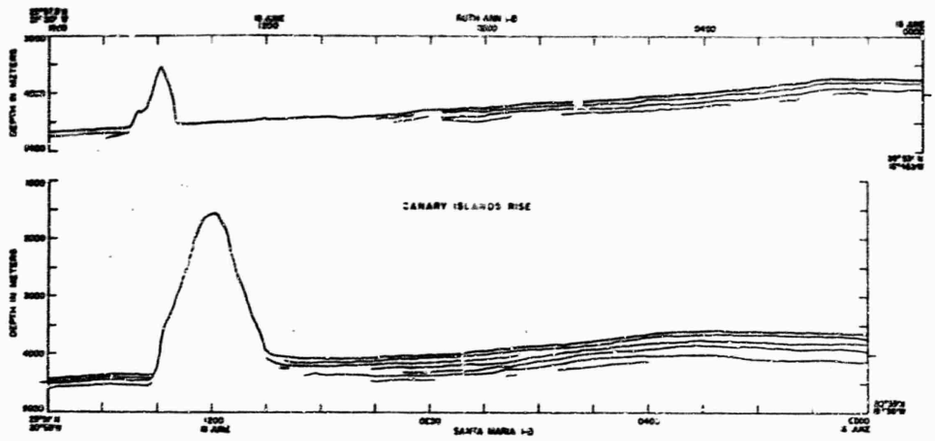

FIG. 11 BATHYMETRIC PROFILES – CANARY ISLAND RISE W/MOUNTS

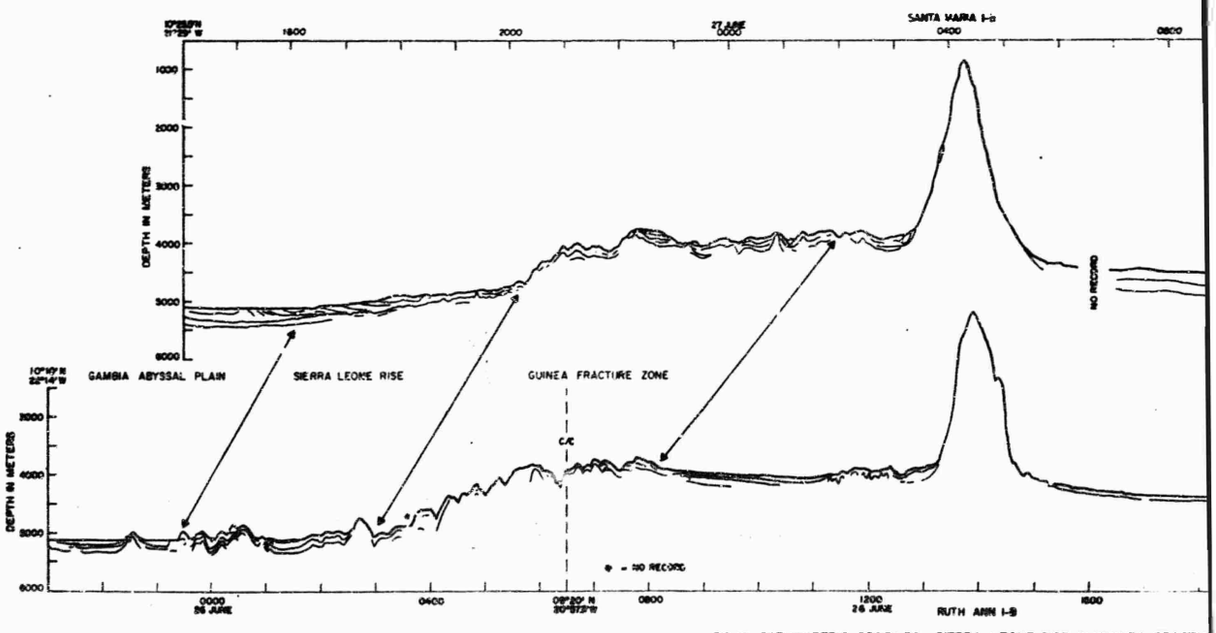

FIG. 13 BATHYMETRIC PROFILES – SIERRA LEONE RISE W/GUINEA FRACTU

A

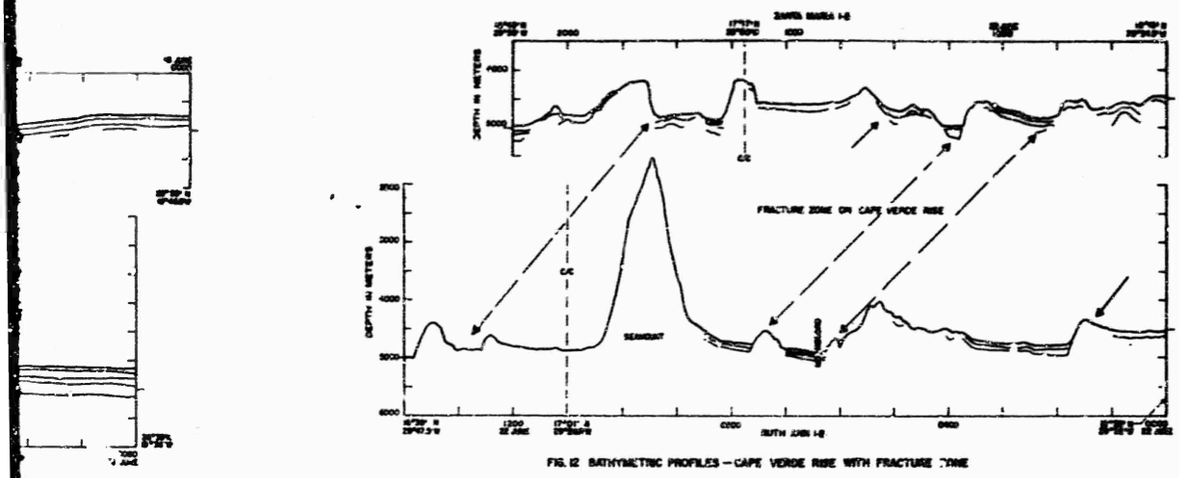

FIG. 12 BATHYMETRIC PROFILES – CAPE VERDE RISE WITH FRACTURE ZONE

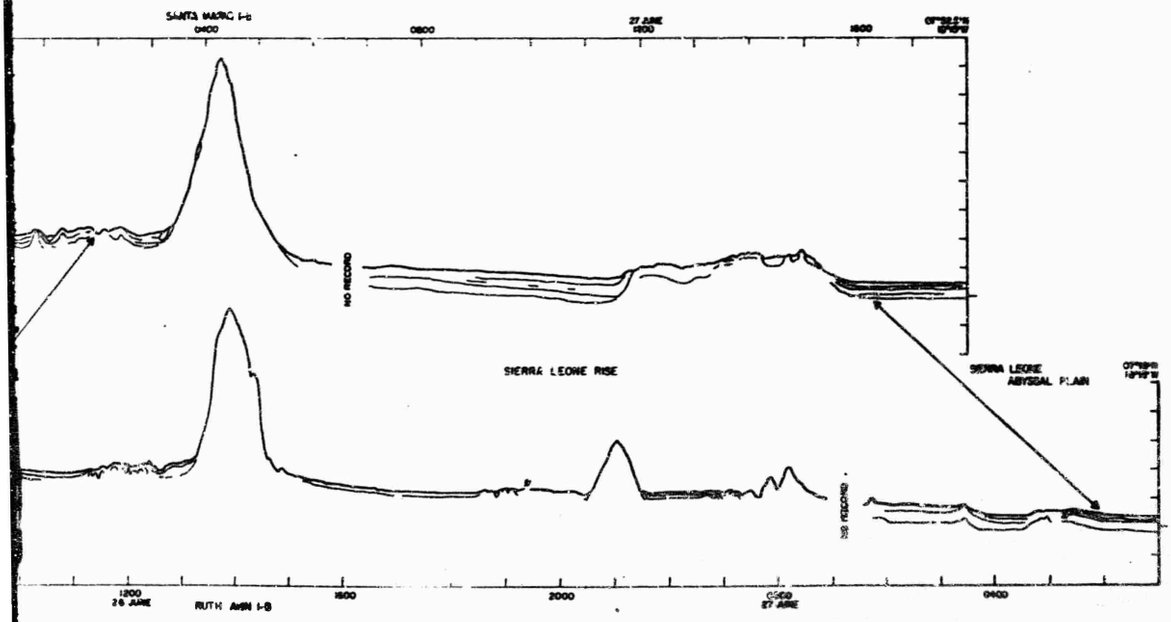

BATHYMETRIC PROFI 3 – SIERRA LEONE RISE W/GUINEA FRACTURE ZONE

B

FIGURE 11
FIGURE 12
FIGURE 13

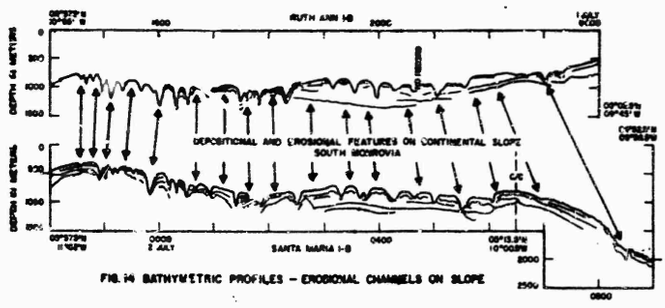

FIG. 14 BATHYMETRIC PROFILES – EROSIONAL CHANNELS ON SLOPE

FIGURE 14

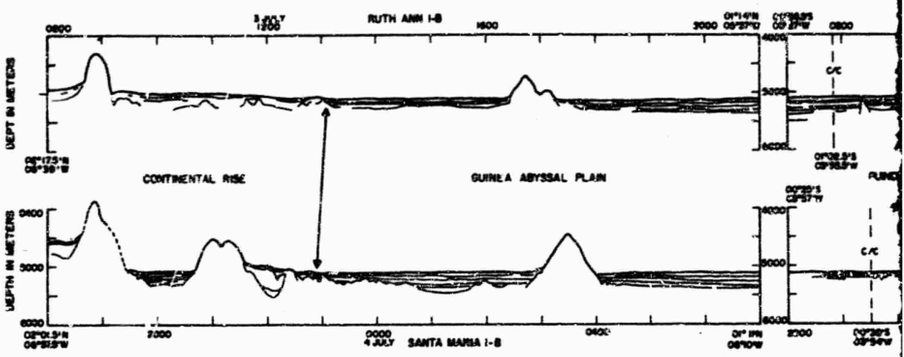

FIG. 15 BATHYMETRIC PROFILES—GUINEA ABYS

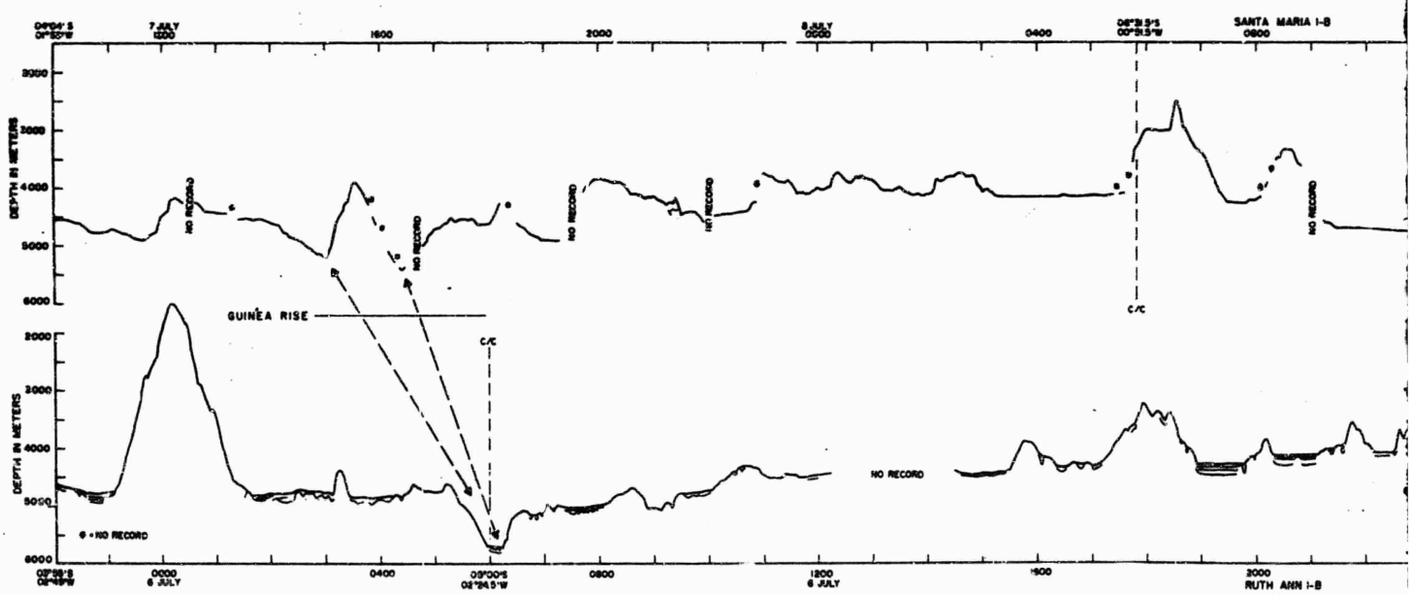

FIG. 16 BATHYMETRIC PROFILES—GUINEA RISE

A

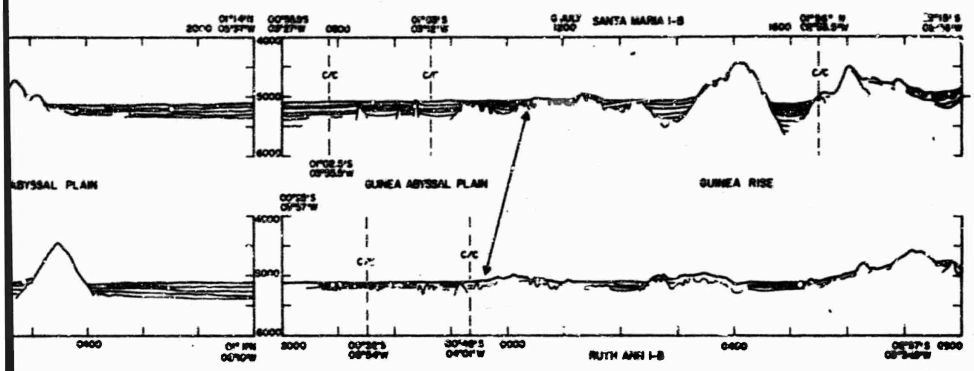

FIG. 15 BATHYMETRIC PROFILES—GUINEA ABYSSAL PLAIN

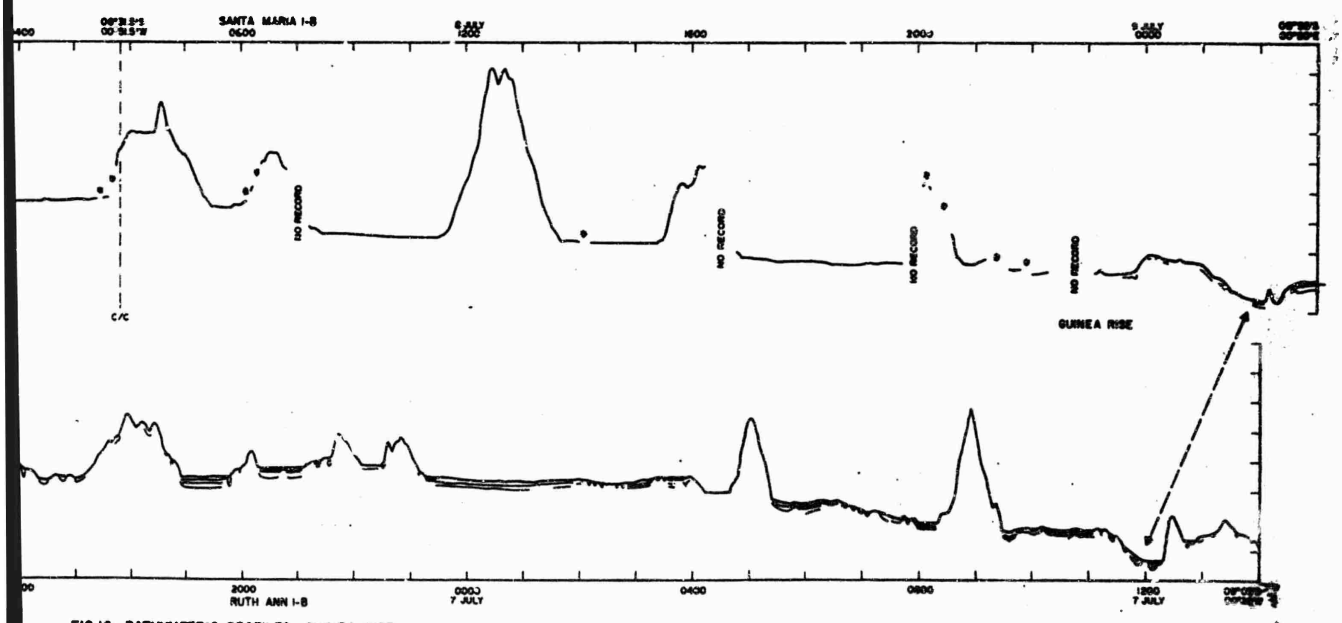

FIG. 16 BATHYMETRIC PROFILES—GUINEA RISE

B

FIGURE 15

FIGURE 16

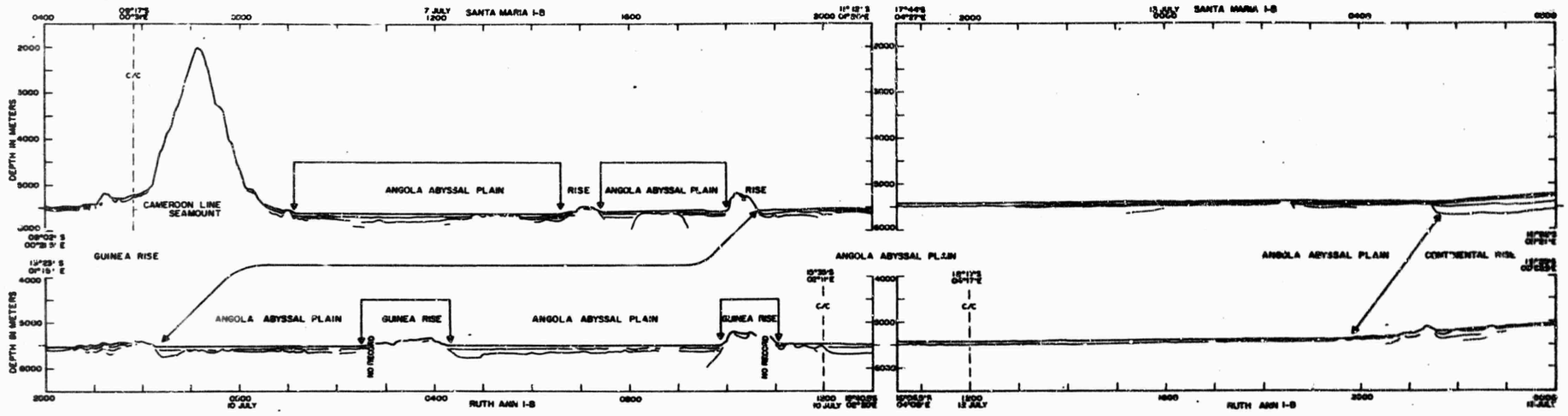

FIG. 17 BATHYMETRIC PROFILES—ANGOLA ABYSSAL PLAIN

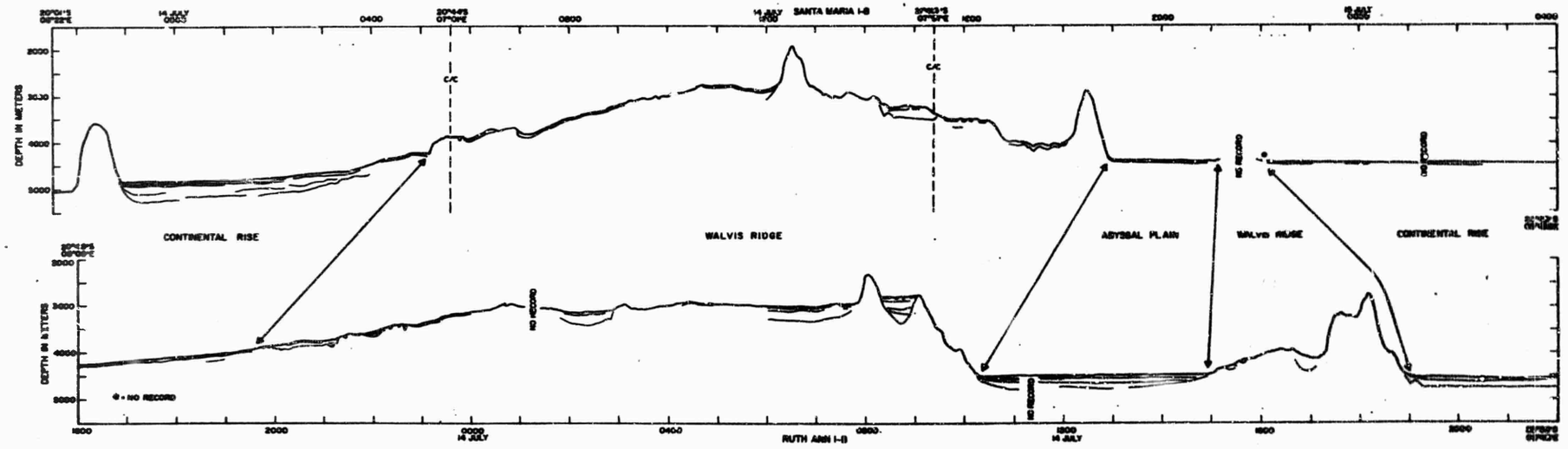

FIG. 18 BATHYMETRIC PROFILES—WALVIS RIDGE

A

FIGURE 17
FIGURE 18

FIG. 19 BATHYMETRIC PROFILES — ORANGE RIVER CANYON

FIG. 20 BATHYMETRIC PROFILES — OLIFANTS RIVER CANYON

FIG. 21 BATHYMETRIC PROFILES - MARGINAL ESCARPMENT ON CONTINENTAL SLOPE

FIG. 22 BATHYMETRIC PROFILES SEABEAM 1 FROM MALLORY GROUP

FIGURE 19

FIGURE 20

FIGURE 21

FIGURE 22

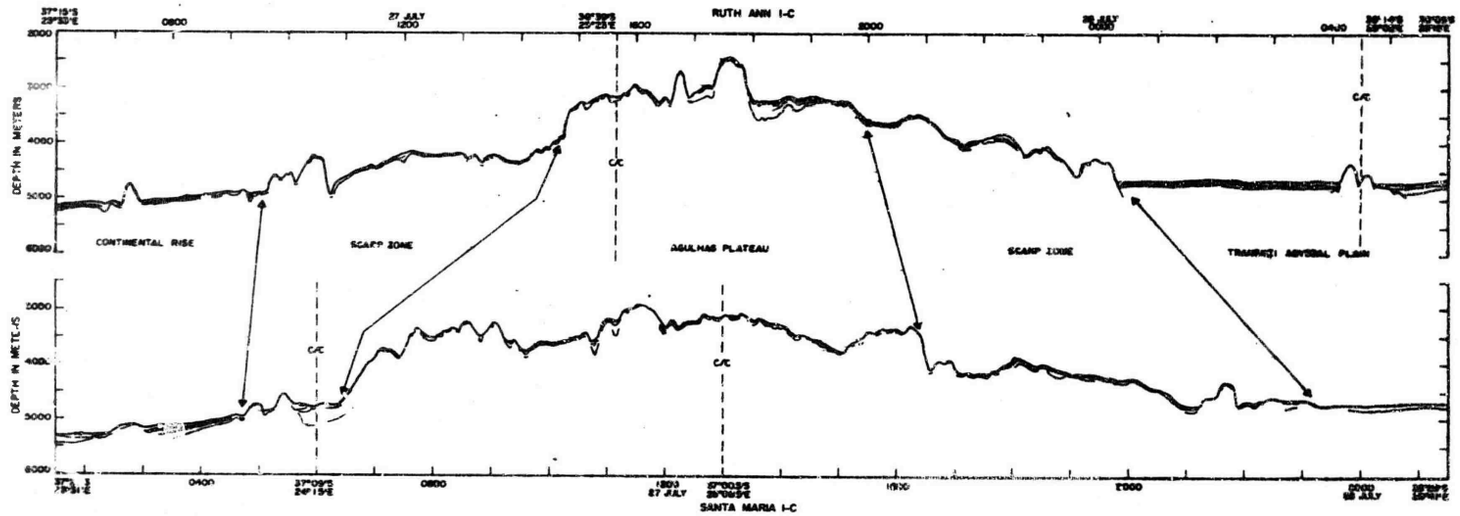

FIG. 23 BATHYMETRIC PROFILES—AGULHAS PLATEAU WITH BORDERING SCARP ZONES

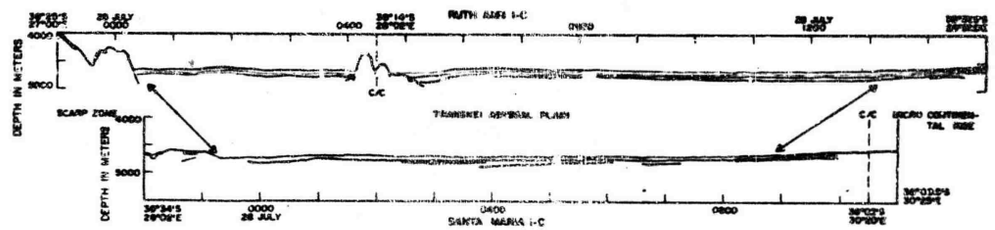

FIG. 24 BATHYMETRIC PROFILES—TRANSKEI ABYSSAL PLAIN

FIGURE 23
FIGURE 24

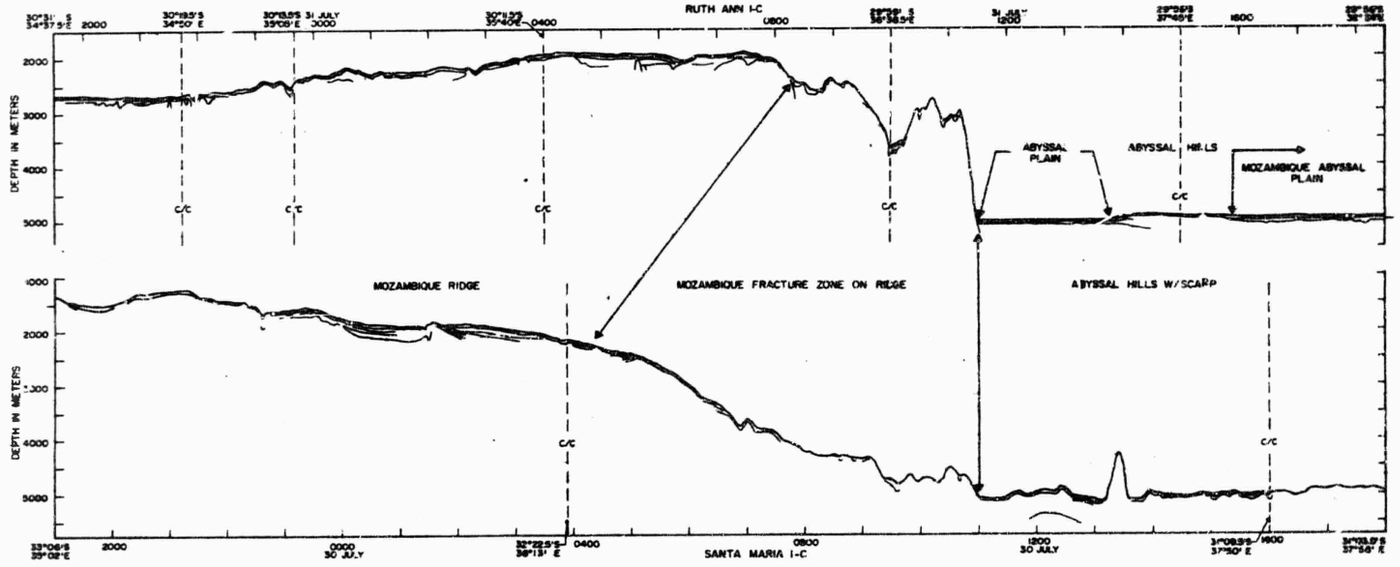

FIG. 25 BATHYMETRIC PROFILES-MOZAMBIQUE RIDGE W/FRACTURE ZONE

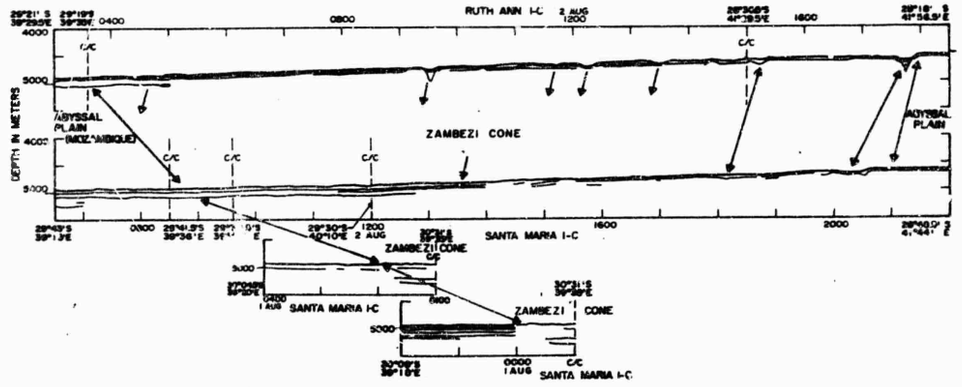

FIG. 26 BATHYMETRIC PROFILES—ZAMBEZI CONE W/ TROUGHS

FIGURE 25
FIGURE 26

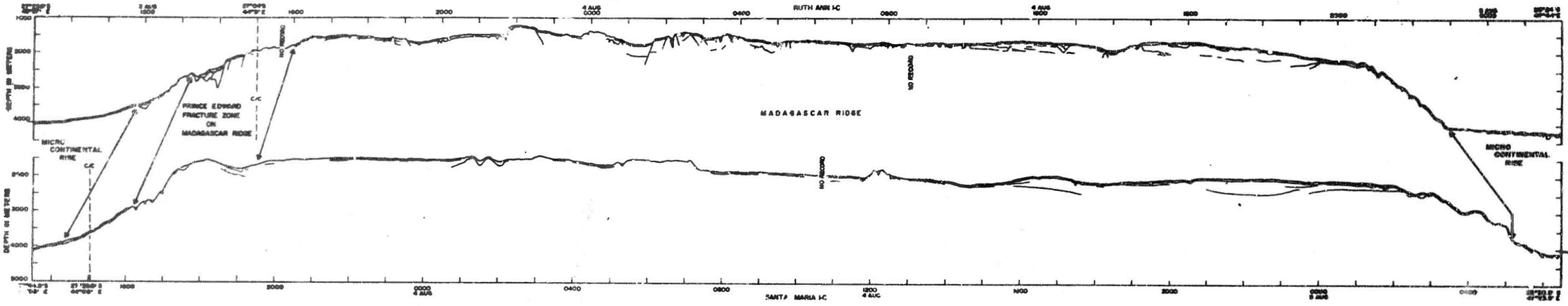

FIG. 27 BATHYMETRIC PROFILES — MADAGASCAR RIDGE W/FRACTURE ZONE

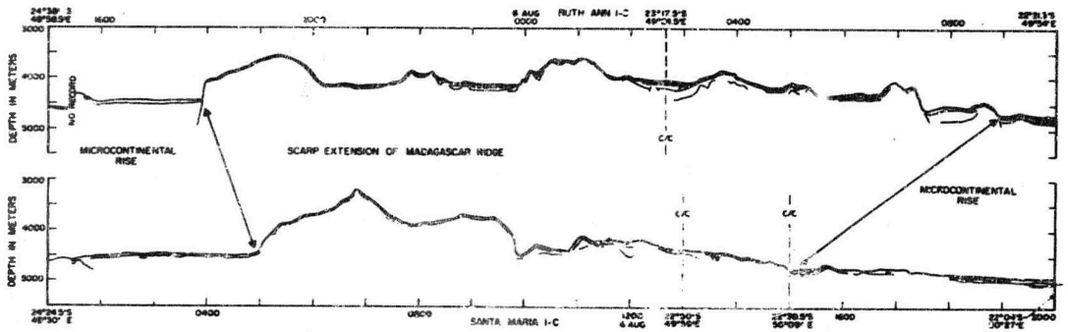

FIG. 28 BATHYMETRIC PROFILES — SCARP EXTENSION OF MADAGASCAR RIDGE

FIGURE 27

FIGURE 28

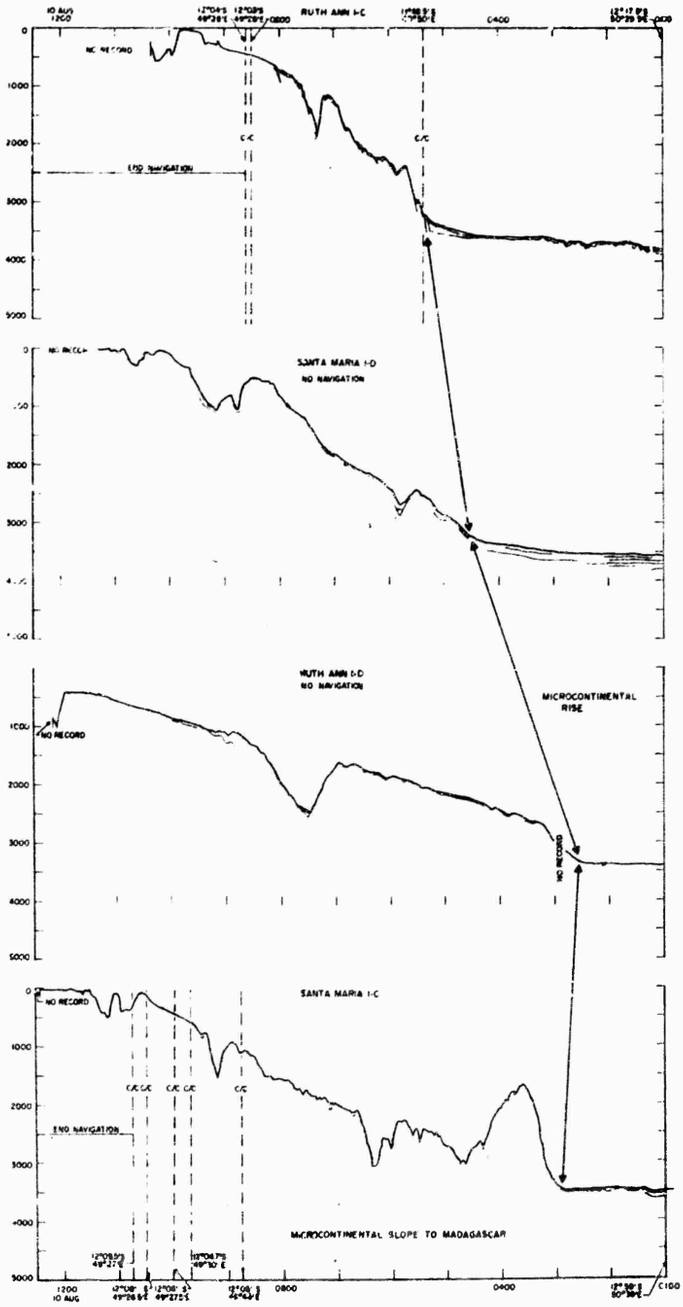

FIG 29 BATHYMETRIC PROFILES – MICROCONTINENTAL SLOPE WITH CANYONS

FIGURE 29

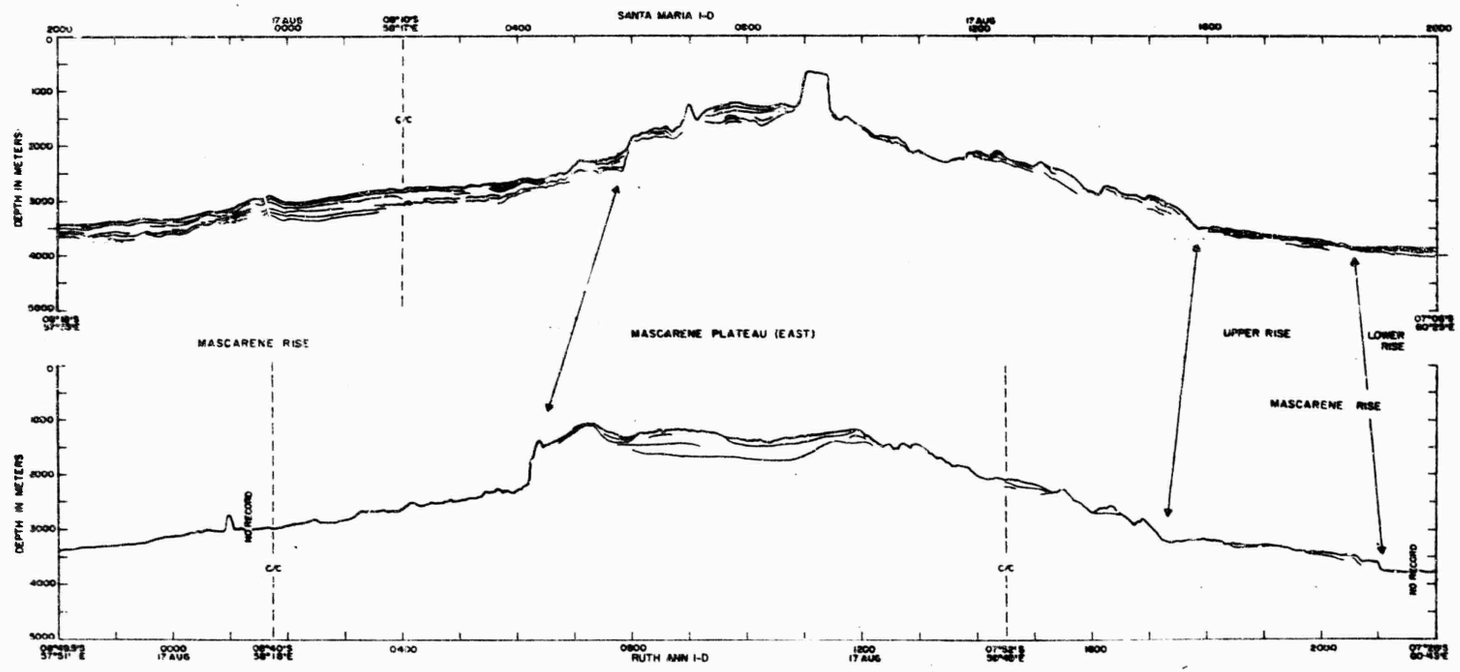

FIG. 30 BATHYMETRIC PROFILES – MASCARENE PLATEAU

FIGURE 30

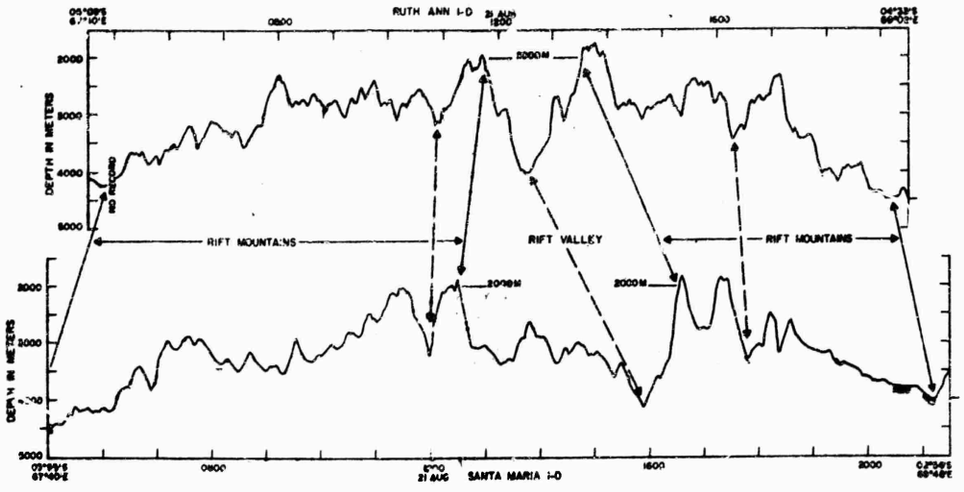

FIG. 31 BATHYMETRIC PROFILES – MID-INDIAN OCEAN RIDGE

FIGURE 31

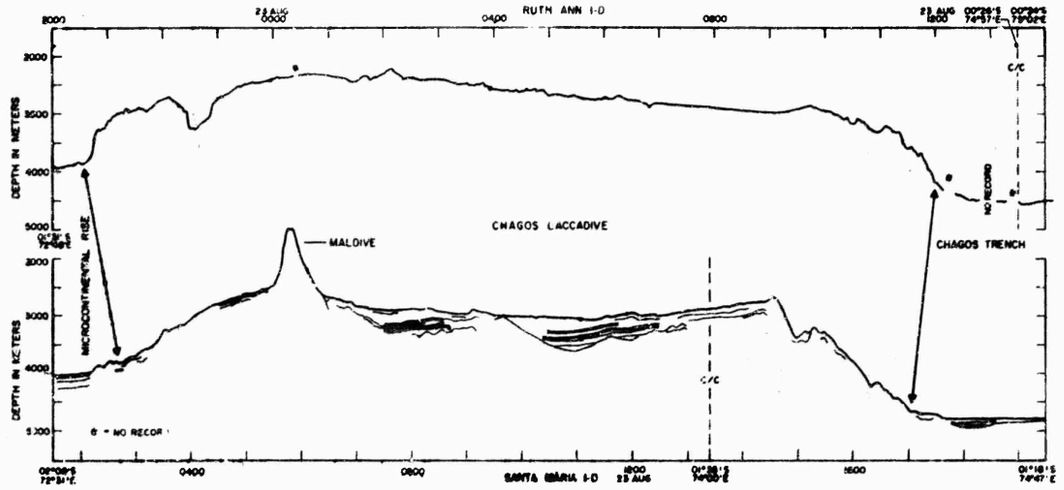

FIG. 32 BATHYMETRIC PROFILES–CHAGOS LACCADIVE WITH MALDIVE

FIGURE 32

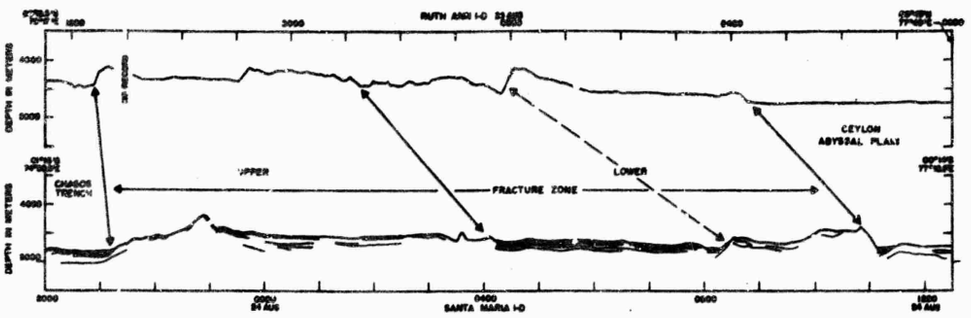

FIG. 33 BATHYMETRIC PROFILES — NNE by ESE FRACTURE ZONE

FIGURE 33

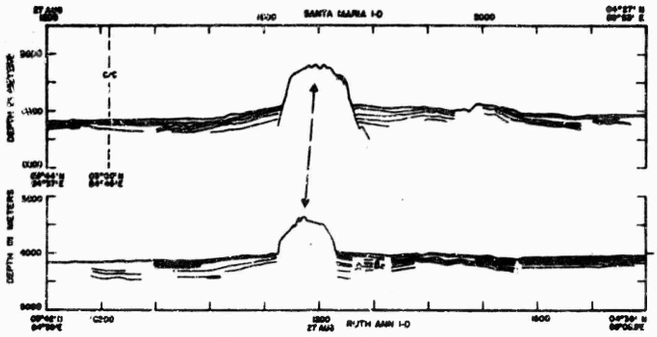

FIG. 34 BATHYMETRIC PROFILES—GANGES CONE WITH SEAMOUNT

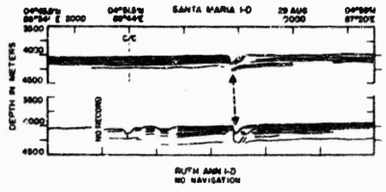

FIG. 35 BATHYMETRIC PROFILES—GANGES CONE WITH TROUGHS

FIGURE 34

FIGURE 35

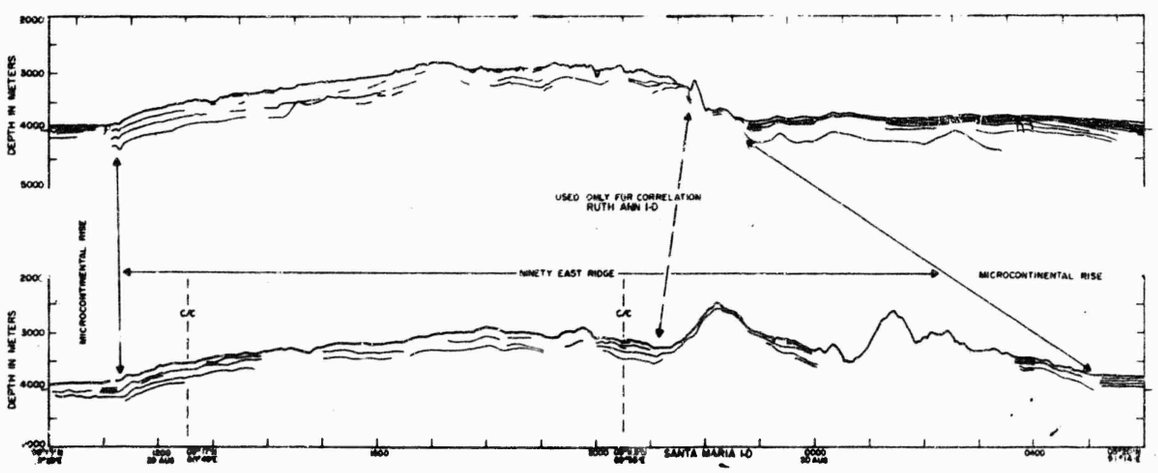

FIG. 36 BATHYMETRIC PROFILES—"NINETY EAST" RIDGE

FIGURE 36

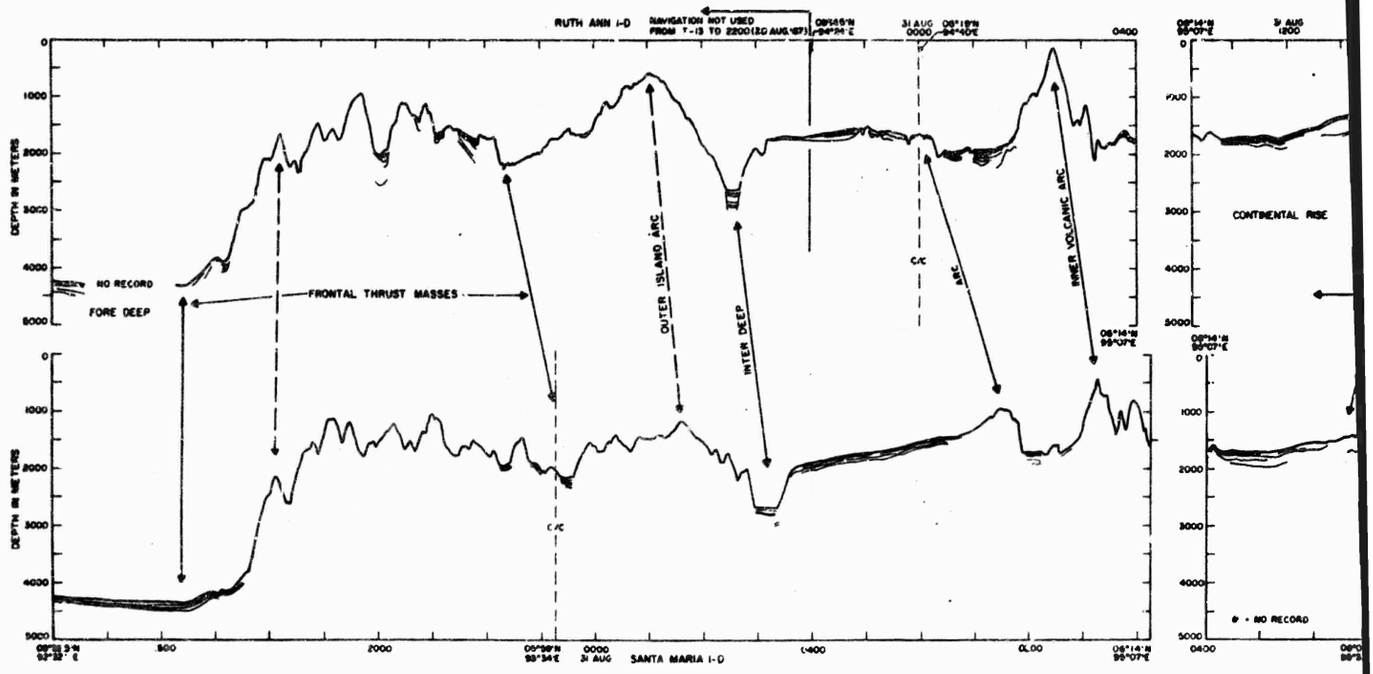

FIG. 37 BATHYMETRIC PROFILES — INDONESIAN ARC

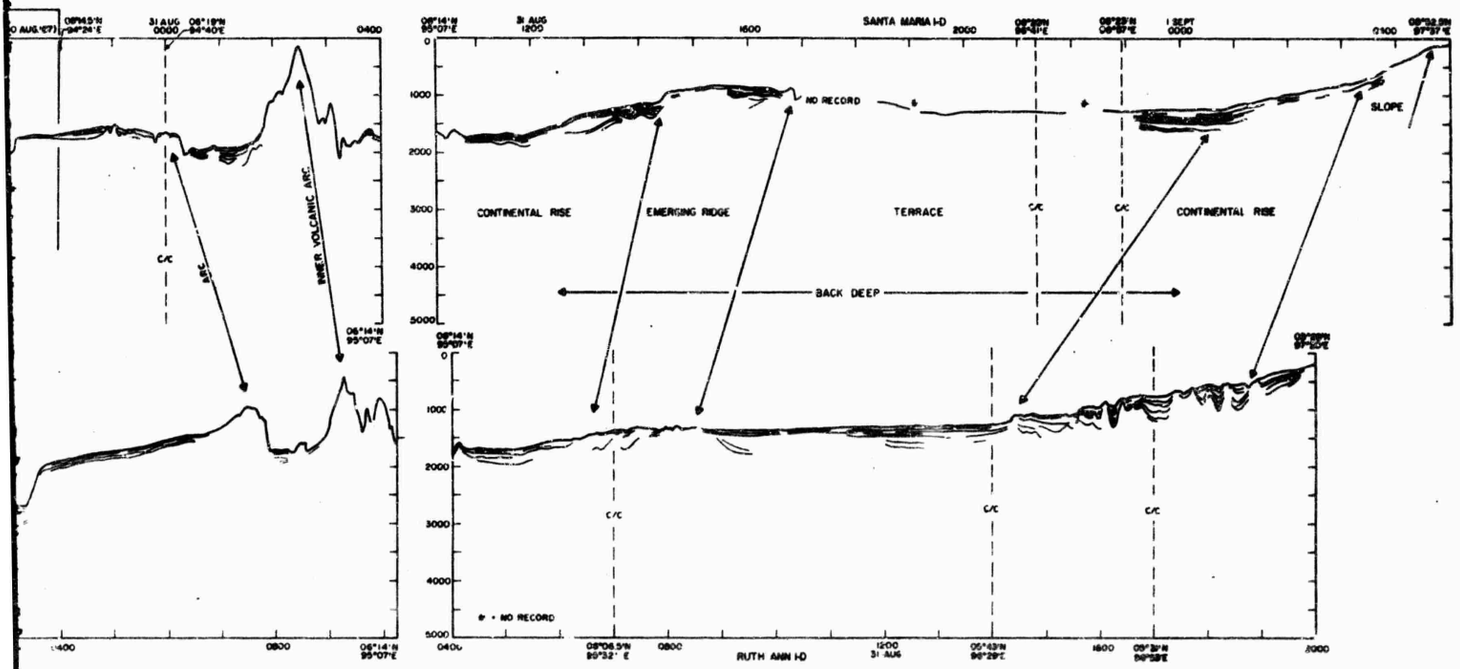

FIG. 37 BATHYMETRIC PROFILES — INDONESIAN ARC

FIGURE 37

PART II

AREA ST VOLUME 2

MAGNETICS

by

D. L. Halpin

VOLUME 2, PART II

TABLE OF CONTENTS

Section | Page

LIST OF FIGURES

Fig. 12 - Bathymetric and magnetic profiles of a seamount in the Mallory Seamount Group

Fig. 13 - Bathymetric and magnetic profiles across a portion of the Agulhas Plateau

Fig. 14 - Bathymetric and magnetic profiles across the Prince Edward Fracture Zone

Fig. 15 - Bathymetric and magnetic profiles across a portion of the Madagascar Ridge Extension

Fig. 16 - Bathymetric and magnetic profiles across the slope and rise east of Diego Suarez

Fig. 17 - Bathymetric and magnetic profiles across a portion of the Mascarene Plateau and Ridge system

Fig. 18 - Bathymetric and magnetic profiles across the Mid-Indian Ocean (Carlsberg) Ridge

Fig. 19 - Bathymetric and magnetic profiles across the Chagos Laccadive Plateau

Fig. 20 - Bathymetric and magnetic profiles across the Ninety East Ridge

SECTION I

ABSTRACT

Marine magnetic surveys in Area ST Cruise 1A permit the extension and greater delineation of the magnetic province boundaries established in Area I (Vajk, 1966a), Area II (Vajk, 1966b), Area SF (Vajk, 1967a) and Area HH (Vajk, 1967b). Cruises 1B - 1D add more data to the growing knowledge of the magnetic field over the oceans. Magnetic provinces and residual anomalies as related to physiographic provinces, (Part I, this volume, Henry, 1968) are discussed.

SECTION II

INTRODUCTION

Total magnetic intensity measurements were made in Area ST from May, 1967 to September, 1967 on the R/V Santa Maria and R/V Ruth Ann. The magnetometer on the R/V Santa Maria was inoperative on Cruises 1C and 1D. Total magnetic intensity data were reduced in the same manner as described in Volume 6, Area I (Vajk, 1966a).

Physiographic provinces mentioned are in accord with those established and illustrated on charts in Part I of this volume (Henry, 1968).

Five maps and five charts are included as well as eighteen profiles showing bathymetry and magnetic anomalies. Figures 1A - 1D are maps of regional magnetic intensity, cruise tracks, and figure locations. Figures 2A - 2D are charts of the magnetic and physiographic provinces.

SECTION III

REGIONAL MAGNETIC FIELD

The regional magnetic field (total magnetic intensity), shown in Figures 1A - 1D, was graphically constructed from the observed magnetic intensity values using Cain's main geomagnetic field for reference (Cain, et. al., 1965). Differences between Cain's main geomagnetic field and the observed magnetic field are variable. For a further discussion of this procedure, refer to Volume 6, Area I (Vajk, 1966a).

The magnetic field observed on the trans-Atlantic cruise is in accord with the magnetic fields established in Areas I, II, SF and HH when all are reduced to the same epoch (Vajk, 1966a, 1966b, 1967a, 1967b).

SECTION IV

RESIDUAL MAGNETIC ANOMALIES AND MAGNETIC PROVINCES

A INTRODUCTION

Residual magnetic anomalies have been reduced from 12-minute readings of total magnetic intensity observed on the R/V Santa Maria and R/V Ruth Ann. These anomalies were used to construct magnetic province charts. Procedures for computation of anomalies and construction of province charts are described in Volume 6 of Area I (Vajk, 1966a) and Volume 2, Part 2 of Area HH (Vajk, 1967b).

Area ST is divided into magnetic provinces (categories) on the basis of amplitude variation of residual anomalies. To describe the variation it is necessary to separate short-wave length variations of magnetic intensity from long-wave length variations. This was accomplished by constructing an average curve, having wave lengths of 120 km or more, on the continuous residual anomaly profile (Vajk, 1967b). Amplitude variations of the short-wave length anomalies are measured from this average curve. The short wave length anomalies are then divided into three categories:

Category	Amplitude variation (gammas)
1	0-100
2	100-500
3	over 500

Areas which fall into the same category are outlined and shown in Figures 2A - 2D.

Magnetic provinces established along the 1A cruise tracks are connected, by dashed lines, with those determined in other Alpine survey areas. This permits extension and further delineation of

previously established magnetic provinces. Magnetic provinces established on cruises 1B - 1D add to the growing knowledge about the magnetic field over the oceans. Discussion of anomalies constituting the magnetic provinces, in relation to physiographic provinces and structural features, is restricted to the local area traversed by the ship and should not be taken as being characteristic of the entire province or structure.

B. CRUISE 1A - TRANS-ATLANTIC

1. Rises

Cruise 1A crossed portions of the Horseshoe Rise, Madeira Rise, lower and upper continental rise north of the Canary Islands. Anomalies related to the Horseshoe Rise increase from a 0-100 gamma variation on the northwest to 100-200 gamma variation on the southeast. Residual anomalies over the Madeira Rise range from 100 to 500 gammas. A magnetic maximum with an intensity of +300 gammas at latitude 33°45'N, longitude 17°40'W may be related to high amplitude anomalies associated with the Horseshoe Seamounts northeast of this area. Anomalies over the continental rises north of the Canary Islands are generally less than 100 gammas in amplitude.

2. Abyssal Hills

Anomalies related to abyssal hills, east and west of the Mid-Atlantic Ridge are variable. The intensities of the magnetic anomalies are in general greater east of the ridge than west of it. East of the ridge values range from less than 100 gammas to greater than 500 gammas. The maximum anomaly value of +510 gammas is located at latitude 33°45'N, longitude 24°45'W. Anomalies over the abyssal hills west of the ridge range from less than 100 gammas to 400 gammas.

3. Abyssal Plains

Two abyssal plains, Sohm and Madeira, are traversed. Residual anomalies are generally small in amplitude but values up to 200 gammas are observed. Higher amplitude anomalies over the Sohm Abyssal Plain are generally found in areas where abyssal hills occur. This is similar to an area of the Sohm further north, in Area I, as reported by Vajk (1966a). Vajk attributed the higher amplitudes to a relatively thin sedimentary section and high relief of buried basement.

4. Mid-Atlantic Ridge

Anomalies over the Mid-Atlantic Ridge are extremely variable. West of the rift valley, smoothed residual anomalies vary between 100 and 500 gammas over the lower step, middle step, rift mountains, western extreme of the rift valley, and western one-fourth of the upper step. The eastern three-fourths of the upper step, west of the rift valley, is characterized by anomalies with amplitudes less than 100 gammas. Residual anomalies related to the rift valley reach a peak positive intensity of +570 gammas (Figures 3 and 4). East of the rift valley the anomaly pattern is somewhat different due to two factors: faults which offset the ridge, and the Atlantis Plato Cruiser Great Meteor Seamount Group which cuts across the middle and upper steps. Where faulting occurs, smoothed residual anomalies are generally less than 100 gammas in amplitude, even over the rift valley. East of the faulted area residual anomalies range from 100 to 500 gammas. The profiles included here are in good agreement with that of the Vema 17 cruise (Heirtzler and LePichon, 1965). The profiles show some symmetry about the rift valley but with only a few tracks no conclusive statement can be made. A few generalizations can be made which characterize these profiles: (1) the major positive residual anomaly is situated east of the axis of the rift

valley, (2) the major negative residual anomaly is situated west of the axis of the rift valley and (3) anomalies east of the rift valley generally have greater peak to peak intensities than those to the west.

5. Bermuda Rise

Residual anomalies range in amplitude from less than 100 gammas to over 500 gammas. Areas containing amplitude variations less than 100 gammas are located near the Bermuda Pedestal and near the eastern edge of the rise. Residual amplitude variations greater than 500 gammas are found in two locations. An 1850 meter high "typical" seamount, (Vajk, 1966a) at latitude 33°25'N, longitude 62°20'W has a peak to peak intensity of 1060 gammas (Figure 5). This appears to be the southern extension of Muir Seamount.

The high amplitude anomaly at latitide 32°35'N, longitude 60°00'W consists of two separate maxima, one coinciding in position with an 850 meter high hill and the other having no direct topographic correlation. A seamount at latitude 32°30'N, longitude 59°10'W has no associated large maxima, but since this is an east-west crossing it is impossible to state whether the seamount is typical or atypical. The eastern edge of the Bermuda Rise appears faulted and there is an associated 150 gamma drop in magnetic intensity.

6. The Horseshoe Seamount

One seamount of the Horseshoe Seamount Group is crossed. Residual anomalies associated with the seamount are of high amplitude (Figure 6). Maximum positive intensity is +725 gammas. Four distinct anomalies are present and are probably due to faults and/or intrusions.

7. Madeira Plateau

Anomalies over the Madeira Plateau are of high amplitude.

Maximum positive intensity is +800 gammas.

C. CRUISE 1B - EASTERN ATLANTIC

1. Continental Slope

The Continental slope, off the west coast of Africa, was crossed in three places; west and south of Monrovia and northwest of Capetown. Anomaly amplitudes over the slope off Monrovia are very small, similar to those off Portugal (Vajk, 1967a; Heirtzler and Hayes, 1967). The slope northwest of Capetown has anomalies of various amplitudes, increasing east and south.

2. Continental Rise

Anomalies over the continental rises are generally less than 100 gammas in amplitude, especially west and south of Monrovia. Higher amplitude anomalies are usually related to seamounts or are situated near larger structures such as Walvis Ridge. In a few areas, i.e., west of the Canary Islands, high amplitude anomalies southwest of the Cape Verde Plateau may represent continuations of the plateau structural elements beneath the rise.

3. Abyssal Hills

Abyssal hills generally have anomalies with amplitudes less than 200 gammas.

4. Abyssal Plains

Four abyssal plains have been crossed. These are the Gambia, Sierra Leone, Guinea and Angola Abyssal Plains. Anomalies over the abyssal plains are generally less than 100 gammas in amplitude. Variations from this low amplitude character are probably due to buried structures. On treverses from plain to rise, the profiles show increasing amplitudes

which may possibly be related to a less complete burial of pre-existing topography. Exceptions to the low amplitude character exist over the Sierra Leone Abyssal Plain in two areas: one at the northwestern boundary near the Sierra Leone Rise and the other at latitude 6°20'N, longitude 17°00'W. The latter appears to be a fault anomaly but topographic correlation is lacking (Figures 7A and 7B). This anomaly may be the reflection of a buried fault, similar to the Guinea Fracture Zone further north. Large amplitude anomalies over the Angola Abyssal Plain are situated in the southern portion (Figures 8A and 8B). The four anomalies have no direct topographic correlation associated with them but may be due to buried NE-SW trending ridge and valley structures which exist to the west and south (Heezen and Tharp, 1961). Maximum positive residual intensity in this area is +700 gammas and maximum negative residual intensity is -600 gammas.

5. Canary Islands Plateau

Anomalies over the Canary Islands Plateau and Slope have peak to peak intensities up to 350 gammas. The higher amplitude anomalies are associated with seamounts and island areas.

6. Rises and Ridges

Three major rises and ridges have been traversed which include: Sierra Leone Rise, Guinea Rise and Ridge, and Walvis Ridge. The Sierra Leone Rise, between the Gambia and Sierra Leone Abyssal Plains, has low amplitude anomalies in the northern third and higher amplitude anomalies in the southern two-thirds. Seamounts on the rise have anomalies up to ±425 gammas. The Guinea Fracture Zone cuts across the rise with anomalies having amplitudes of less than 200 gammas. Anomalies over the Guinea Rise are generally less than 100 gammas with the exception of local high amplitude anomalies associated with seamounts. The Guinea Ridge, occupying the central portion of the Guinea Rise, is a northeast-southwest trending

volcanic ridge (Fairbridge, 1966). Anomalies increase in amplitude from the flanks toward the central portion of the ridge. Seamounts and large hills on the ridge have individual anomalies with peak to peak intensities up to 750 gammas (Figure 9). Anomalies over Walvis Ridge have large amplitudes up to +630 gammas. The anomaly shown on Figure 10 is taken from the Ruth Ann traverse of the ridge which has an amplitude of 300 gammas. This northeast-southwest trending ridge is divided into two sections, each with a southeast-facing fault scarp. Anomalies are apparently in association with these scarps.

D. CRUISE 1C - SOUTHWEST INDIAN OCEAN

1. Continental Slope

The continental slope south of Capetown generally has low amplitude anomalies. Two exceptions to this exist at latitude 36°35'S, longitude 19°09'E and at latitude 37°50'S, longitude 19°55'E. The first of these appears to be a fault anomaly with a peak to peak intensity of 1275 gammas, although there is no correlative expression from bathymetric records (Figure 11). The second, situated at or near the base of the slope has a maximum positive intensity of 750 gammas.

2. Continental Rise

Anomalies over the continental rise southeast of Capetown are of low amplitude on the west but increase in amplitude, to approximately 350 gammas, near the flank of the Agulhas Plateau. This increase in amplitude is broken only by the presence of a high amplitude anomaly, associated with a seamount of the Mallory Seamount Group, at latitude 37°35'S, longitude 22°25'E (Figure 12). This anomaly is negative with a minimum intensity of approximately -250 gammas.

3. Abyssal Plains

Three abyssal plains were crossed and include the Transkei, Mozambique and Malagasy. Anomalies over the Transkei have amplitudes

less than 100 gammas with two exceptions: the southwestern portion where anomalies reach +450 gammas and in the northeastern portion where an apparent fault anomaly has a peak to peak intensity of 325 gammas. Anomalies over the Mozambique Abyssal Plain range in amplitude from 50 to 375 gammas. Magnetic records were not obtained over the Malagasy Abyssal Plain.

4. Zambesi Cone

Anomalies related to the Zambesi Cone are of two types: low amplitude anomalies over the flanks of the cone and higher amplitude anomalies (100-300 gammas) over the channeled central portion.

5. Agulhas Plateau

The Agulhas Plateau has a symmetrical anomaly pattern (Figure 13). The higher central portion is positive with three distinct anomalies having intensities up to +720 gammas. Anomalies over the flank of the plateau are essentially negative, have smaller amplitudes and a minimum intensity of -290 gammas. East and west of the flank areas the amplitudes again increase.

6. Mozambique Ridge System

Anomalies over the Mozambique Ridge, Slopes, Rise and Fracture Zone generally range in amplitude from 100 to 375 gammas. The fracture zone anomalies are less than 200 gammas. A few local areas with anomaly amplitudes less than 100 gammas exist on the rise west of Mozambique Ridge.

7. Madagascar Microcontinental System

The Madagascar Microcontinental System including the island of Madagascar, Prince Edward Fracture Zone, Madagascar Ridge, Madagascar Ridge Scarp Extension Slope and Rise have anomalies of various amplitudes. Anomalies over the rise are generally less than 100 gammas in amplitude except where they are associated with faults or are adjacent

to high amplitude areas such as the scarp extension. Anomalies related to the Prince Edward Fracture Zone, on the western side of the ridge, have large amplitudes with a minimum intensity of -820 gammas (Figure 14). Anomalies over the ridge have large amplitudes with only a few local exceptions. In general, residual anomalies are positive over the southwestern three-fourths of the ridge and negative over the northeastern one-fourth. An exception to the pattern is a broad positive anomaly (+580 gammas) in the negative zone. The ridge scarp extension contains high amplitude anomalies with peak to peak intensities to 550 gammas (Figure 15). Anomalies associated with the slope east and southeast of Diego Suarez are of high amplitude. A fault anomaly is apparent at the base east of Diego Suarez (Figure 16). Upslope from the fault, amplitudes of the anomalies decrease.

E. CRUISE 1D - TRANS-INDIAN OCEAN

1. Rises

Rises east and northeast of Diego Suarez, adjacent to the Mascarene Plateau and east of the Ninety East Ridge generally have anomalies with amplitudes less than 200 gammas. Anomalies over the rises where amplitudes are larger are probably due to adjacent or buried structural features.

2. Abyssal Hills

Anomalies over the abyssal hills west of the Mid-Indian Ridge and east of the Chago Laccadive are generally quite small in amplitude. Locally, anomalies attain amplitudes greater than 100 gammas.

3. Abyssal Plains

Three abyssal plains that were crossed are the Mascarene, Madingley, and Ceylon. Anomalies over the Mascarene Abyssal Plain have peak to peak variations of approximately 170 gammas. The Madingley Abyssal Plain, in general, has anomalies with amplitudes greater than 100

gammas. Anomalies over the Ceylon Abyssal Plain are generally less than 100 gammas. An exception to this is an anomaly which has a peak to peak intensity of 250 gammas, at latitide 0°59'N, longitude 78°25'E. This anomaly may be related to a buried portion of the western flank of a ridge which trends NNE-SSW off the southern tip of India (Heezen and Tharp, 1964).

4. Ganges Cone

Anomalies over the Ganges Cone are of low amplitude except in areas where seamounts exist. Anomalies in association with seamounts attain peak to peak intensities of up to 475 gammas.

5. Mascarene Plateau and Ridge System

Anomalies over the Mascarene Plateau and Ridge System are generally less than 200 gammas in amplitude with a few exceptions. The largest residual anomalies are found in association with the western ridge at latitude 9°45'S, longitude 56°10'E (Figure 17). These anomalies have peak to peak intensities of up to 770 gammas. Anomalies associated with the plateau are generally of low amplitude.

6. Mid-Indian Ocean Ridge (Carlsberg Ridge)

Anomalies over the Carlsberg Ridge are symmetrical about the rift valley anomaly (Figure 18). The rift valley anomaly has an average intensity of about -200 gammas. The magnetic profile is quite similar to those in an area to the northwest (Matthews et al , 1965).

7. Chagos Laccadive Plateau

The Chagos Laccadive Plateau contains anomalies which are generally less than 200 gammas in amplitude (Figure 19). The central portion has entirely positive residual anomalies whereas the eastern and western portions have negative anomalies or a positive-negative combination. Residual anomalies over the Chagos trench, east of the plateau, have an intensity of +275 gammas.

8. Ninety East Ridge

Anomalies over the Ninety East Ridge are generally less than 100 gammas in amplitude (Figure 20). One exception to this is a +225 gamma residual anomaly over the eastern-most slope of the ridge.

9. Island Arc System

The complex double arc system contains anomalies of very low amplitude. The largest anomaly, with an intensity of +260 gammas, is associated with the inner volcanic arc and adjacent interdeep. A slight negative anomaly of -100 gammas is associated with a portion of the back deep.

V - REFERENCES

Alldredge, L.R., Van Voorhis, G.D., and Davis, T.M. 1963. A magnetic profile around the world. J. Geophys. Res., 68 (12): 3679-3692.

Bowin, C.O., and Vogt, P. 1966. Magnetic lineation between Carlsberg Ridge and Seychelles Bank, Indian Ocean. J. Geophys. Res., 71 (10): 2625-2630.

Cain, J.C., Daniels, W.E., Hendricks, S.J., and Jensen, D.C. 1965. An evaluation of the main geomagnetic field, 1942-1962. J. Geophys. Res., 70: 3647-3674.

Cann, J.R., and Vine, F.J. 1966. An area of the crest of the Carlsberg Ridge: Petrology-Magnetic survey. Phil. Trans. Roy. Soc. London, A, 259 (1099): 198-217.

Cox, A., Dalrymple, G.B., and Doell, R.C. 1967. Reversals of the earth's magnetic field. Sci. Am., 216: 44-54.

Encyclopedia of Oceanography 1966. R.W. Fairbridge, editor, Reinhold Publishing Corp., New York: 1021 pp.

Graham, K.W.T., and Hales, A.L. 1965. Surface-ship gravity measurements in the Agulhas Bank area, south of South Africa. J. Geophys. Res., 70 (16): 4005-4011.

Green, R.W.E., and Hales, A.L. 1966. Seismic refraction measurements in the southwest Indian Ocean. J. Geophys. Res., 71 (6): 1637-1647.

Heezen, B.C., Ewing, M., and Miller, E.T. 1953. Trans-Atlantic profile of total magnetic intensity and topography, Dakar to Barbados. Deep-Sea Res., 1: 25-33.

Heezen, B.C., and Tharp, M. 1957. Physiographic diagram, Atlantic Ocean, In: The floors of the oceans, I, The North Atlantic. Geol. Soc. Am. Spec. Papers, 65: 122 pp.

Heezen, B.C., and Tharp, M. 1961. Physiographic diagram of the South Atlantic Ocean, the Caribbean Sea, the Scotia Sea, and the eastern margin of the South Pacific Ocean. Geol. Soc. Am., New York.

Heezen, B.C., and Tharp, M. 1964. Physiographic diagram of the Indian Ocean, the Red Sea, the South China Sea, the Sulu Sea and the Celebes Sea. Geol. Soc. Am., New York.

Heezen, B.C., and Tharp, M. 1966. Physiography of the Indian Ocean. Phil. Trans. Roy. Soc. London, A., 259: 137-149.

Heezen, B.C., Tharp, M., and Ewing, M. 1959. The floors of the oceans, I, The North Atlantic. Geol. Soc. Am. Spec. Papers, 65: 122 pp.

Heirtzler, J.R. 1965. Marine geomagnetic anomalies. J. Geomagnet. Geoelec., Kyoto, 17 (3-4): 227-236.

Heirtzler, J.R., and Hayes, D.E. 1967. Magnetic boundaries in the North Atlantic Ocean. Science, 157: 185-187.

Heirtzler, J.R., and Hirshman, J. 1960. Measurements of the geomagnetic field near Capetown. J. Geophys. Res., 65 (9): 3016-3018.

Heirtzler, J.R., and LePichon, X. 1965. Crustal structure of the mid-ocean ridges. 3. Magnetic anomalies over the Mid-Atlantic Ridge. J. Geophys. Res., 70 (16): 4013-4033.

Henry, J.A. 1968. Area ST, Volume 2, Part I, Bathymetry and Subbottom Profiling. Prepared by Alpine Geophysical Associates, Inc. U. S. Naval Oceanographic Office. SP-97-ST-2-I.

Keller, F., Jr., Meuschke, J.L., and Alldredge, L.R. 1954. Aeromagnetic surveys in the Aleutian, Marshall, and Bermuda Islands. Trans. Am. Geophys. Union, 35 (4): 558-572.

Krause, D.C. 1964. Guinea Fracture Zone in the Equatorial Atlantic. Science, 146: 57-59.

Matthews, D.H., Vine, F.J., and Cann, J.R. 1965. Geology of an area of the Carlsberg Ridge, Indian Ocean. Bull. Geol. Soc. Am., 76: 675-682.

Peter, G., Weeks, L., and Burns, R.E. 1966. A reconnaissance geophysical survey in the Andaman Sea and across the Andaman-Nicobar Arc. J. Geophys. Res., 71 (2): 495-509.

Taylor, P.T. 1966. Geothermal and magnetic survey off the coast of Sumatra, 2-Interpretation and discussion of results. Tokyo Univ. Earthquake Res. Inst. Bull., 44 (2): 531-540.

Vacquier, V., and Taylor, P.T. 1966. Geothermal and magnetic survey off the coast of Sumatra, 1-Presentation of data. Tokyo Univ. Earthquake Res. Inst. Bull., 44 (2): 531-540.

Vajk, R. 1966a. Area I, Volume 6, Magnetics. Prepared by Alpine Geophysical Associates, Inc. U. S. Naval Oceanographic Office SP-96-I-6.

Vajk, R. 1966b. Area II, Volume 6, Magnetics. Prepared by Alpine Geophysical Associates, Inc. U. S. Naval Oceanographic Office SP-96-II-6.

Vajk, R. 1967a. Area SF, Volume 6, Magnetics. Prepared by Alpine

Geophysical Associates, Inc. U. S. Naval Oceanographic Office SP-96-SF-6.

Vajk, R. 1967b. Area HH, Volume 2, Part 2, Magnetics. Prepared by Alpine Geophysical Associates, Inc. U. S. Naval Oceanographic Office SP-96-H-2-2.

Vine, F.J., and Matthews, D.H. 1963. Magnetic anomalies over oceanic ridges. Nature, 199 (4897): 947-949.

Weeks, L.A., Harbison, R.N., and Peter, G. 1967. Island arc system in Andaman Sea. Bull. Am. Assoc. Petrol. Geologists, 51 (9): 1803-1815.

Wilson, J.T. 1965. A new class of faults and their bearing on continental drift. Nature, 207 (4995): 343-347.

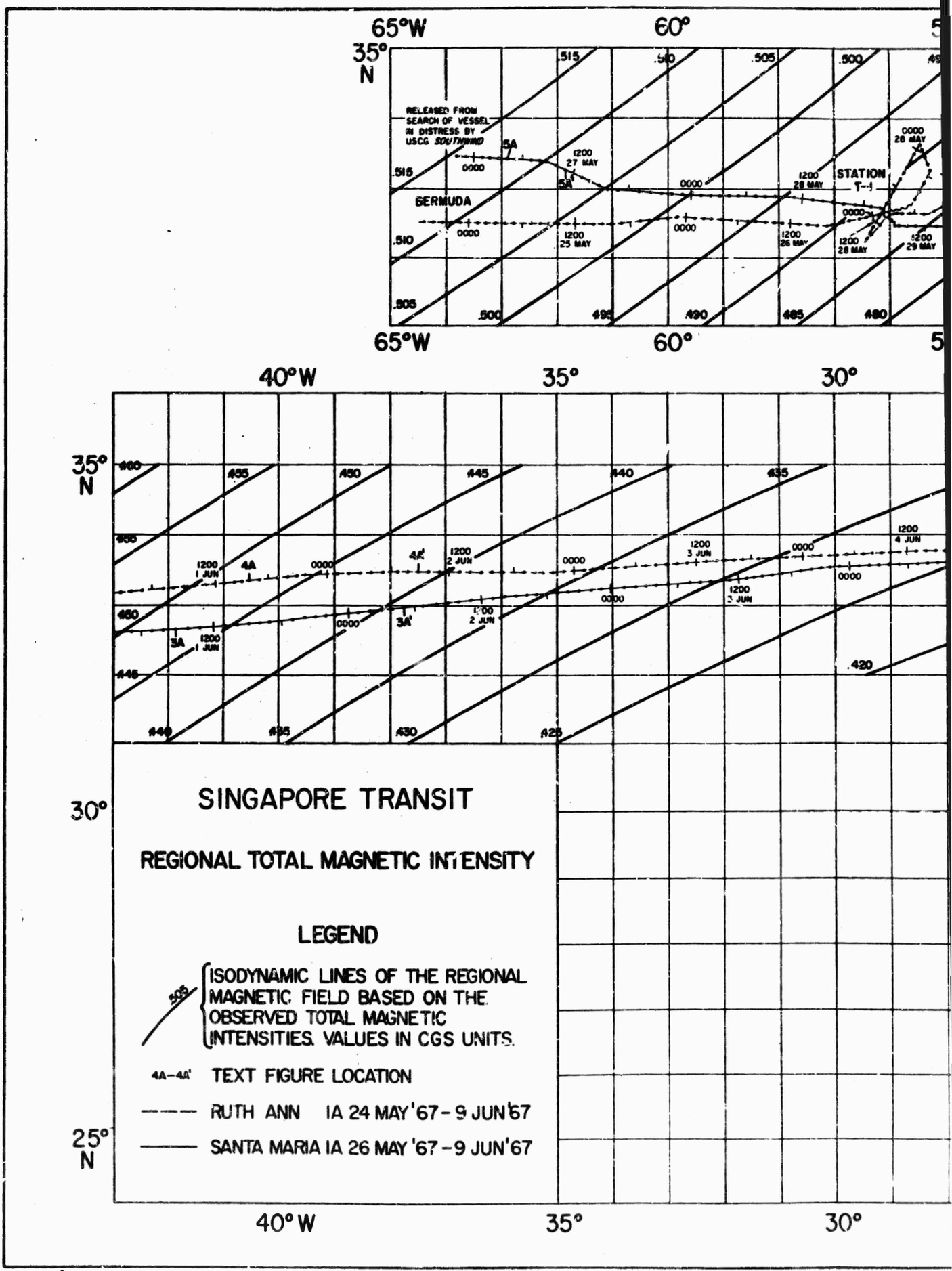
65°W
60°
35° N
RELEASED FROM SEARCH OF VESSEL IN DISTRESS BY USCG SOUTHWIND
BERMUDA
STATION T-1
0000 28 MAY
1200 27 MAY
1200 28 MAY
1200 25 MAY
1200 26 MAY
1200 29 MAY
.515
.510
.505
.500
.495
.490
.485
.480
40°W
35°
30°
35° N
30°
25° N
1200 1 JUN
1200 2 JUN
1200 3 JUN
1200 4 JUN
4A
4A'
3A
3A'
.460
.455
.450
.445
.440
.435
.430
.425
.420
SINGAPORE TRANSIT
REGIONAL TOTAL MAGNETIC INTENSITY
LEGEND
ISODYNAMIC LINES OF THE REGIONAL MAGNETIC FIELD BASED ON THE OBSERVED TOTAL MAGNETIC INTENSITIES. VALUES IN CGS UNITS.
4A–4A' TEXT FIGURE LOCATION
RUTH ANN IA 24 MAY '67 – 9 JUN '67
SANTA MARIA IA 26 MAY '67 – 9 JUN '67

A

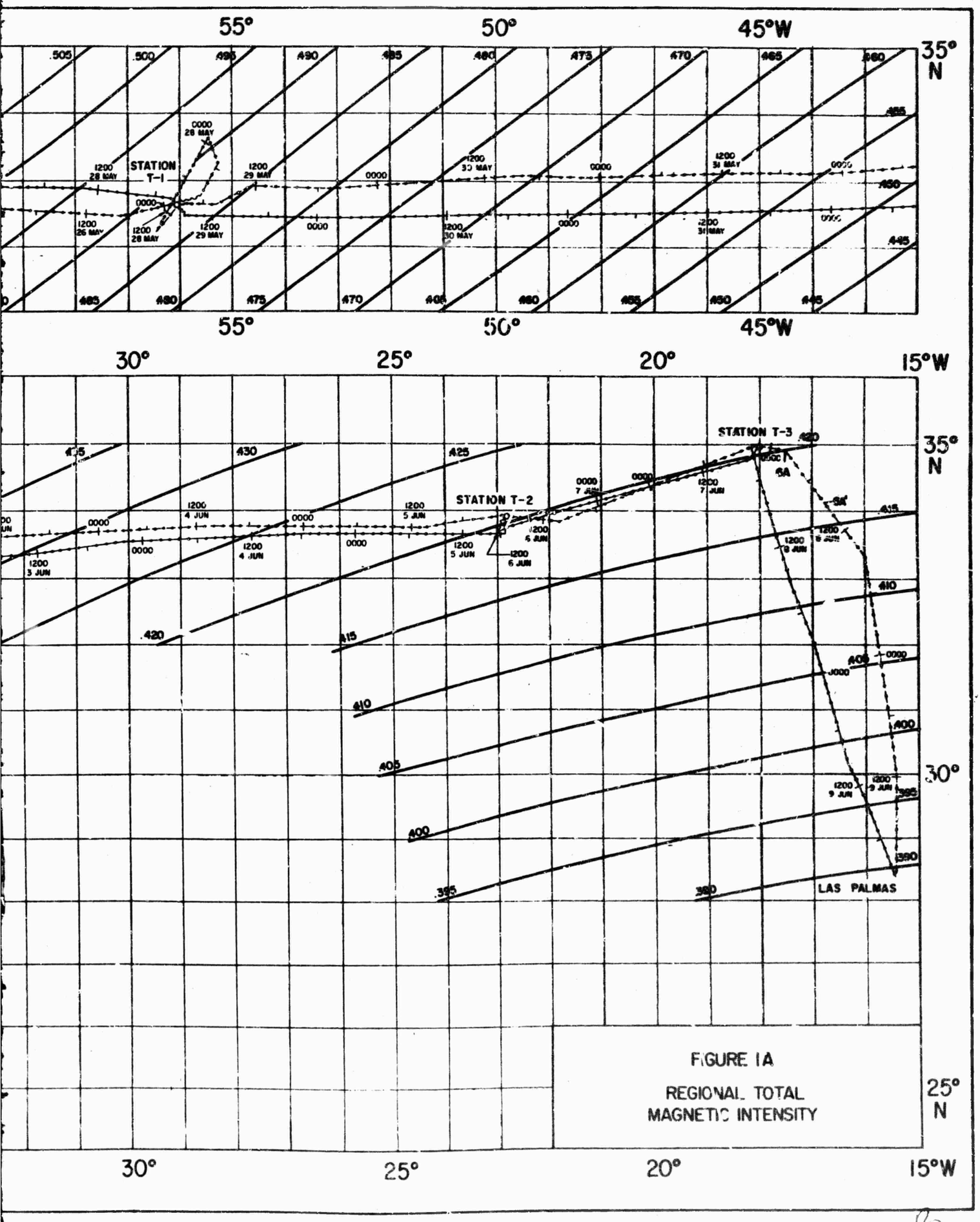

FIGURE 1A

REGIONAL TOTAL MAGNETIC INTENSITY

B

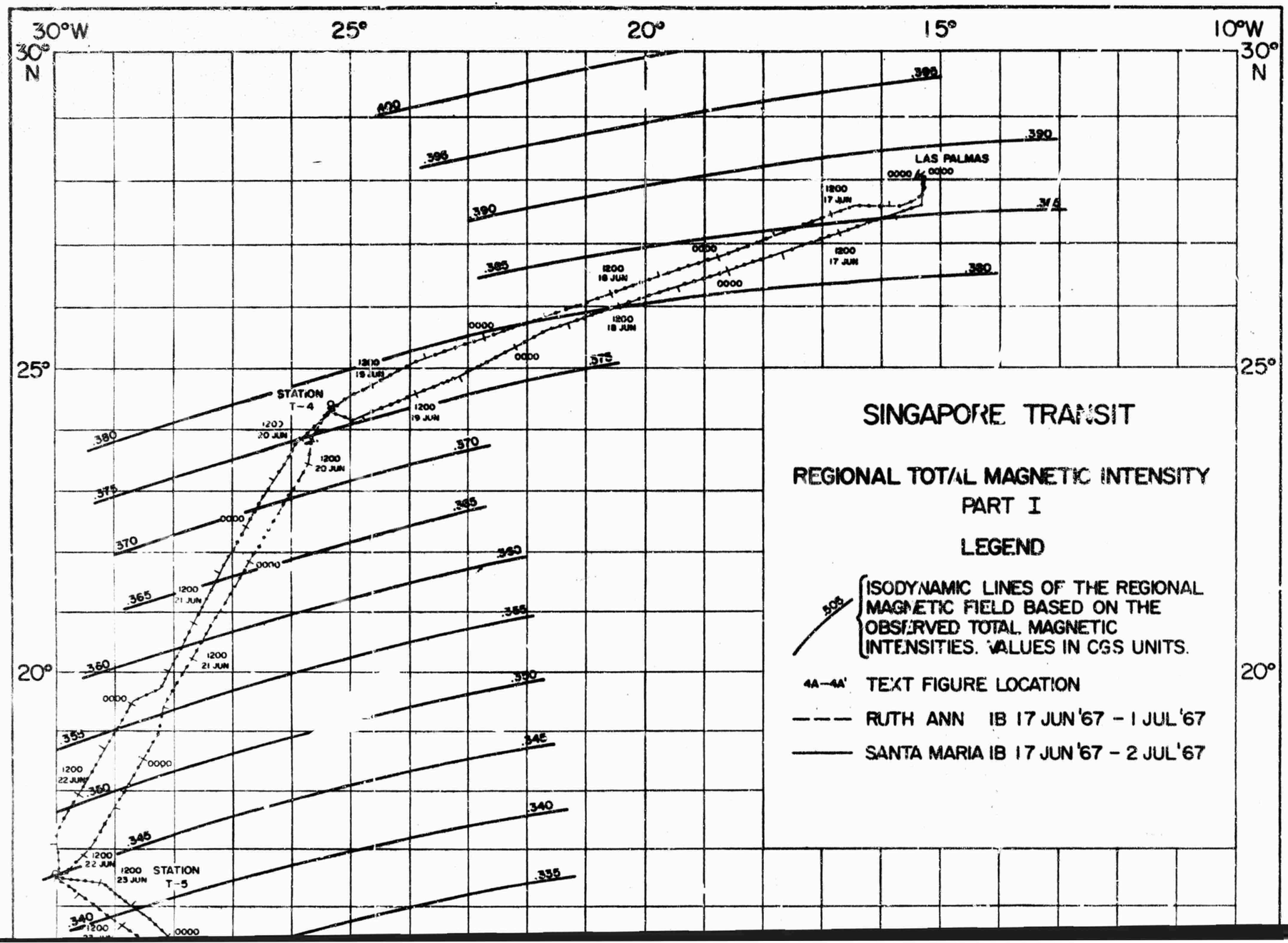
30°W
25°
20°
15°
10°W
30° N
25°
20°
LAS PALMAS
STATION T-4
STATION T-5
SINGAPORE TRANSIT
REGIONAL TOTAL MAGNETIC INTENSITY
PART I
LEGEND
ISODYNAMIC LINES OF THE REGIONAL MAGNETIC FIELD BASED ON THE OBSERVED TOTAL MAGNETIC INTENSITIES. VALUES IN CGS UNITS.
4A–4A' TEXT FIGURE LOCATION
RUTH ANN IB 17 JUN '67 – 1 JUL '67
SANTA MARIA IB 17 JUN '67 – 2 JUL '67

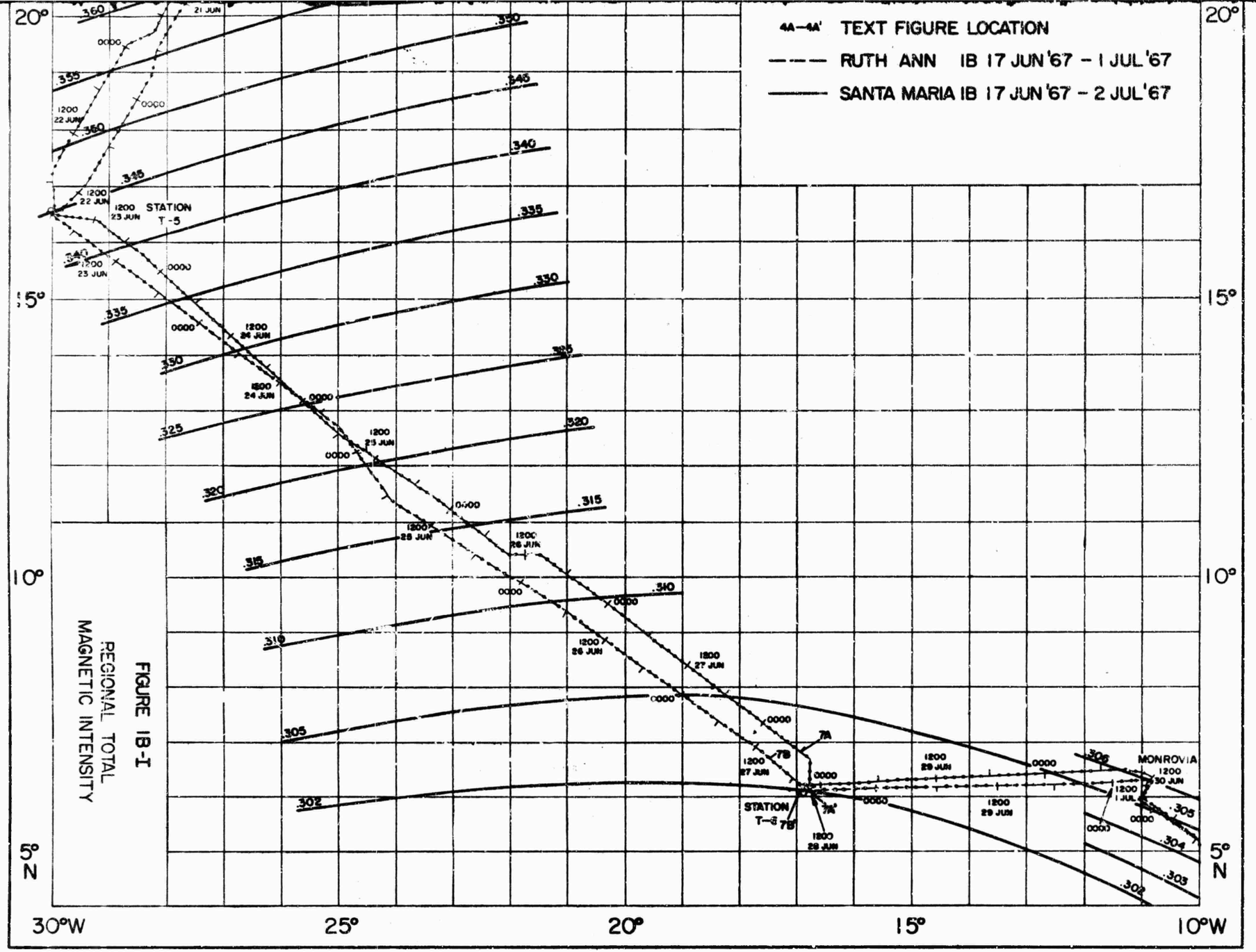

FIGURE IB-I

REGIONAL TOTAL MAGNETIC INTENSITY

FIGURE IB-I

B

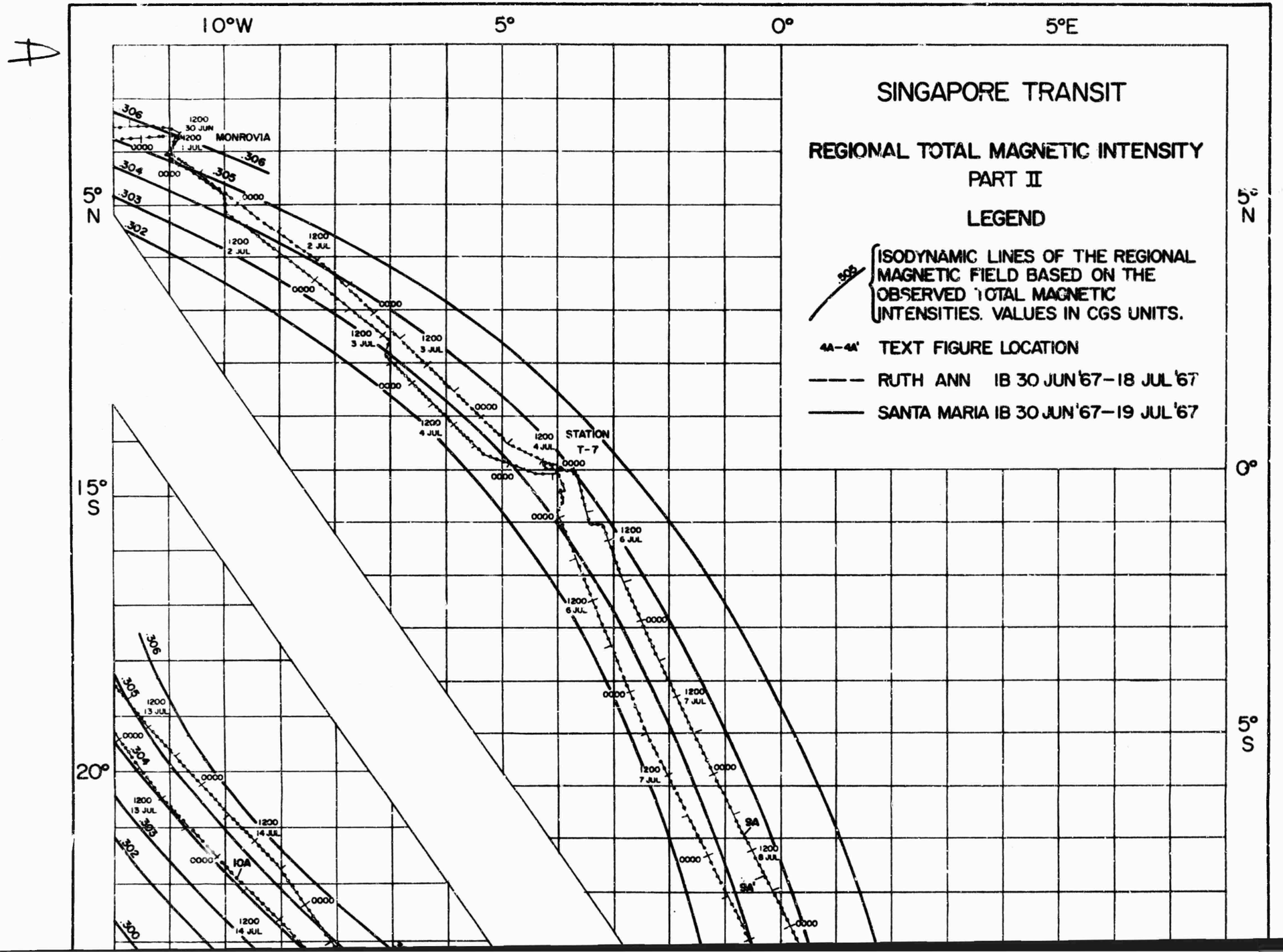
10°W
5°
0°
5°E
5° N
15° S
20°
5° N
0°
5° S
SINGAPORE TRANSIT
REGIONAL TOTAL MAGNETIC INTENSITY
PART II
LEGEND
ISODYNAMIC LINES OF THE REGIONAL MAGNETIC FIELD BASED ON THE OBSERVED TOTAL MAGNETIC INTENSITIES. VALUES IN CGS UNITS.
4A-4A' TEXT FIGURE LOCATION
RUTH ANN IB 30 JUN '67 – 18 JUL '67
SANTA MARIA IB 30 JUN '67 – 19 JUL '67
MONROVIA
STATION T-7
1200 30 JUN
0000 1 JUL
1200 2 JUL
1200 3 JUL
1200 4 JUL
1200 6 JUL
1200 7 JUL
1200 8 JUL
1200 13 JUL
1200 14 JUL
306
305
304
303
302
300
4A
4A'
104

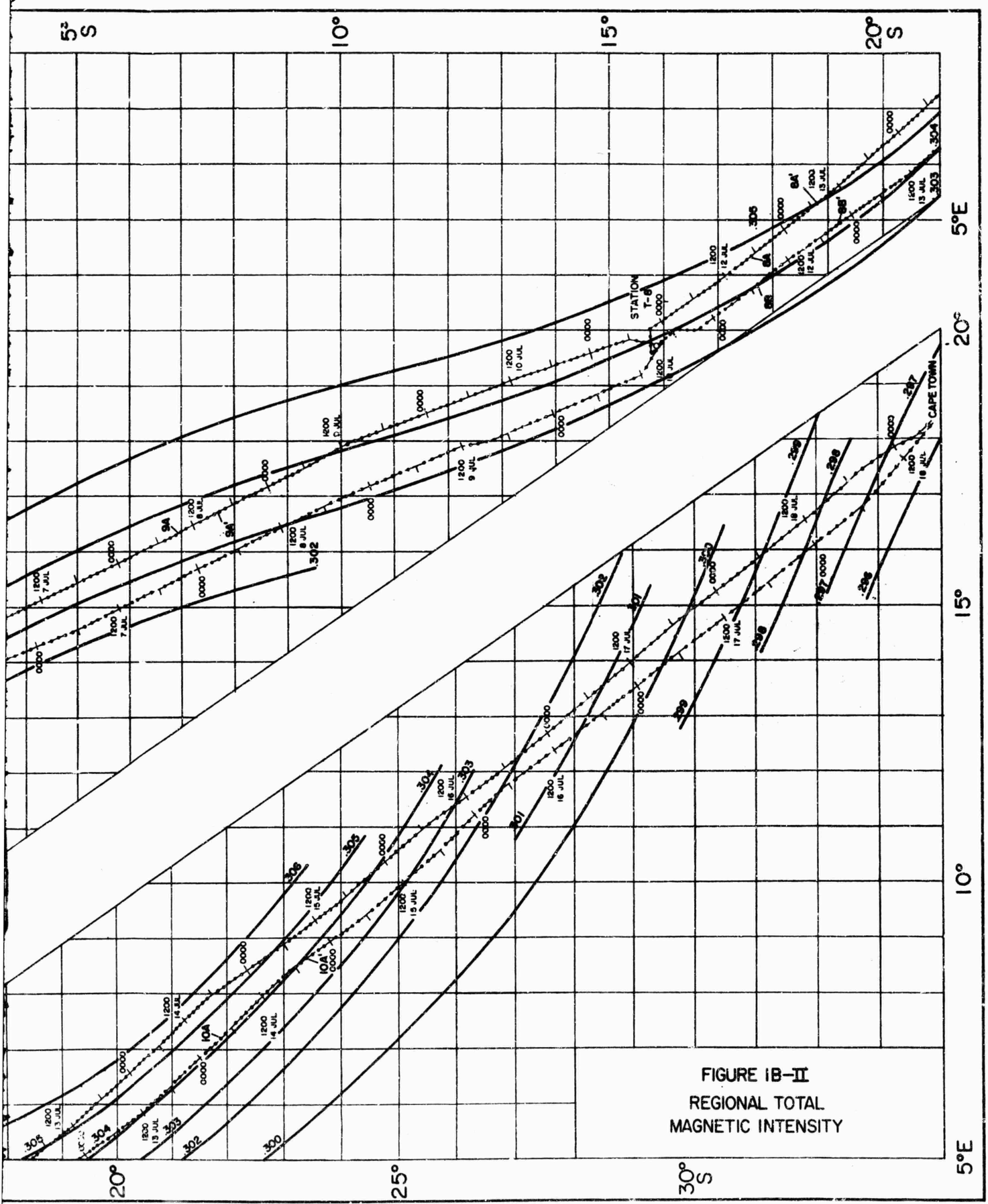

FIGURE 1B-II

B

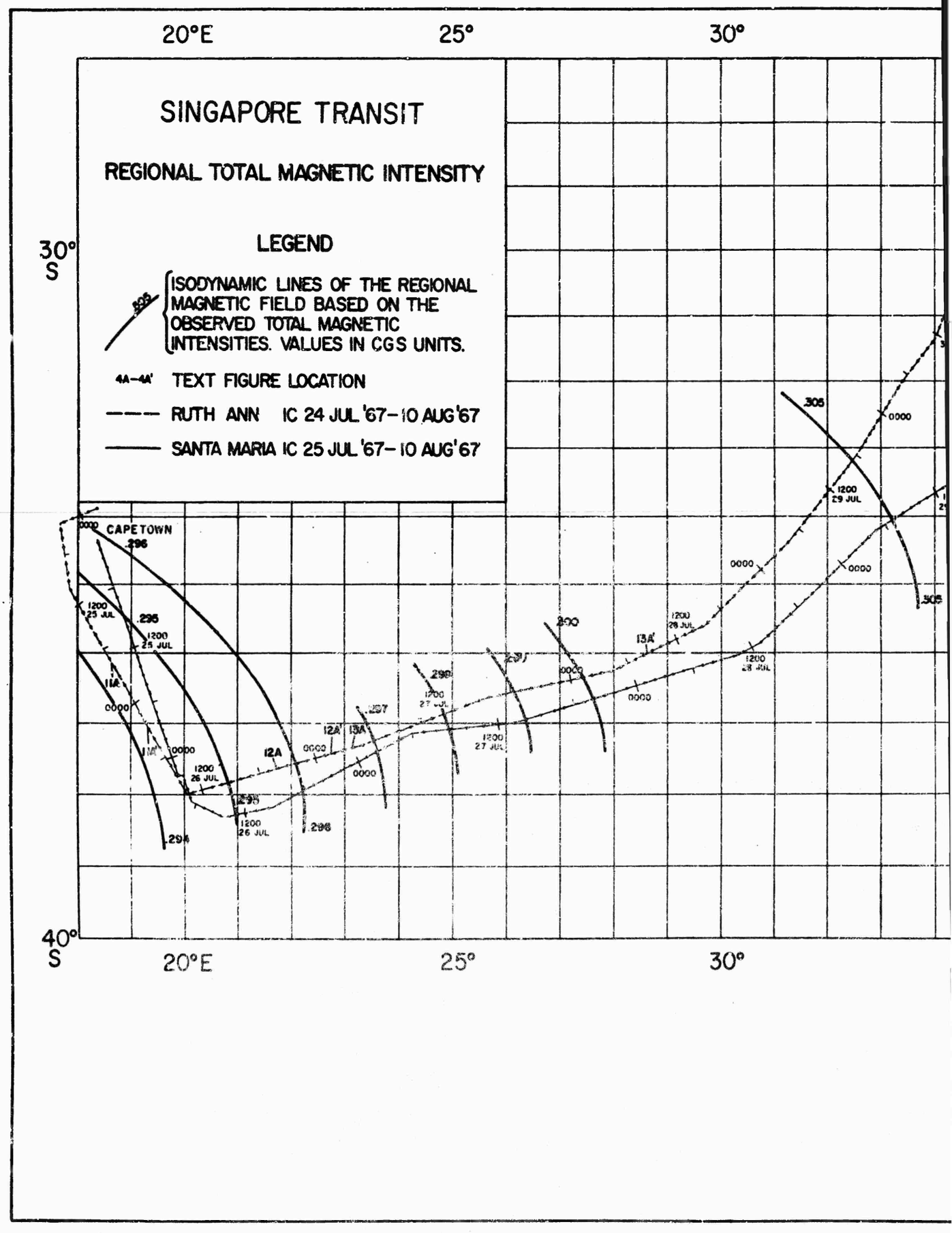
20°E
25°
30°
SINGAPORE TRANSIT
REGIONAL TOTAL MAGNETIC INTENSITY
LEGEND
ISODYNAMIC LINES OF THE REGIONAL MAGNETIC FIELD BASED ON THE OBSERVED TOTAL MAGNETIC INTENSITIES. VALUES IN CGS UNITS.
4A–4A' TEXT FIGURE LOCATION
RUTH ANN IC 24 JUL '67–10 AUG '67
SANTA MARIA IC 25 JUL '67–10 AUG '67
30° S
40° S
CAPE TOWN
296
295
294
298
300
305
0000
1200
25 JUL
26 JUL
27 JUL
28 JUL
29 JUL
11A
11A'
12A
12A'
13A
13A'

A

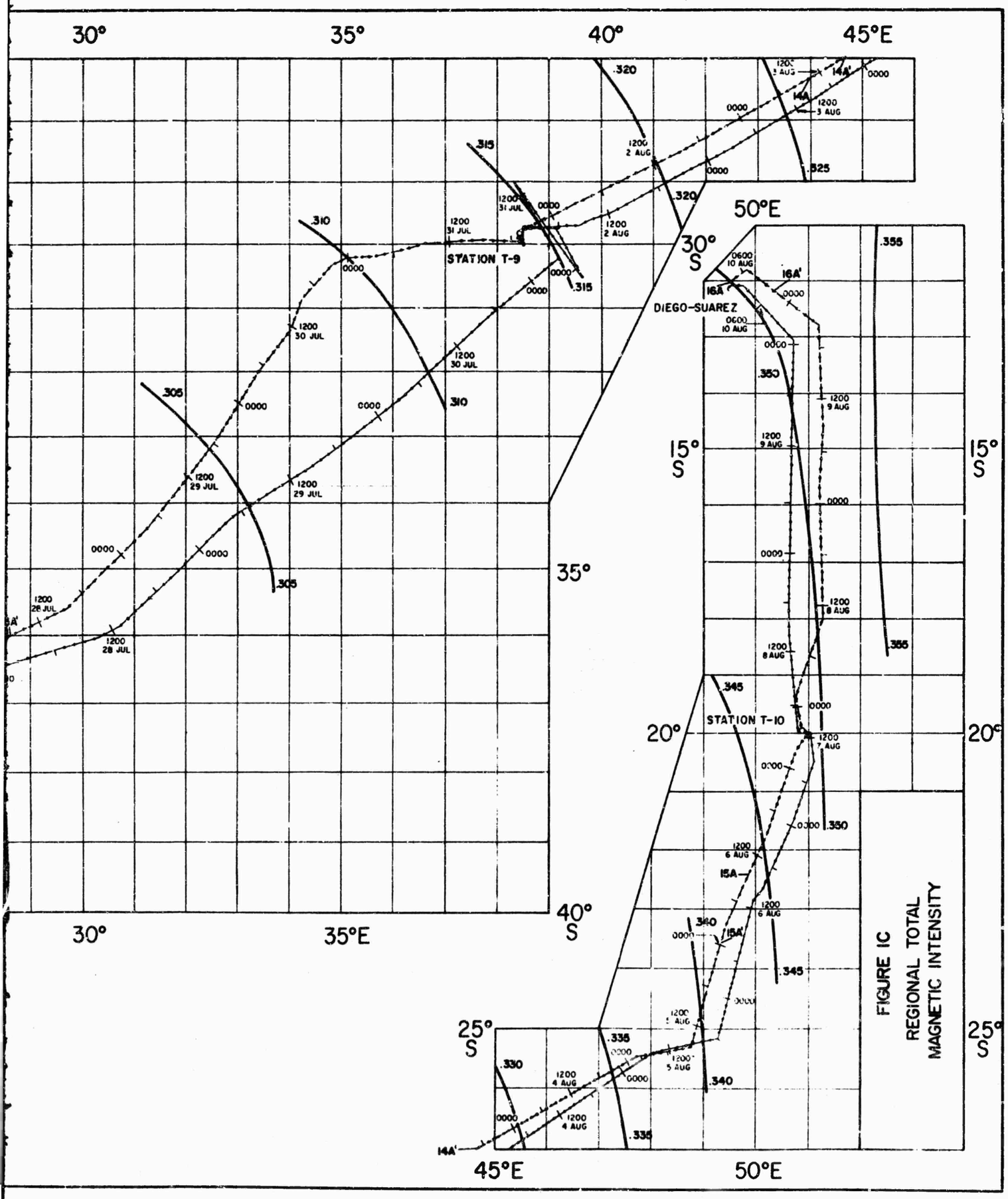
30°
35°
40°
45°E
50°E
30°
S
15°
S
35°
40°
S
20°
25°
S
30°
35°E
45°E
50°E
STATION T-9
STATION T-10
DIEGO-SUAREZ
.320
.315
.310
.305
.325
.355
.350
.345
.340
.335
.330
0000
0600
10 AUG
1200
31 JUL
1200
2 AUG
1200
30 JUL
1200
29 JUL
1200
28 JUL
1200
9 AUG
1200
8 AUG
1200
7 AUG
1200
6 AUG
1200
5 AUG
1200
4 AUG
1200
3 AUG
14A
14A'
15A
15A'
16A
16A'
FIGURE IC
REGIONAL TOTAL
MAGNETIC INTENSITY

FIGURE IC

B

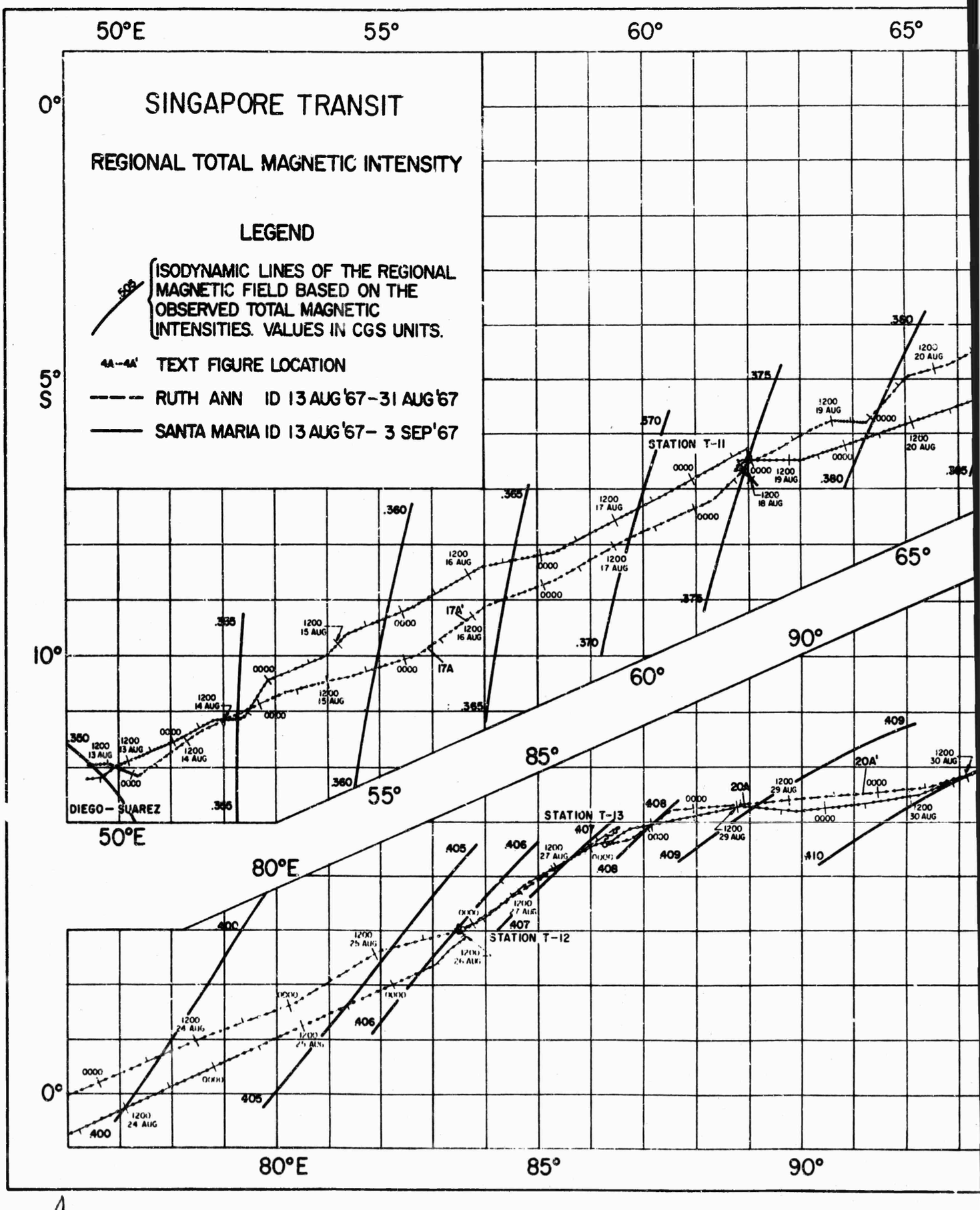
50°E
55°
60°
65°
0°
5° S
10°
80°E
85°
90°
SINGAPORE TRANSIT
REGIONAL TOTAL MAGNETIC INTENSITY
LEGEND
ISODYNAMIC LINES OF THE REGIONAL MAGNETIC FIELD BASED ON THE OBSERVED TOTAL MAGNETIC INTENSITIES. VALUES IN CGS UNITS.
4A–4A' TEXT FIGURE LOCATION
RUTH ANN ID 13 AUG '67 – 31 AUG '67
SANTA MARIA ID 13 AUG '67 – 3 SEP '67
STATION T-11
STATION T-12
STATION T-13
DIEGO-SUAREZ
17A
17A'
20A
20A'

A

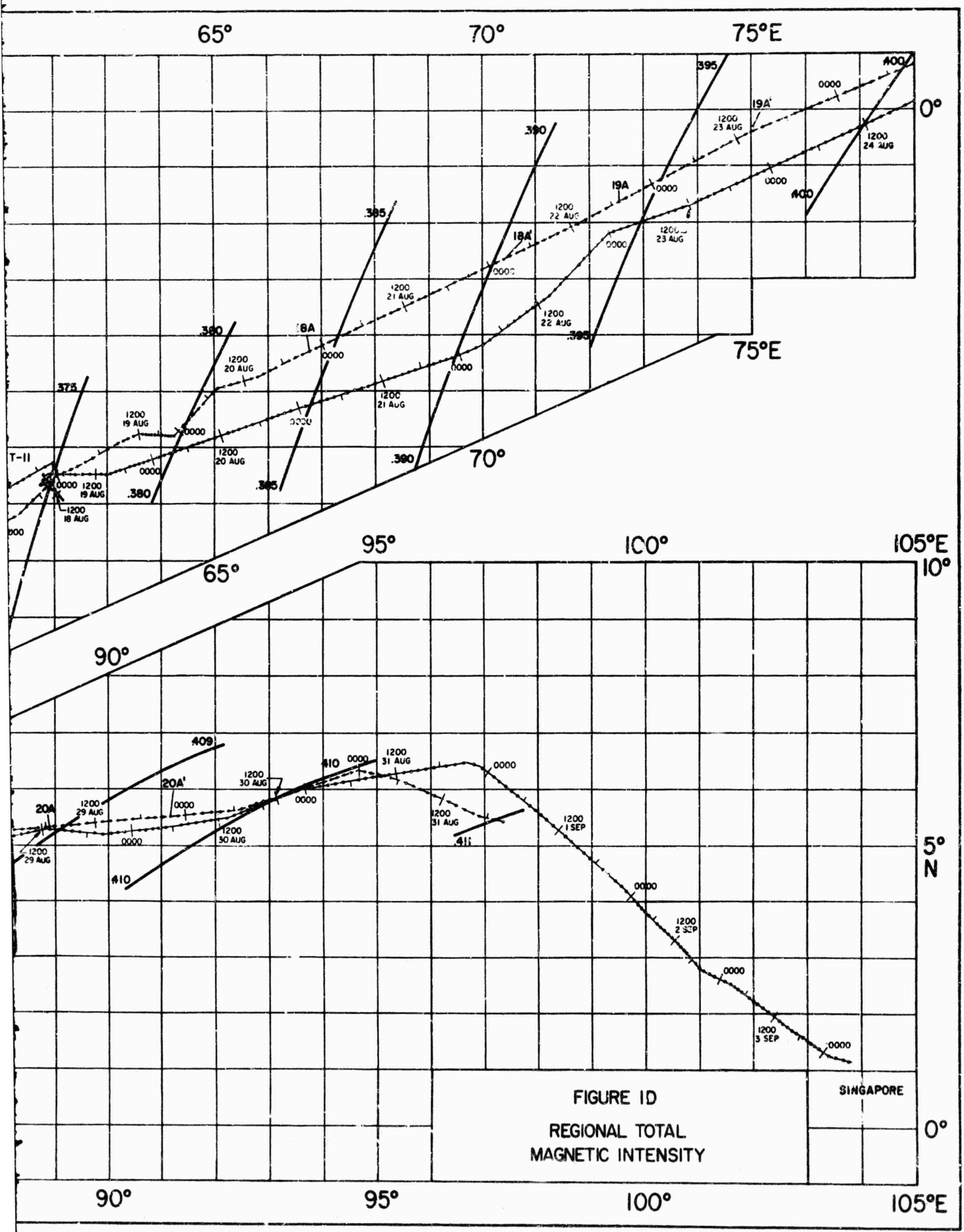

FIGURE 1D

REGIONAL TOTAL
MAGNETIC INTENSITY

B FIGURE 1D

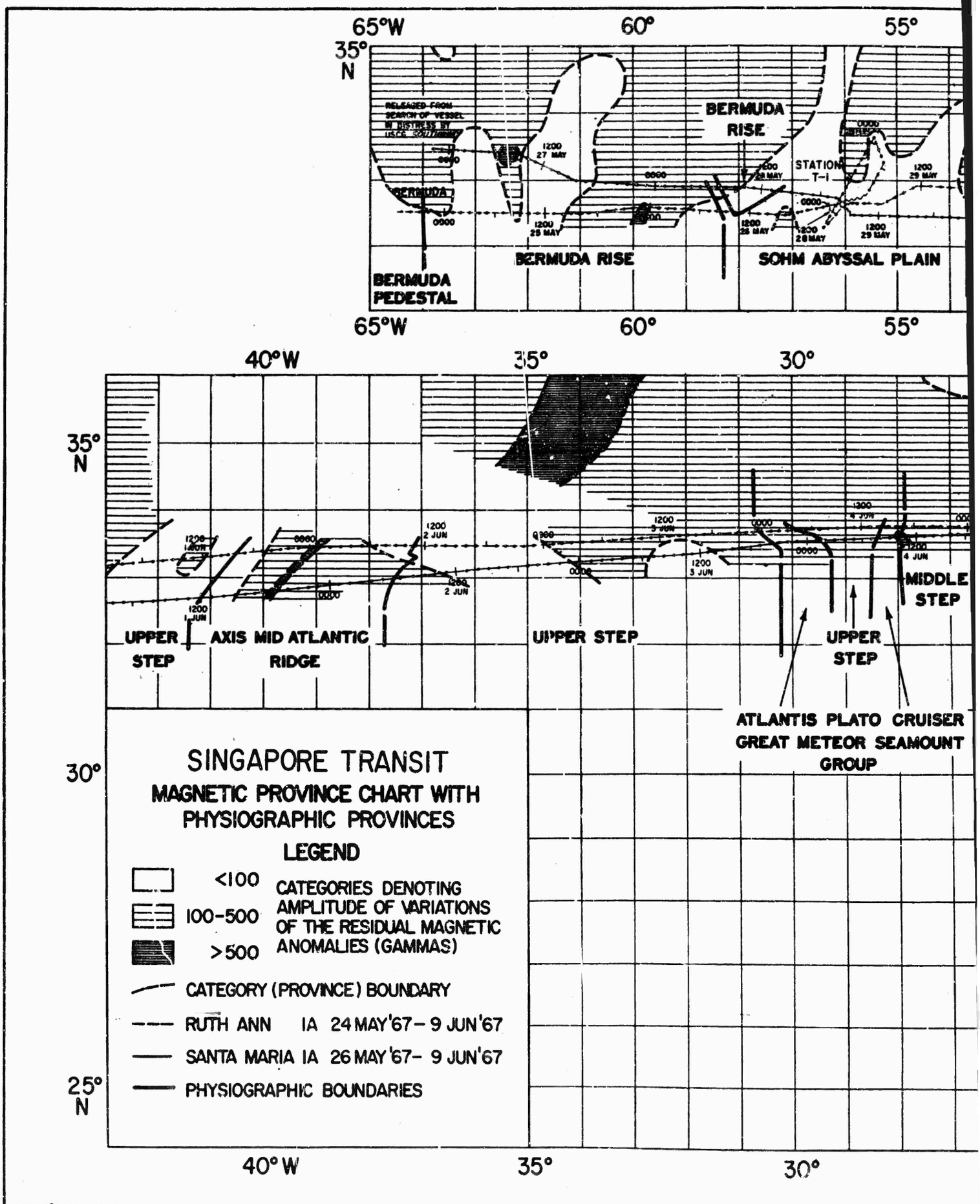
65°W
60°
55°
35° N
BERMUDA RISE
STATION T-i
BERMUDA
BERMUDA PEDESTAL
BERMUDA RISE
SOHM ABYSSAL PLAIN
40°W
35°
30°
35° N
UPPER STEP
AXIS MID ATLANTIC RIDGE
UPPER STEP
UPPER STEP
MIDDLE STEP
ATLANTIS PLATO CRUISER
GREAT METEOR SEAMOUNT GROUP
30°
25° N
SINGAPORE TRANSIT
MAGNETIC PROVINCE CHART WITH PHYSIOGRAPHIC PROVINCES
LEGEND
<100
100-500
>500
CATEGORIES DENOTING AMPLITUDE OF VARIATIONS OF THE RESIDUAL MAGNETIC ANOMALIES (GAMMAS)
CATEGORY (PROVINCE) BOUNDARY
RUTH ANN IA 24 MAY'67 – 9 JUN'67
SANTA MARIA IA 26 MAY'67 – 9 JUN'67
PHYSIOGRAPHIC BOUNDARIES

A

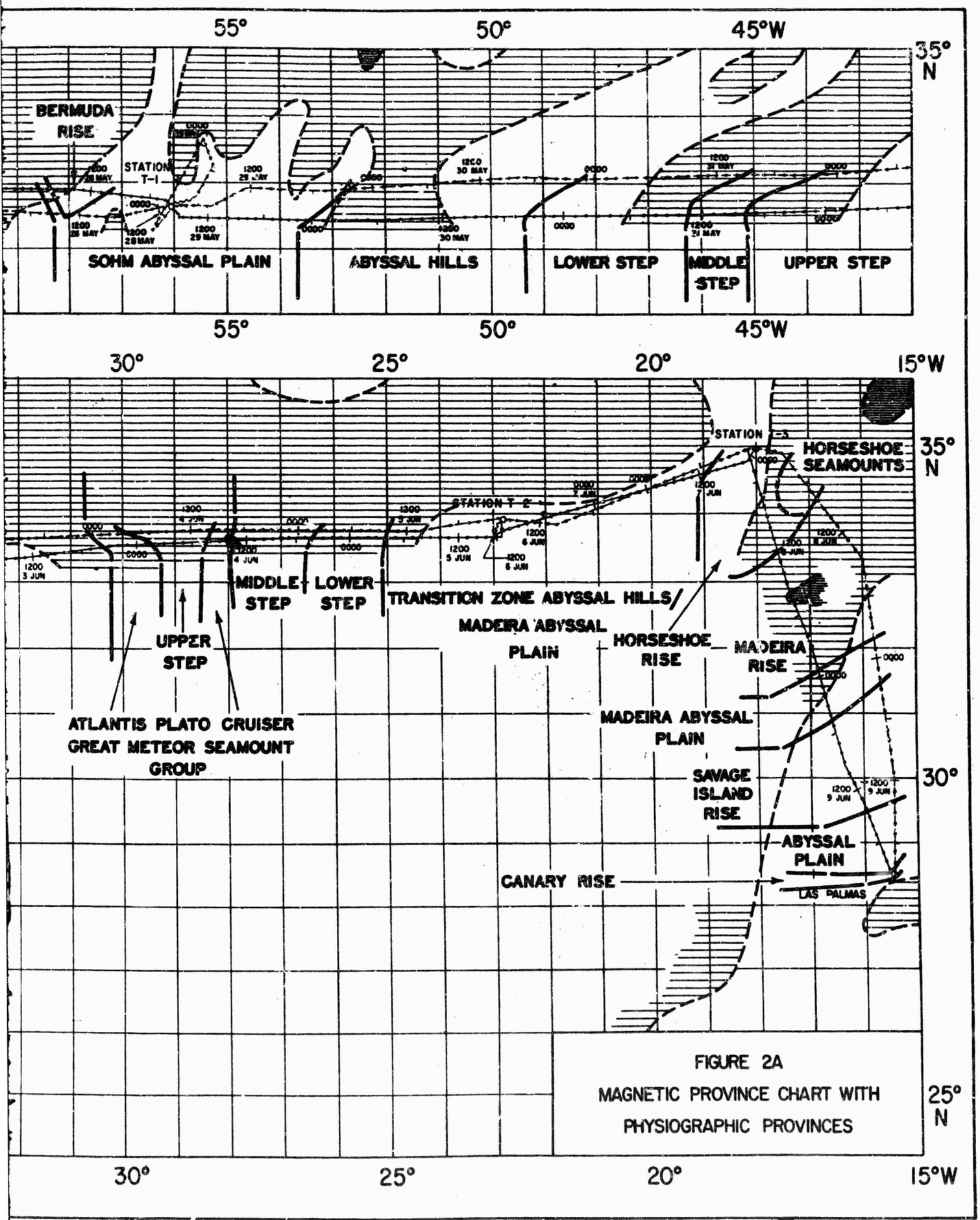

FIGURE 2A
MAGNETIC Pprovince CHART WITH
PHYSIOGRAPHIC PROVINCES

B FIGURE 2A

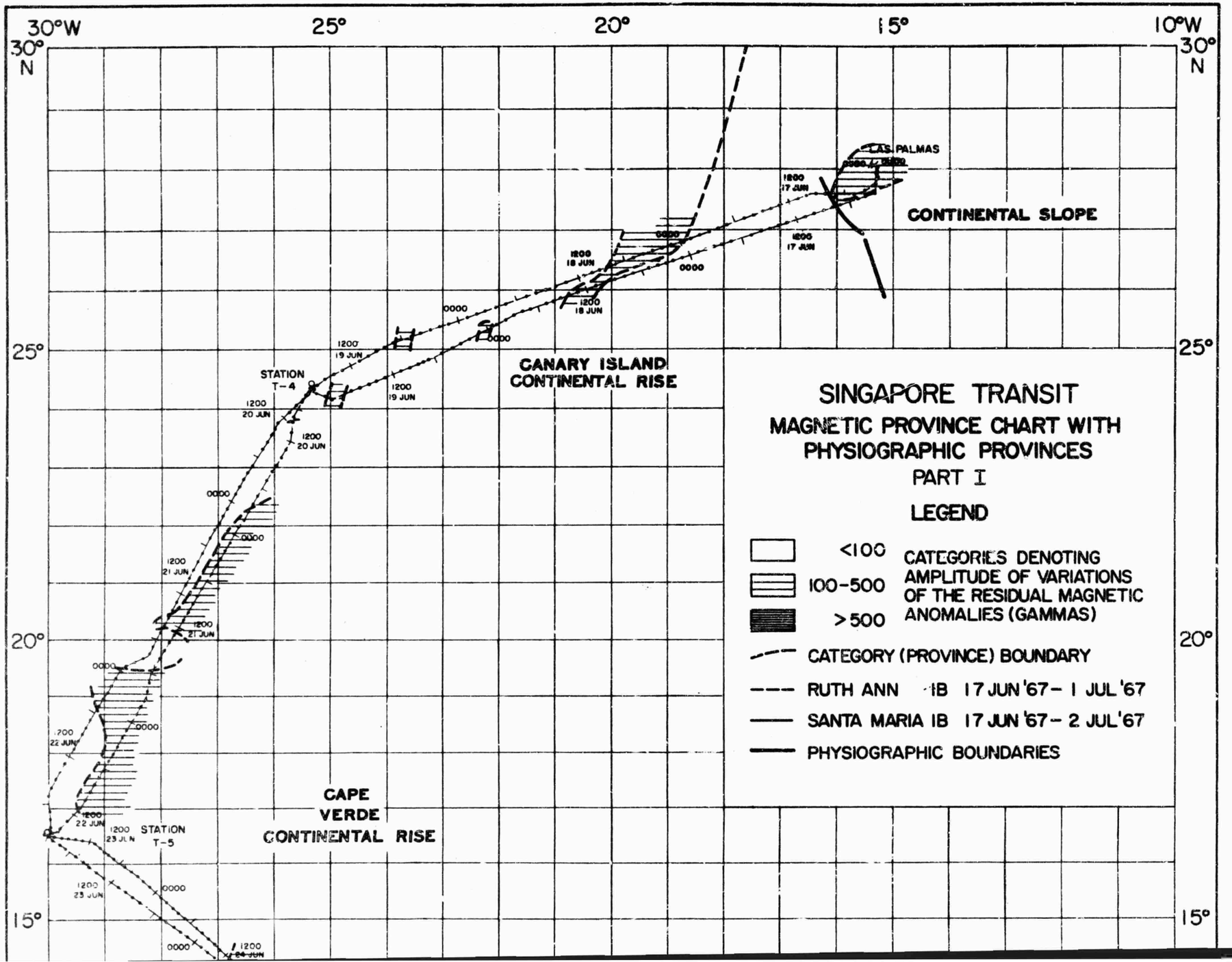
30°W
25°
20°
15°
10°W
30° N
25°
20°
15°
LAS PALMAS
CONTINENTAL SLOPE
CANARY ISLAND CONTINENTAL RISE
STATION T-4
STATION T-5
CAPE VERDE CONTINENTAL RISE
1200 17 JUN
1200 18 JUN
1200 19 JUN
1200 20 JUN
1200 21 JUN
1200 22 JUN
1200 23 JUN
0000
SINGAPORE TRANSIT
MAGNETIC PROVINCE CHART WITH PHYSIOGRAPHIC PROVINCES
PART I
LEGEND
<100
100-500
>500
CATEGORIES DENOTING AMPLITUDE OF VARIATIONS OF THE RESIDUAL MAGNETIC ANOMALIES (GAMMAS)
CATEGORY (PROVINCE) BOUNDARY
RUTH ANN IB 17 JUN '67 – 1 JUL '67
SANTA MARIA IB 17 JUN '67 – 2 JUL '67
PHYSIOGRAPHIC BOUNDARIES

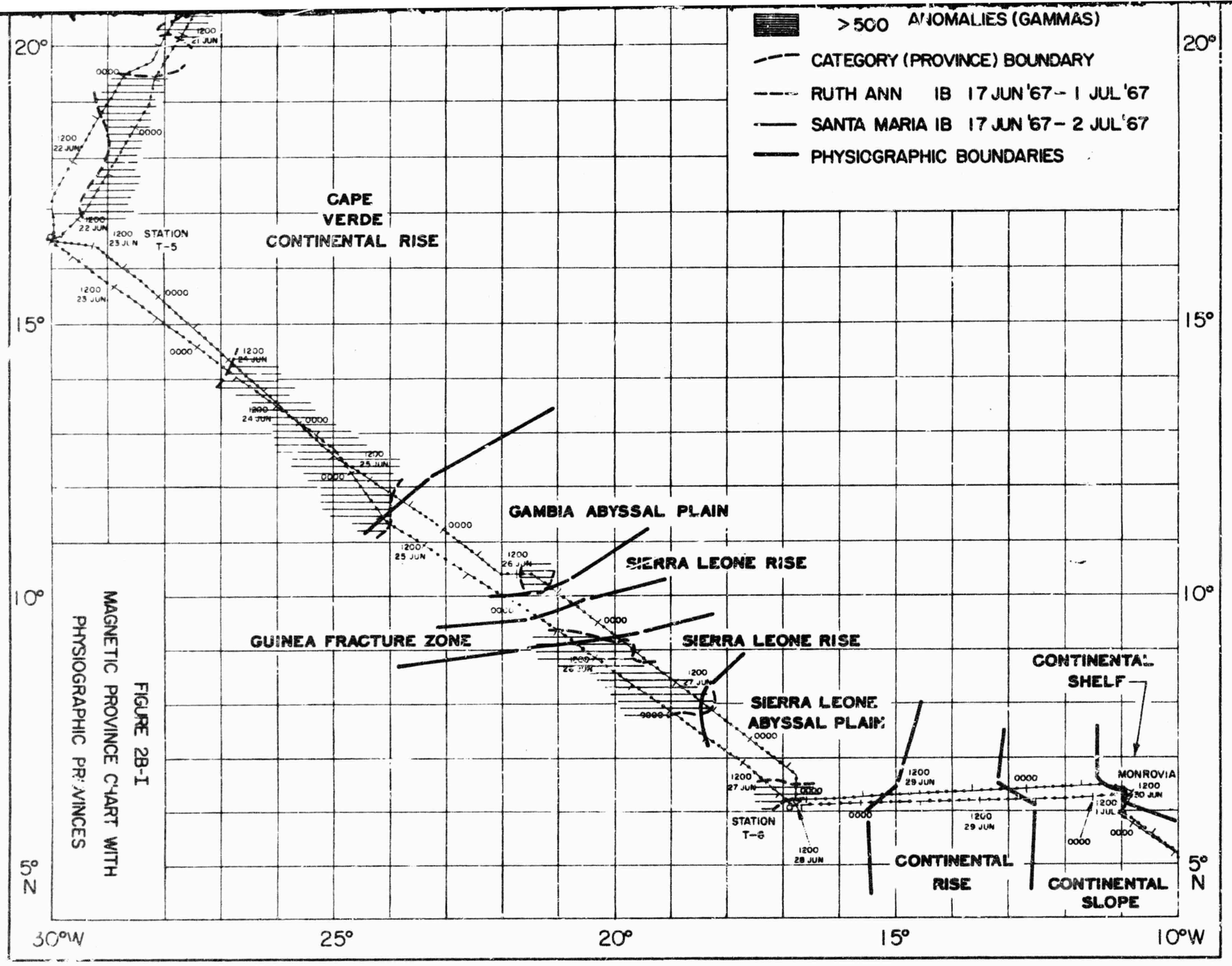

FIGURE 2B-I MAGNETIC PROVINCE CHART WITH PHYSIOGRAPHIC PROVINCES

FIGURE 2B-I

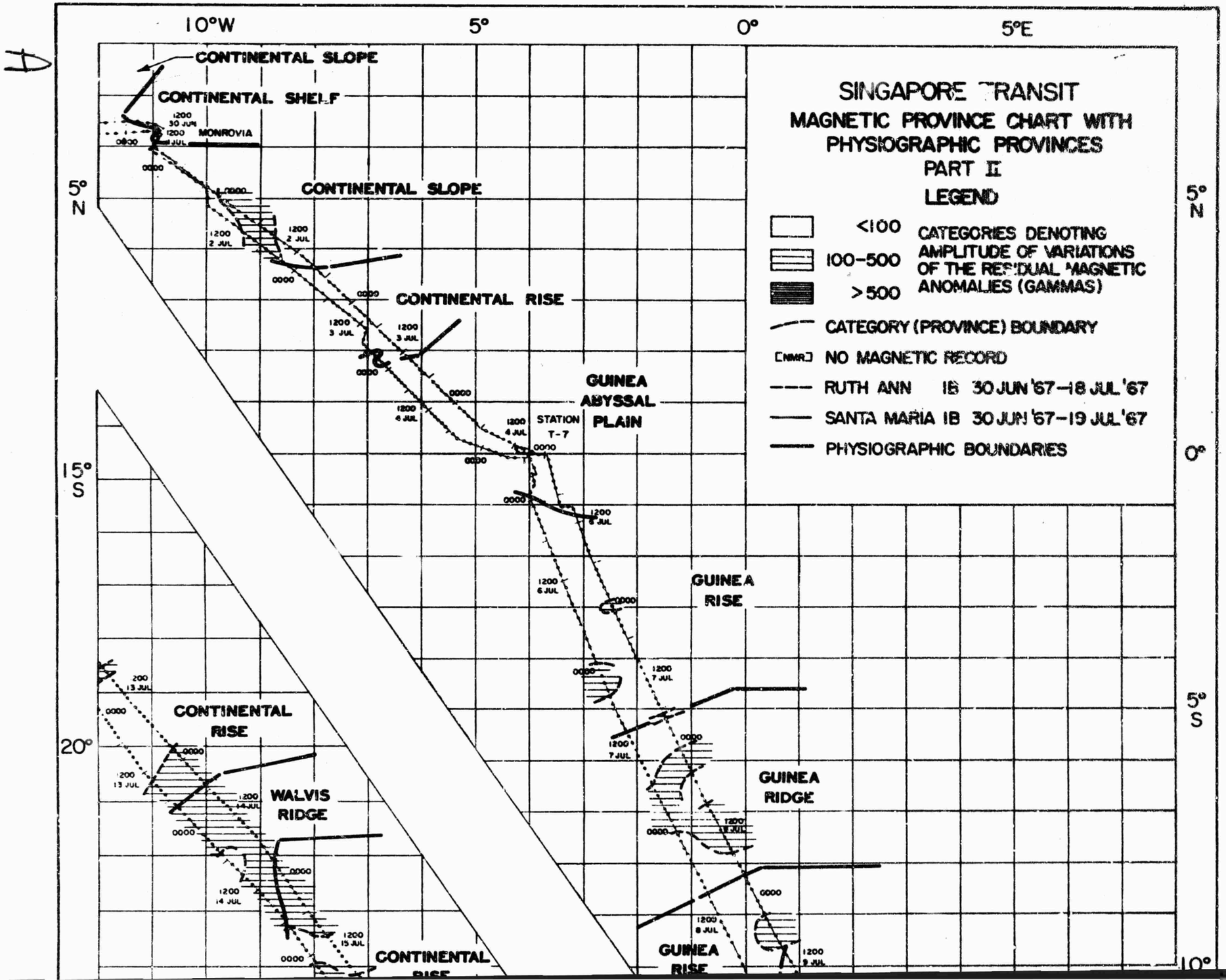
10°W
5°
0°
5°E
5° N
15° S
20°
10°
CONTINENTAL SLOPE
CONTINENTAL SHELF
MONROVIA
CONTINENTAL SLOPE
CONTINENTAL RISE
GUINEA ABYSSAL PLAIN
STATION T-7
GUINEA RISE
CONTINENTAL RISE
WALVIS RIDGE
GUINEA RIDGE
CONTINENTAL RISE
GUINEA RISE
SINGAPORE TRANSIT
MAGNETIC PROVINCE CHART WITH PHYSIOGRAPHIC PROVINCES
PART II
LEGEND
<100 CATEGORIES DENOTING AMPLITUDE OF VARIATIONS OF THE RESIDUAL MAGNETIC ANOMALIES (GAMMAS)
100-500
>500
CATEGORY (PROVINCE) BOUNDARY
NMR NO MAGNETIC RECORD
RUTH ANN IB 30 JUN '67-18 JUL '67
SANTA MARIA IB 30 JUN '67-19 JUL '67
PHYSIOGRAPHIC BOUNDARIES

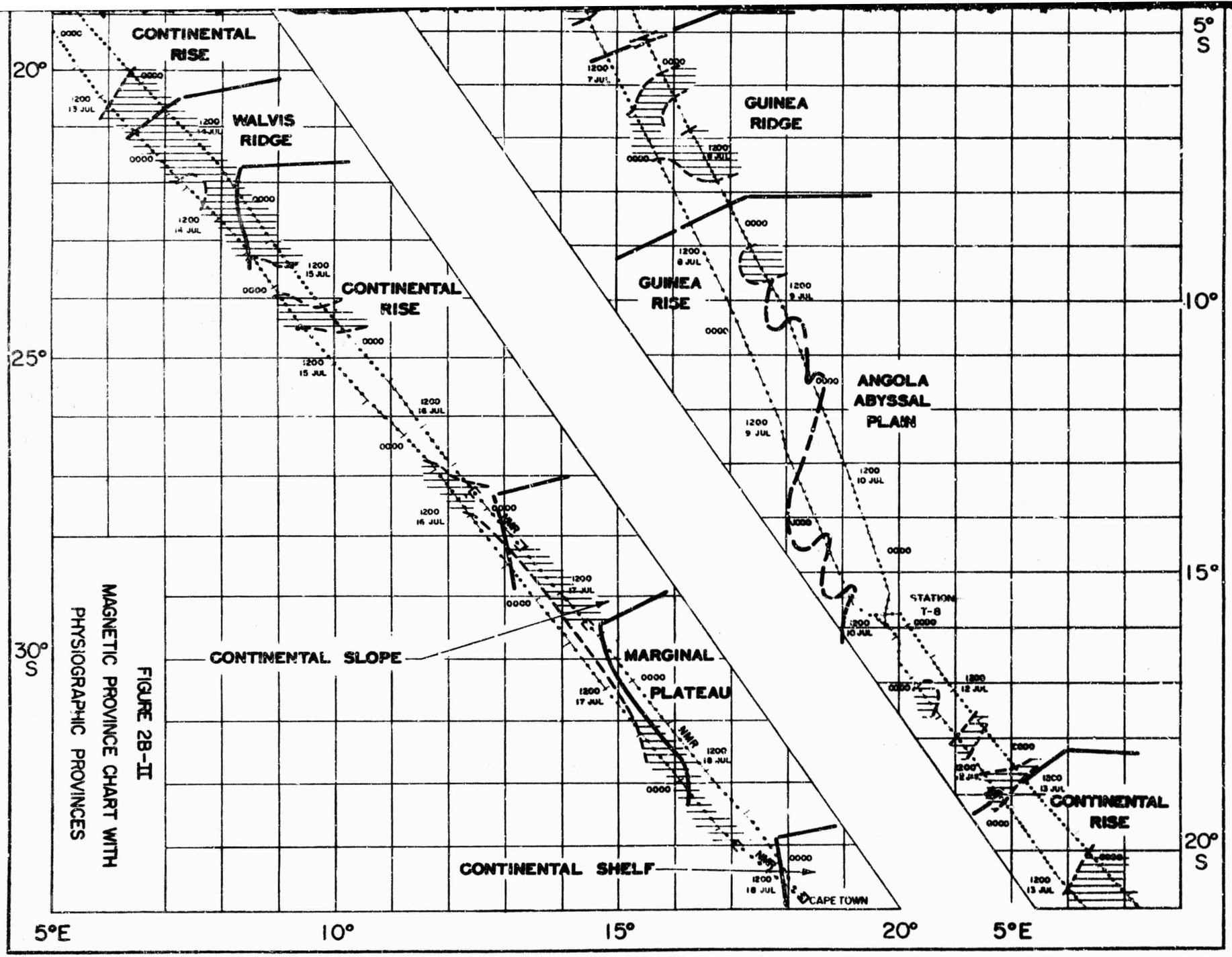

FIGURE 2B-II

B

FIGURE 2B-II

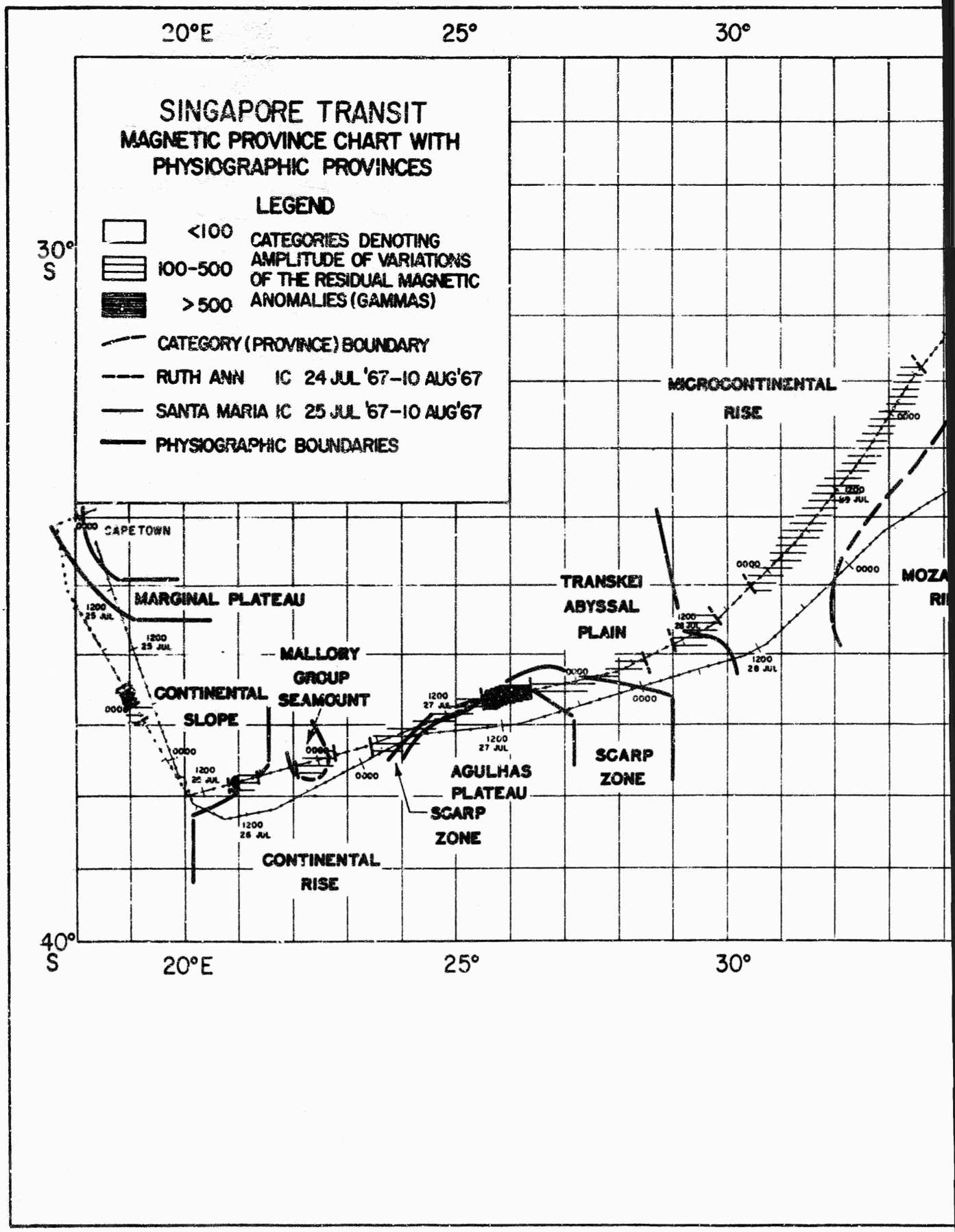
20°E
25°
30°
SINGAPORE TRANSIT
MAGNETIC PROVINCE CHART WITH
PHYSIOGRAPHIC PROVINCES
LEGEND
<100
100-500
>500
CATEGORIES DENOTING AMPLITUDE OF VARIATIONS OF THE RESIDUAL MAGNETIC ANOMALIES (GAMMAS)
CATEGORY (PROVINCE) BOUNDARY
RUTH ANN IC 24 JUL '67–10 AUG'67
SANTA MARIA IC 25 JUL '67–10 AUG'67
PHYSIOGRAPHIC BOUNDARIES
30° S
40° S
CAPETOWN
MARGINAL PLATEAU
CONTINENTAL SLOPE
MALLORY GROUP SEAMOUNT
CONTINENTAL RISE
AGULHAS PLATEAU SCARP ZONE
TRANSKEI ABYSSAL PLAIN
SCARP ZONE
MICROCONTINENTAL RISE
MOZA
RI

A

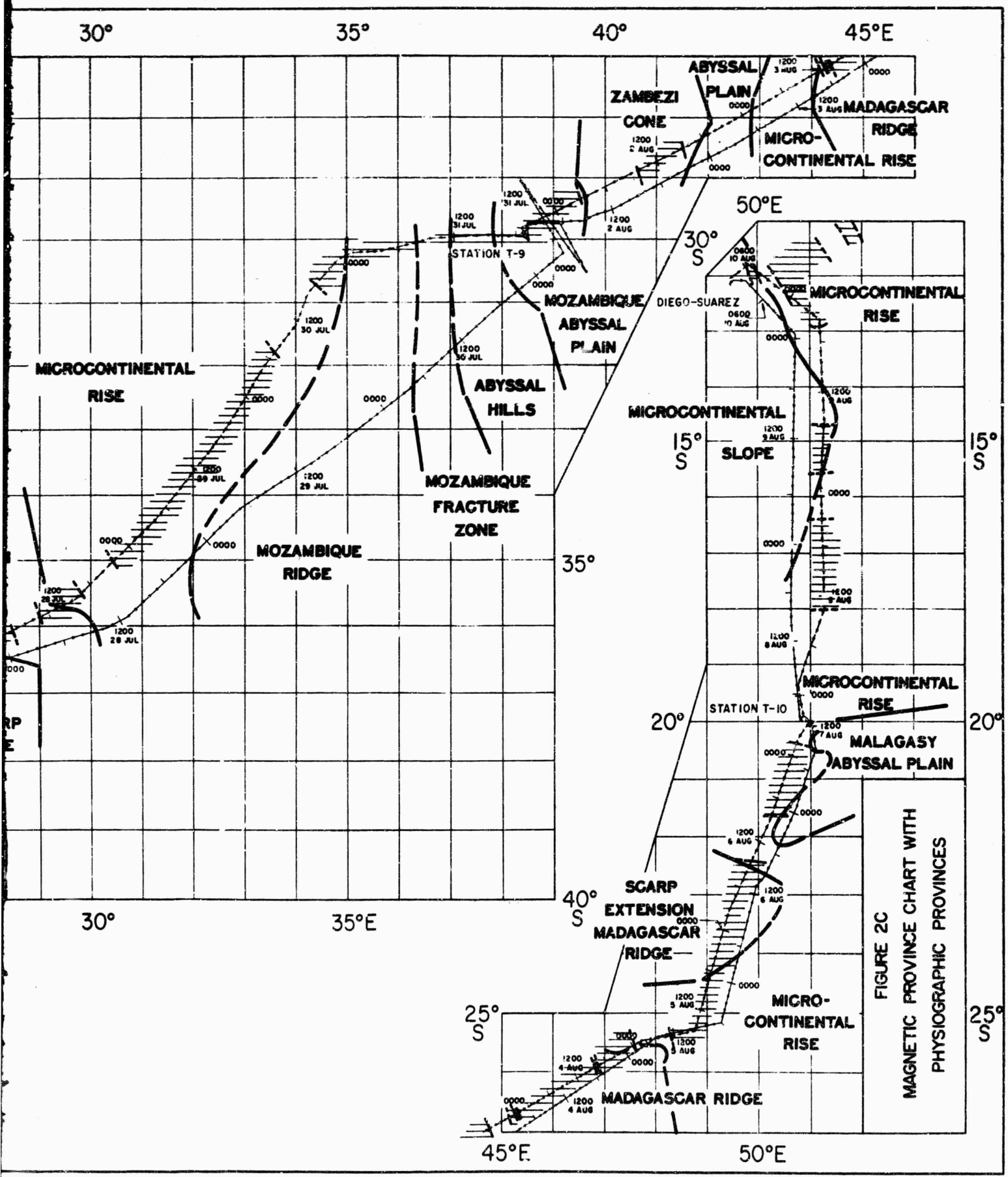
30°
35°
40°
45°E
50°E
30°
S
15°
S
20°
S
25°
S
40°
S
35°
30°
35°E
45°E
50°E
ABYSSAL PLAIN
ZAMBEZI CONE
MADAGASCAR RIDGE
MICRO-CONTINENTAL RISE
STATION T-9
MOZAMBIQUE ABYSSAL PLAIN
DIEGO-SUAREZ
MICROCONTINENTAL RISE
MICROCONTINENTAL RISE
ABYSSAL HILLS
MICROCONTINENTAL SLOPE
MOZAMBIQUE FRACTURE ZONE
MOZAMBIQUE RIDGE
MICROCONTINENTAL RISE
STATION T-10
MALAGASY ABYSSAL PLAIN
SCARP
EXTENSION
MADAGASCAR RIDGE
MICRO-CONTINENTAL RISE
MADAGASCAR RIDGE
FIGURE 2C
MAGNETIC PROVINCE CHART WITH PHYSIOGRAPHIC PROVINCES

B

FIGURE 2C

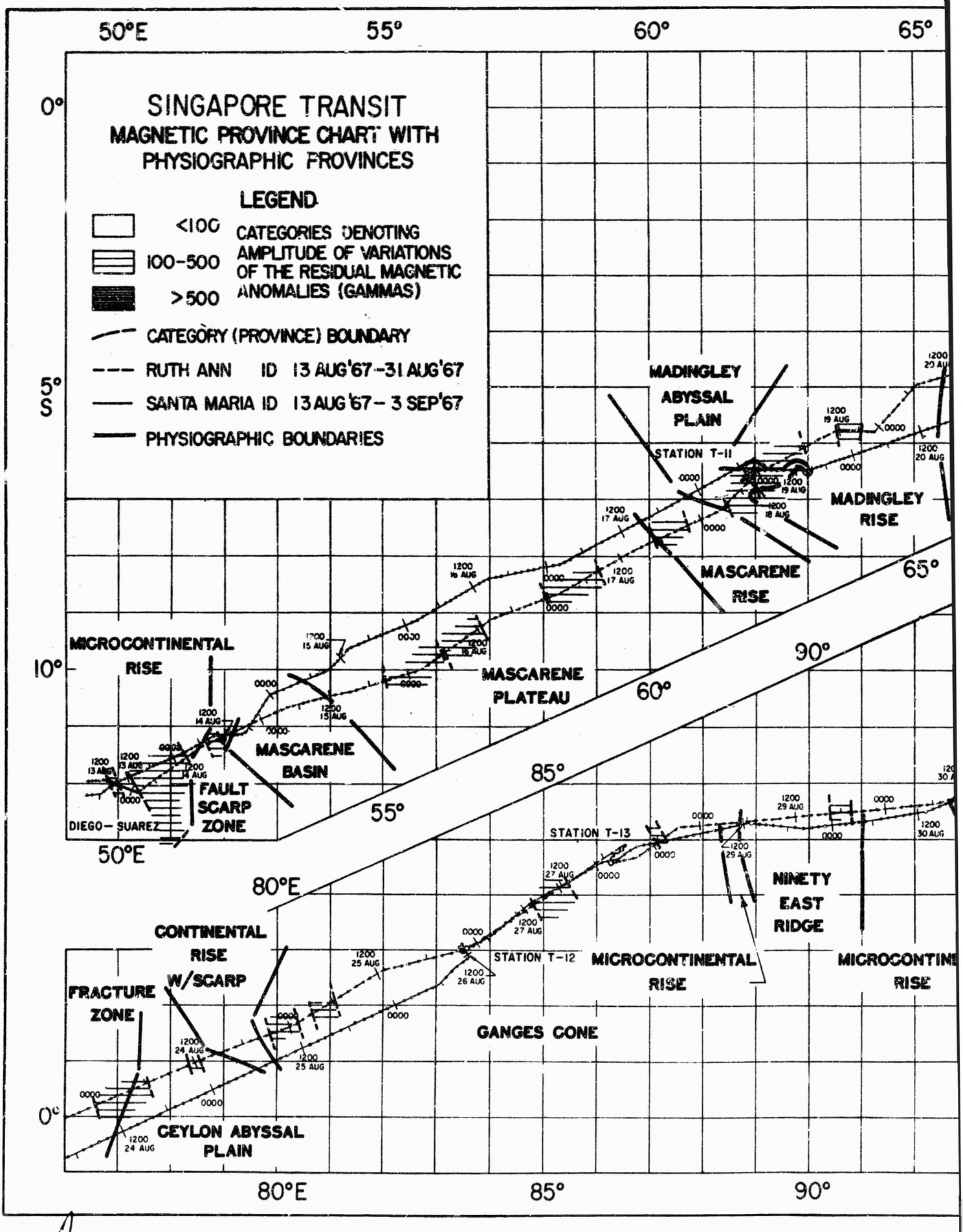
SINGAPORE TRANSIT
MAGNETIC PROVINCE CHART WITH PHYSIOGRAPHIC PROVINCES
LEGEND
<100
100-500
>500
CATEGORIES DENOTING AMPLITUDE OF VARIATIONS OF THE RESIDUAL MAGNETIC ANOMALIES (GAMMAS)
CATEGORY (PROVINCE) BOUNDARY
RUTH ANN ID 13 AUG'67-31 AUG'67
SANTA MARIA ID 13 AUG'67 - 3 SEP'67
PHYSIOGRAPHIC BOUNDARIES
50°E
55°
60°
65°
0°
5° S
10°
80°E
85°
90°
MADINGLEY ABYSSAL PLAIN
MADINGLEY RISE
STATION T-11
MASCARENE RISE
MASCARENE PLATEAU
MASCARENE BASIN
MICROCONTINENTAL RISE
FAULT SCARP ZONE
DIEGO-SUAREZ
STATION T-13
NINETY EAST RIDGE
MICROCONTINENTAL RISE
STATION T-12
CONTINENTAL RISE W/SCARP
FRACTURE ZONE
GANGES CONE
CEYLON ABYSSAL PLAIN

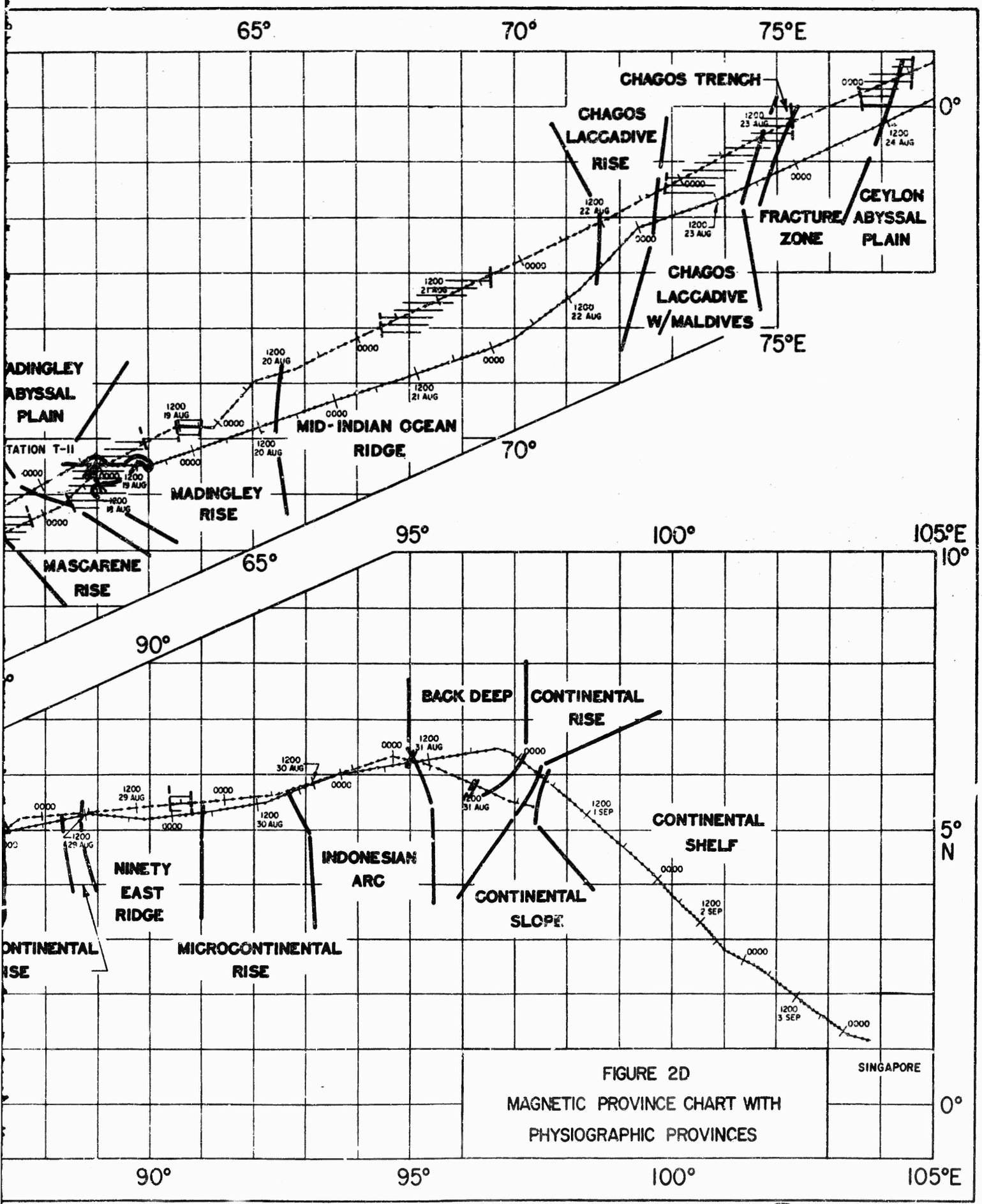

FIGURE 2D
MAGNETIC PROVINCE CHART WITH
PHYSIOGRAPHIC PROVINCES

B FIGURE 2D

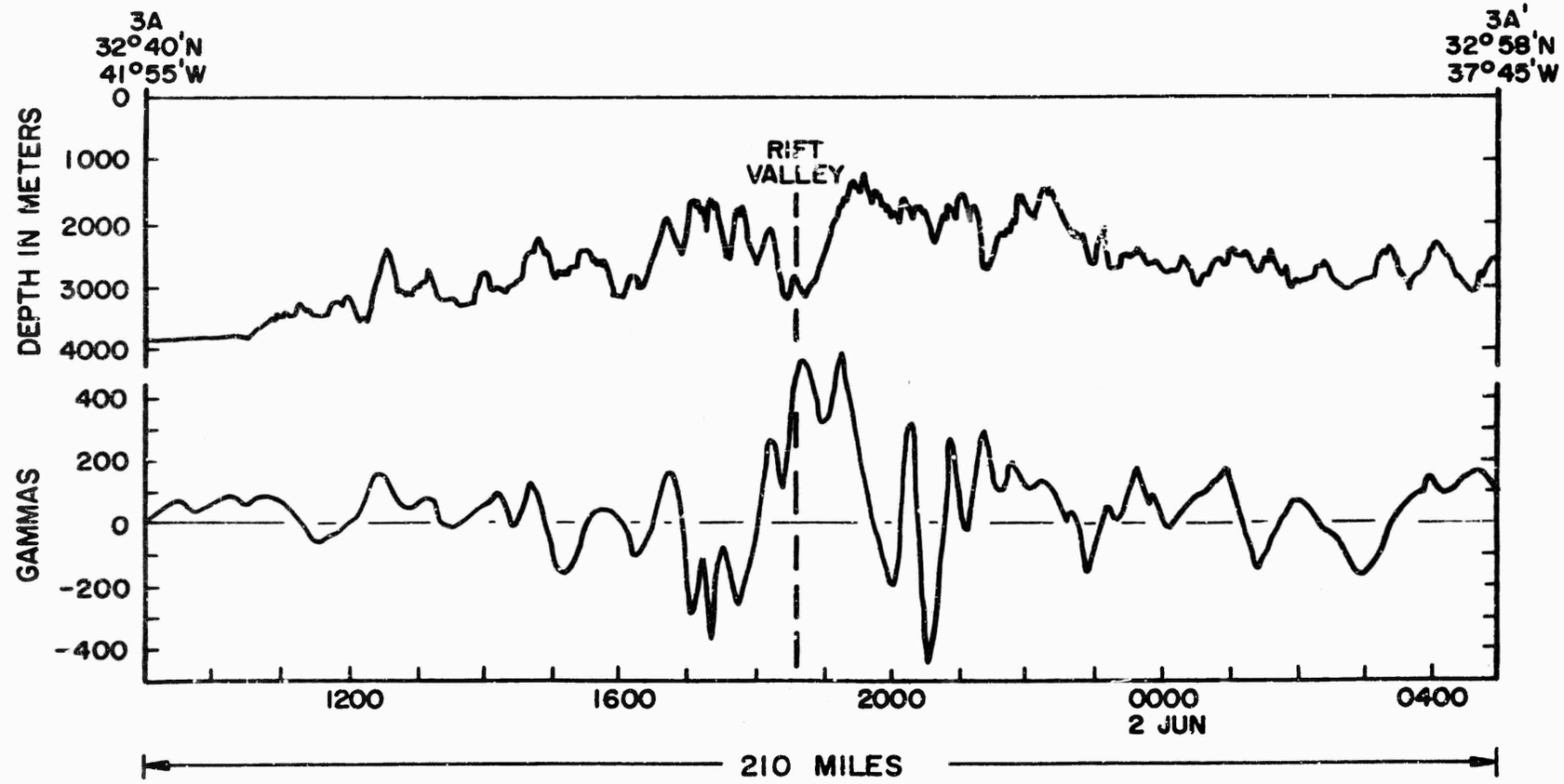

FIG. 3 BATHYMETRIC AND MAGNETIC PROFILES ACROSS THE CENTRAL PORTION OF THE MID-ATLANTIC RIDGE

FIGURE 3

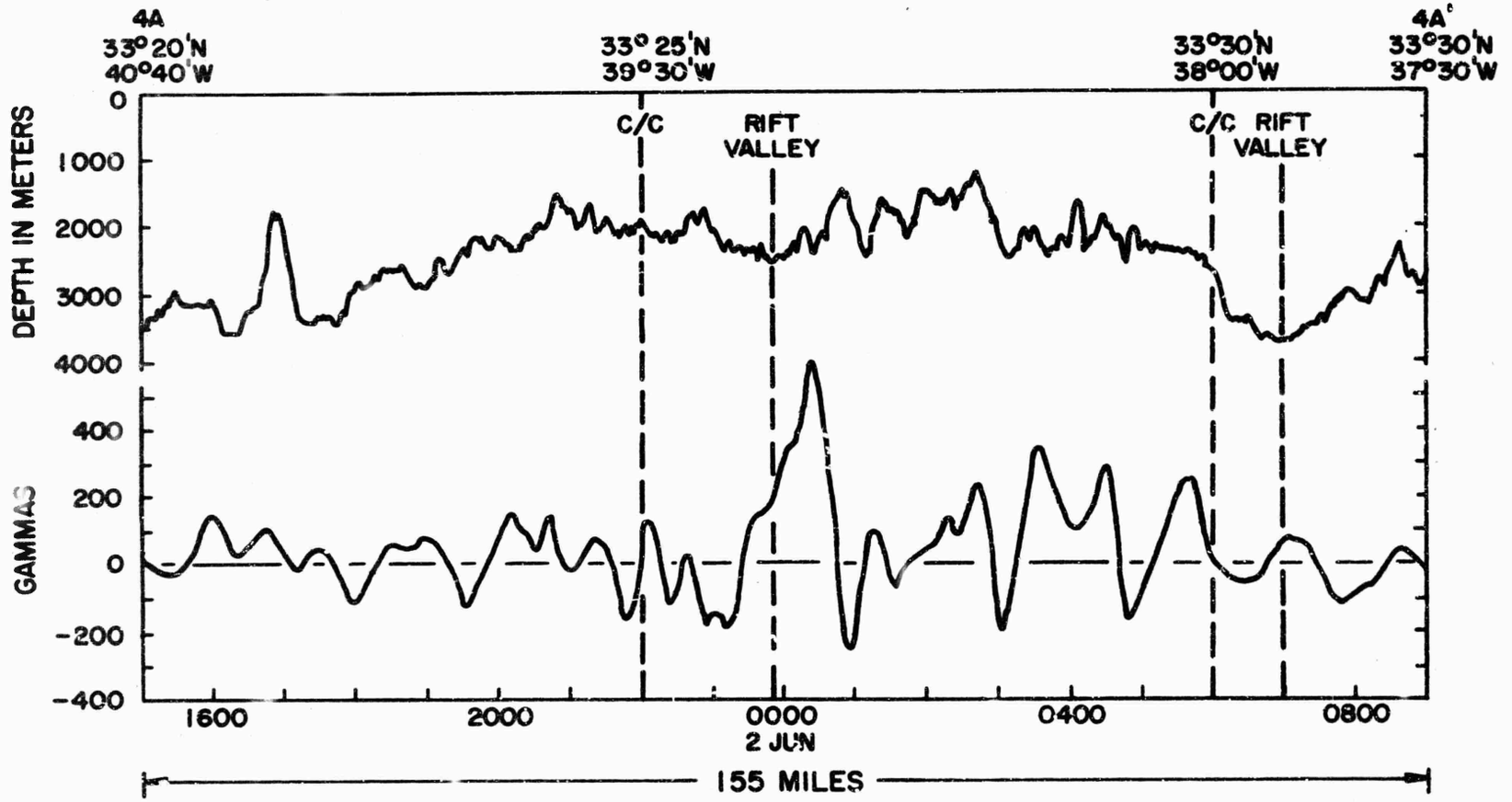

FIG. 4 BATHYMETRIC AND MAGNETIC PROFILES ACROSS THE CENTRAL PORTION OF THE MID-ATLANTIC RIDGE

FIGURE 4

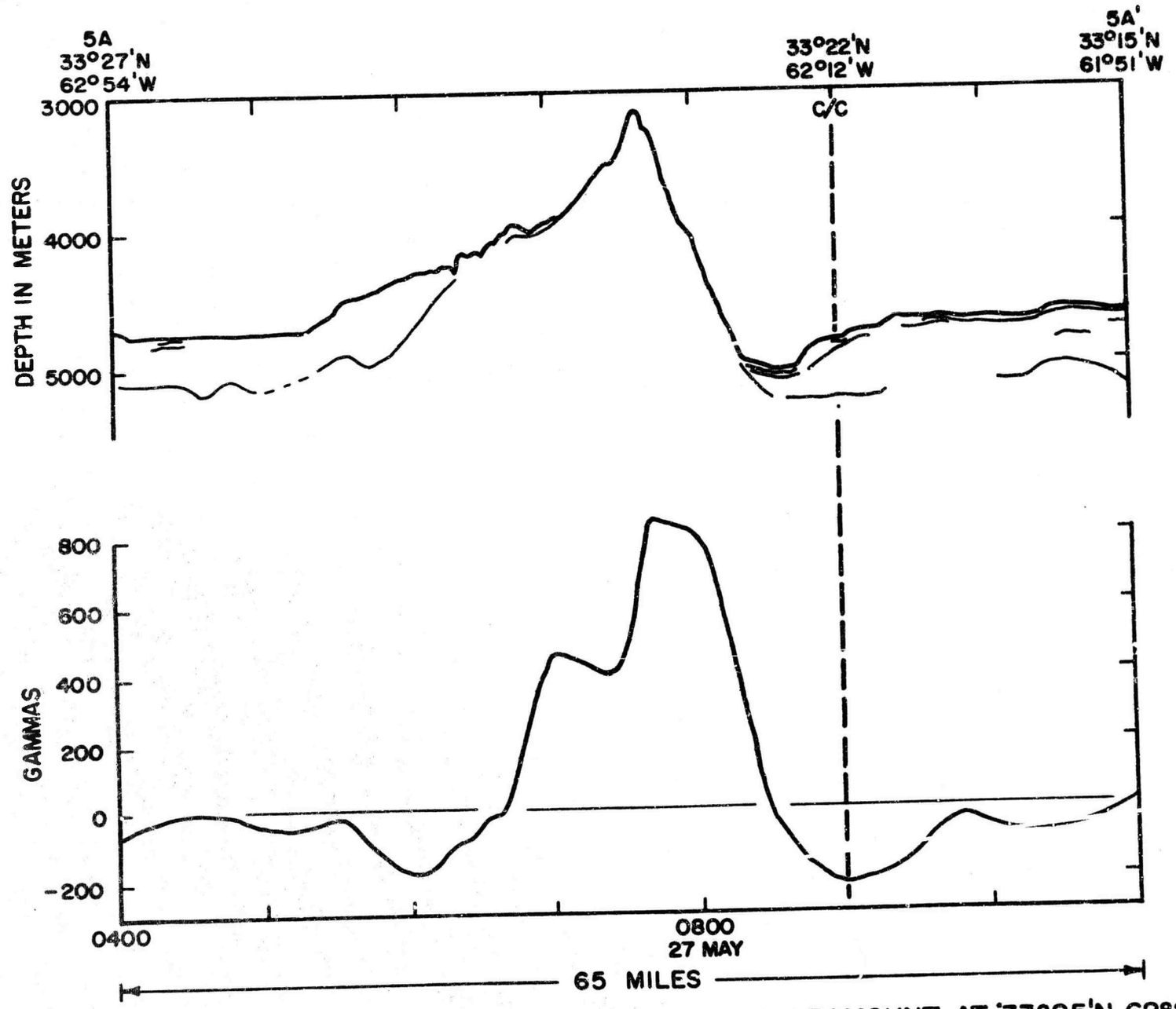

FIG. 5 BATHYMETRIC AND MAGNETIC PROFILES ACROSS A SEAMOUNT AT 33°25'N, 62°20'W.

FIGURE 5

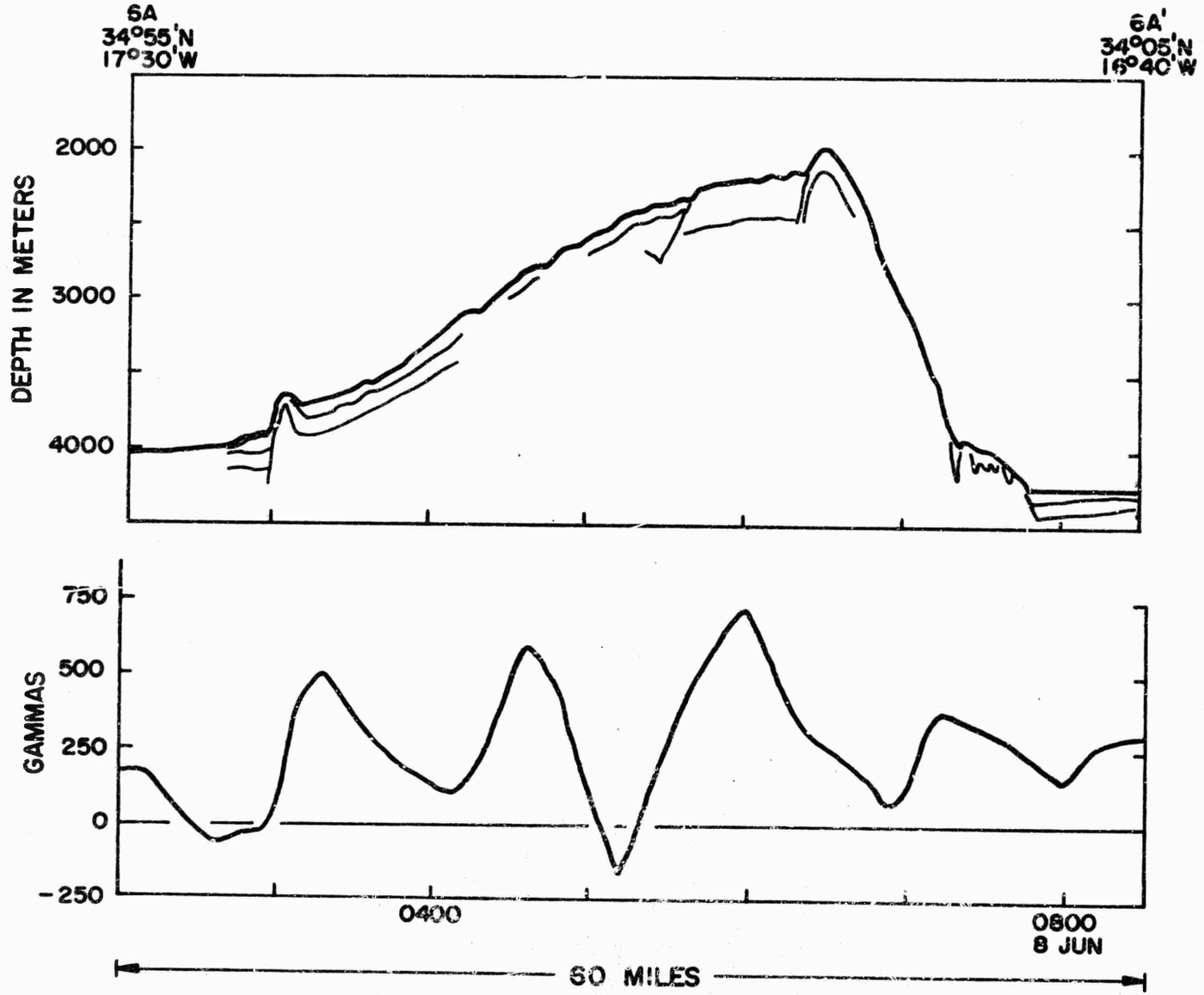

FIG.6 BATHYMETRIC AND MAGNETIC PROFILES ACROSS A SEAMOUNT IN THE HORSESHOE SEAMOUNT GROUP

FIGURE 6

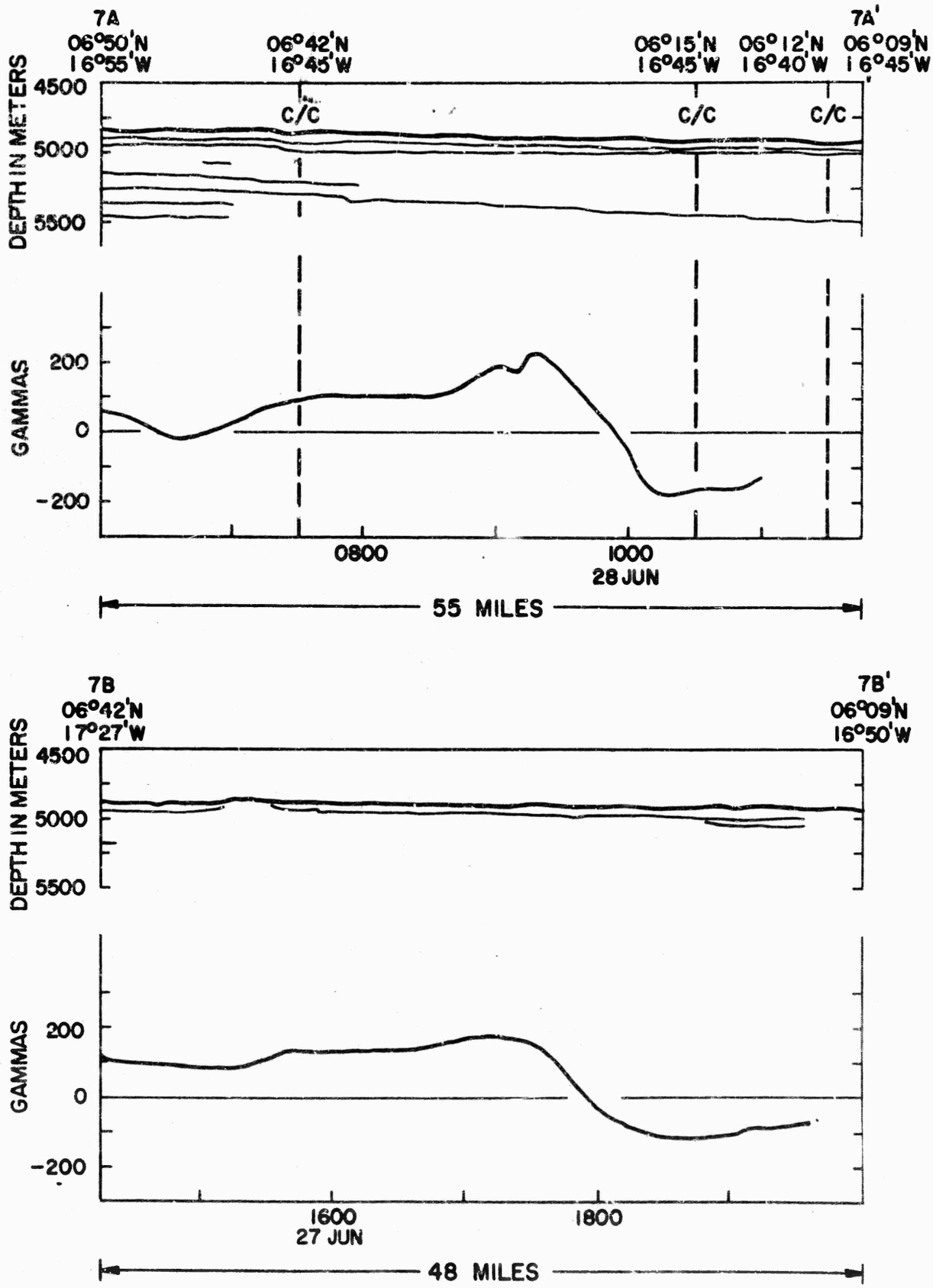

FIGS. 7A & 7B BATHYMETRIC AND MAGNETIC PROFILES AT 06°20'N, 17°00'W

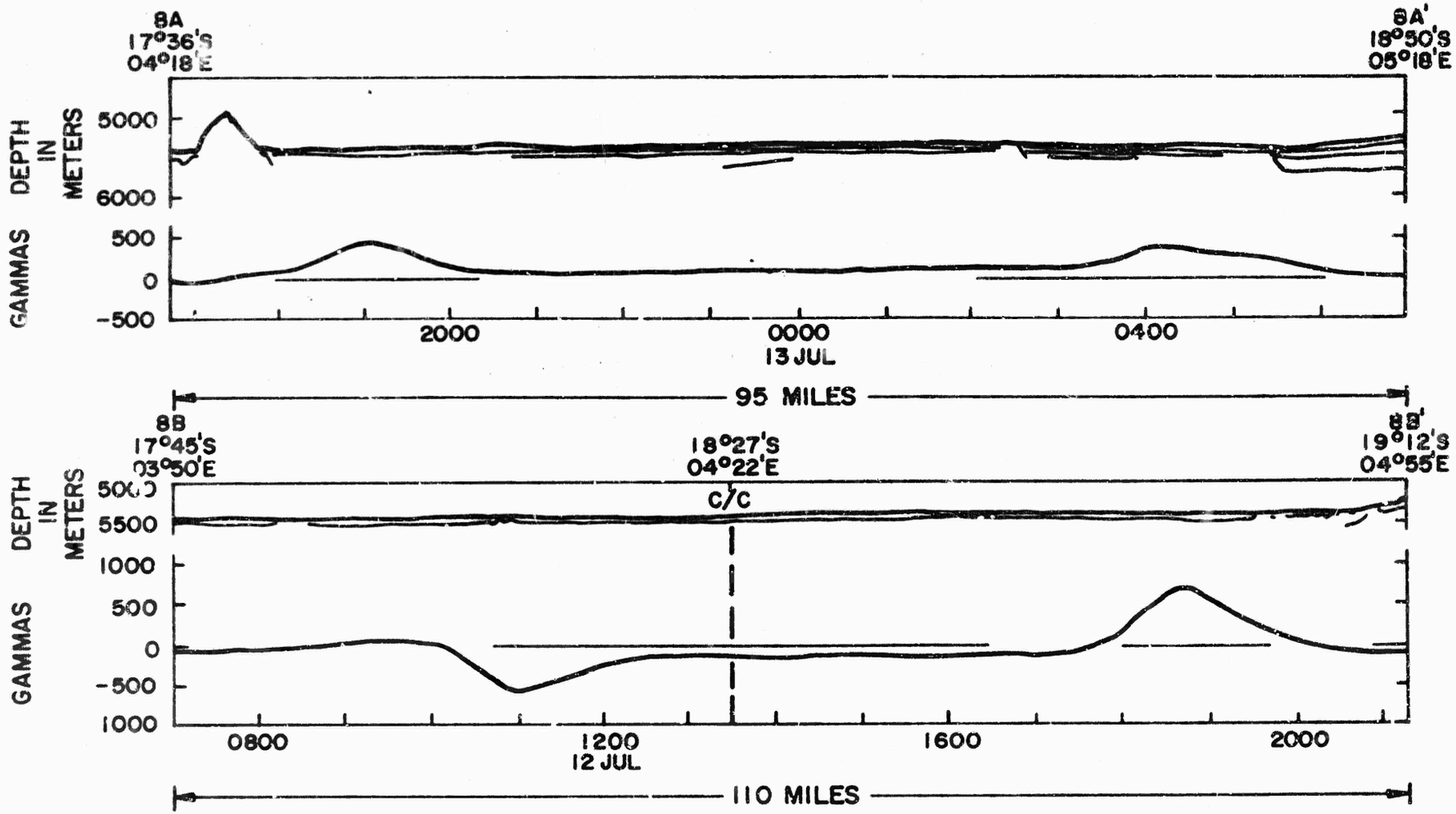

FIG. 8A & 8B BATHYMETRIC AND MAGNETIC PROFILES AT THE SOUTHEASTERN END OF THE ANGOLA ABYSSAL PLAIN

FIG. 8A & 8B

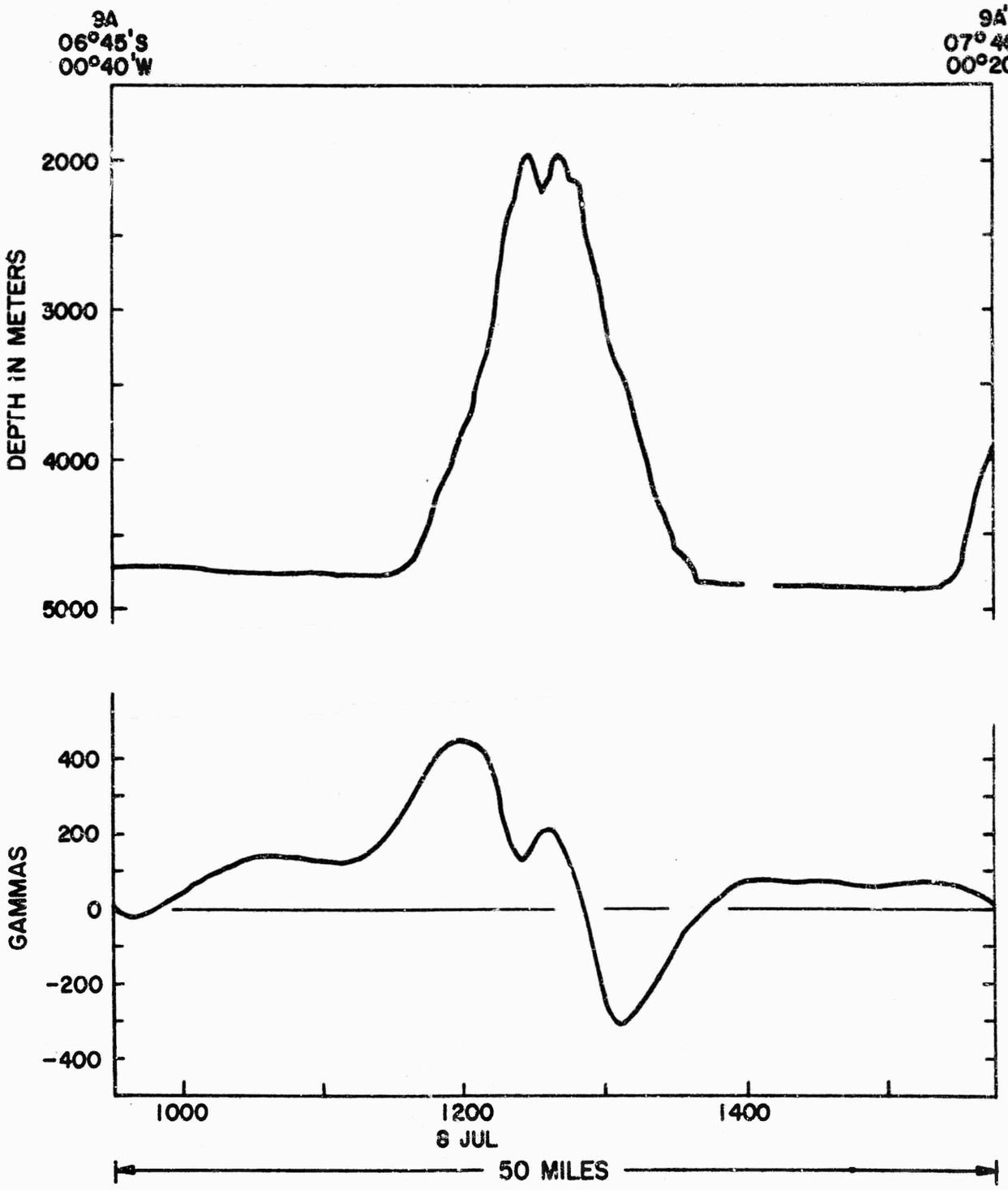

FIG. 9 BATHYMETRIC AND MAGNETIC PROFILES OF A SEAMOUNT ON GUINEA RIDGE

FIGURE 9

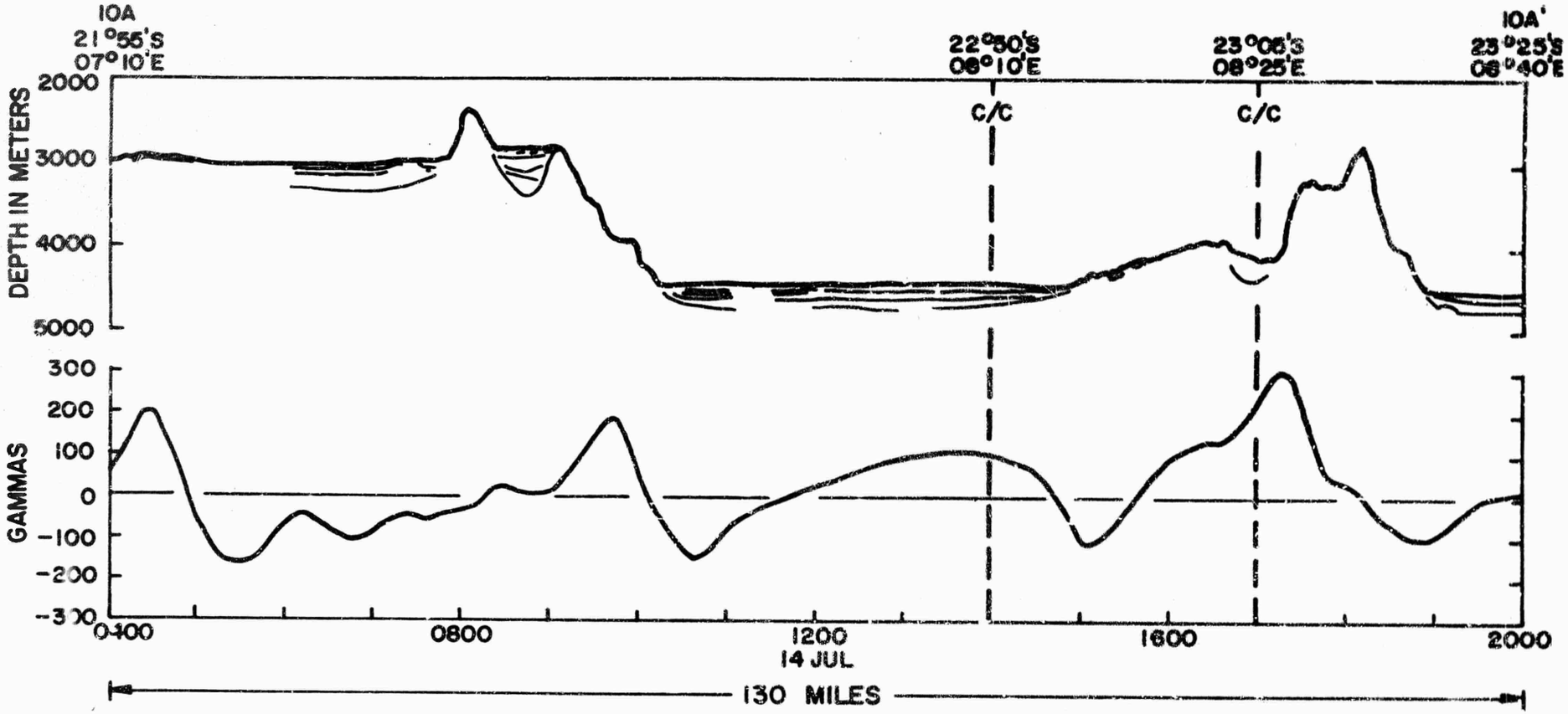

FIG. 10 BATHYMETRIC AND MAGNETIC PROFILES ACROSS A PORTION OF WALVIS RIDGE

FIGURE 10

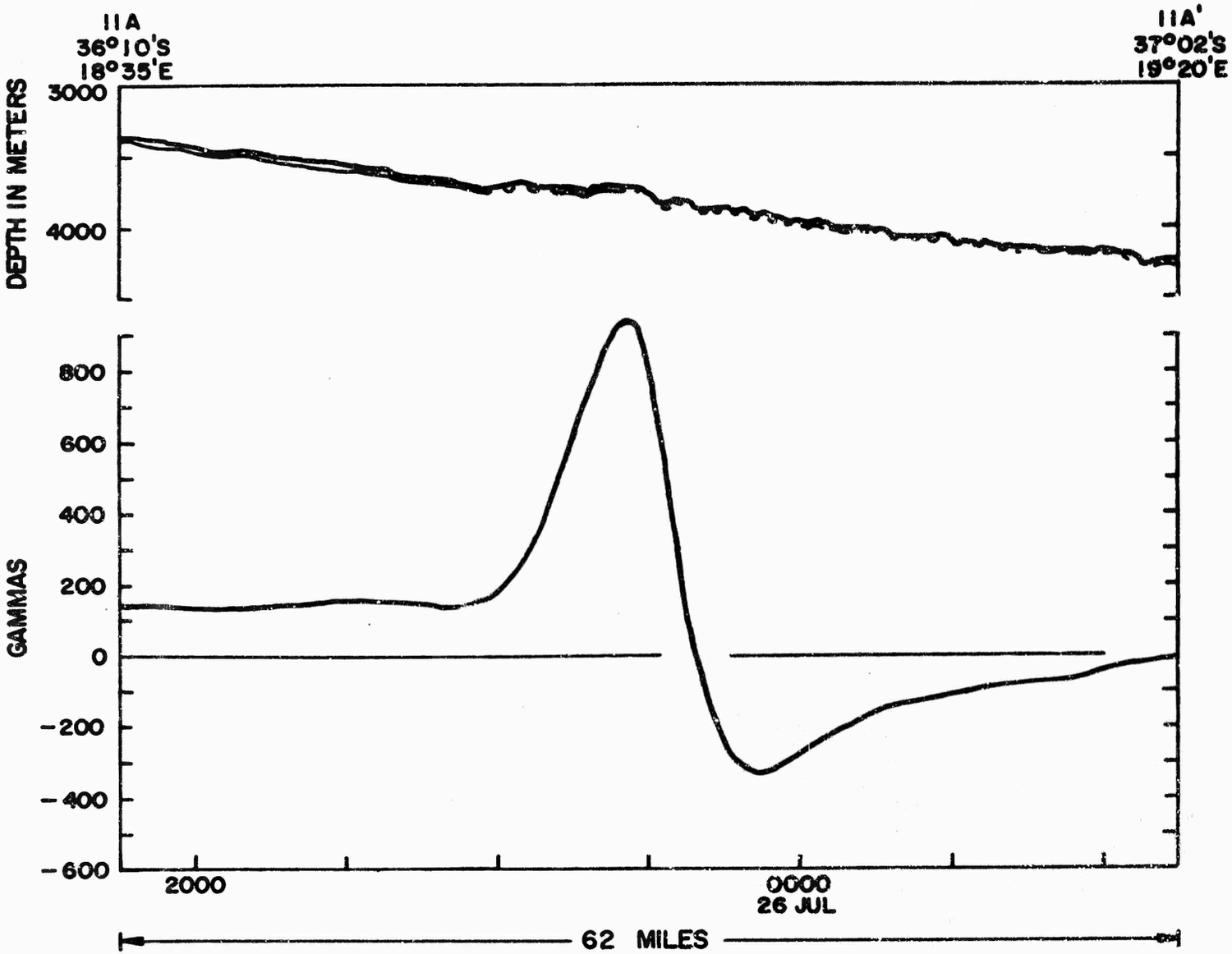

FIGURE 11

FIG. 11 BATHYMETRIC AND MAGNETIC PROFILES ACROSS THE SLOPE SOUTH OF CAPETOWN

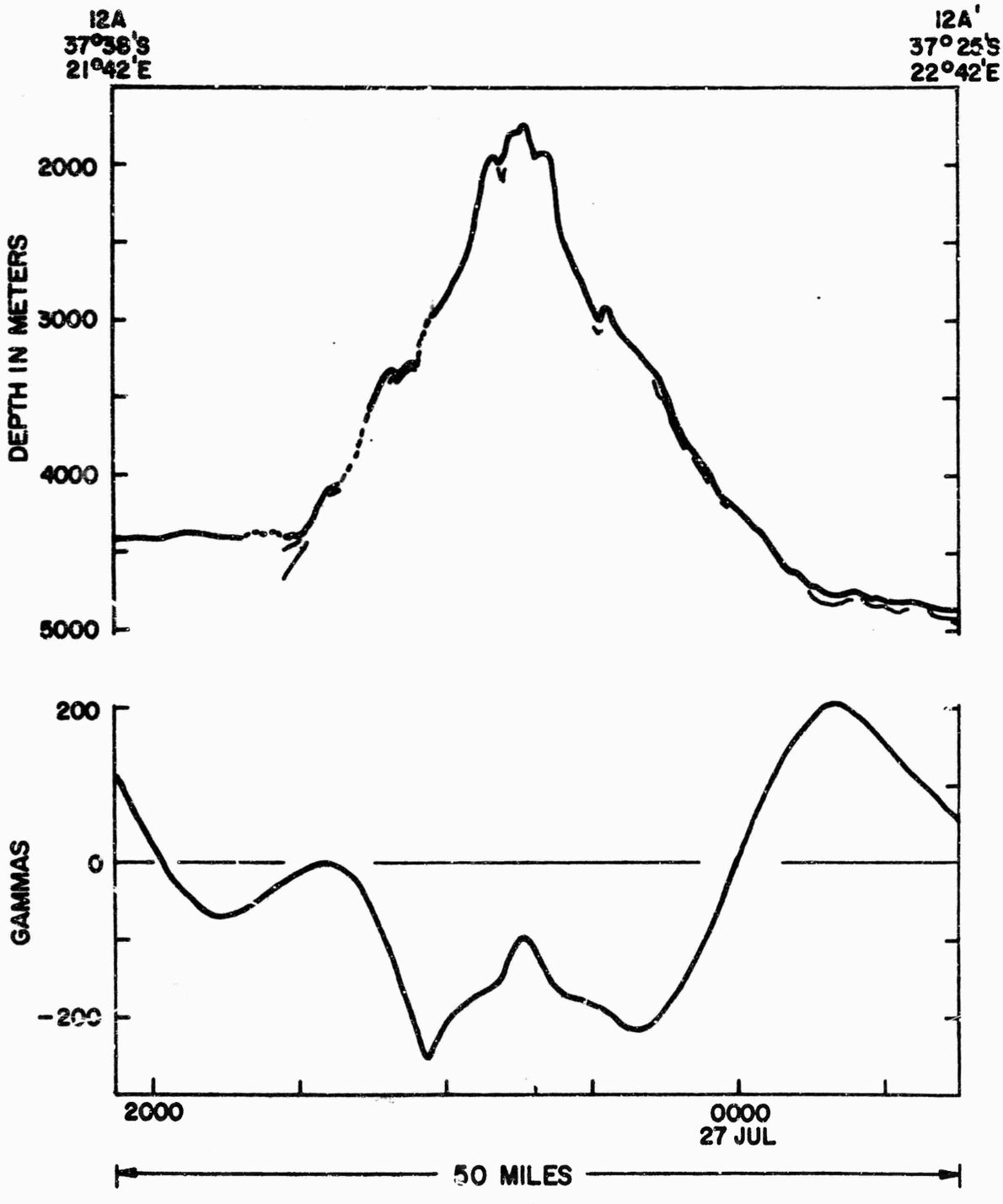

FIG. 12 BATHYMETRIC AND MAGNETIC PROFILES OF A SEAMOUNT IN THE MALLORY SEAMOUNT GROUP

FIGURE 12

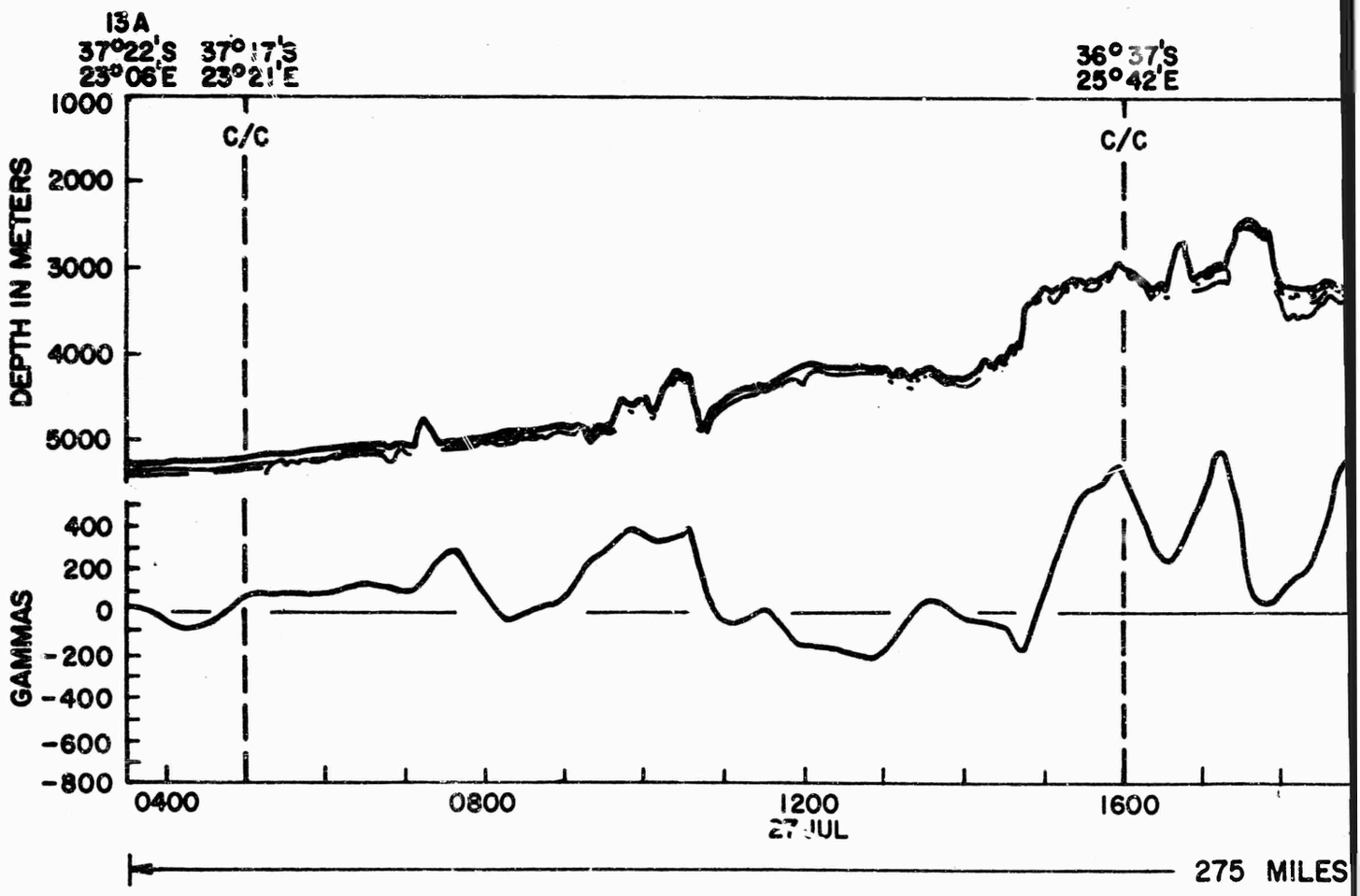

FIG. 13 BATHYMETRIC AND MAGNETIC PROFILES ACROS

A

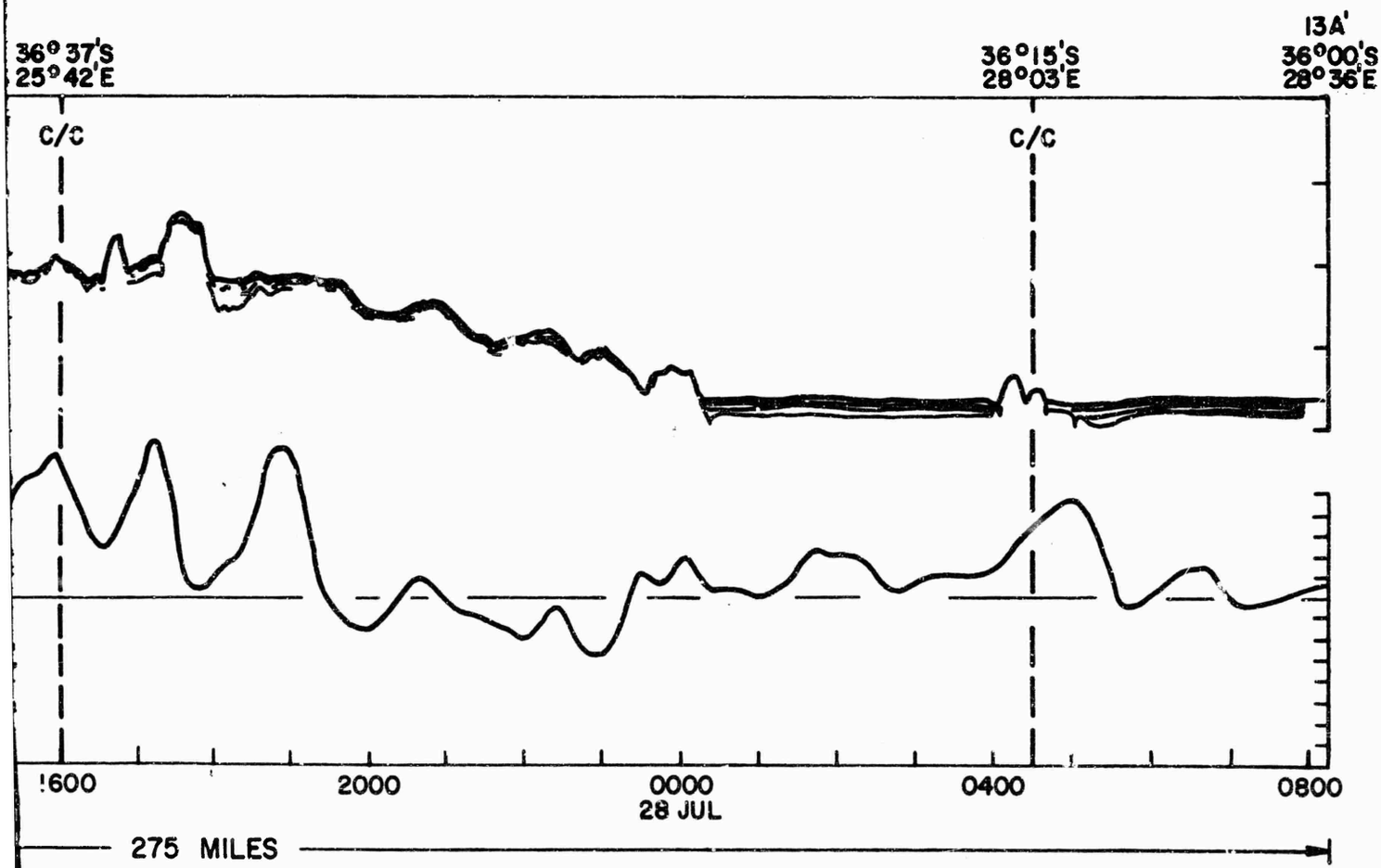

PROFILES ACROSS A PORTION OF THE AGULHAS PLATEAU

B

FIGURE 13

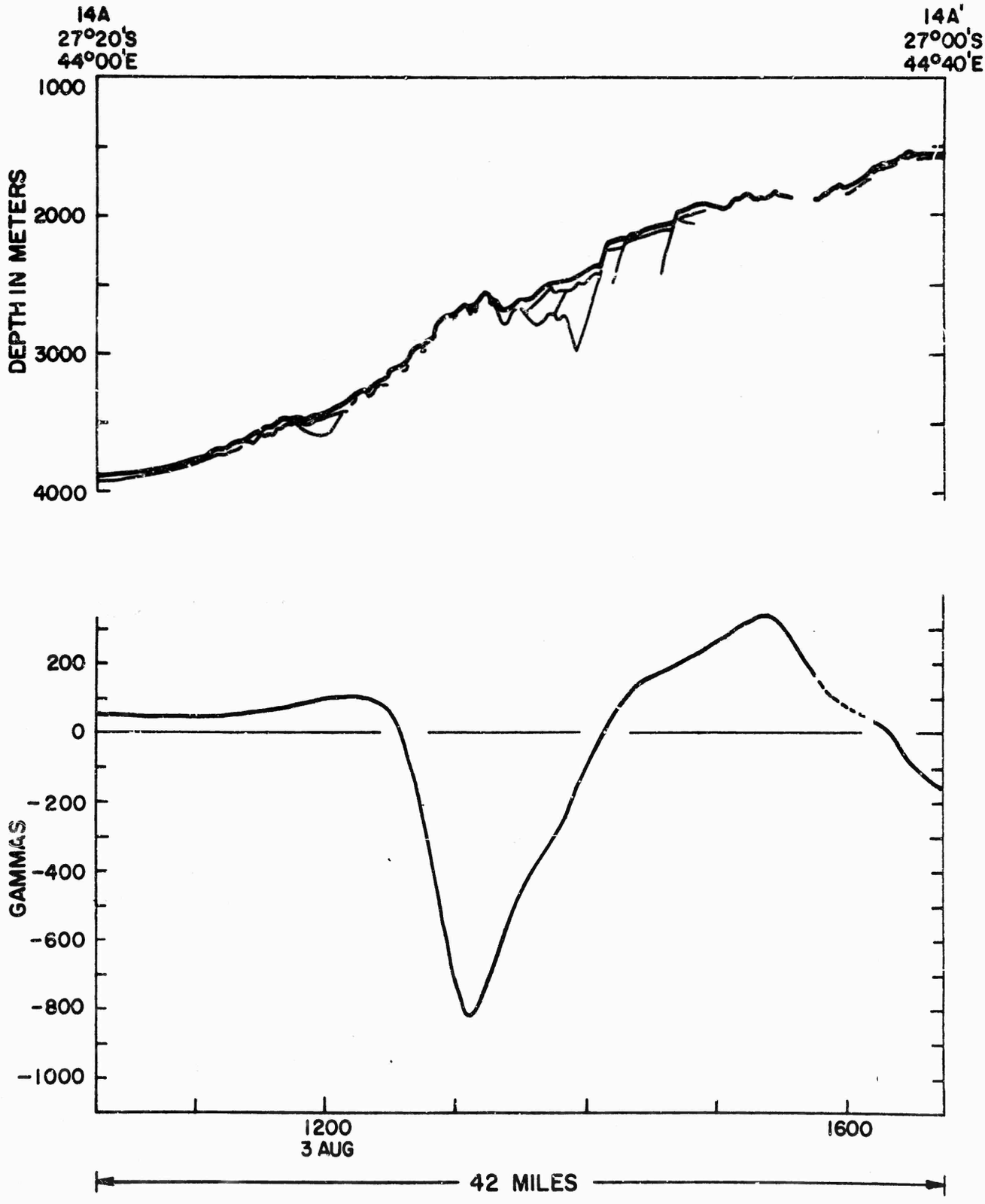

FIG. 14 BATHYMETRIC AND MAGNETIC PROFILES ACROSS THE PRINCE EDWARD FRACTURE ZONE

FIGURE 14

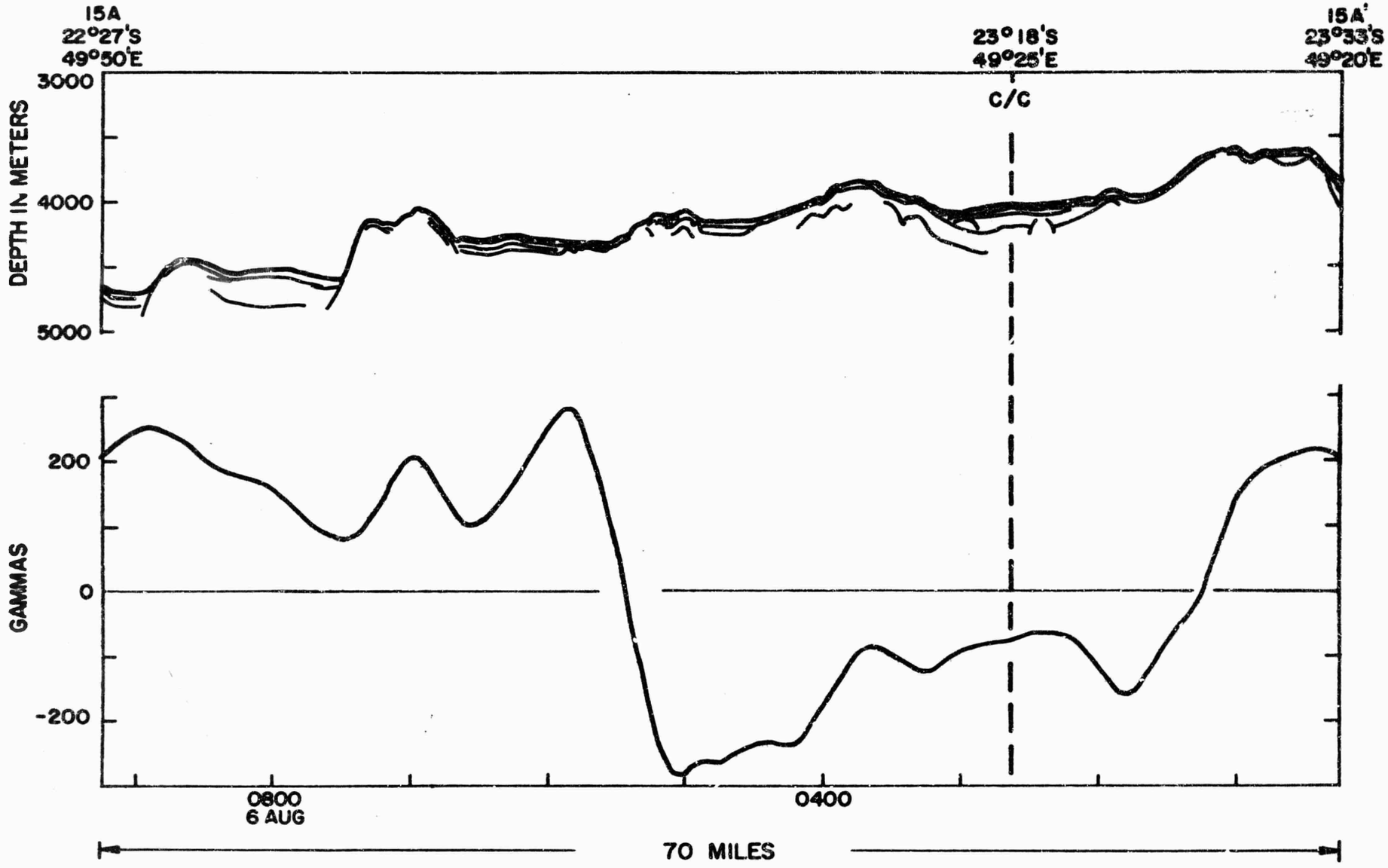

FIGURE 15

FIG. 15 BATHYMETRIC AND MAGNETIC PROFILES ACROSS A PORTION OF THE MADAGASCAR RIDGE EXTENSION

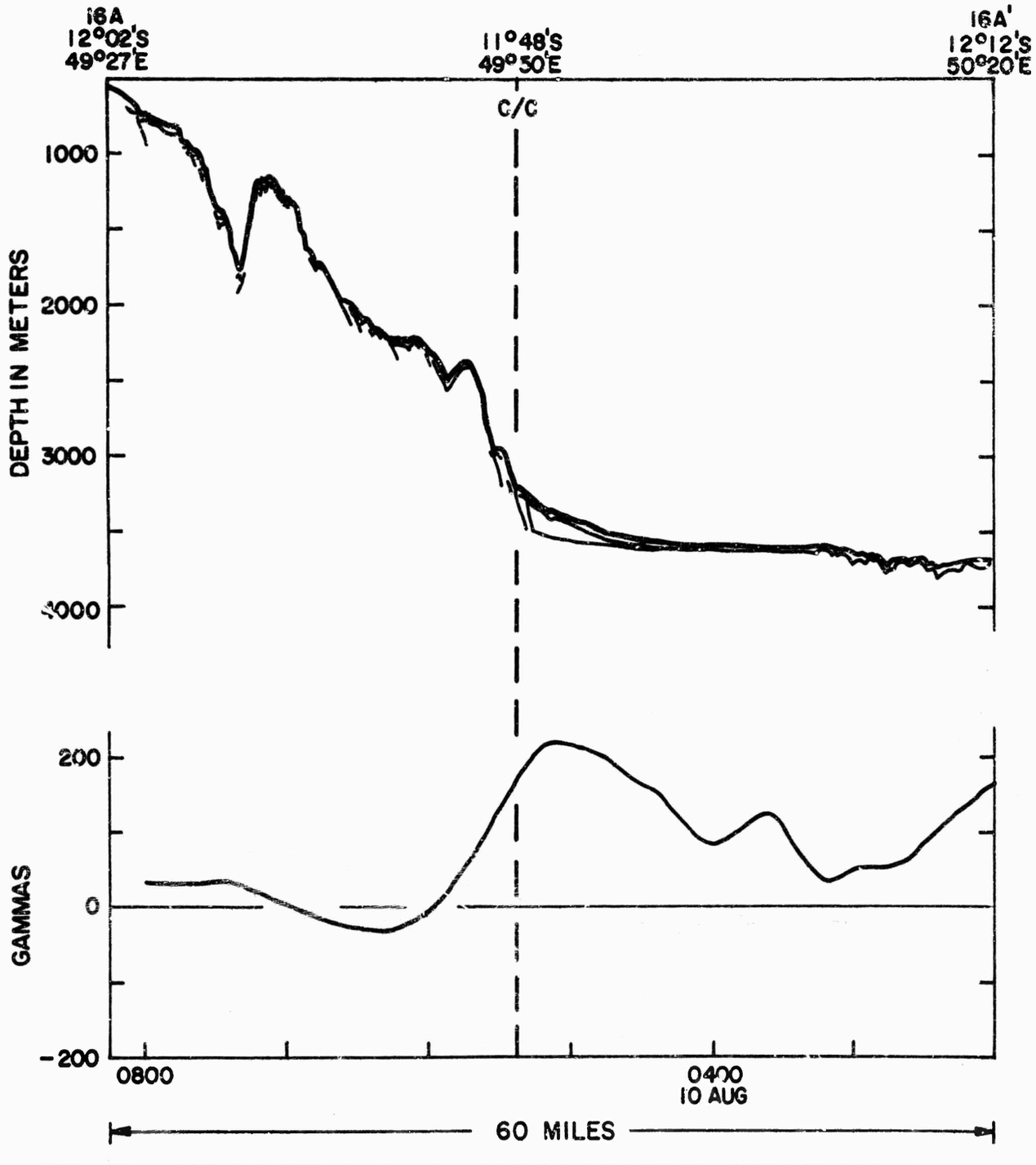

FIG. 16 BATHYMETRIC AND MAGNETIC PROFILES ACROSS THE SLOPE AND RISE EAST OF DIEGO SUAREZ

FIGURE 16

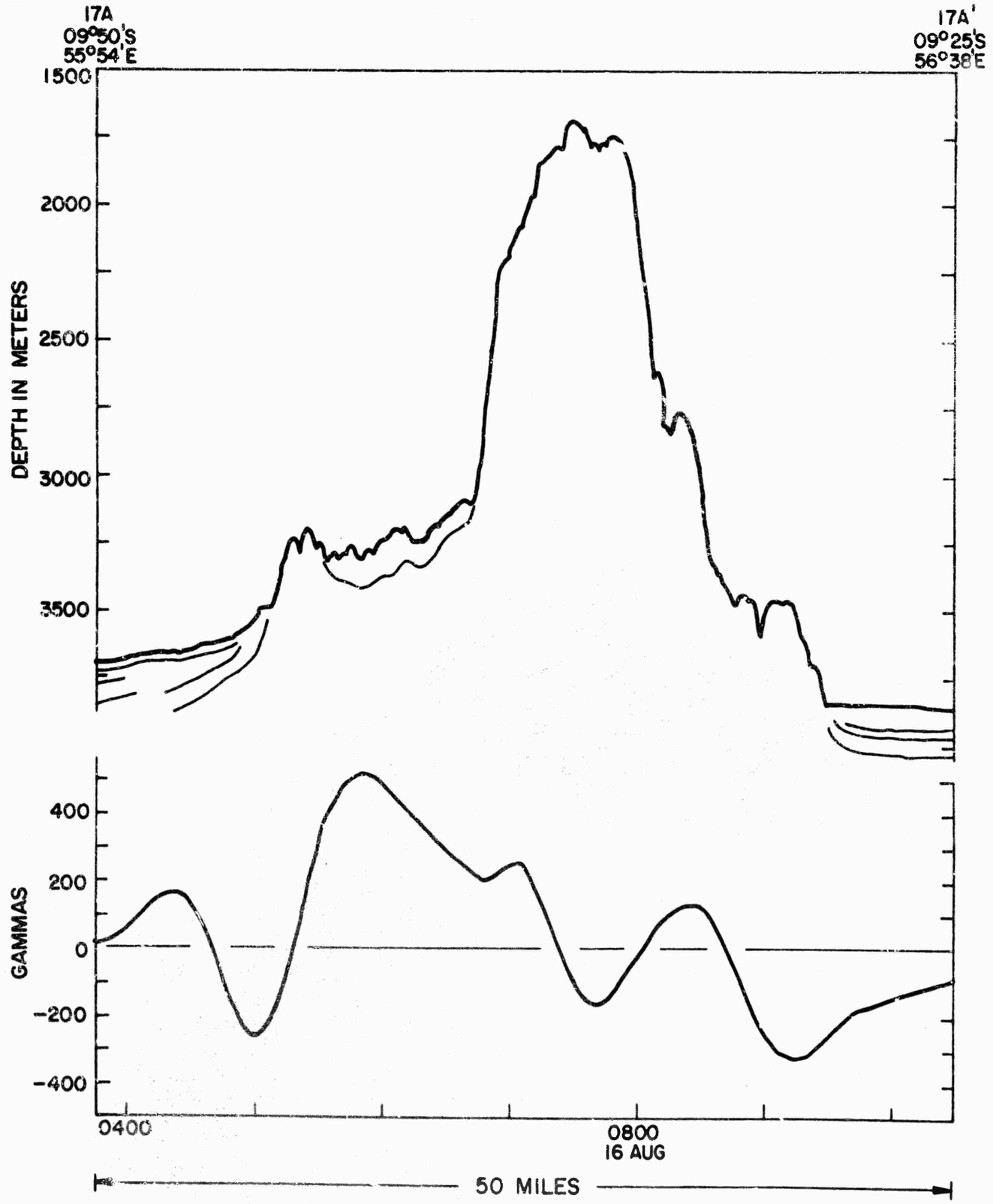

FIG. 17 BATHYMETRIC AND MAGNETIC PROFILES ACROSS A PORTION OF THE MASCARENE PLATEAU AND RIDGE SYSTEM

FIGURE 17

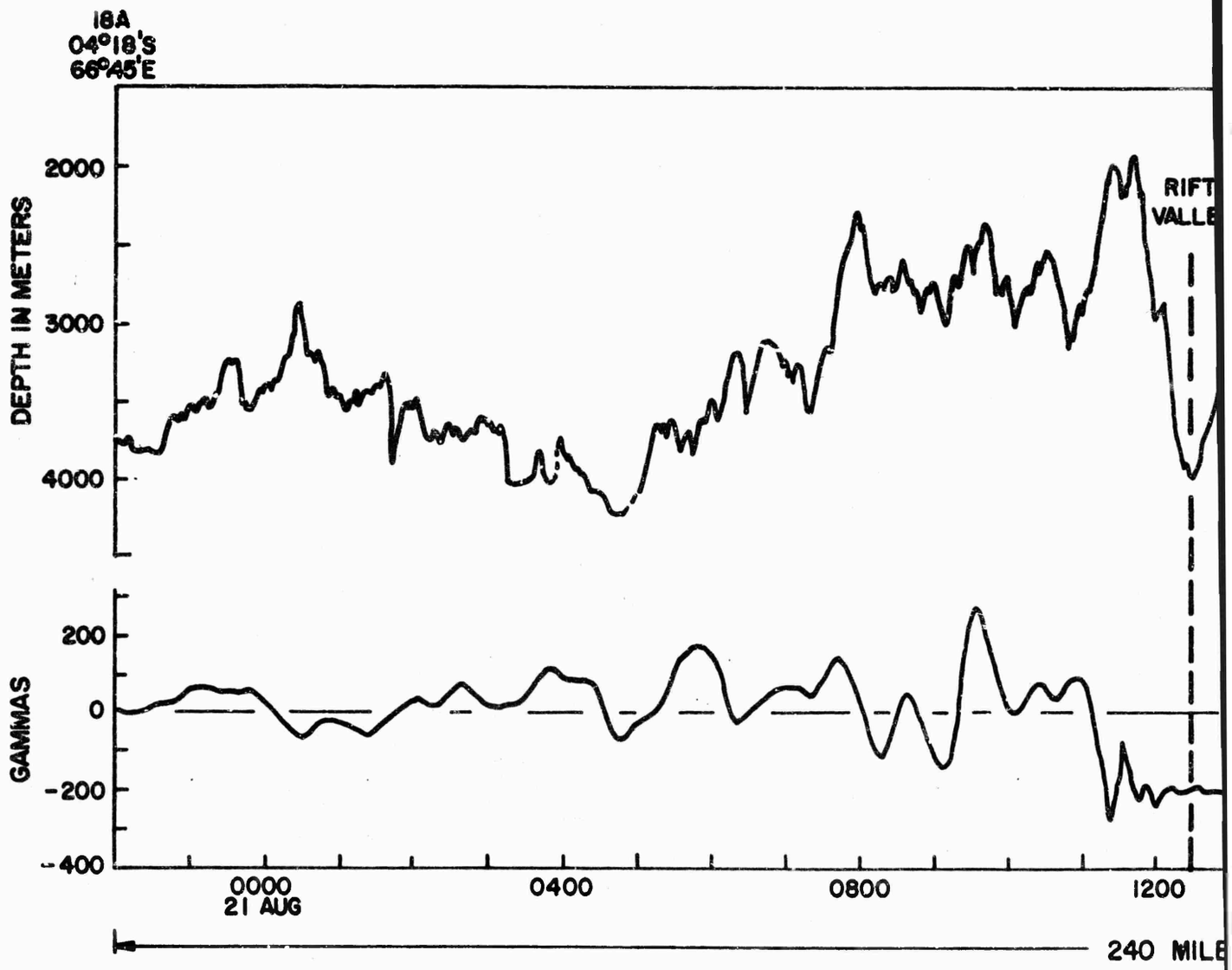

FIG. 18 BATHYMETRIC AND MAGNETIC PROFILES ACROS

A

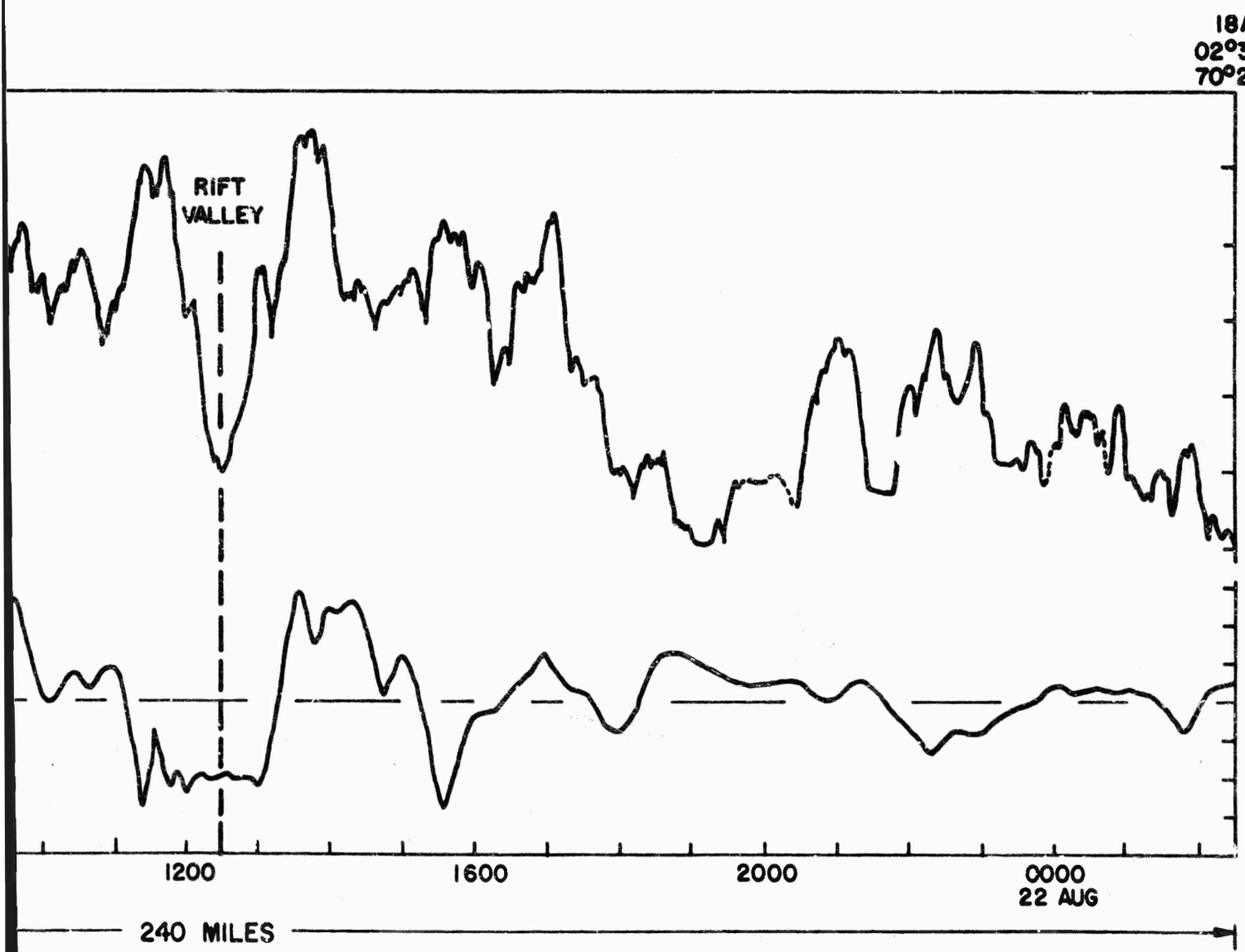

PROFILES ACROSS THE MID-INDIAN OCEAN (CARLSBERG) RIDGE

B

FIGURE 18

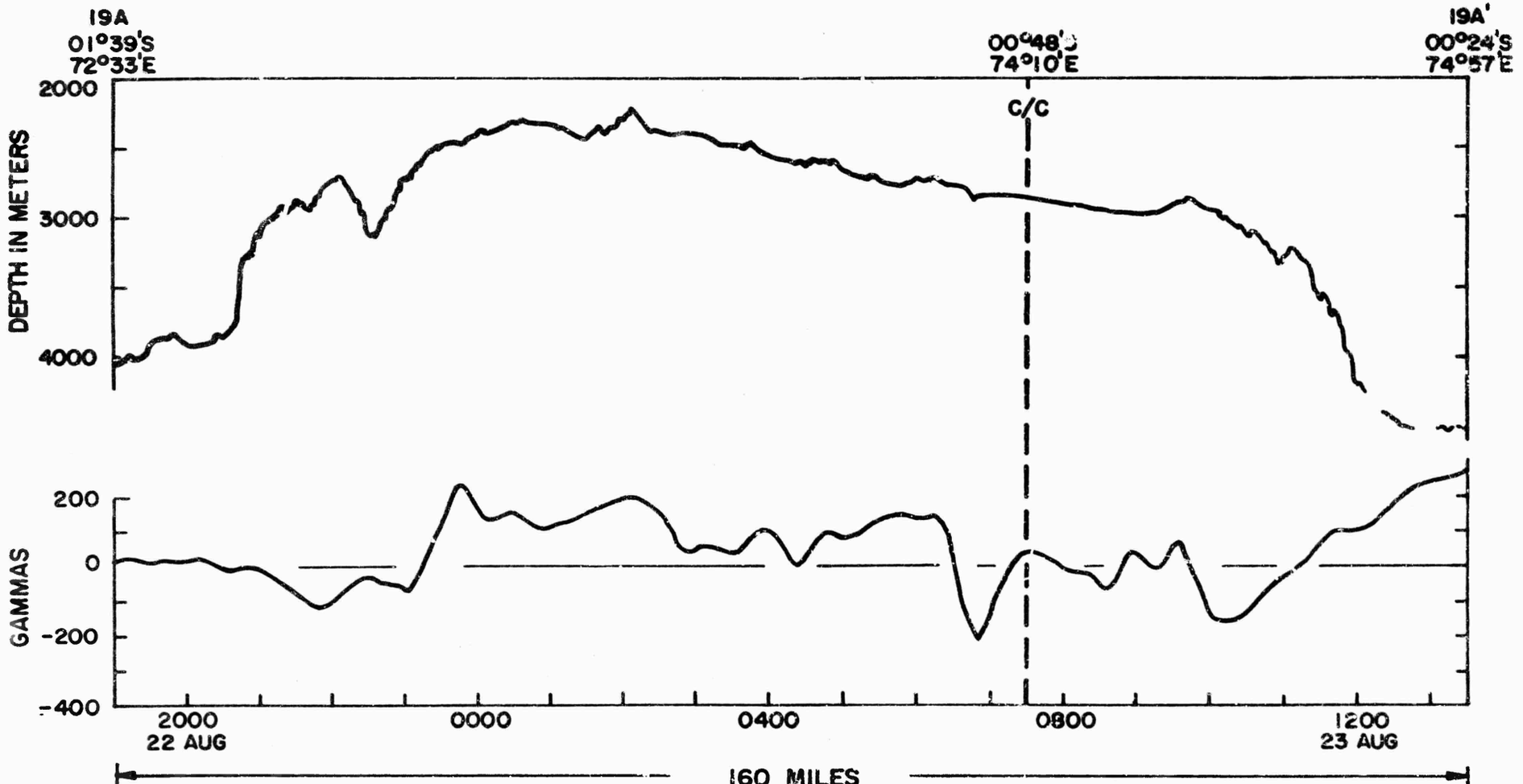

FIGURE 19

FIG. 19 BATHYMETRIC AND MAGNETIC PROFILES ACROSS THE CHAGOS–LACCADIVE PLATEAU

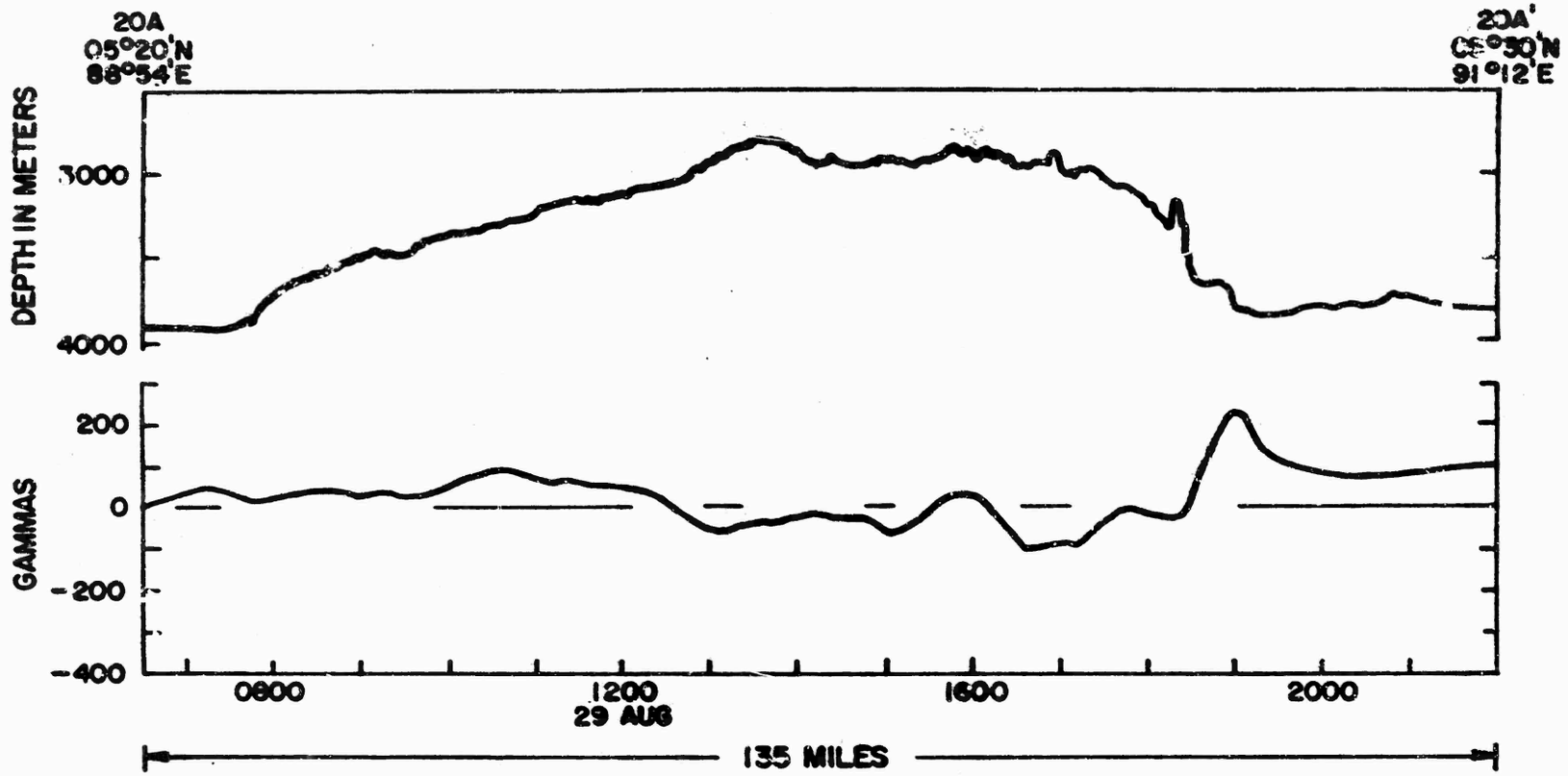

FIG. 20 BATHYMETRIC AND MAGNETIC PROFILES ACROSS THE NINETY EAST RIDGE

FIGURE 20

PART III

AREA ST VOLUME 2

CORE DATA

by

C. Lair and P. Sanko

VOLUME 2, PART III

TABLE OF CONTENTS

VOLUME 2, PART III

LIST OF PLATES

LIST OF TABLES

LIST OF FIGURES IN APPENDIX

I - Introduction

As part of the transit survey by the R/V Santa Maria and R/V Ruth Ann, eight core and six camera stations were occupied by the R/V Ruth Ann. The core and camera locations were made to correspond to acoustic station locations and are numbered according to the acoustic station numbers. From these stations seven piston cores, three in the south eastern Atlantic Ocean and four in the Indian Ocean, were recovered and five of the camera stations produced bottom photographs. The sediment was analyzed to determine its physical properties, calcium carbonate content and acoustic properties. These various properties are then related to each other and to a general geologic description of the sediment in order to point out trends between the several variables. A description of the physiographic provinces in which the cores were taken is found in Part I (Henry, 1969) of this volume.

II - Shipboard Procedures

A. Cores

The cores were taken with a Ewing-type piston corer using a 1200 pound weight-stand and modified by inserting a polycarbonate liner inside the core pipe. This yields a core of about two and a quarter inches in diameter. Normal shipboard procedures for coring were employed (Alpine Geophysical Associates, Inc., 1965). The liner was extruded, labeled, cut, and sealed in five foot sections. The sections were then stored upright in the hold with the uppermost sediment at the top. Shipment to the laboratory was done in Conex boxes in order to keep the cores vertical during the transit period.

B. Bottom Photographs

Stereo photographs were taken of the ocean bottom using two EG&G cameras, model 204, equipped with a specially corrected Hopkins f4.5 35mm lens to overcome distortions resulting from the water, glass, and air interfaces. The lenses were in focus for an underwater depth of seven feet. No shutter was used due to the depth of operation, and exposure was obtained by flashing the two strobe units at 15 second intervals. Fifty foot rolls of Plus X Pan 35 mm film was used in each camera. A timing device prevented the film from advancing until the cameras had reached the bottom. Proper focal distance was maintained by measuring direct and bottom reflected signals of a pinger mounted on the camera frame. An EG&G current vane was employed to observe bottom currents. This vane can be

seen in the corner of most photographs. A more detailed description of the EG&G camera and its use aboard the R/V Ruth Ann is found in Volume 7, Area 15 (May, 1969). The bottom photographs reproduced in this volume represent the most typical bottom features of the station area. A few pictures, however, have been added to show unusual or interesting features that are not necessarily observed in the other photographs taken at the same station.

III - Methods Used to Determine the Various Physical Properties

Upon arrival at the laboratory, sound-speed measurements are taken across the diameter, every five centimeters down the length of the core. The core is rotated with sound-speed measurements taken at an arbitrary 0 degrees, 90 degrees, 180 degrees, and 270 degrees to avoid any abnormal reading due to possible air bubbles occurring between the liner and sediment. The core is then cut longitudinally and the sediment is photographed, sampled, and described. Samples for physical properties analysis are taken primarily in areas which display sound-speed anomalies and in areas which exhibit a different lithology from previously sampled sediment in the core.

Samples are analyzed to determine moisture content, porosity, void ratio, bulk density, specific gravity, calcium carbonate content and particle size distribution.

Sound-speed values are plotted with depth to show trends down the length of the core (Figures: 13-19). A core diagram and description accompanies each figure to aid in correlating the various sound-speed values with sediment type. The lines connecting the sound-speed value points are meant to show up trends and should not be considered as indicating actual

values between points. Tables I through VII, which follow the core descriptions give the physical property values and corresponding sound-speed values of each sample.

Calculations of sound-speed values and of the various physical property values presented here are made using an IBM 1130 computer.

A. Sound-Speed

Sound-speed measurements were made using a pulse technique. An ultrasonic pulse of a known frequency is transmitted through the liner containing the core sample, and a similar pulse is transmitted through a liner containing distilled water. The sound-speed of the sediment is calculated from the delay in arrival time due to the sediment, with respect to the sound-speed of distilled water at 1 atmosphere of pressure.

An Underwater Systems' sediment velocimeter, model USI 101, was used to make the measurements. The unit consists of two transmitting and receiving crystals, each pair submerged in a water tank. A pulse generator and amplifier cause the transmitting crystals to resonate at 400 kHz. The received signals are amplified and displayed on a dual trace oscilloscope, and the difference between the two pulses is measured using the oscilloscope's time delay system. Sound-speed values are calculated using the equation:

$$C_s = C_w \frac{1}{1 - \frac{\Delta t \, C_w}{d}}$$

Where C_s is the sound velocity through the sediment, C_w is the sound velocity through distilled water, Δt is the difference in time of arrival for the pulse through the sediment as compared to the reference

pulse (distilled H_2O) and d is the core sample thickness.

The sound-speed values presented in this report are corrected to in-situ values for temperature and pressure (Hamilton, 1963, 1965) using the formula V m/sec = 1449.14 + Vp + Vs + Vt + Vstp taken from the U. S. Naval Oceanographic Office's Tables of Sound-Speed in Sea Water (SP-58). Bottom water velocity was computed for each core station using the same tables. The bottom water temperature was obtained from the sound velocimeter profiles taken at the core station. A graph of the corrected sound-speed values for each core appears next to the core diagrams in Figures 13-19.

B. Water Content

The water or moisture content (w) is the ratio, expressed as a percentage, of the weight of water in a given mass of sediment to the weight of the solid particles.

Samples of a size to yield a dry weight of 10 to 20 grams are placed in a covered aluminum container and weighed to the nearest milligram. The sediment is then dried for 24 hours at a temperature of 110° ± 5°C, cooled in a desiccator, and weighed again to the nearest milligram. Water content is calculated as follows:

$$\text{Water content (w)} = \left[\frac{\text{weight of water}}{\text{weight of oven dried sediment}} \right] \times 100$$

C. Specific Gravity

Specific gravity (G) is the ratio of the weight in air of a given volume of material, at a stated temperature, to the weight in air

of an equal volume of distilled water at a stated temperature.

The specific gravity of solids is determined with calibrated 50 ml. stoppered pycnometer bottles which are preweighed to the nearest milligram. Oven dried and desiccated sediment samples, weighing from 10 to 15 grams, are ground to a powder and placed in pycnometer bottles, which are then weighed to the nearest milligram to determine the weight of sample used. The bottles are filled half-way with de-aired distilled water and allowed to stand overnight, prior to being boiled under a vacuum for 5 minutes. After cooling and filling with water, the bottles are weighed to the nearest milligram and the temperature of the water taken to the nearest degree centigrade. Specific gravity is calculated as follows:

$$G = \frac{Wo}{Wo + (Wa - Wb)} \times K$$

where

G = specific gravity at 20°C

Wo = weight of sample in grams

Wa = weight of pycnometer filled with water as taken from the pycnometer calibration curve

Wb = weight of the pycnometer filled with water and sediment

K = temperature correction factor used to reduce results to 20°C

D. Bulk Density, Void Ratio and Porosity

Bulk density or wet unit weight (γ wet) is the weight (solids plus water) per unit of total volume of sediment mass, irrespective of the degree of saturation. Bulk density is calculated as follows:

$$\gamma \text{ wet} = \frac{W \text{ wet}}{V \text{ wet}}$$

$$= \frac{W \text{ wet}}{V \text{ dry} + Ww}$$

$$= \frac{W \text{ wet}}{\frac{W \text{ dry}}{G} + Ww}$$

where:

γ wet = bulk density

W wet = wet weight

V wet = wet volume

V dry = dry volume

Ww = weight of water

W dry = dry weight

G = specific gravity of solid particles

Void ratio (e) is the ratio of the volume of void space to the volume of solid particles in a given sediment mass.

$$e = \frac{Vv}{V \text{ dry}}$$

$$e = \frac{Ww}{V \text{ dry}}$$

$$e = \frac{Ww}{\frac{W \text{ dry}}{G}}$$

$$e = \frac{G\ (Ww)}{W \text{ dry}}$$

where:

e = void ratio

Vv = volume of voids

V dry = volume of solid particles

Ww = weight of water

W dry = weight of solid particles

G = specific gravity of solid particles

Porosity (η) is the ratio, usually expressed as a percentage, of the volume of voids of a given sediment mass to the total volume of the sediment mass.

$$\eta = \frac{e}{e + 1} \times 100$$

where:

η = Porosity

e = void ratio

E. Grain Size Analysis

Grain size distribution is determined using the procedures outlined by Folk (1965). Samples which will yield a dry weight of 10 to 15 grams are soaked for at least 24 hours in dispersant (2.5 g sodium metaphosphate/ liter) and wet sieved through a 62 micron sieve. The fraction retained on the sieve is dried, weighed and sieved at 1/2 phi intervals, whereas the fraction passing the 62 micron sieve is pipetted at one phi intervals. The results are plotted as cumulative curves on probability graph paper and the statistical parameters of Folk (1965), graphic mean (M_z), inclusive graphic standard deviation (θ_I), inclusive graphic skewness (SK_I), and transformed kurtosis (K_G) are computed.

F. Calcium Carbonate ($CaCO_3$)

The calcium carbonate content is determined using a volumetric gas measuring apparatus developed by Hulsemann (1965). CO_2 is generated by adding a 2N solution of HCl to the sediment. The amount of $CaCO_3$ present is calculated from the amount of CO_2 generated using the formula:

$$\% \ CO_3^{--} = \frac{v(P-M)}{w(T+t)} \ 0.0961$$

where v = observed volume of CO_2 in ml.

P = barometric pressure in mm Hg.

M = Vapor pressure of water in mm Hg: dependent on the lowest temperature in the system.

w = weight of the sample in grams.

T = room temperature in °C; in order to compensate for variations between the beginning and the end of the analysis, the average of the two is entered.

t = 273.16 (conversion factor for changing temperature from degrees centigrade to degrees Kelvin)

0.0961 = constant resulting from the conversion of the barometric pressure to cgs units, the gas constant, and the molecular weight of CO_3^{--}

G. Shear Strength

Shear strength, expressed in tons/meter^2, is a measure of the maximum resistance of a material to shearing stresses. Shear strength was measured, using a Geonor fall-cone penetrometer at 10 cm intervals down the length of the freshly opened cores. The amount of cone penetration into the sediment was related to shear strength by means of Hansbo's tables (1957).

IV Description of Cores and Bottom Photographs

A. Station T-4

Core 1B-1

Core 1B-1 was taken at the base of the Canary Island Rise (Henry 1969) in 5240 meters of water with coordinates of 24°22'N and 25°24'W. Ten and a half meters of sediment were recovered consisting of intercalating layers of foraminiferal sands, silts and lutites. The amount of foraminiferal sand decreases in abundance with depth while silts and lutite become the predominant sediment type below 3 meters. Layers of coccolith ooze occur between 641-653 cm, 661-690 cm, 693-715 cm and from 1025-1040 cm. The coarse fraction material consists mostly of foraminiferal tests with a moderate amount of sub-angular quartz grains present. In many of the sand layers the majority of the tests appear to be juvenile. Radiolarians occur in minor amounts in the foraminiferal sand layers, predominantly in the upper portions of the core. Sound-speed for this core shows a great deal of variation depending on the type of sediment present. On the whole, velocities are high with readings above 1.500 km/sec for the lutite and coccolith ooze layers to over 1.850 km/sec for one of the sand layers below 1.5 meters.

B. Station T-6

Core 1B-2

Core 1B-2 was taken on the Sierra Leone Abyssal Plain in 4930 meters of water at 6°10'N and 16°15'W. "PESR" profiles show a flat abyssal bottom with concordant sub-bottoms. The sediment recovered consists predominantly

TABLE I

ACOUSTIC AND PHYSICAL PROPERTIES

Ship: RA Core: 1b-1 Area: ST Cr: 1B

Sample Depth cm	Sediment Type	C_s km/sec	n %	ω	G	γ wet	$CaCO_3$ %	e	M_z ϕ	σ_I ϕ	SK_I	K_G	τ t/m^2
20	Lutite	1.586	68.3	79.2	2.71	1.54	50.0	2.151	7.87ϕ	2.16ϕ	-0.22	1.83	0.60
35	Foram Sand	1.599	66.3	73.2	2.68	1.57	--	1.967	--	--	--	--	--
45	Lutite	1.582	68.7	79.8	2.74	1.55	33.0	2.190	8.07ϕ	1.86ϕ	-0.20	1.66	--
60	Foram Sand	1.721	59.6	55.1	2.68	1.68	50.2	1.477	4.43ϕ	2.18ϕ	0.60	2.00	2.6
80	Foram Sand	1.800	45.3	30.8	2.68	1.92	--	0.829	3.70ϕ	1.28ϕ	0.24	2.64	1.66
95	Foram Sand	1.773	53.1	39.4	2.87	1.88	--	1.132	3.83ϕ	1.71ϕ	0.53	2.66	--
110	Foram Sand	1.815	48.1	34.3	2.70	1.88	42.7	0.925	3.33ϕ	1.10ϕ	0.30	2.32	8.8
145	Foram Sand	1.769	57.5	50.1	2.70	1.72	54.6	1.355	3.30ϕ	1.86ϕ	0.41	2.77	--
165	Foram Sand	1.854	42.2	26.9	2.71	1.99	44.2	0.729	3.17ϕ	0.78ϕ	0.30	1.64	--
180	Foram Sand	1.892	38.9	23.4	2.71	2.05	50.5	0.637	2.93ϕ	1.43ϕ	0.52	3.23	2.8
190	Lutite	1.588	70.5	89.9	2.66	1.49	39.6	2.394	10.80ϕ	2.18ϕ	-0.23	0.87	0.81
195	Lutite	1.591	71.1	94.3	2.60	1.46	6.8	2.458	9.57ϕ	2.77ϕ	-0.11	0.77	--
210	Lutite	1.593	71.1	91.0	2.69	1.49	35.4	2.456	9.80ϕ	2.70ϕ	-0.13	0.74	1.20
220	Foram Sand	1.682	54.9	45.2	2.69	1.76	--	1.216	4.43ϕ	1.93ϕ	0.27	1.79	2.3
240	Foram Sand	1.805	50.0	37.0	2.70	1.85	29.8	1.000	4.47ϕ	1.20ϕ	0.39	2.55	--

TABLE I (continued)

ACOUSTIC AND PHYSICAL PROPERTIES

Ship: RA Core: 1B-1 Area: ST Cr: 1B

Sample Depth cm	Sediment Type	C_s km/sec	n %	ω	G	γ wet	$CaCO_3$ %	e	M_z ϕ	σ_I ϕ	SK_I	K_G	τ t/m^2
260	Foram Sand	--	61.0	58.0	2.69	1.66	44.0	1.563	3.90ϕ	2.11ϕ	0.40	2.68	--
280	Foram Sand	1.818	46.8	31.5	2.78	1.95	--	0.878	4.17ϕ	1.57ϕ	0.55	3.24	10.3
295	Foram Sand	1.691	55.2	45.9	2.68	1.76	--	1.232	4.43ϕ	2.12ϕ	0.55	2.28	--
305	Lutite	1.617	61.4	59.1	2.69	1.65	--	1.591	7.87ϕ	3.46ϕ	-0.04	0.74	--
315	Lutite	1.586	72.8	99.0	2.70	1.46	38.2	2.674	9.63ϕ	2.66ϕ	-0.07	0.80	--
335	Lutite	1.594	70.5	89.7	2.66	1.49	--	2.387	8.33ϕ	2.94ϕ	0.24	0.70	--
340	Silt	1.594	52.0	40.1	2.69	1.82	--	1.083	5.30ϕ	1.84ϕ	0.62	2.80	0.62
345	Lutite	1.582	74.1	111.9	2.55	1.40	14.4	2.857	9.97ϕ	2.30ϕ	0.03	0.88	--
365	Silt	1.712	52.0	40.0	2.70	1.82	25.9	1.083	5.03ϕ	1.84ϕ	0.56	2.40	--
375	Lutite	1.574	70.5	89.2	2.67	1.49	--	2.387	9.57ϕ	2.68ϕ	-0.02	0.64	--
385	Silty Lutite	1.596	68.7	81.2	2.70	1.53	--	2.196	9.23ϕ	3.22ϕ	-0.14	1.04	--
400	Lutite	1.598	67.1	74.8	2.72	1.57	--	2.036	9.07ϕ	3.11ϕ	-0.08	0.96	1.20
420	Lutite	1.591	71.4	91.8	2.72	1.49	--	2.501	10.10ϕ	2.35ϕ	-0.01	0.86	0.77
440	Lutite	1.593	68.6	79.6	2.74	1.55	28.9	2.188	4.77ϕ	1.82ϕ	0.57	2.31	1.12
465	Foram Sand	1.734	48.0	34.4	2.68	1.88	--	0.924	--	--	--	--	--

TABLE I (continued)

ACOUSTIC AND PHYSICAL PROPERTIES

Ship: RA Core: 1B-1 Area: ST Cr: 1B

Sample Depth cm	Sediment Type	C_s km/sec	η %	ω	G	γ wet	$CaCO_3$ %	e	M_z ϕ	σ_I ϕ	SK_I	K_G	τ t/m^2
480	Lutite	1.580	72.3	96.3	2.73	1.48	44.5	2.631	9.40ϕ	2.92ϕ	-0.11	0.92	0.61
490	Sandy Lutite	1.623	60.2	56.2	2.69	1.67	--	1.513	5.67ϕ	2.82ϕ	0.63	1.51	0.45
500	Lutite	1.585	69.2	85.1	2.64	1.51	6.1	2.252	8.90ϕ	2.24ϕ	-0.02	1.14	1.01
525	Silt	1.585	75.4	110.1	2.78	1.44	--	3.068	7.87ϕ	2.56ϕ	0.39	1.31	--
530	Coarse Silt	1.623	70.5	85.9	2.78	1.53	--	2.391	5.93ϕ	1.78ϕ	0.59	2.30	2.4
555	Coarse Silt	--	68.1	77.3	2.76	1.56	53.0	2.134	4.63ϕ	1.82ϕ	0.48	2.59	--
570	Lutite	1.539	68.4	78.4	2.75	1.56	9.2	2.159	9.43ϕ	2.61ϕ	-0.01	0.80	1.85
600	Lutite	1.535	67.6	77.6	2.68	1.55	2.4	2.085	9.50ϕ	2.70ϕ	-0.02	0.70	1.15
615	Silt	1.627	52.4	40.1	2.74	1.83	13.8	1.100	5.47ϕ	1.61ϕ	0.58	2.72	--
630	Lutite	1.534	68.9	81.2	2.73	1.54	47.5	2.219	8.90ϕ	1.42ϕ	-0.09	1.64	1.85
655	Silt	1.561	57.5	50.1	2.69	1.72	31.8	1.350	6.43ϕ	2.41ϕ	0.64	1.89	--
680	Coccolith ooze	1.550	62.4	61.4	2.70	1.64	83.8	1.659	9.53ϕ	2.44ϕ	-0.05	1.95	17.6
700	Coccolith ooze	1.565	64.4	66.6	2.71	1.61	72.4	1.807	8.43ϕ	3.48ϕ	-0.28	1.42	3.2
710	Coccolith ooze	1.546	66.2	71.3	2.74	1.59	42.8	1.955	9.57ϕ	2.66ϕ	-0.03	0.87	1.28

TABLE I (continued)

ACOUSTIC AND PHYSICAL PROPERTIES

Ship: RA Core: 1B-1 Area: ST Cr: 1B

Sample Depth cm	Sediment Type	C_s km/sec	η %	ω	G	γwet	$CaCO_3$ %	e	M_z ϕ	σ_I ϕ	SK_I	K_G	τ t/m^2
720	Lutite	1.536	70.0	85.4	2.73	1.52	26.6	2.332	9.20ϕ	1.90ϕ	-0.06	1.89	0.99
740	Lutite	1.543	67.2	75.2	2.72	1.57	20.0	2.050	8.53ϕ	2.07ϕ	-0.33	1.26	1.08
750	Lutite	1.542	67.4	75.4	2.73	1.57	34.6	2.064	8.77ϕ	2.63ϕ	-0.13	1.41	0.92
770	Lutite	1.566	59.4	53.9	2.71	1.70	32.7	1.460	7.07ϕ	2.55ϕ	0.66	1.11	1.47
795	Lutite	1.548	65.1	67.9	2.73	1.61	15.3	1.861	9.17ϕ	2.72ϕ	0.06	0.70	--
800	Lutite	1.543	65.9	71.6	2.70	1.58	--	1.935	9.50ϕ	2.55ϕ	0.04	0.71	1.75
815	Lutite	1.551	65.4	69.6	2.71	1.59	57.6	1.890	7.63ϕ	2.96ϕ	-0.15	1.25	--
895	Foram Sand	1.657	55.4	46.0	2.70	1.76	36.5	1.242	4.03ϕ	1.89ϕ	0.37	2.10	--
915	Foram Sand	1.615	63.9	65.7	2.69	1.61	56.2	1.771	3.83ϕ	2.27ϕ	0.49	2.34	--
965	Foram Sand	1.633	59.4	54.3	2.69	1.69	48.1	1.462	3.57ϕ	1.77ϕ	0.43	2.49	--
1010	Foram Sand	1.619	61.6	59.3	2.70	1.66	61.2	1.606	3.37ϕ	2.18ϕ	0.54	2.46	4.2
1030	Coccolith ooze	1.571	62.8	62.3	2.70	1.63	76.9	1.684	7.80ϕ	3.85ϕ	-0.22	0.96	4.0
1050	Lutite	1.535	72.0	93.8	2.73	1.49	47.3	2.569	10.07ϕ	2.60ϕ	-0.13	0.91	1.12

TABLE II

ACOUSTIC AND PHYSICAL PROPERTIES

Ship: RA Core: 1B-2 Area: ST Cr: 1B

Sample Depth cm	Sediment Type	C_s km/sec	η %	ω	G	γ_{wet}	$CaCO_3$ %	e	M_z ϕ	σ_I ϕ	SK_I	K_G	τ t/m^2
20	Lutite	1.512	82.6	174.6	2.72	1.30	8.7	4.749	10.17ϕ	2.38ϕ	-0.09	0.81	0.084
55	Lutite	1.519	85.1	225.9	2.53	1.23	--	5.726	10.50ϕ	2.26ϕ	-0.14	0.82	--
100	Lutite	1.537	77.1	125.3	2.68	1.39	4.8	3.361	6.07ϕ	3.49ϕ	0.13	0.57	0.50
145	Lutite	1.516	83.1	189.2	2.59	1.27	--	4.907	9.17ϕ	3.42ϕ	-0.30	1.11	--
165	Lutite	1.517	83.5	194.1	2.61	1.27	--	5.077	9.27ϕ	3.14ϕ	-0.12	0.98	--
190	Lutite	1.521	85.7	223.8	2.67	1.24	--	5.992	8.80ϕ	3.82ϕ	-0.27	0.86	0.27
240	Brittle Lutite	1.519	82.1	172.3	2.66	1.30	--	4.584	9.97ϕ	2.57ϕ	-0.12	0.79	3.7
250	Lutite	1.520	84.9	211.5	2.66	1.25	3.7	5.640	--	--	---	---	0.039
260	Brittle Lutite	1.512	80.2	153.4	2.64	1.33	--	4.059	10.77ϕ	2.23ϕ	-0.29	0.87	0.46
280	Lutite	1.512	79.7	149.6	2.63	1.33	2.8	3.937	10.80ϕ	2.17ϕ	-0.19	0.91	0.87
305	Lutite	1.518	75.2	113.0	2.68	1.42	--	3.035	10.20ϕ	2.51ϕ	-0.21	0.79	--
330	Lutite	1.511	81.4	161.0	2.71	1.32	8.5	4.368	9.07ϕ	3.38ϕ	-0.12	0.91	0.425
350	Slightly Indurated Lutite	1.521	82.5	170.8	2.75	1.31	--	4.700	8.63ϕ	3.05ϕ	0.08	0.86	3.6
430	Lutite	1.519	85.9	231.2	2.63	1.23	--	6.097	10.00ϕ	3.04ϕ	-0.14	1.01	0.97

TABLE II (continued)

ACOUSTIC AND PHYSICAL PROPERTIES

Ship: RA Core: 1B-2 Area: ST Cr: 1B

Sample Depth cm	Sediment Type	C_s km/sec	η %	ω	G	γ_{wet}	$CaCO_3$ %	e	M_z ϕ	σ_I ϕ	SK_I	K_G	τ t/m^2
505	Lutite	1.510	82.1	171.8	2.67	1.30	--	4.589	10.00ϕ	2.35ϕ	-0.00	0.79	--
525	Lutite	1.525	82.0	169.6	2.68	1.30	--	4.549	10.47ϕ	2.48ϕ	-0.20	0.71	--
590	Lutite	1.518	83.8	201.0	2.57	1.26	--	5.185	10.63ϕ	2.31ϕ	-0.23	0.84	0.44
650	Lutite	1.511	80.6	159.6	2.59	1.31	5.3	4.149	10.03ϕ	2.63ϕ	-0.21	0.71	0.495
720	Lutite	1.511	82.1	171.5	2.68	1.30	--	4.600	10.87ϕ	2.17ϕ	-0.29	0.92	0.33
740	Lutite	1.507	83.4	135.3	2.68	1.36	--	3.637	10.97ϕ	2.03ϕ	-0.21	0.95	0.96
770	Lutite	1.517	82.3	174.9	2.65	1.29	--	4.649	9.83ϕ	3.01ϕ	-0.27	0.93	1.80
865	Lutite	1.509	77.6	136.1	2.54	1.35	--	3.467	11.17ϕ	1.86ϕ	-0.21	0.91	--
900	Lutite	1.514	83.0	188.3	2.58	1.27	--	4.868	10.97ϕ	2.04ϕ	-0.24	0.87	1.90
955	Lutite	1.516	79.3	144.5	2.65	1.34	2.0	3.831	9.37ϕ	2.81ϕ	-0.08	0.64	--
985	Brittle Lutite	1.528	83.9	197.9	2.64	1.26	--	5.230	9.13ϕ	3.21ϕ	-0.10	0.98	--
995	Brittle Lutite	1.520	84.8	219.5	2.64	1.23	1.0	5.576	9.97ϕ	2.80ϕ	-0.16	1.01	--
1020	Lutite	1.518	81.0	156.7	2.72	1.33	1.9	4.262	10.33ϕ	2.46ϕ	-0.21	0.77	0.65
1080	Lutite	1.516	80.0	167.9	2.37	1.28	1.4	3.994	10.83ϕ	2.12ϕ	-0.25	0.82	0.71

of olive green silty lutite marked by slight color variations and local areas of induration. The indurated lutite areas appear to consist of angular pebble size clay aggregates and indurated laminar clay beds. The remainder of the sediment cored is very moist and plastic. Porosity values calculated from the amount of water present in a sample show very little variation between the brittle indurated layers and the remainder of the sediment. Sound-speed measurements are relatively constant along the length of the core, falling between 1.550 and 1.600 km/sec.

C. Station T-7

Core 1B-3

Core 1B-3 was taken in the Guinea Basin at 00°00'N and 03°55'W and at a depth of 5110 meters of water. The "PESR" records for station T-7 show a flat bottom area with slopes for the most part being approximately 0°. Shallow sub-bottoms are abundant and concordant with the topography. Eleven meters of sediment were recovered consisting of olive gray to olive green lutite. Color variations are slight but occur in distinct zones with sharp upper and lower boundaries. The top 20 cm of core has the only appreciable percentage of foraminiferal tests. Sediment between 150-375 cm is slightly diatomaceous. Below 5 meters the sediment consists principally of a moist grayish olive lutite intercalated with short zones of a firmer, brittle olive green lutite. Sound-speed values show slight variations but remain between 1.500 km/sec and 1.550 km/sec. There is a slight decrease in the average velocity with depth in the core.

Bottom Photographs

The bottom photographs were taken in 5100 meters of water.

TABLE III

ACOUSTIC AND PHYSICAL PROPERTIES

Ship: RA Core: 1B-3 Area: ST Cr: 1B

Sample Depth cm	Sediment Type	C_s km/sec	η %	ω	G	γwet	$CaCO_3$ %	e	M_z ϕ	σ_I ϕ	SK_I	K_G	τ t/m^2
10	Lutite	1.519	84.9	205.1	2.74	1.26	13.7	5.625	9.00ϕ	1.47ϕ	0.25	2.50	0.017
85	Lutite	1.512	81.9	176.5	2.56	1.28	--	4.525	--	--	--	--	--
115	Lutite	1.523	83.3	196.5	2.54	1.26	--	5.003	10.77ϕ	2.17ϕ	-0.22	0.82	--
150	Lutite	1.525	85.8	230.2	2.62	1.23	39.9	6.035	9.83ϕ	3.10ϕ	-0.23	1.10	0.18
170	Lutite	1.537	90.5	374.8	2.55	1.15	11.6	9.566	10.33ϕ	2.82ϕ	-0.30	1.10	0.33
250	Lutite	1.523	86.2	256.7	2.43	1.20	5.7	6.241	10.97ϕ	1.9[illegible]	-0.18	0.82	0.31
255	Lutite	1.527	89.4	324.3	2.58	1.17	--	8.393	11.00ϕ	2.04ϕ	-0.28	0.94	--
280	Lutite	1.523	82.1	187.0	2.45	1.26	6.6	4.591	10.67ϕ	2.20ϕ	-0.15	0.77	0.31
310	Lutite	1.522	84.1	212.8	2.48	1.24	5.7	5.279	10.93ϕ	1.97ϕ	-0.19	0.81	0.18
365	Lutite	1.533	90.1	362.3	2.51	1.15	7.5	9.119	10.90ϕ	2.02ϕ	-0.21	0.81	--
405	Lutite	1.520	85.1	216.1	2.62	1.24	12.0	5.693	11.00ϕ	1.99ϕ	-0.22	0.88	--
490	Lutite	1.515	79.5	148.2	2.60	1.33	--	3.868	10.73ϕ	2.18ϕ	-0.22	0.83	0.60
510	Silty Lutite	1.525	64.2	67.3	2.66	1.60	5.6	1.794	8.67ϕ	2.85ϕ	0.38	0.60	0.70
535	Lutite	1.515	79.2	150.4	2.52	1.32	2.0	3.802	11.40ϕ	1.66ϕ	-0.19	0.89	--
560	Lutite	1.533	87.1	271.1	2.48	1.19	21.4	6.734	10.30ϕ	2.23ϕ	-0.06	0.82	0.60

TABLE III (continued)

ACOUSTIC AND PHYSICAL PROPERTIES

Ship: RA Core: 1B-3 Area: ST Cr: 1B

Sample Depth cm	Sediment Type	C_s km/sec	η %	ω	G	γ wet	$CaCO_3$ %	e	M_z ϕ	θ_I ϕ	SK_I	K_G	τ t/m^2
585	Lutite	1.522	85.3	214.3	2.71	1.25	10.3	5.825	10.40ϕ	2.26ϕ	-0.09	0.80	--
610	Lutite	1.512	78.4	142.0	2.55	1.34	--	3.632	11.33ϕ	1.69ϕ	-0.23	0.89	0.48
700	Lutite	1.536	89.9	347.9	2.56	1.16	--	8.940	10.30ϕ	2.50ϕ	-0.17	0.92	1.40
735	Lutite	1.516	81.9	173.3	2.60	1.29	--	4.521	10.63ϕ	2.81ϕ	-0.35	1.28	--
830	Lutite	1.521	82.9	178.0	2.72	1.29	--	4.843	10.87ϕ	1.99ϕ	-0.16	0.76	3.7
910	Lutite	1.510	74.9	116.4	2.56	1.39	--	2.988	11.77ϕ	1.34ϕ	-0.17	0.86	0.88
1065	Lutite	1.510	75.0	110.9	2.70	1.43	2.5	2.997	11.07ϕ	2.04ϕ	-0.26	0.94	--

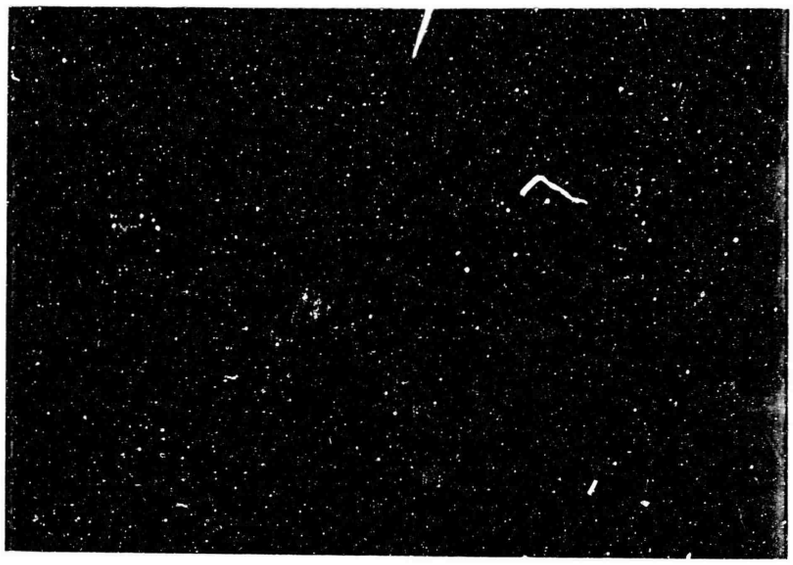

FIG. 1

FIG. 2

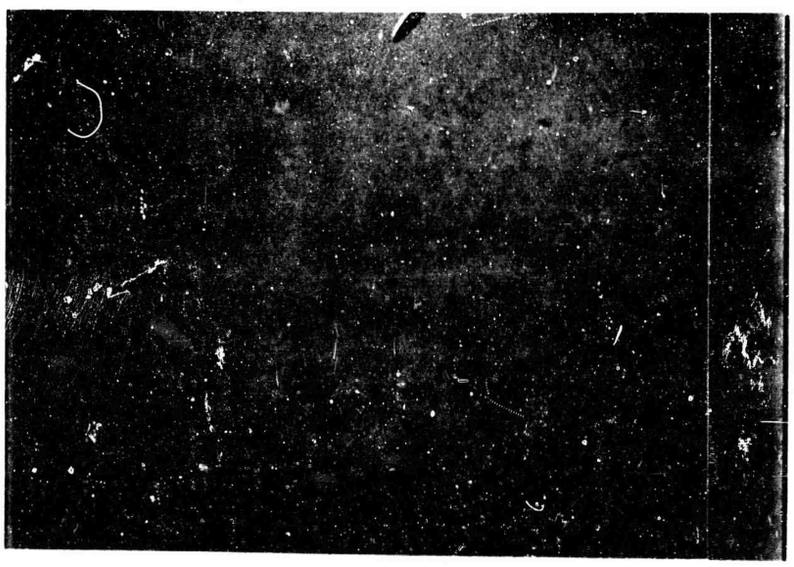

FIG. 3

PLATE I

They depict a smooth flat bottom with very little relief and very few tracks or burrows. Two interesting pictures were taken of fish just off the bottom (Plate I).

D. Station T-9

Core 1C-1

Core 1C-1 is located on the Mozambique Abyssal Plain. The core was taken at 29°58'S and 38°31'E and at a depth of 4945 meters of water. The core is 5.25 meters long and consists mostly of medium grain quartzitic sand except for a layer of foraminiferal sand occurring between 115 and 125 cm. The sand grains are sub-angular to angular in shape suggesting a proximity to the source. A small percentage of shell fragments is present throughout the core. Sound-speed measurements show values exceeding 1.800 km/sec for the sand layers while sound-speed values for the foraminiferal sand are approximately 1.670 km/sec.

Bottom Photographs

Camera station T-9 was taken at 30°00'S and 38°30'E and at a depth of 5100 meters of water. The pictures show a very low relief bottom with no evidence of benthonic life observed (Plate II). The camera station lies approximately two miles south of the core location.

E. Station T-10

Core 1C-2

Core 1C-2 is located on the Continental rise east of Madagascar, an area referred to as "micro-continental rise" (Henry, 1969).

TABLE IV

ACOUSTIC AND PHYSICAL PROPERTIES

Ship: RA Core: 1C-1 Area: ST Cr: 1C

Sample Depth cm	Sediment Type	C_s km/sec	η %	ω	G	γ_{wet}	$CaCO_3$ %	e	M_x ϕ	θ_I ϕ	SK_I	K_G	τ t/m^2
60	Sand	1.926	27.2	14.0	2.67	2.22	3.9	0.373	2.10ϕ	0.81ϕ	0.06	0.92	13.4
85	Sand	1.878	31.7	17.3	2.67	2.14	10.8	0.463	1.93ϕ	0.96ϕ	0.15	1.01	--
100	Sand	1.843	34.0	19.2	2.67	2.11	13.6	0.514	2.47ϕ	1.30ϕ	0.12	1.41	16.9
120	Foram Sand	1.798	51.2	38.8	2.69	1.83	25.6	1.047	3.77ϕ	2.22ϕ	0.33	1.54	7.9
205	Sand	1.860	28.7	15.1	2.65	2.18	3.8	0.402	1.97ϕ	1.10ϕ	0.16	0.92	--
245	Sand	--	32.6	18.1	2.67	2.13	9.8	0.483	2.17ϕ	1.14ϕ	0.16	1.00	--
250	Sand	--	32.7	18.2	2.66	2.12	8.4	0.485	2.30ϕ	1.37ϕ	0.23	1.34	7.3
295	Sand	--	23.6	11.6	2.66	2.27	12.3	0.308	2.10ϕ	1.13ϕ	0.08	1.04	--
330	Sand	--	29.1	15.4	2.66	2.18	3.0	0.410	2.13ϕ	1.06ϕ	0.12	0.96	7.7
350	Sand	1.843	33.2	18.6	2.67	2.12	7.8	0.497	2.33ϕ	1.22ϕ	0.22	1.12	7.7
490	Sand	1.863	31.9	17.5	2.67	2.14	5.3	0.468	2.30ϕ	1.17ϕ	0.11	1.20	8.3

TABLE V

ACOUSTIC AND PHYSICAL PROPERTIES

Ship: RA Core: 1C-2 Area: ST Cr: 1C

Sample Depth cm	Sediment Type	C_s km/sec.	η %	ω	G	γ wet	$CaCO_3$ %	e	M_z ϕ	θ_I ϕ	SK_I	K_G	τ t/m^2
5	Lutite	1.524	71.2	89.6	2.76	1.51	--	2.475	--	--	--	--	--
15	Fine Sand	1.563	54.2	43.7	2.69	1.78	9.2	1.181	3.50ϕ	1.98ϕ	0.33	2.77	--
80	Sand	1.763	30.3	16.2	2.69	2.18	7.6	0.435	1.68ϕ	1.09ϕ	0.07	1.01	4.5
130	Sand	1.772	36.5	21.5	2.68	2.07	7.9	0.575	1.70ϕ	1.10ϕ	0.18	1.11	7.3
145	Sand	1.797	32.8	18.2	2.68	2.13	10.4	0.487	1.47ϕ	1.21ϕ	0.09	1.02	--
190	Silt	1.513	81.7	160.5	2.78	1.33	--	4.468	4.63ϕ	1.01ϕ	0.46	4.51	1.58
205	Sand	1.742	32.4	17.8	2.69	2.15	5.1	0.480	1.67ϕ	1.53ϕ	0.35	1.45	--
240	Silty Lutite	1.500	83.2	177.2	2.79	1.30	--	4.945	7.00ϕ	3.18ϕ	0.14	0.94	2.5

STATION T-9

FIG. 1

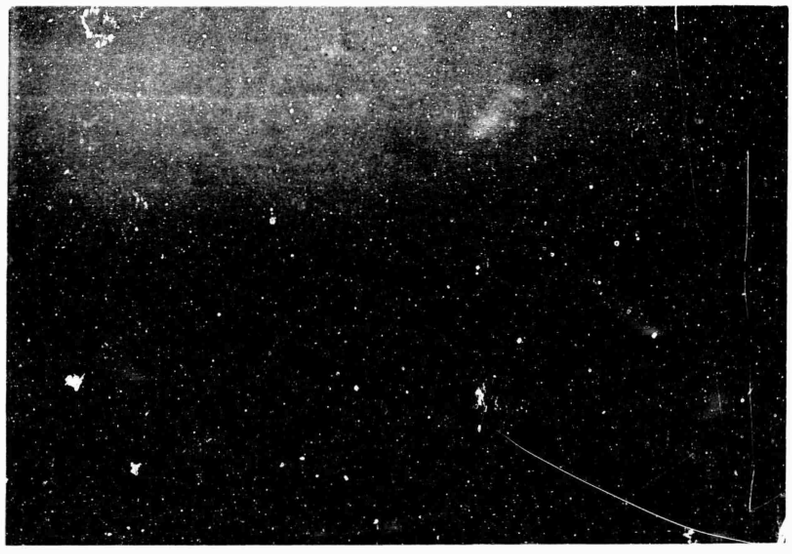

STATION T-10

FIG. 2

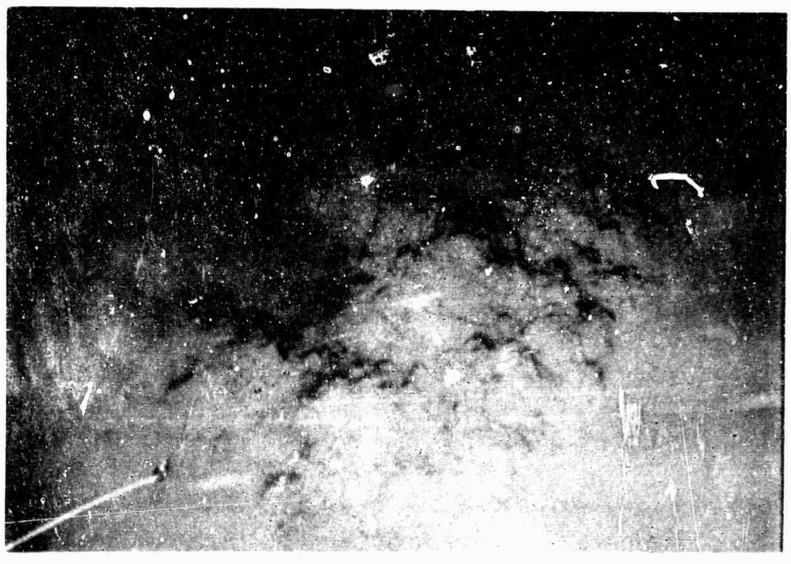

STATION T-10

FIG. 3

PLATE 2

The core was taken at 20°00's and 51°00'E at a depth of 4820 meters, and has a total length of 2.5 meters. The sediment recovered consists predominantly of lutaceous silt and quartzitic sand zones. The top 15 cm of core is of yellowish brown lutaceous sandy silt, moderately plastic and has a coarse fraction consisting predominantly of mica flakes (biotite). The sediment alters at 15 cm to a quartzitic sand for a depth of ~145 cm. The sediment below 160 cm is an olive gray lutaceous silt with quartz grains and mica flakes being the predominant coarse fraction material. A sand layer similar to that found between 15 and 160 cm reoccurs between 202 and 209 cm.

Sound-speed values show two definite groupings based on sediment type. Sound-speed values for the quartzitic sand layers averaged ~1.750 km/sec while the lutaceous silts areas have values averaging about 1.500 km/sec.

Bottom Photographs

Camera station T-10 was taken a few miles away from the core position at 19°57'S and 50°57'E and at approximately 4500 meters depth. The lowering at this station was used principally to adjust the focal length and to position the two strobe units. The weighted line, which can be seen in the pictures (Plate II), has calibrated markings and was used to determine the best shooting distance. The pictures recovered show a fine grain, low relief sediment bottom, most of which is obscured by the clouds of sediment caused by the dragging of the calibration line. The reflecting specks observed on most of the negatives are probably mica flakes sent into suspension by the calibration line.

F. Station T-11

Core 1D-1

The core was taken on the Madingley Abyssal Plain at 06°40'S and 62°00'E and in 3980 meters of water. Nearly five meters of good core were

TABLE VI

ACOUSTIC AND PHYSICAL PROPERTIES

Ship: RA Core: 1D-1 Area: ST Cr: 1D

Sample Depth cm	Sediment Type	C_s km/sec	η %	ω	G	γwet	$CaCO_3$ %	e	M_z ϕ	θ_I ϕ	SK_I	K_G	τ t/m^2
70	Foram Sand	1.545	63.0	62.0	2.74	1.65	88.2	1.704	4.43ϕ	1.88ϕ	0.48	2.27	17.6
125	Foram Sand	1.563	60.1	54.6	2.75	1.70	94.1	1.505	4.47ϕ	1.63ϕ	0.45	2.49	--
155	Foram Sand	1.611	50.8	37.0	2.79	1.88	94.3	1.034	4.43ϕ	1.33ϕ	0.33	2.46	--
190	Coccolith ooze and Foram Sand	--	62.9	61.9	2.73	1.64	94.9	1.693	6.77ϕ	3.63ϕ	0.31	0.91	4.5
280	Foram Sand	1.560	59.4	52.9	2.76	1.72	100.0	1.462	4.47ϕ	1.68ϕ	0.45	2.40	13.9
350	Foram Sand	1.536	61.8	58.6	2.75	1.67	93.8	1.616	5.30ϕ	2.37ϕ	0.59	2.03	8.5
365	Foram Sand	1.546	59.9	54.9	2.72	1.69	100.0	1.495	5.47ϕ	2.42ϕ	0.60	1.92	--
490	Foram Sand	1.541	61.2	56.9	2.76	1.69	90.7	1.574	5.80ϕ	2.52ϕ	0.61	2.03	9.7
525	Foram Sand	1.531	60.5	55.5	2.76	1.70	90.5	1.532	5.47ϕ	2.44ϕ	0.60	1.94	--
610	Foram Sand	1.529	59.6	54.1	2.72	1.70	88.3	1.474	5.47ϕ	2.32ϕ	0.58	1.98	4.6
675	Foram Sand	1.548	60.7	55.9	2.75	1.69	95.5	1.541	4.70ϕ	1.69ϕ	0.39	2.25	--

recovered consisting predominantly of a uniform foraminiferal sand. Two layers of coccolith ooze and silt size foramineral tests occur from 179-181 cm and 189-193 cm, accounting for the only breaks in continuity.

Sound-speed values, on the whole, average between 1.500 km/sec. and 1.550 km/sec. A high value is found from 165 to 175 cm which correlates with the coccolith ooze layers. Calcium carbonate content ranges from 88 to 100% as can be expected.

G. Station T-12

Bottom Photographs

Camera station T-12 was taken at 03°00'N and 83°30'E in approximately 4400 meters of water. The bottom pictures depict a low relief bottom with an abundance of tracks, burrows and plants (Plates III, IV, V). The sediment surface in all the pictures taken at T-12 appears slightly granular and the limited amount of sediment placed in suspension when the current vane touched the bottom suggests possibly a fine sand or silt bottom.

H. Station T-13

Core 1D-3

Core 1D-3 was taken on the southern central portion of the Ganges cone at 04°37'N latitude and 86°28'E longitude and in 4400 meters of water. The core is 1.25 meters in length and consists predominantly of silts and silty lutite. The top 45 cm. consists of foraminiferal lutite altering to olive green silt. The bottom 10 cm of core consist of an olive gray lutite similar to that found at the very top of the core. The dominant coarse fraction materials are mica flakes, angular quartz grains and foraminiferal tests. Foraminiferal tests are absent below 45 cm and where present constitute the

TABLE VII

ACOUSTIC AND PHYSICAL PROPERTIES

Ship: RA Core: 1D-3 Area: ST Cr: 1D

Sample Depth cm	Sediment Type	C_s km/sec	η %	ω	G	γ wet	$CaCO_3$ %	e	M_z ϕ	θ_I ϕ	SK_I	K_G	τ t/m^2
15	Foram Lutite	1.492	72.6	98.4	2.69	1.46	57.3	2.652	8.17ϕ	3.83ϕ	-0.15	0.83	-
50	Silt	1.543	60.9	57.1	2.72	1.68	3.4	1.557	6.57ϕ	2.21ϕ	0.52	1.62	2.5
55	Silt	1.621	47.2	32.6	2.74	1.92	4.7	0.895	5.23ϕ	1.34ϕ	0.26	1.95	-
60	Silt	1.539	55.6	45.4	2.75	1.78	-	1.253	6.23ϕ	2.40ϕ	0.42	1.74	4.4
70	Silt	1.610	46.1	31.3	2.72	1.93	4.7	0.855	5.10ϕ	2.00ϕ	0.21	1.54	2.0
95	Sandy Silt	1.690	44.4	29.3	2.72	1.96	7.1	0.707	4.37ϕ	1.42ϕ	0.23	1.48	-
110	Silt	1.655	44.1	28.8	2.74	1.97	5.7	0.789	5.23ϕ	1.46ϕ	0.26	2.05	4.3

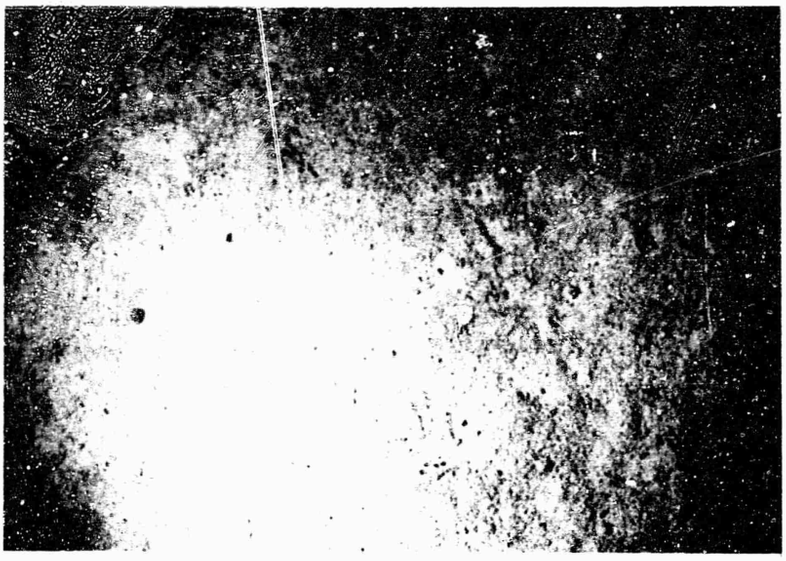

FIG. 1

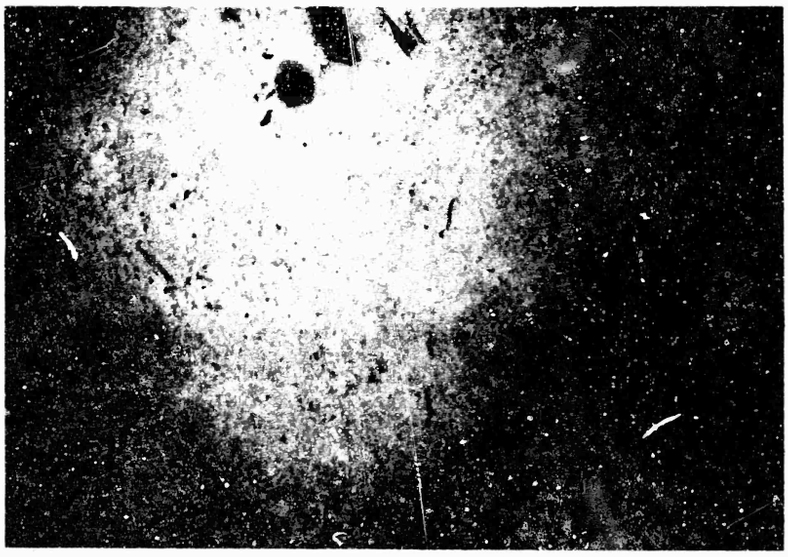

FIG. 2

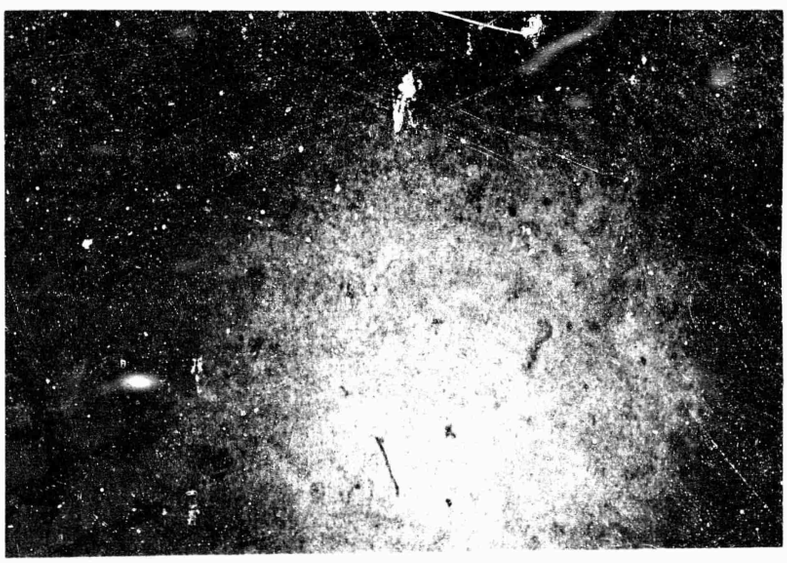

FIG. 3

PLATE 3

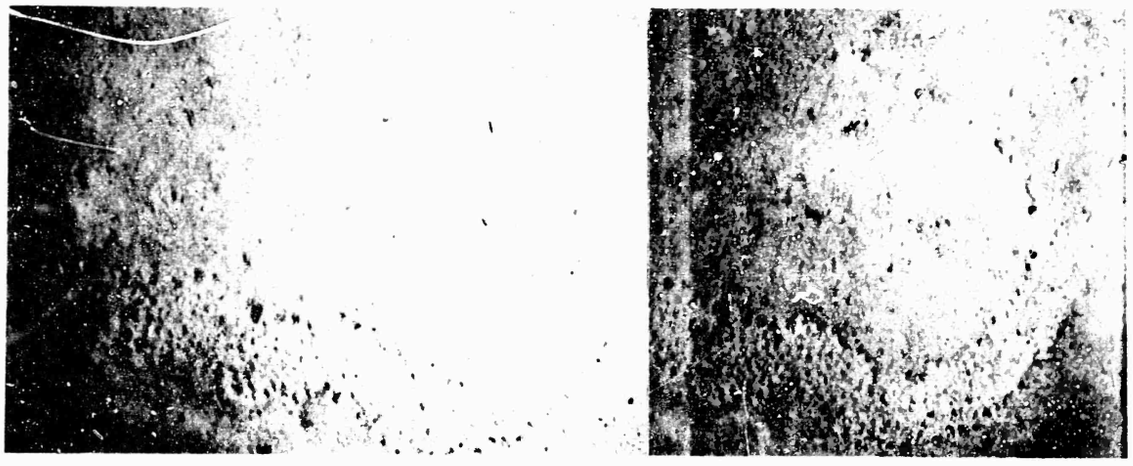

FIG. 1

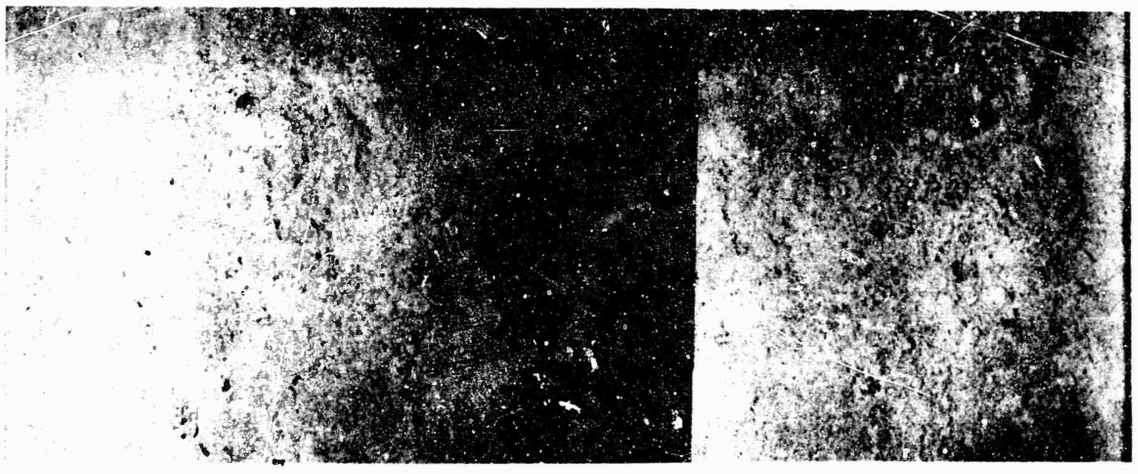

FIG. 2

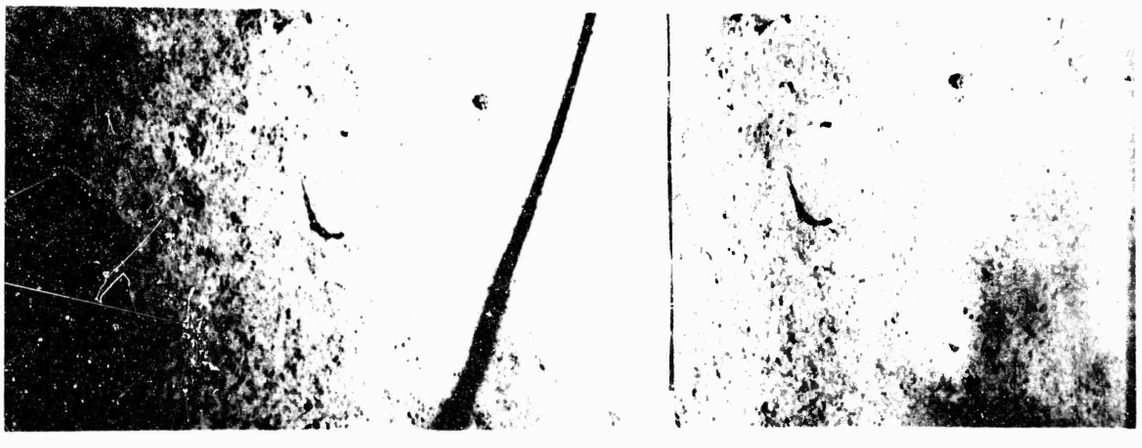

FIG. 3

PLATE 4

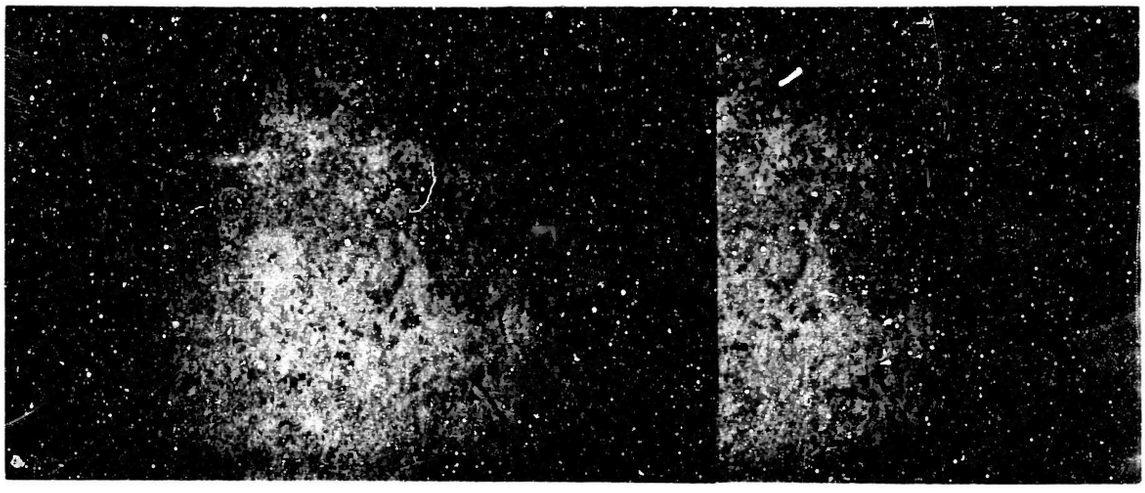

FIG. 1

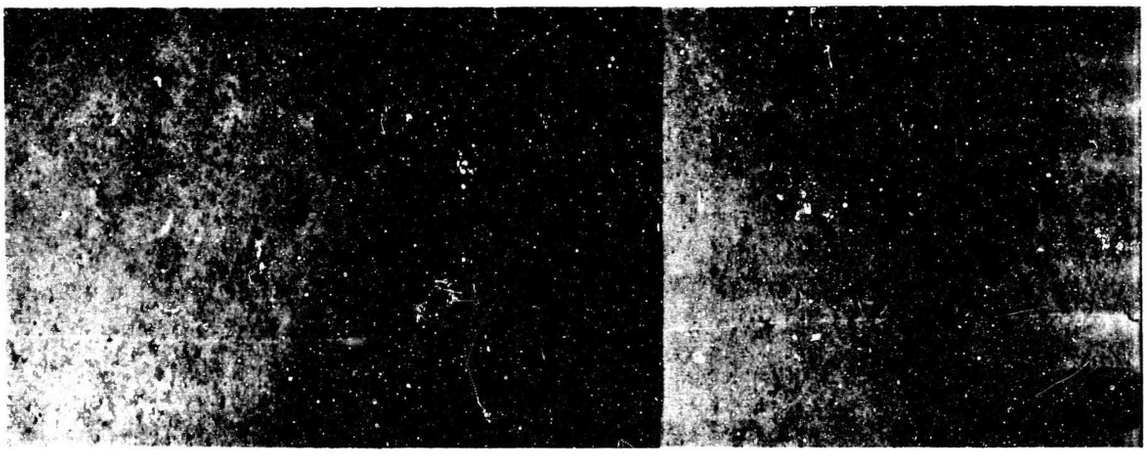

FIG. 2

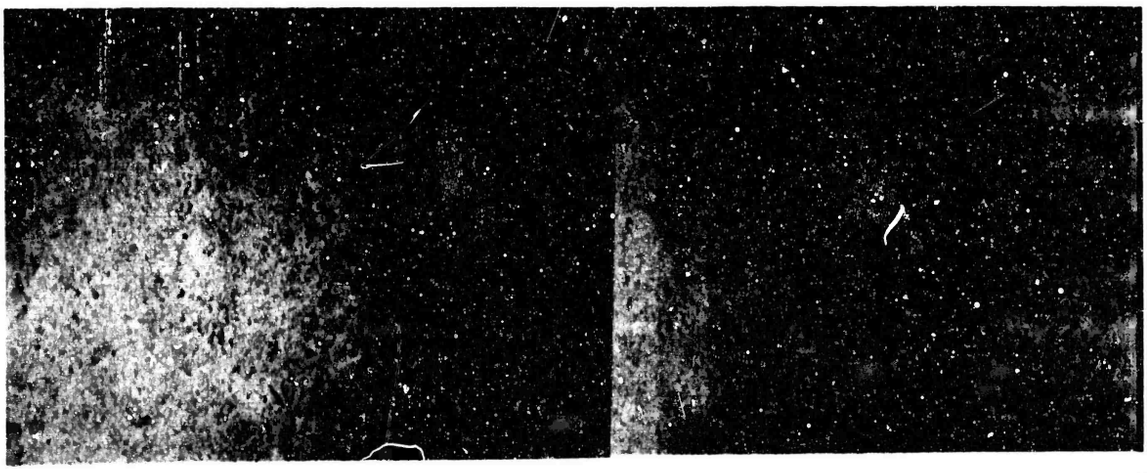

FIG. 3

PLATE 5

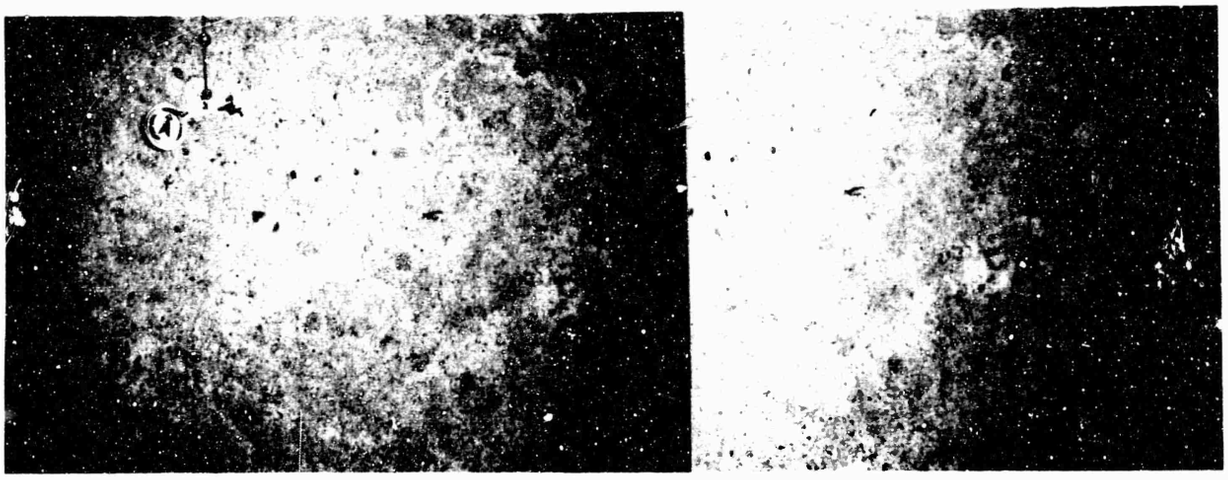

FIG. 1

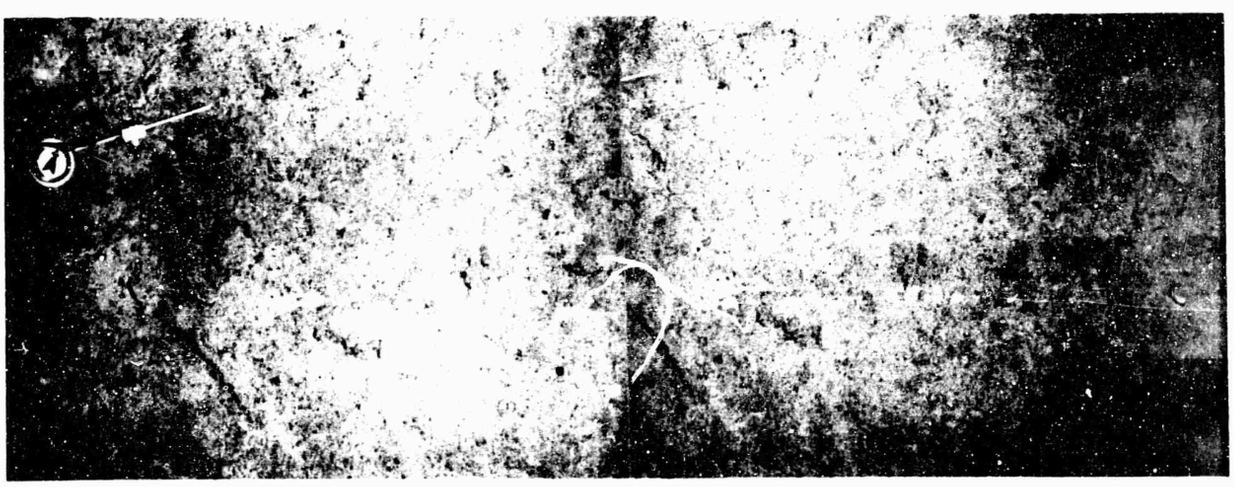

FIG. 2

FIG. 3

PLATE 6

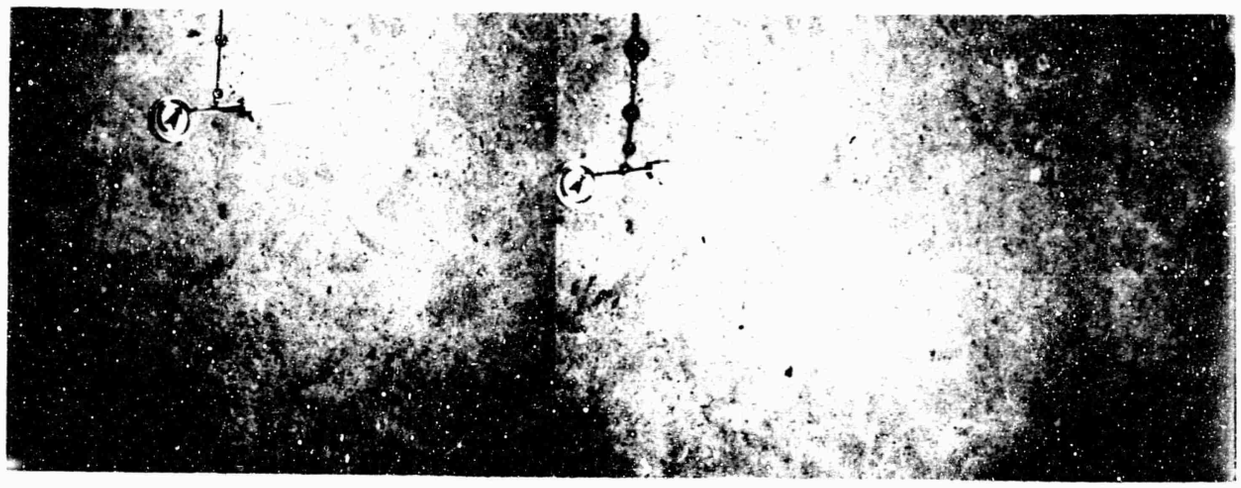

FIG. 1

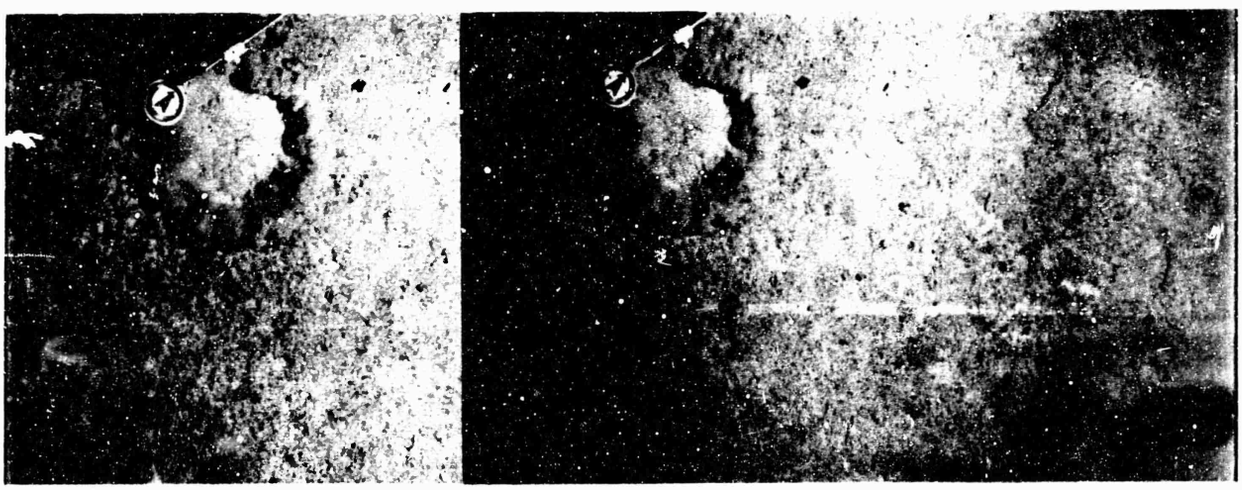

FIG. 2

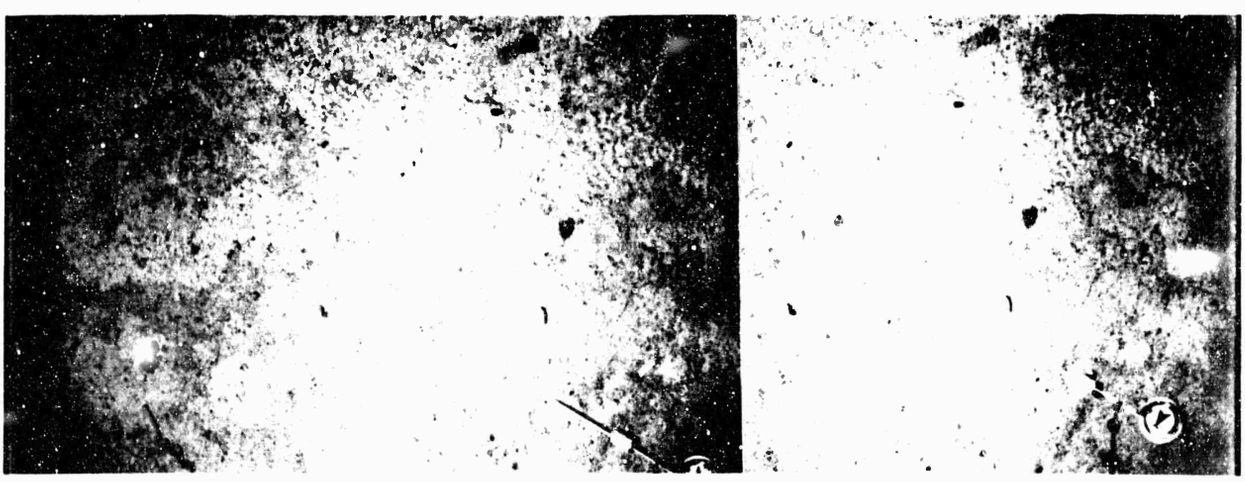

FIG. 3

PLATE 7

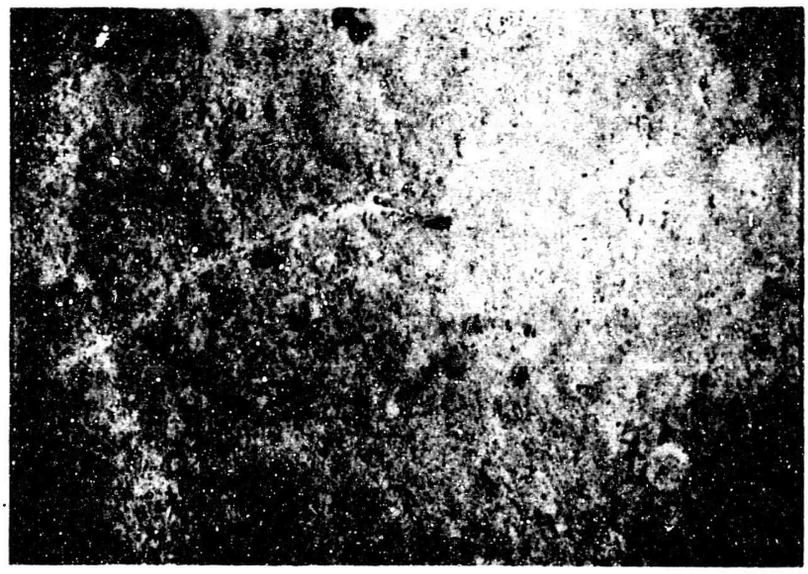

FIG. 1

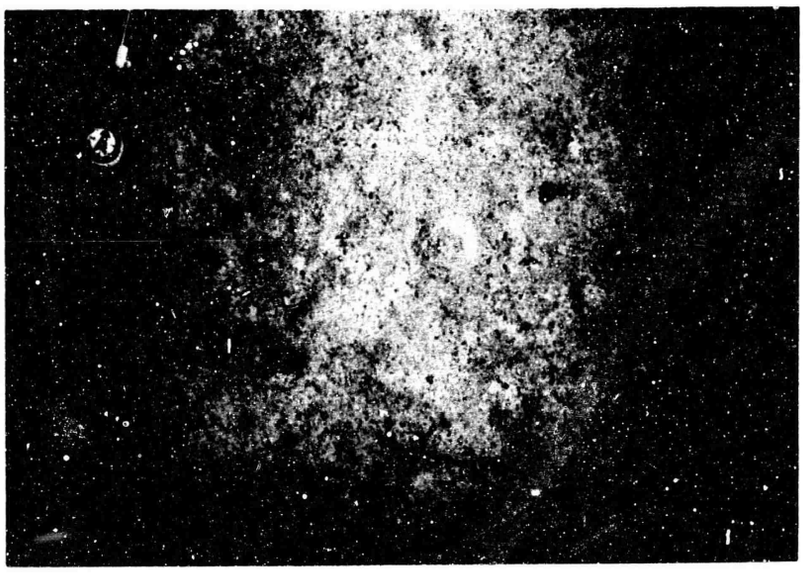

FIG. 2

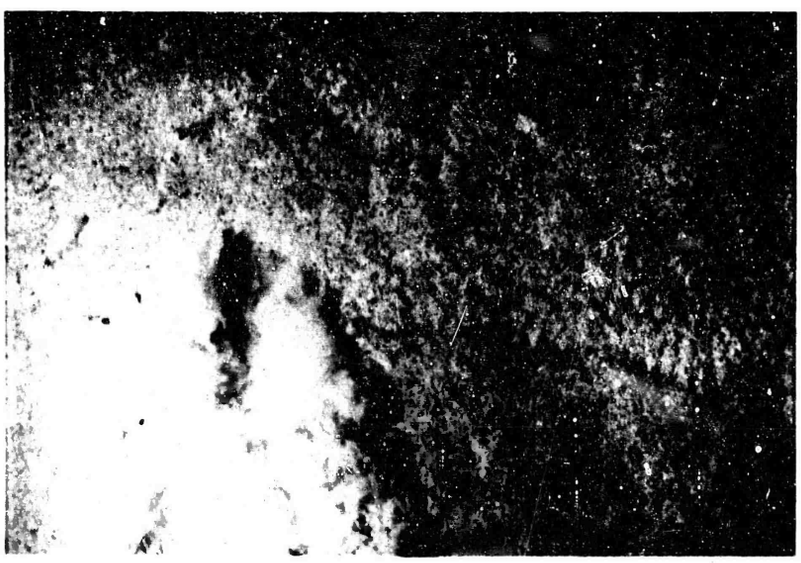

FIG. 3

PLATE 8

dominant coarse fraction material. Quartz grains, although present throughout the silt zone, become abundant ($\sim$ 30%) only below one meter.

Sound-speed values fall into two groups corresponding to sediment type. The top 45 cm of core have an average velocity of 1.500 km/sec. which is normal for this type of sediment. Below 45 cm the sediment, consisting of silt, has an average velocity of $\sim$ 1.700 km/sec.

Bottom Photographs

The bottom photographs taken at T-13 show a low relief bottom consisting possibly of a silt or sand and marked by an abundance of tracks, trails, burrows and excrement (Plates VI, VII, VIII). No change is observed in the topography from the beginning to the end of the camera lowering. The average water depth at T-13 was 4040 meters.

SUMMARY

During the Singapore Transit, new equipment and procedures were tested. The cores and bottom photographs were taken in conjunction with the acoustic program, and their location coincides with acoustic stations. Emphasis has been placed on the sound-speed values of the sediment cored, its physical properties and the size distribution of its particles. The physical property values, derived by calculating the amount of water in the sediment, form parabolic curves when plotted against sound-speed. The minimum sound-speed (~1.500 km/sec) corresponds to a bulk density value of 1.42, a moisture content of 140%, a void ratio of 3.000 and a porosity of 82%. In general these values agree with those observed for Area 17 and Area 6; however, upon closer observation of Figures 1-4 it can be seen that there are two parabolic curves formed. The two curves are representative of a difference in sediment type which have similar property values but different sound-speeds. Identifying each point in the graphs showed that the curve having the higher sound-speed for a given moisture content, void ratio etc. represents foraminiferal sands while the other curve represents lutites, silty lutite and mineral sands.

Specific gravity when plotted against sound-speed produced an L-shaped curve. The size parameters: mean diameter, transformed kurtosis, standard deviation, and graphic skewness, did not show any clear cut relationship with sound-speed except for the mean diameters. Sound-speed increases with an increase in the mean diameter (decreasing phi units). Sound-speed increases most rapidly between 6ϕ and 2ϕ

showing less variation for the silty lutites and the lutites. There is a greater scattering of points for the coarser sediment but this is due mainly to the lack of distinction between foraminiferal sands and mineral sands.

The cores analyzed in this report are important in that they consist of sediments having greater variation in sound-speeds (Fig. 13-19) than previously analyzed at Alpine Geophysical Associates, Inc. The high sound-speed (~1.900 km/sec) allowed extension of the physical property versus sound-speed curves beyond what had been observed in either Area 17 or Area 6.

VI APPENDIX

TABLE VIII

CORE STATION SUMMARY

R/V Ruth Ann — Area ST — Cruises 1B, 1C, 1D

Core Designation	Latitude	Longitude	PRESR. Depth	Physiographic Province	Core Length	Date Taken	Acoustic Station No.
RA-ST-1B-1	24°27'N	25°24'W	5240 m	Canary Island Rise	1064 cm	19 June 1967	T-4
RA-ST-1B-2	06°10'N	16°15'W	4930 m	Sierra Leone Abyssal Plain	1120 cm	27 June 1967	T-6
RA-ST-1B-3	00°00'N	03°55'W	5110 m	Guinea Basin Abyssal Plain	1125 cm	4 July 1967	T-7
RA-ST-1C-1	29°58'S	32°31'W	4945 m	Mozambique Abyssal Plain	530 cm	1 August 1967	T-9
RA-ST-1C-2	20°00'S	51°00'E	4820 m	Continental Rise	250 cm	7 August 1967	T-10
RA-ST-1D-1	06°40'S	62°00'E	3980 m	Madingley Abyssal Plain	485 cm	18 August 1967	T-11
RA-ST-1D-2	02°59'N	83°31'E	4240 m	Ganges Cone	No core	26 August 1967	T-12
RA-ST-1D-3	04°37'N	86°28'E	4040 m	Ganges Cone	125 cm	28 August 1967	T-13

TABLE IX

CAMERA STATION SUMMARY

R/V Ruth Ann — Area ST — Cruises 1B, 1C, 1D

Acoustic Station	Date	Latitude	Longitude	PESR. Depth	Plate Number	Description
T-7	4 July 1967	00°00'	03°55'W	5110 m	I	Smooth flat bottom, tracks and burrows not abundant. Two pictures show fish just off the bottom.
T-9	31 July-1 August 1967	30°00'S	38°30'E	5100 m	II	Pictures not very distinct. Bottom appears to have very little relief and few tracks or excrements were observed.
T-10	7 August 1967	19°57'S	50°57'E	4500 m	II	Fine grain sediment bottom. Mica flakes sent into suspension by dragging of calibration line seen as light specks on many pictures.
T-11	18 August 1967	06°40'S	62°00'E	3980 m	--	No pictures recovered. Camera malfunctioned.
T-12	26 August 1967	03°00'N	83°30'E	4400 m	III IV V	Low relief bottom marked by an abundance of tracks, plants and excrements. Surface sediment appears to be either sand or silt.
T-13	28 August 1967	04°37'N	86°28'E	4040 m	VI VII VIII	Low relief bottom consisting of sand or silt with an abundance of tracks, trails, burrows and excrement.

TABLE X

SYMBOLS

C_s	Sound-speed of sediment at a given temperature and pressure
C_w	Sound-speed of distilled water at a given temperature and pressure
η	Porosity; the ratio, expressed as a percentage, of the volume of voids of a given sediment to the total volume of the sediment (ASTM 1964)
γ wet	Bulk density (wet unit weight); total weight per unit of total volume of sediment irrespective of the degree of saturation (ASTM 1964)
w	Moisture content; the ratio expressed as a percentage of the weight of water in a given sediment, to the weight of solid particles (ASTM 1964)
G	Specific gravity; the ratio of the weight in air of a given volume of sediment solids at 20°C to the weight in air of an equal volume of distilled water at 20°C (ASTM 1964)
e	Void ratio; the ratio of the volume of void space to the volume of solid particles in a given sediment (ASTM 1964)
τ	Shear strength; the maximum resistance of a soil to shearing stresses expressed in tons/m^2 (ASTM 1964)
M_z	Graphic mean; the measure of the average particle size, obtained by Folk's formula $M_z = (\phi 16 + \phi 15 + \phi 84)/3$ and expressed in ϕ units (Folk 1965)
θ_I	Inclusive graphic standard deviation; a measure of sorting obtained using Folk's formul $= \frac{\phi 84-\phi 16}{4} + \frac{\phi 95-\phi 5}{6.6}$ expressed in ϕ units (Folk 1965)
SK_I	Inclusive graphic skewness; a measure of the displacement of the medina from the mean. Values are obtained using Folk's formula $SK_I = \frac{\phi 16 + \phi 84 - 2\phi 50}{2(\phi 84 - \phi 16)} + \frac{\phi 5 + \phi 95 - 2\phi 50}{2(\phi 95 - \phi 5)}$ (Folk 1965)
K_G	Graphic kurtosis; a measure of the ratio between the sorting in the tails of the curve and the sorting in the central portion of the curve. Values are obtained using Folk's formula $K_G = \frac{\phi 95 - \phi 5}{2.44\ (\phi 75-\phi 25)}$ (Folk 1965)

TABLE XI

CORE DESCRIPTIVE SYMBOLS

SEDIMENT GRAIN SIZE

SAND 

SILT 

LUTITE 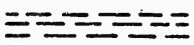

CONTACTS BETWEEN SEDIMENT LAYERS

GRADATIONAL CONTACT 

SHARP HORIZONTAL CONTACT

SHARP IRREGULAR CONTACT 

OTHERS

LAMINA OF INDURATED LUTITE 

BURROWS AND INCLUSIONS
(SUCH AS PEBBLES, ASH, ETC.) 

SPACE CONTAINING NO SEDIMENT 

NUMBERS IN CENTER OF CORE DIAGRAM ARE MUNSELL SOIL COLOR CODE DESIGNATING SEDIMENT COLOR WHEN CORES WERE OPENED IN THE LABORATORY

COLOR CODE CHART

(MUNSELL SOIL COLOR CHART
re NATIONAL BUREAU OF STANDARDS
RESEARCH PAPER RP 1239)

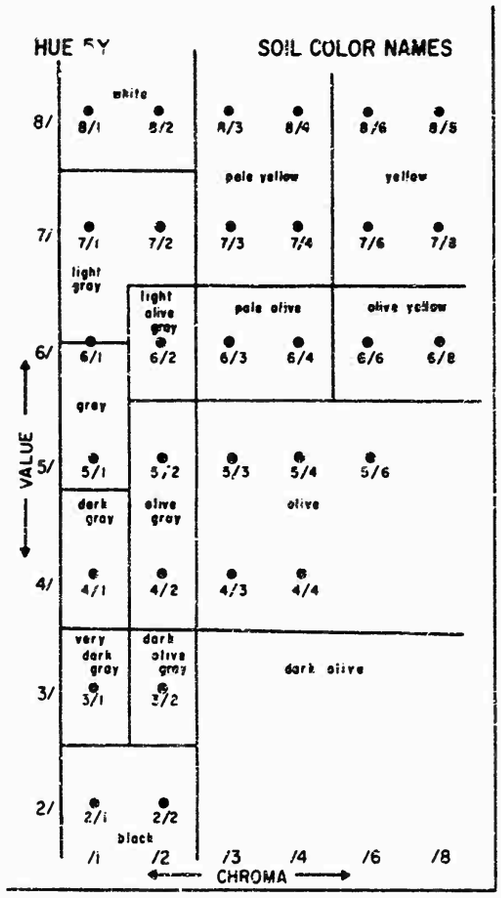

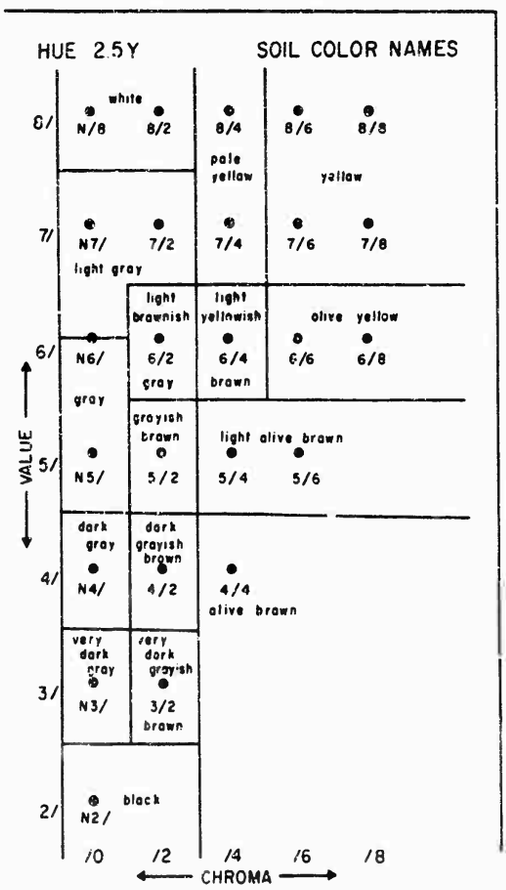

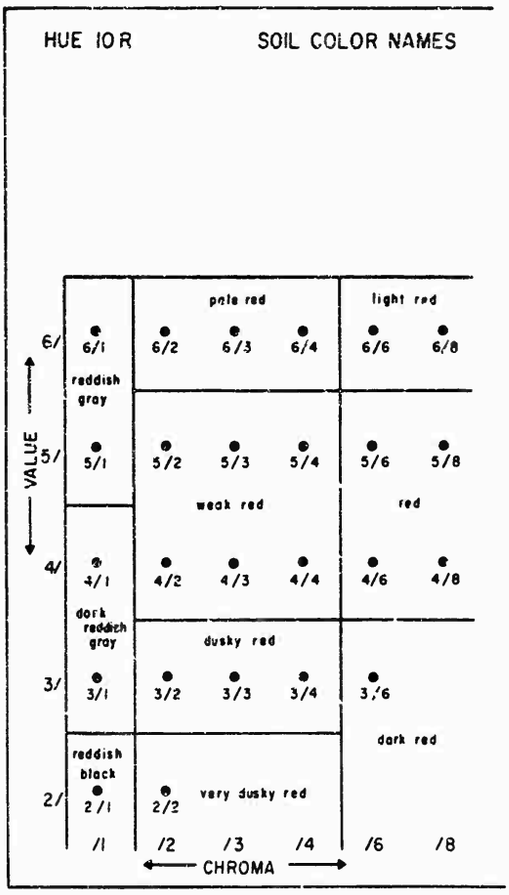

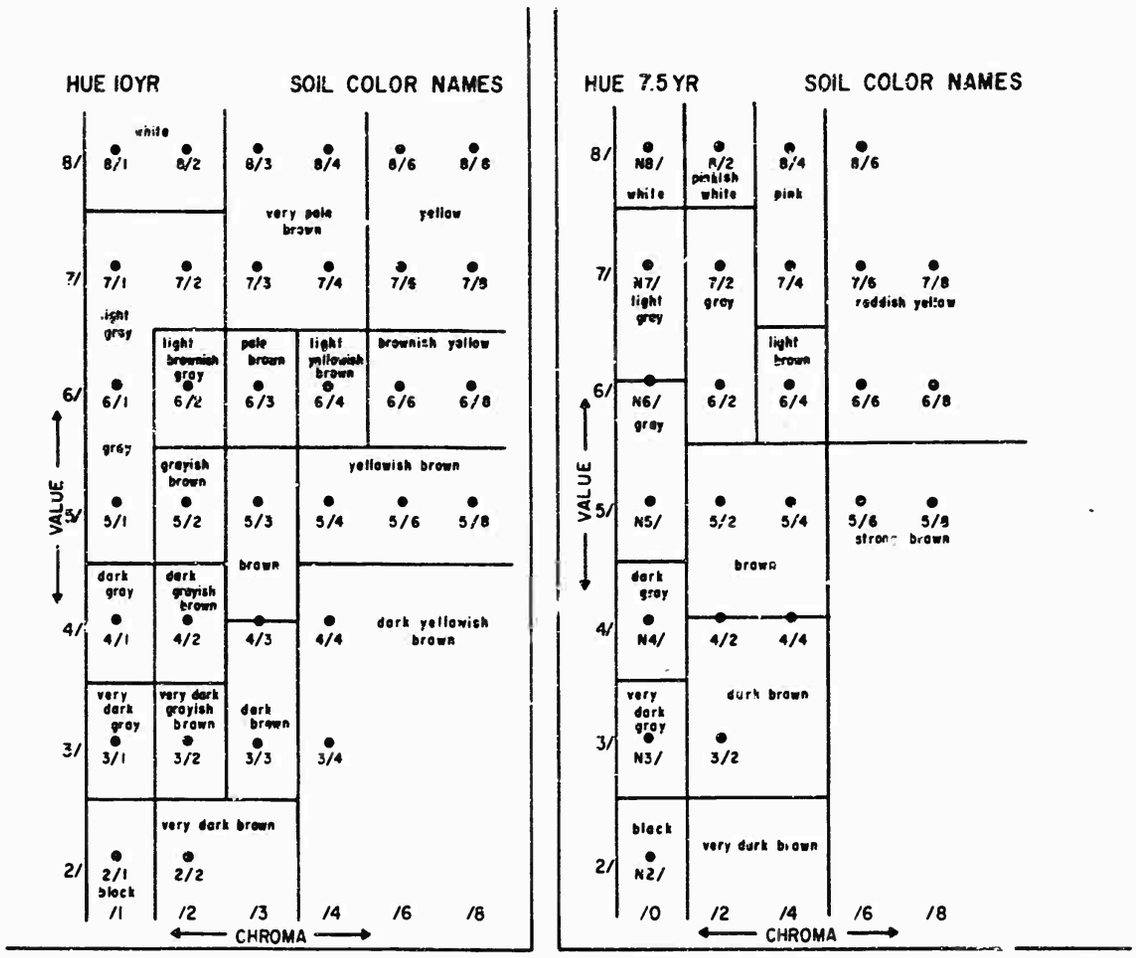
HUE 10YR
SOIL COLOR NAMES
white
8/1
8/2
8/3
8/4
8/6
8/8
very pale brown
yellow
7/1
7/2
7/3
7/4
7/6
7/8
light gray
light brownish gray
pale brown
light yellowish brown
brownish yellow
6/1
6/2
6/3
6/4
6/6
6/8
gray
grayish brown
yellowish brown
5/1
5/2
5/3
5/4
5/6
5/8
brown
dark gray
dark grayish brown
dark yellowish brown
4/1
4/2
4/3
4/4
very dark gray
very dark grayish brown
dark brown
3/1
3/2
3/3
3/4
very dark brown
2/1
2/2
black
/1
/2
/3
/4
/6
/8
VALUE
CHROMA
HUE 7.5YR
SOIL COLOR NAMES
N8/
white
8/2
pinkish white
8/4
pink
8/6
N7/
light gray
7/2
gray
7/4
7/6
reddish yellow
7/8
light brown
N6/
gray
6/2
6/4
6/6
6/8
N5/
5/2
5/4
5/6
strong brown
5/8
brown
dark gray
N4/
4/2
4/4
very dark gray
dark brown
N3/
3/2
black
very dark brown
N2/
/0
/2
/4
/6
/8
VALUE
CHROMA
HUE 5YR
SOIL COLOR NAMES
white
8/1
pinkish white
8/2
8/3
8/4
pink
7/1
7/2
7/3
7/4
7/6
7/8
light gray
pinkish gray
reddish yellow
light reddish brown
6/1
5/2
6/3
6/4
6/6
6/8
gray
reddish gray
5/1
5/2
5/3
5/4
5/6
5/8
dark gray
dark reddish gray
reddish brown
yellowish red
4/1
4/2
4/3
4/4
4/6
4/8
very dark gray
3/1
3/2
3/3
3/4
dark reddish brown
black
2/1
2/2
/1
/2
/3
/4
/6
/8
VALUE
CHROMA
HUE 2.5YR
SOIL COLOR NAMES
pale red
light reddish brown
light red
N6/
6/2
6/4
6/6
6/8
gray
N5/
5/2
5/4
5/6
5/8
weak red
reddish brown
red
dark gray
N4/
4/2
4/4
4/6
4/8
very dark gray
dusky red
N3/
3/2
3/4
3/6
black
very dusky red
dark reddish brown
dark red
N2/
2/2
2/4
/0
/2
/4
/6
/8
VALUE
CHROMA

VII - REFERENCES AND BIBLIOGRAPHY

Anonymous. 1965. Instrument Manual for Sediment Coring Apparatus. Prepared by Alpine Geophysical Associates, Inc., Norwood, N. J. 19 pp.

Anonymous. 1964. Procedure for Testing Soils, 4th ed. American Society for testing and materials. Philadelphia. 535 pp.

Anonymous. 1962. Tables of sound-speed in sea water. Oceanographic Analysis Division. U. S. Naval Oceanographic Office, SP-58.

Fairbridge, R., Gordon, A., and Olaussen, E. 1965. Atlantic Ocean, Encyclopedia of Oceanography, R. Fairbridge (editor), Reinhold Publishing Company, New York: 56-84.

Folk, Robert L., 1965. Petrology of Sedimentary Rocks, Hemphills, Austin. 159 pp.

Hamilton, Edwin L. 1964. Consolidation characteristics and related properties of sediment from experimental mohole (Guadalupe Site). J. Geophys. Res. 69 (20): 4257-4269.

Hamilton, Edwin L. 1963. Sediment sound velocity measurements made in-situ from the Bathyscaphe Trieste. J. Geophys. Res. 68 (21): 5991-5998.

Hamilton, Edwin L. 1965. Sound-speed and related physical properties of sediments from experimental Mohole (Guadalupe Site) Geophysics. 30 (2): 257-261.

Hansbo, Sven. 1957. A new approach to the determination of shear strength of clay by the Fall Cone Test. Royal Swedish Geotechnical Institute Proceedings 14: 46 pp.

Heezen, B.C. and Tharp, M. 1966. Physiography of the Indian Ocean. Phil. Trans. Roy. Soc. London, A, 259: 137-149.

Heezen, B.C. and Tharp, M. 1965. A symposium on Continental Drift VIII, tectonic fabric of the Atlantic and Indian Oceans and Continental Drift. Phil. Trans. Roy. Soc. London, A, 258: 90-106.

Heezen, B.C. and Tharp, M. 1965. Descriptive Sheet to Accompany Physiographic Diagram of the Indian Ocean. Geological Society of America.

Heezen, B.C. and Tharp, M. 1964. Physiographic diagram of the Indian Ocean, the Red Sea, the South China Sea, the Sulu Sea, and the Celebes Sea. Geol. Soc. Am. New York.

Heezen, B.C. and Tharp, M. 1961. Physiographic diagram of the South Atlantic Ocean, the Caribbean Sea, the Scotia Sea, and the eastern margin of the South Pacific Ocean. Geol. Soc. Am. New York.

Henry, James A. 1969. Area ST, Volume 2, Part 1, Bathymetry and Subbottom Profiling. Prepared by Alpine Geophysical Associates, Inc. U. S. Naval Oceanographic Office, SP-97-ST-2-1.

Hulsemann, Jobst. 1965. On the routine analysis of carbonates in unconsolidated sediments. J. Sediment Petrol. 36: 622-625.

Krumbien and Sloss. 1963. Stratigraphy and Sedimentation, 2nd ed., W.H. Freeman and Company, San Francisco. 497 pp.

Laughton, A.S. 1957. Sound propagation in compacted ocean sediments. Geophysics. 22 (2): 233-260.

Rodriguez, M. H., Jr. 1968. Area ST, Volume 2, Part 5, Hydrographic Station Data. Prepared by Alpine Geophysical Associates, Inc. U.S. Naval Oceanographic Office, SP-97-ST-2-5.

Shipek, C. J. 1966. Photo analysis of the sea floor microrelief. U. S. Navy Electronic Laboratory, Report 1374. San Diego. 70 pp.

Shumway, G. 1960. Sound-speed and absorption studies of marine sediments by a Resonance Method. Part I. Geophysics. 25 (2): 451-467.

Shumway, G. 1960. Sound-speed and absorption studies of marine sediments by a Resonance Method. Part II. Geophysics. 25 (3): 659-682.

Shumway, G. 1958. Sound velocity versus temperature in water saturated sediments. Geophysics. 23 (3): 494-505.

Siddiquie, H. N. 1967. Recent Sediments of the Bay of Bengal. Marine Geology (5): 249-291.

Sutton, G. H., Berckhemer, Hans, and Nafe, John E. 1957. Physical analysis of deep sea sediments. Geophysics. 22 (4): 779-812.

Williams, H., Turner, F. J., and Gilbert, C.M. 1954. Petrography. W. H. Freeman and Company, San Francisco.

Wood, A.B. 1949. A Textbook of Sound. G. Bell and Sons LTD., London. 578 pp.

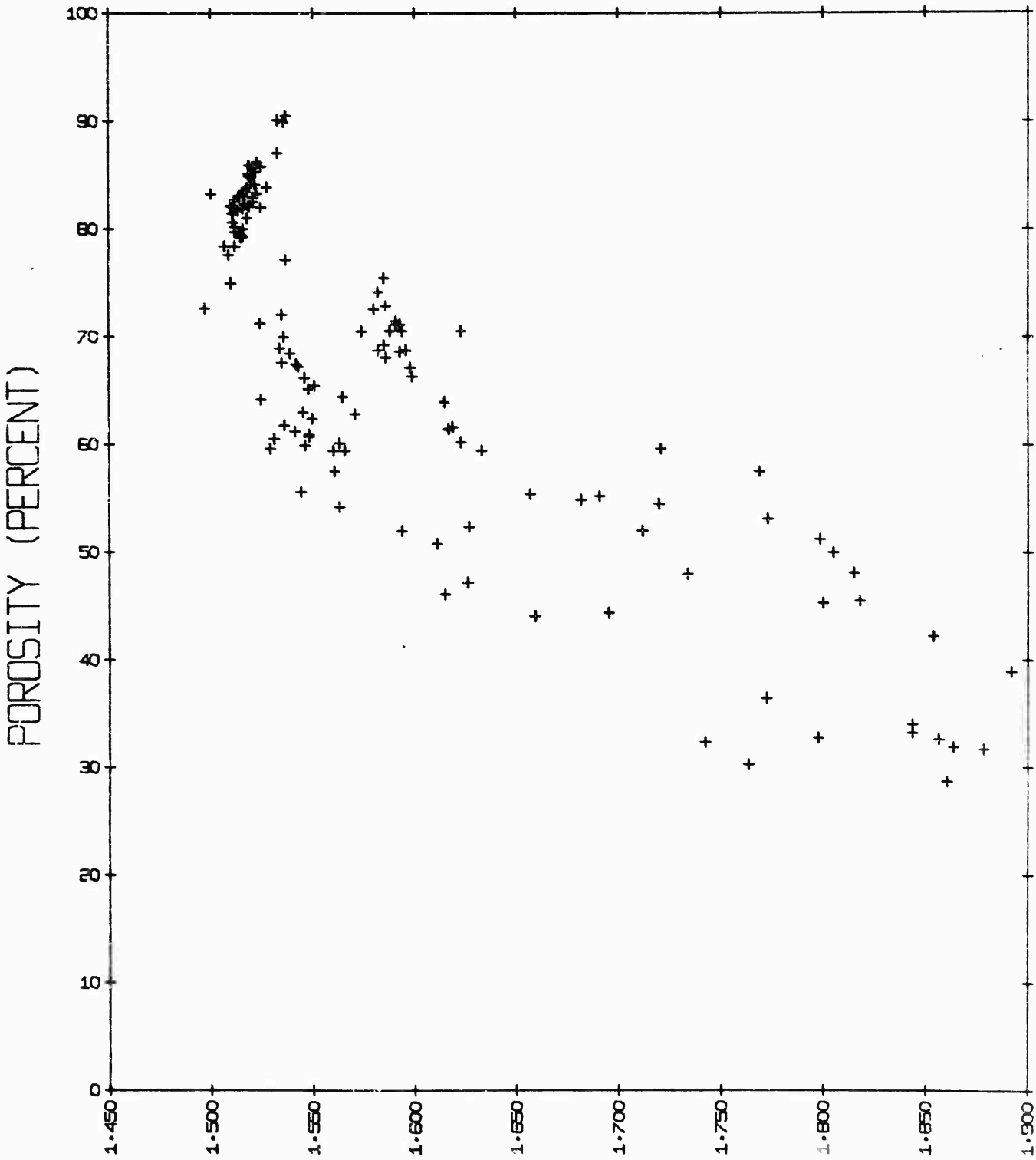

POROSITY VS. CORRECTED SOUND SPEED

FIGURE 1

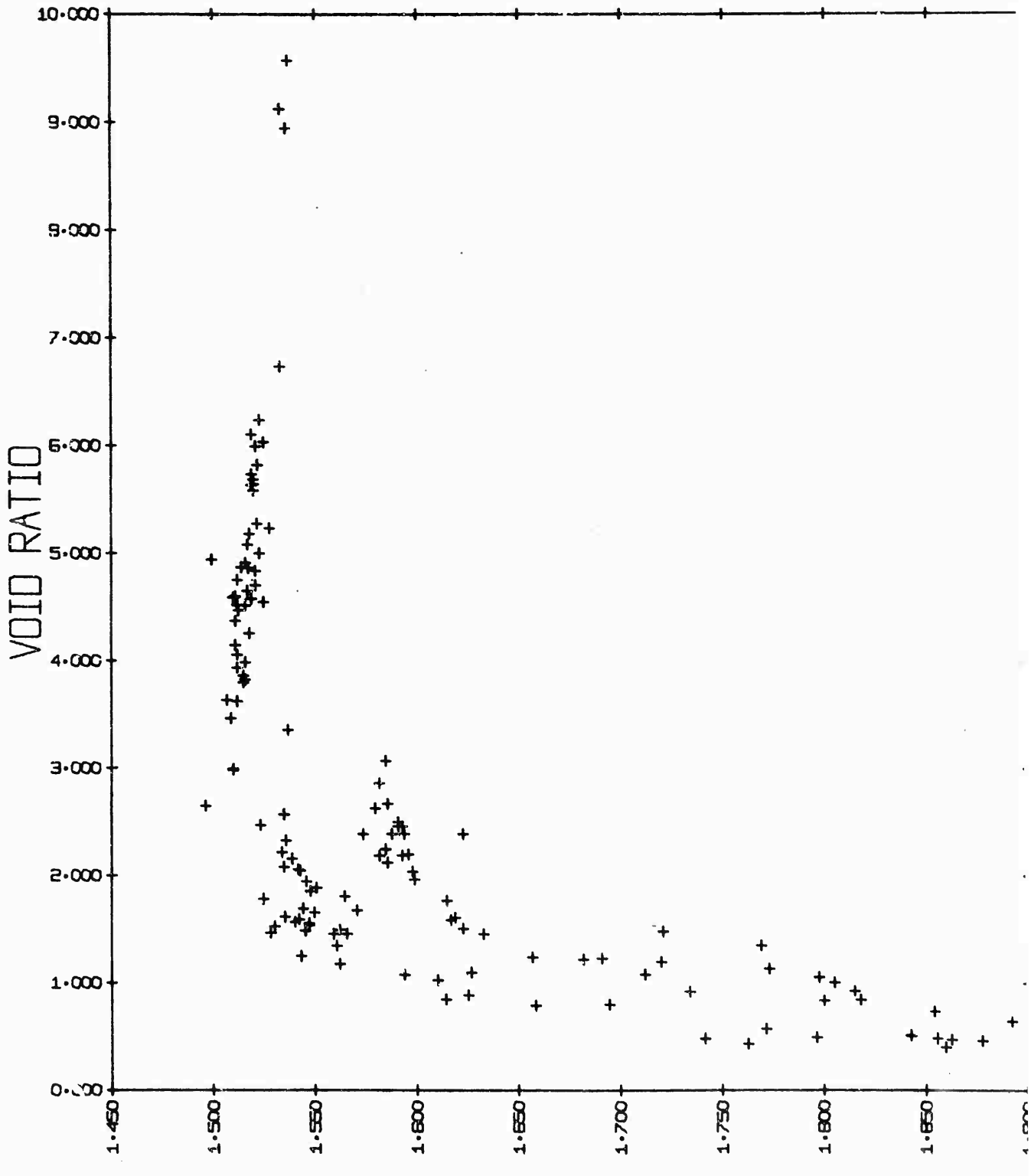

VOID RATIO VS. CORRECTED SOUND SPEED

FIGURE 2

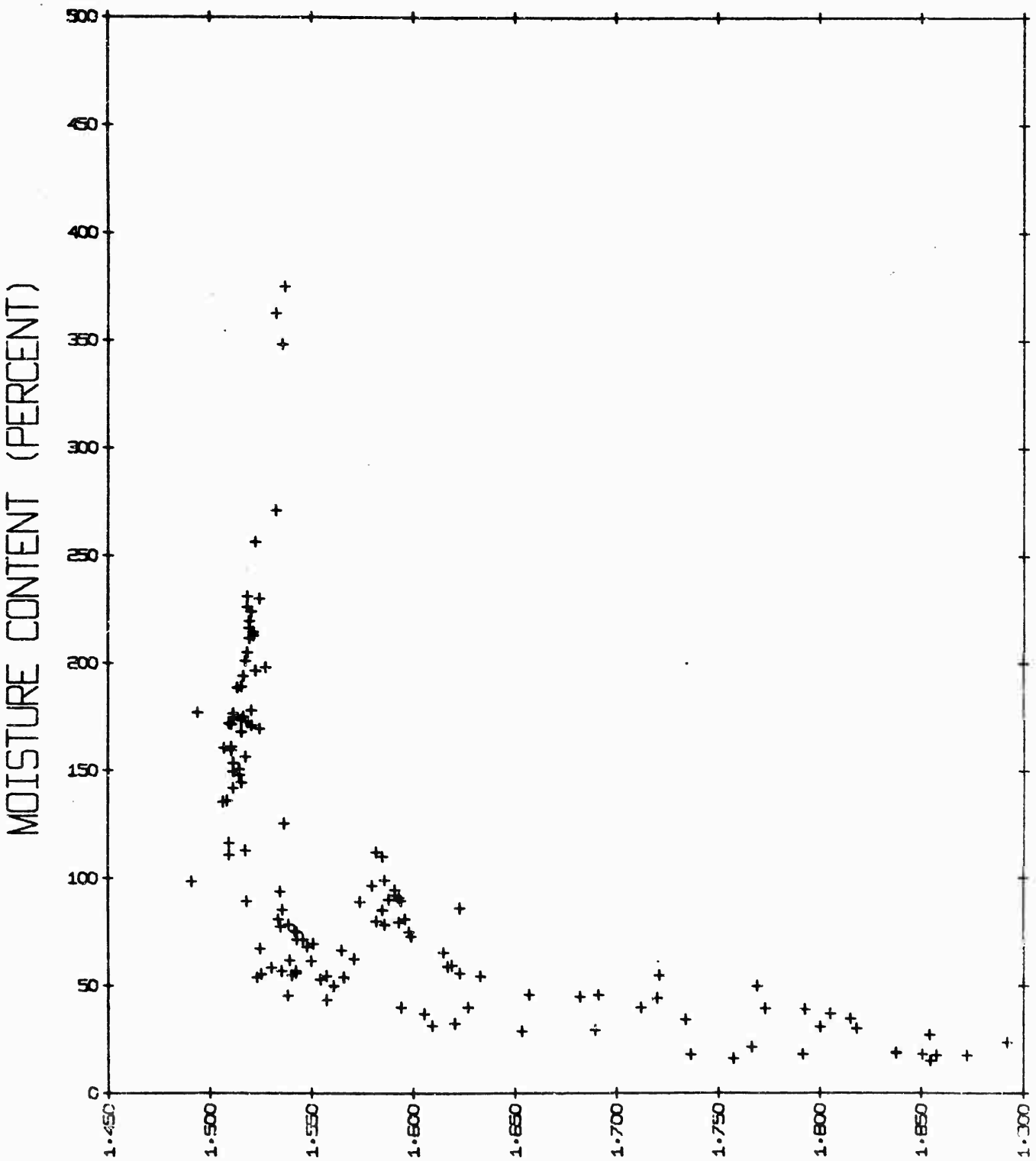

MOISTURE CONTENT VS. CORRECTED SOUND SPEED

FIGURE 3

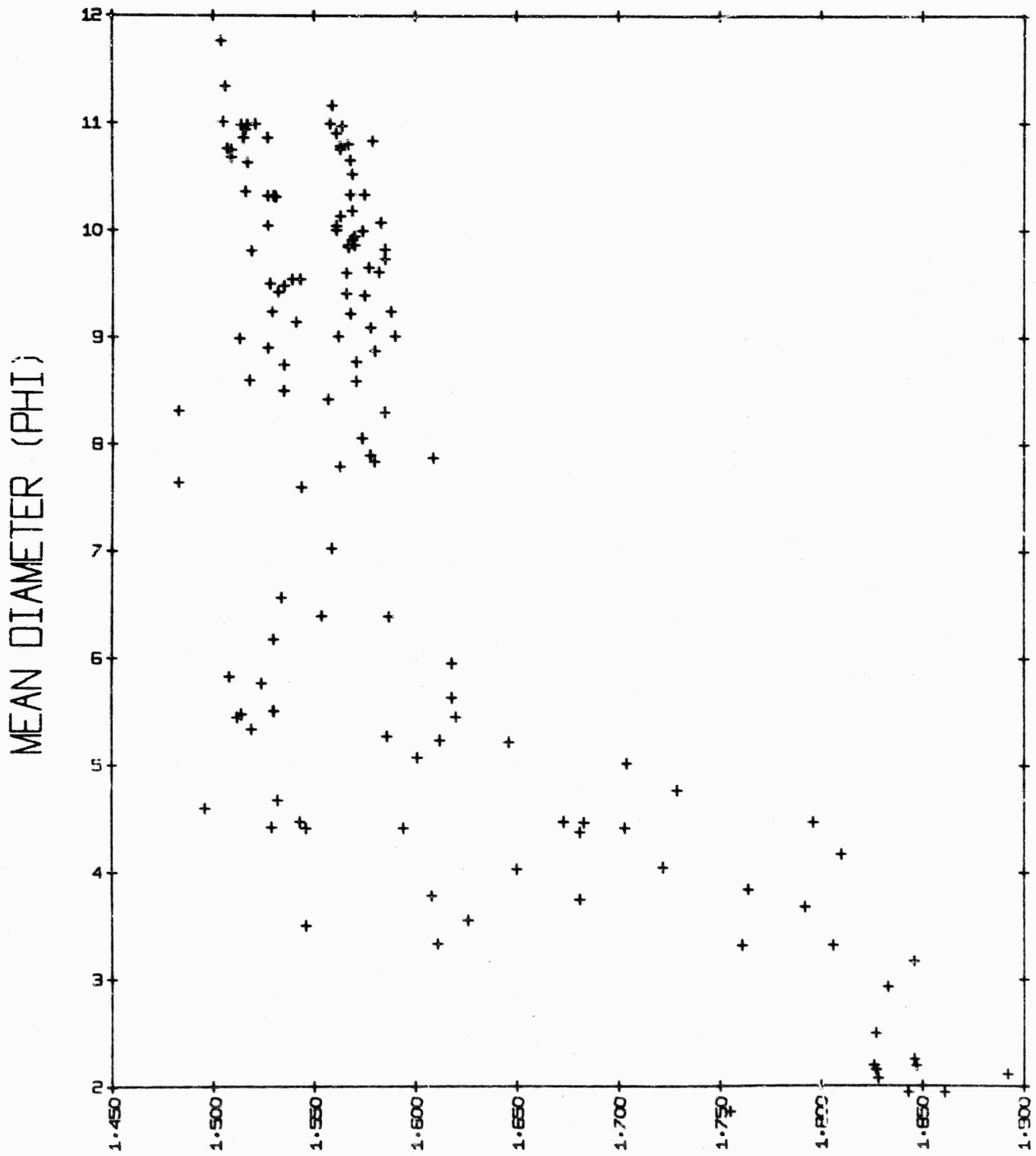

MEAN DIAMETER VS. CORRECTED SOUND SPEED

FIGURE 4

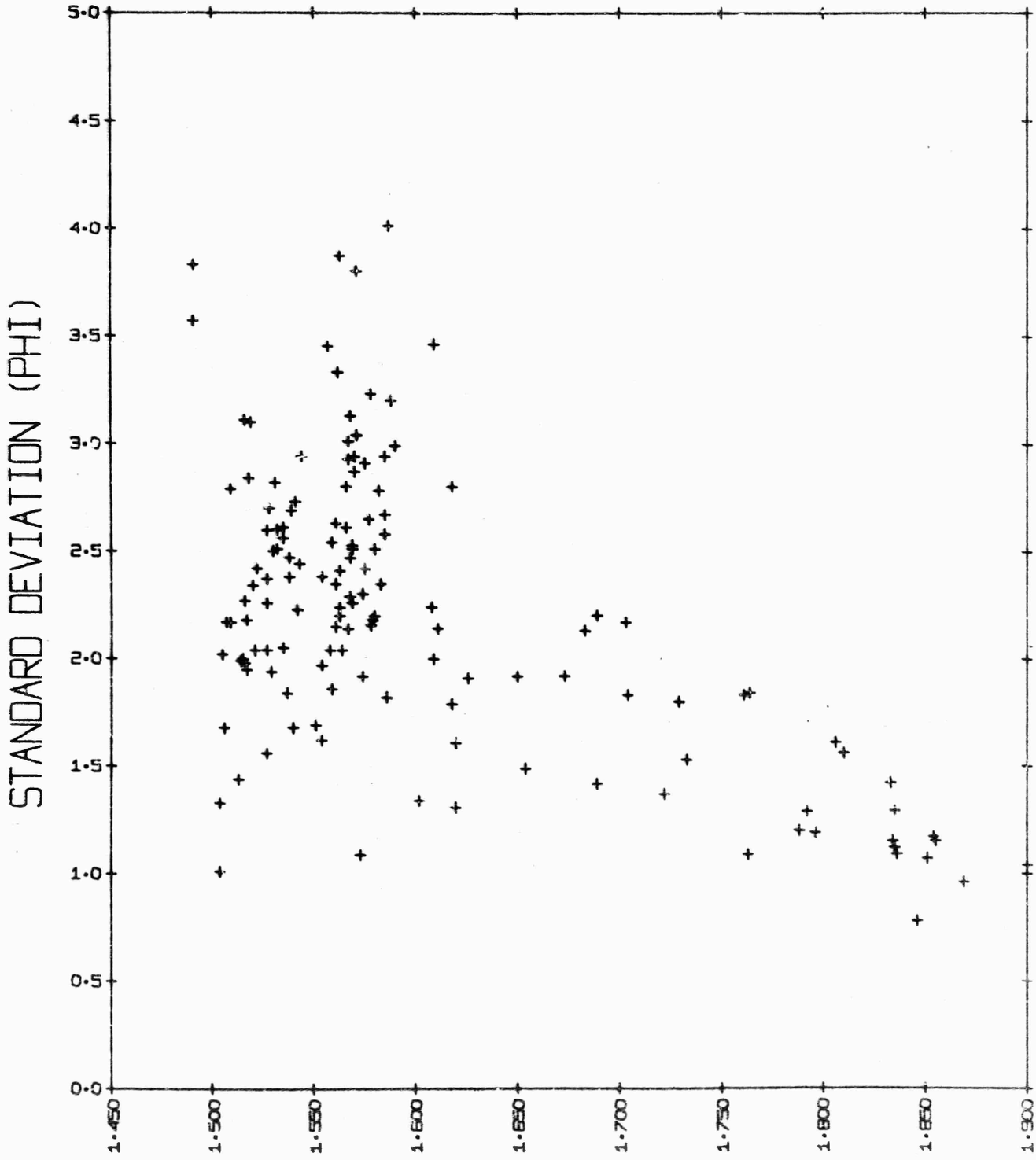

STANDARD DEVIATION VS. CORRECTED SOUND SPEED

FIGURE 5

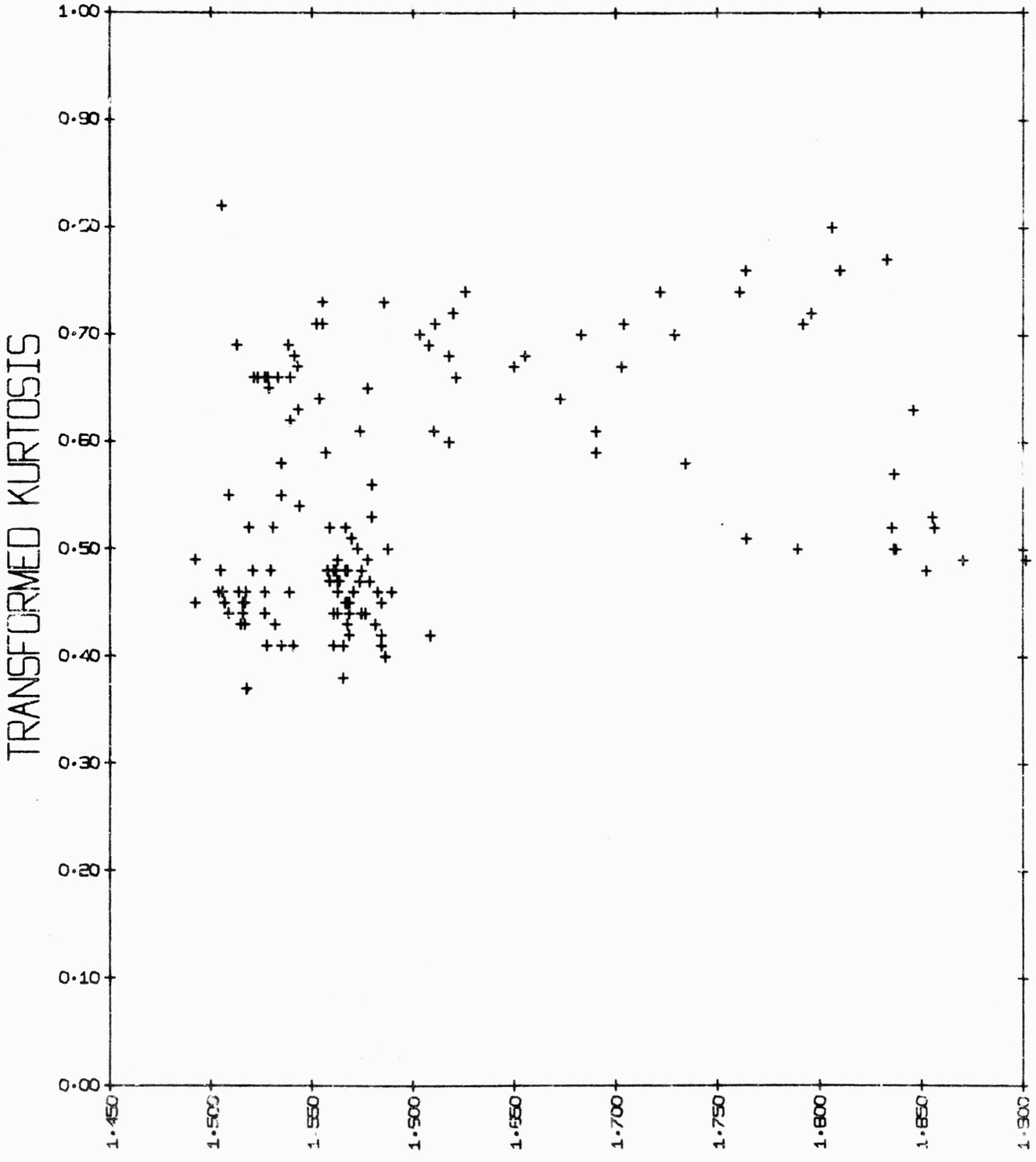

TRANSFORMED KURTOSIS VS. CORRECTED SOUND SPEED

FIGURE 6

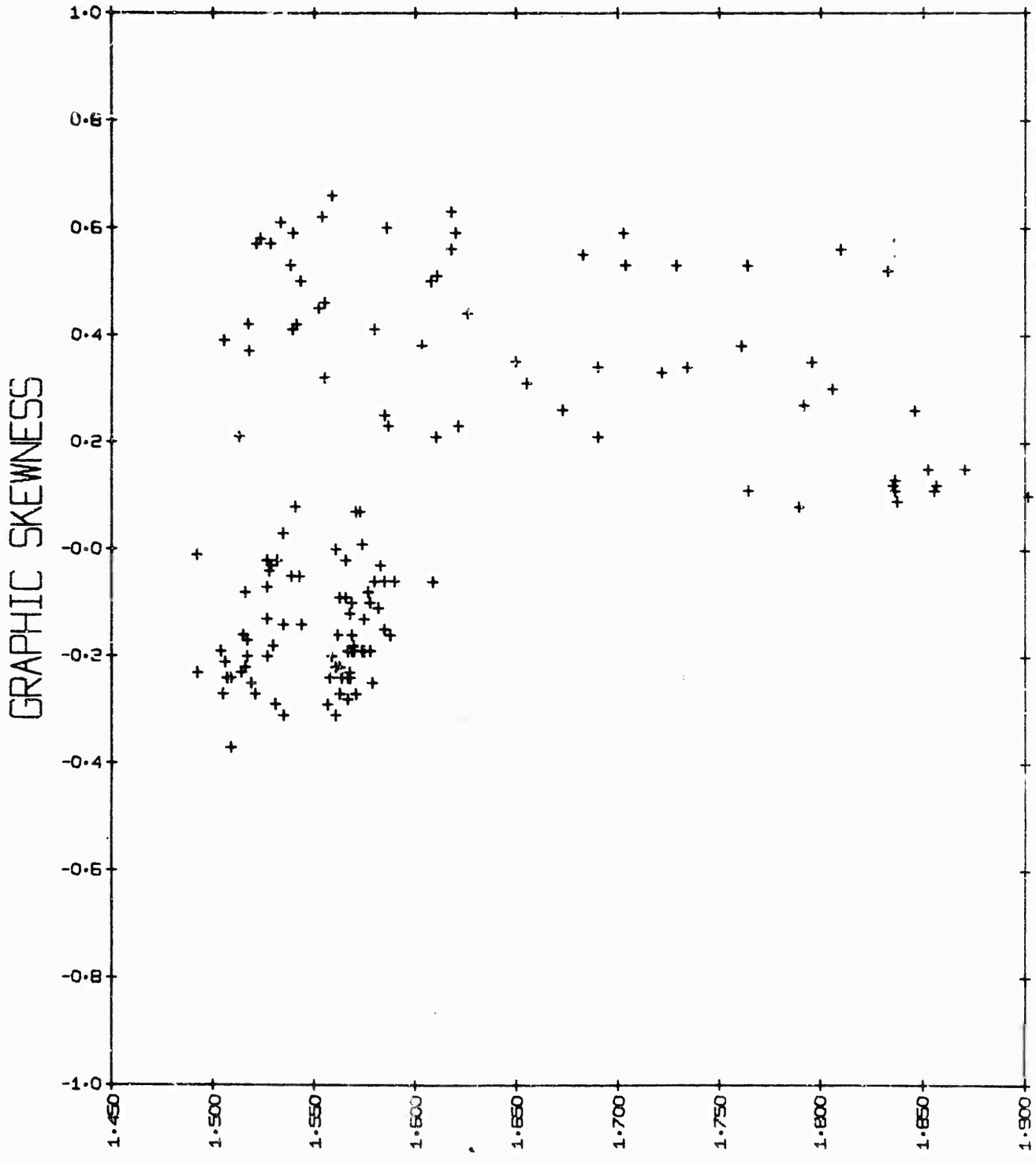

GRAPHIC SKEWNESS VS. CORRECTED SOUND SPEED

FIGURE 7

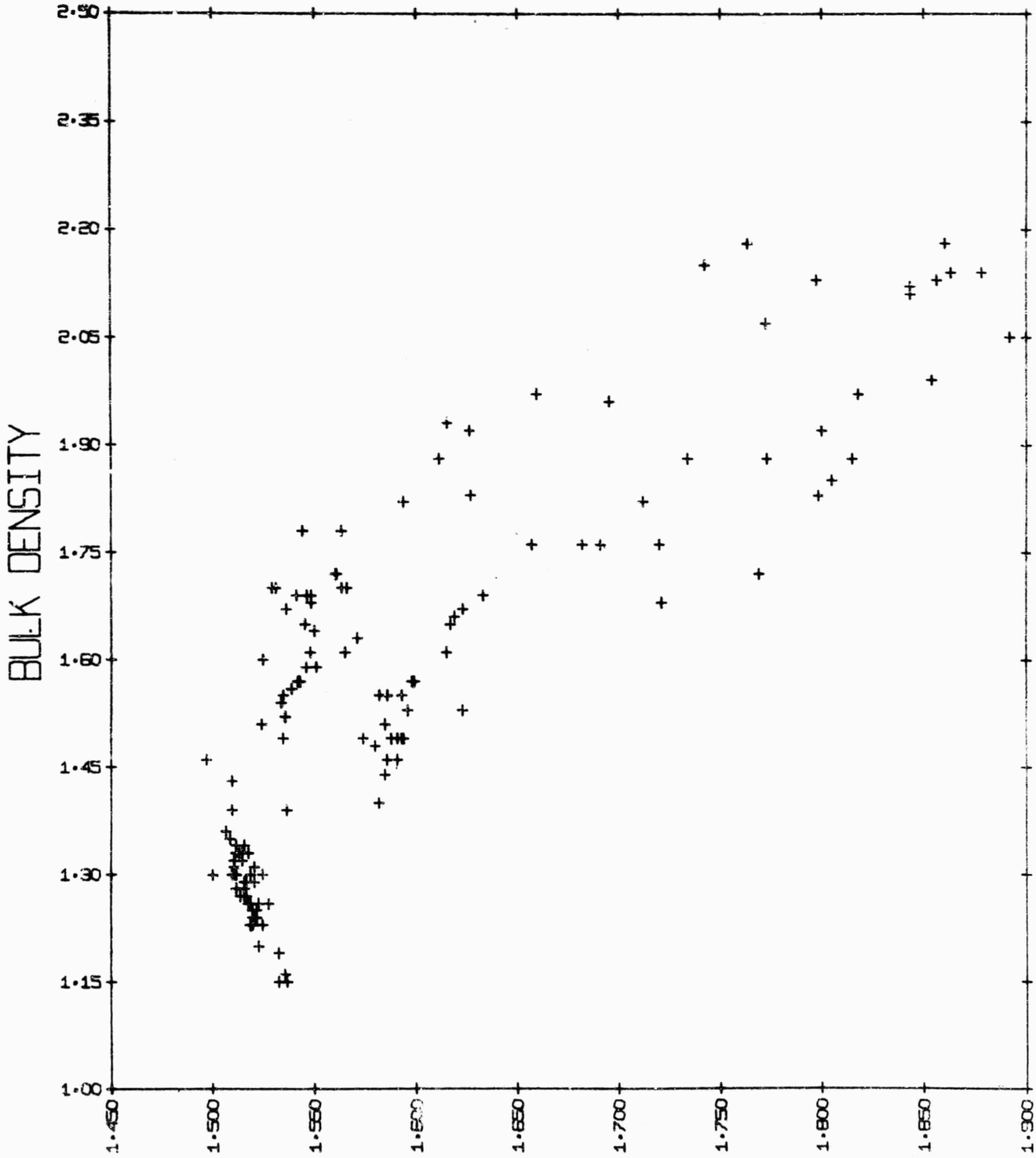

BULK DENSITY VS. CORRECTED SOUND SPEED

FIGURE 8

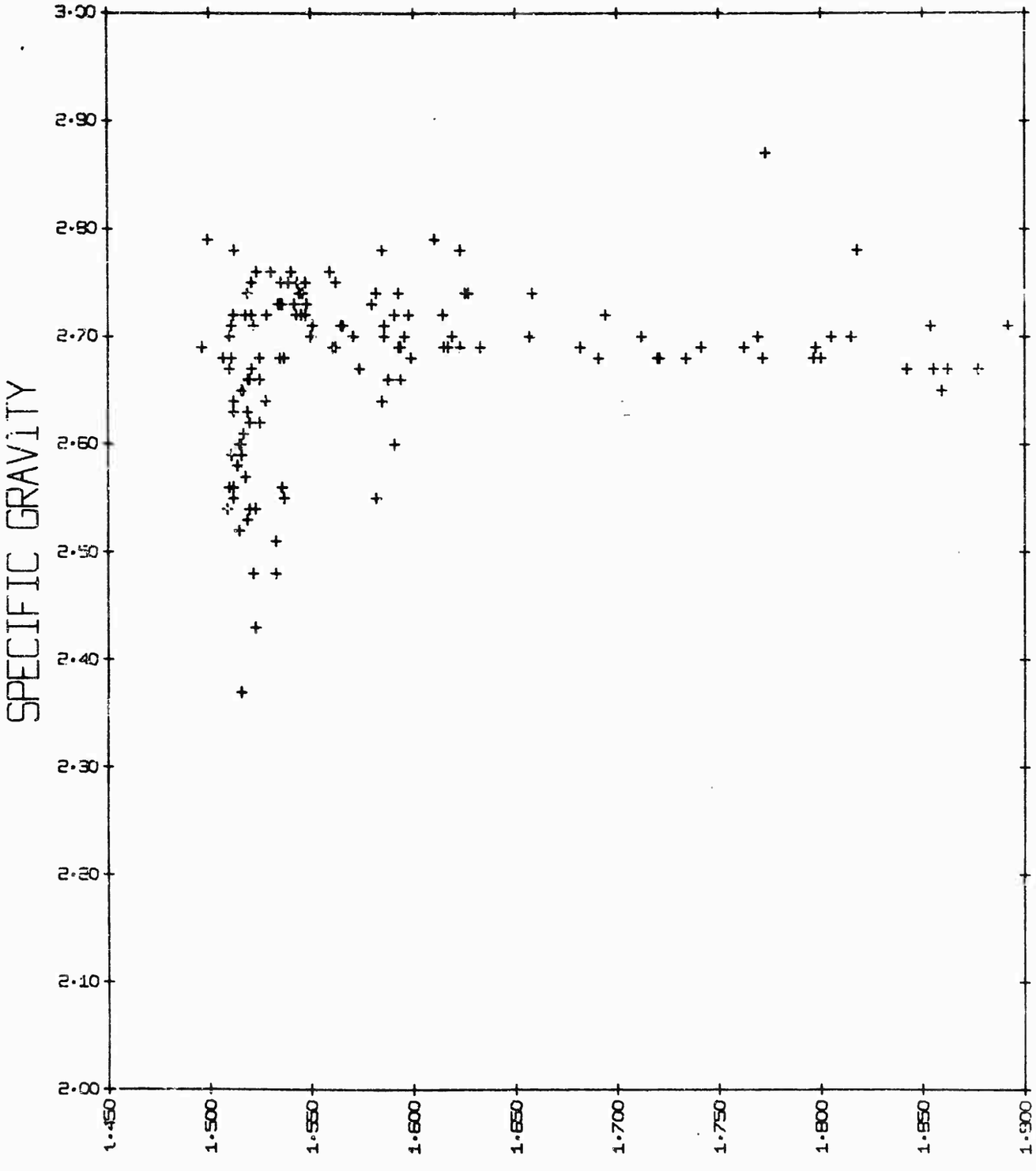

SPECIFIC GRAVITY VS. CORRECTED SOUND SPEED

FIGURE 9

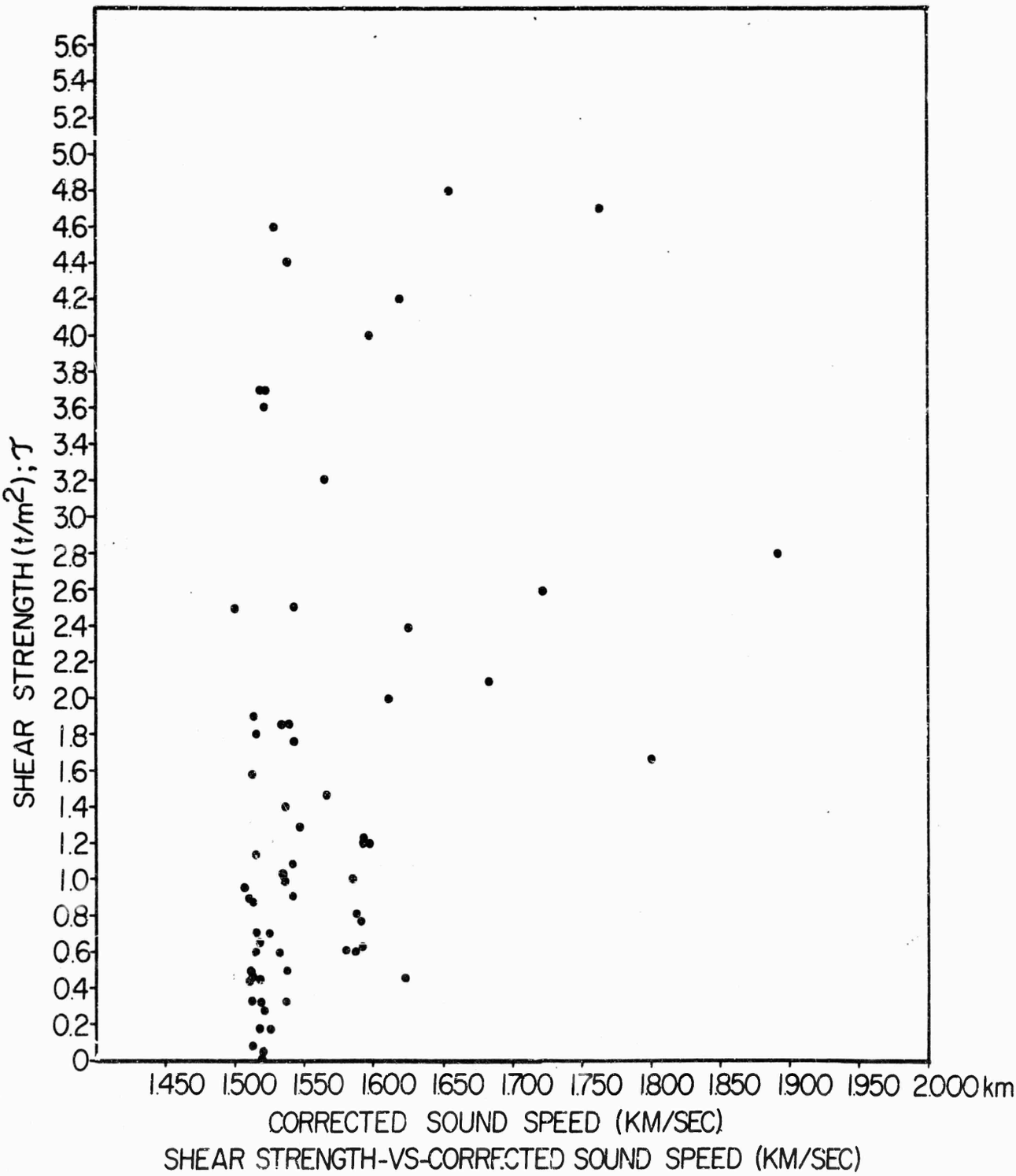

SHEAR STRENGTH-VS-CORRECTED SOUND SPEED (KM/SEC)

FIGURE 10

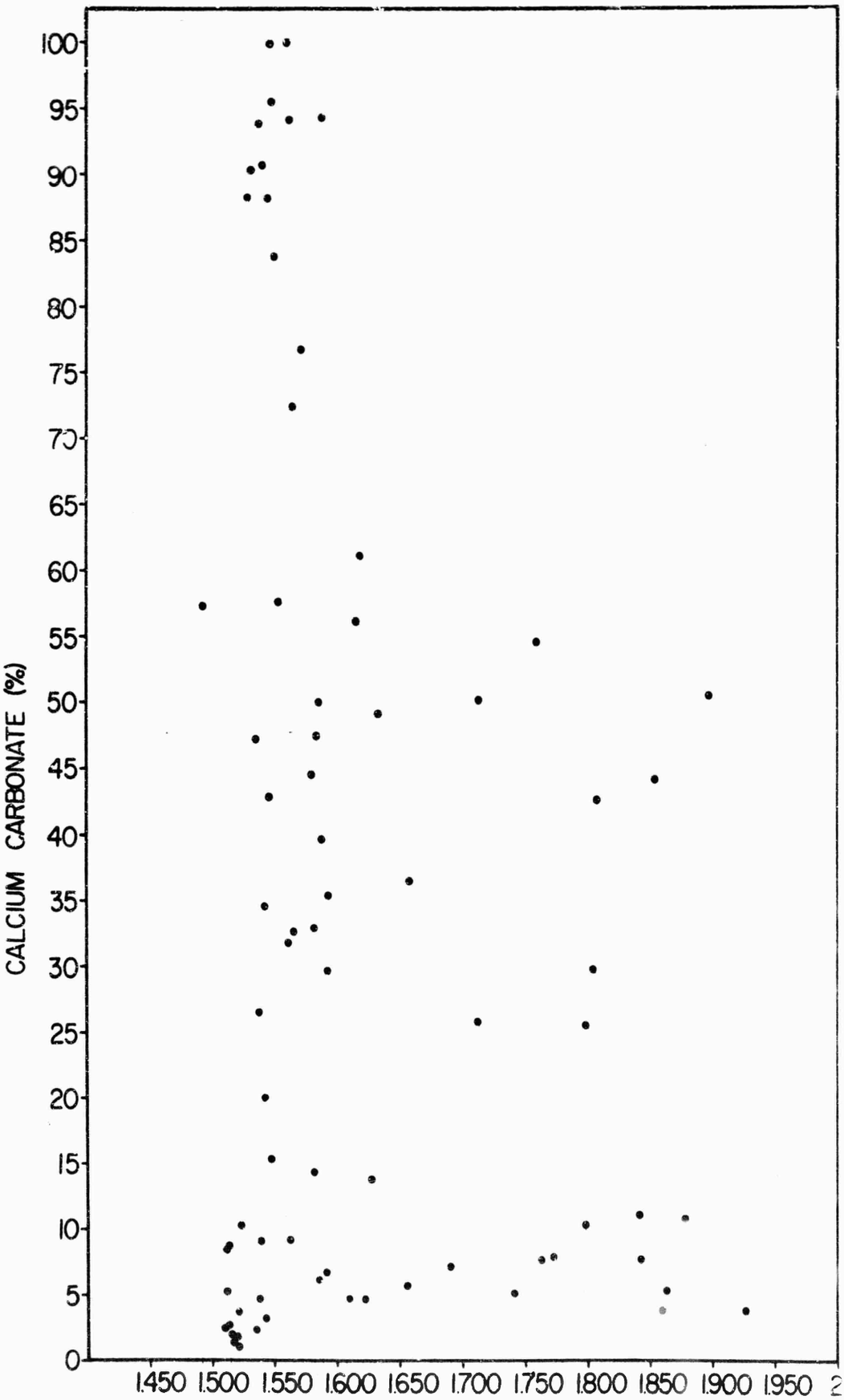

CALCIUM CARBONATE(%)-VS-CORRECTED SOUND SPEED (KM./SEC)

FIGURE 11

A


40°
60°
70°
80°
90°
30°
20°
10°
0°
20°
T-11
T-12
T-13
T-10
T-9
30°
40°
50°
60°
70°
80°
90°
PHYSIOGRAPHIC DIAGRAM OF THE
SOUTH ATLANTIC OCEAN
AND
INDIAN OCEAN
The Red Sea, the South China Sea, the Sulu Sea and the Celebes Sea
BY BRUCE C. HEEZEN AND MARIE THARP
LAMONT GEOLOGICAL OBSERVATORY
DEPARTMENT OF GEOLOGY
Columbia University
0
4000
8000
4000
2000
80-200
1000
5000
6000 METERS
FIGURE 12
PHYSIOGRAPHIC PROVINCES
WITH
CORE AND CAMERA LOCATIONS

B

FIGURE 12

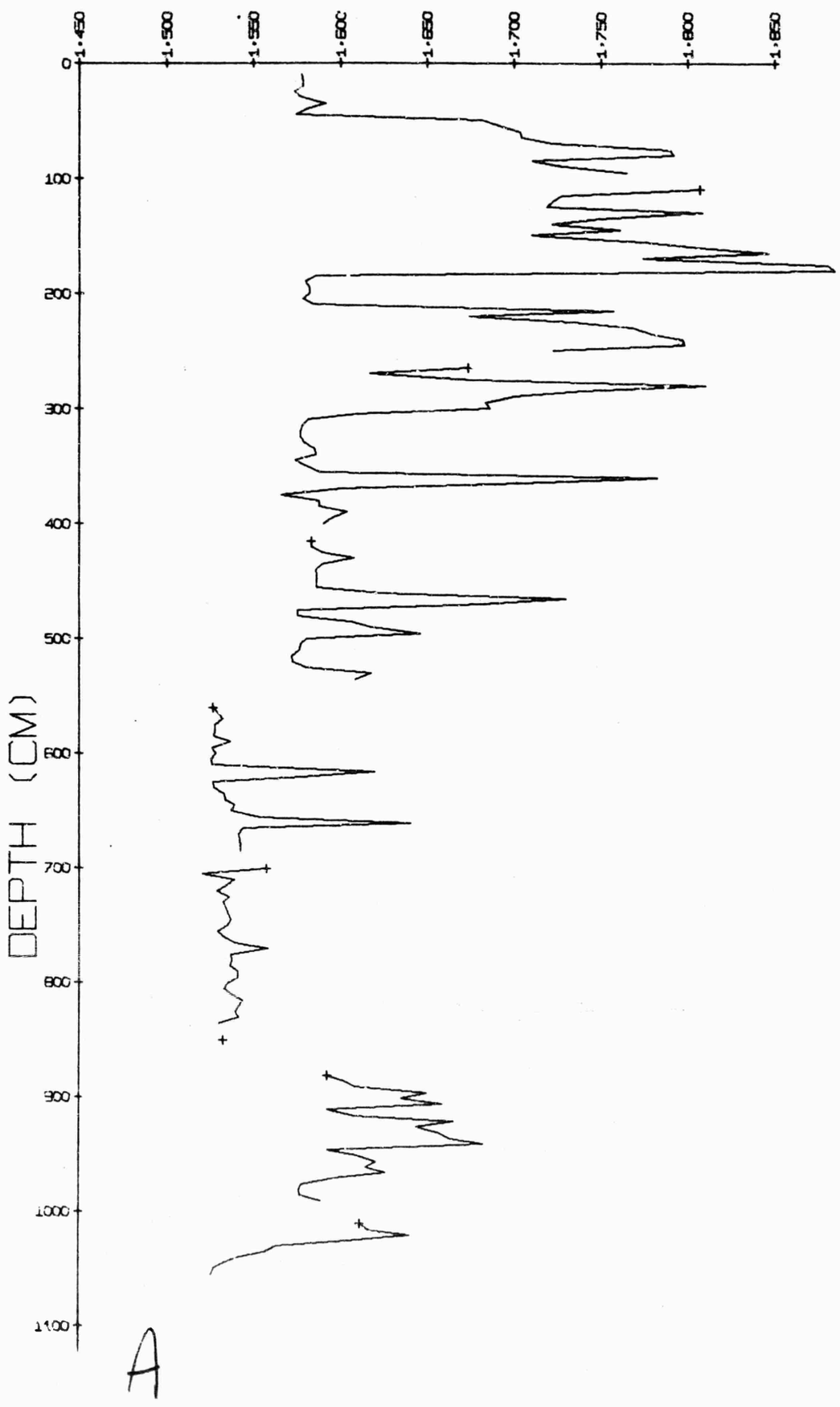
RA -ST - 1B - 1
SOUND SPEED (KM/SEC)
1.450
1.500
1.550
1.600
1.650
1.700
1.750
1.800
1.850
0
100
200
300
400
500
600
700
800
900
1000
1100
DEPTH (CM)
A

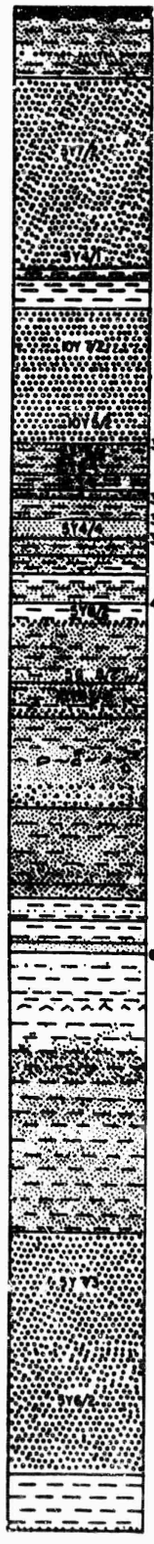

0-10 CM	NO SEDIMENT
10-80 CM	SILTY LUTITE WITH INTERCALATING BEDS OF LIGHT YELLOWISH BROWN (10YR 6/3) AND BROWN (7.5 Y 5/4) LUTITE. SEDIMENT BEST DESCRIBED AS A HIGHLY MOTTLED "RED CLAY". FORAMINIFERAL SAND LAYER OCCURS BETWEEN 34 AND 36CM. CHARP BOTTOM CONTACT.
80-304 CM	FORAMINIFERA SAND, DARK GRAY(5Y 4/1) ALTERING TO A LIGHT GRAYISH OLIVE (5Y 5/2) BELOW 214CM. TEST ARE PREDOMINANTLY SILT SIZE AND DISPLAY BEDDING DUE TO SLIGHT COLOR VARIATIONS. THE CONTINUITY OF THE LAYER IS INTERRUPTED BETWEEN 183-193CM BY A LAYER OF UNIFORM LUTITE, PALE OLIVE (10Y 6/1) AND A LAYER OF SILTY LUTITE BROWN (10YR 5/3) BETWEEN 193-214CM. A MICROLAMINA OF FORAMINIFERA SAND SEPARATES THE TWO LAMINAE. SHARP BOTTOM CONTACT.
304-336 CM	SILTY LUTITE, LIGHT BROWNISH GRAY (2.5Y 6/2) GRADING AT 310CM TO A PALE OLIVE (10Y 6/1), SILTY LUTITE. MOTTLE BURROWING AT TOP BUT ABSENT BELOW 329CM. SHARP BOTTOM CONTACT.
336-341 CM	FORAMINIFERA SAND, DARK OLIVE GRAY (5Y 3/4), OF SILT SIZE TESTS PREDOMINANTLY GLOBIGERINA SP. SMALL PERCENTAGE OF QUARTZ GRAINS PRESENT. SHARP BOTTOM CONTACT.
341-357 CM	LUTITE, COLOR ALTERING FROM PALE OLIVE TO OLIVE OCCURS AT 348 CM. BURROWING PROMINENT BETWEEN 341 AND 345 CM. SHARP BOTTOM CONTACT.
357-372 CM	FORAMINIFERA SAND, OLIVE (5Y 4/4). SIMILAR TO 336-341CM. SHARP BOTTOM CONTACT.
372-417 CM	FORAMINIFERAL LUTITE, OCCURRING IN 10CM. LAYERS WITH WELL DEFINED COLOR BOUNDARIES. DARK GRAYISH BROWN (2.5YR 3/2) OCCURS BETWEEN 372-382 CM, PALE OLIVE (10Y 6/1) FROM 382-394CM, BROWNISH GRAY (10YR 6/2) FROM 394-405CM AND BROWN (10YR 5/3) FROM 405-417 CM. MOTTLE BURROWING IS SLIGHT THROUGHOUT THE ZONE. SHARP BOTTOM CONTACT.
417-429 CM	LUTITE, LIGHT GREENISH GRAY (5GY 8/2) WITH SOME BURROWS. BURROWS FILLED WITH SEDIMENT FROM OVERLYING LAYERS. SHARP BOTTOM CONTACT.
429-432 CM	FORAMINIFERA SAND AND LUTITE LAYER, LIGHT GREENISH GRAY (5GY 8/2). SHARP BOTTOM CONTACT.
432-452 CM	SILTY LUTITE, PALE ORANGE (10YR 7/2) GRADING WITH DEPTH TO YELLOWISH BROWN (10YR 6/2) SILTY LUTITE AT 440 CM. CONTACT REGION (~440CM) IS EXTENSIVELY MOTTLE BURROWED. COLOR CONTACT NOT DISTINCT DUE TO MOTTLING.
452-471 CM	SILTY LUTITE, LIGHT GREENISH GRAY (5G 8/2) SIMILAR IN APPEARANCE TO THE 417-429 CM ZONE, GRADES WITH DEPTH TO A FORAMINIFERAL SANDY SILT (10YR 6/2). MOTTLE BURROWING PRESENT. BURROWS FILLED WITH PALE ORANGE AND YELLOWISH BROWN LUTITE. SHARP BOTTOM CONTACT.
471-497 CM	SILTY LUTITE, PALE ORANGE (10YR 7/2) SHOWING EXTENSIVE MOTTLE BURROWING GRADES WITH DEPTH TO A FORAMINIFERAL SANDY SILT WITH A MODERATE PERCENTAGE OF LUTITE STILL PRESENT. FORAMINIFERAL SANDY SILT DISPLAYS BEDDING OF A MEDIUM GRAY (4) AND DUSKY YELLOW (5Y 6/4). COLORS BETWEEN 495-497CM. SHARP BOTTOM CONTACT.
497-523 CM	SILTY LUTITE, MODERATE YELLOWISH BROWN (10YR 5/4), MOTTLE BURROWING SLIGHT, GRADES TO DIATOMACEOUS SILTY, GRAY (10YR 6/1), AT 523 CM. BOTTOM CONTACT BLURRED BY BURROWING.
523-542 CM	FORAMINIFERA SILT LAYERS: 523-528 CM GRAY (10YR 6/1) 528-539 CM GRAY (10YR 5/1) GRADES TO DARK GRAY (10YR 4/1) 539-542 CM GRAY (10YR 6/1)
542-560 CM	SANDY SILT, LIGHT GRAY (10YR 7/1) WITH DARK GRAY (10YR 4/1) AND VERY PALE BROWN (10YR 7/3) SANDY SILT BED. SHARP BOTTOM CONTACT.
560-615 CM	SILTY LUTITE, BROWN (7.5 Y 5/4) MOTTLED WITH PALE ORANGE (10YR 8/2) LUTITE. GRADES TO LIGHT OLIVE GRAY (5Y 6/2) SILTY LUTITE WITH BLACK SILT INCLUSIONS. SILT CONTENT DECREASES WITH DEPTH. SHARP BOTTOM CONTACT.
615-622 CM	FORAMINIFERA SILT LAYERS. 618 CM - 616 CM SILT, OLIVE (5Y 4/4) 616 CM - 617 CM SILT, OLIVE (5Y 5/4) } 5° ANGLE 617 CM - 618 CM SILTY LUTITE, PALE YELLOW (5Y 7/3) 618 CM - 620 CM SILTY LUTITE, LIGHT OLIVE GRAY (5Y 5/2) 620 CM - 622 CM SILT PALE OLIVE (5Y 6/3) SHARP HORIZONTAL BOTTOM CONTACT.
622-635CM	LUTITE, WHITE (5Y 8/2) WITH HORIZONTAL BEDS OF BLACK SILT. BASE OF ZONE IS SLIGHTLY SILTY. SHARP BOTTOM CONTACT.
635-641 CM	LUTITE, LIGHT BROWNISH GRAY (10YR 6/2) SLIGHTLY SILTY. BURROWING AND MOTTLING AT BASE.
641-653 CM	COCCOLITH OOZE, PALE ORANGE (10YR 8/1) PLASTIC, SOME FORAMINIFERA TESTS. BURROWS CONTAIN LIGHT BROWN LUTITE FROM OVERLYING ZONE. GRADATIONAL BOTTOM CONTACT. (DISTURBED)
653-661 CM	SILT, LIGHT BROWNISH GRAY (10YR 6/2), MOTTLED. SHARP BASAL CONTACT.
661-715 CM	COCCOLITH OOZE, PALE ORANGE (10YR 9/2). SMALL FORAMINIFERA CONTENT. VERY PLASTIC AND UNIFORM IN APPEARANCE. GRADING TO LIGHT YELLOWISH BROWN (10YR 6/2) LUTITE (703CM) SLIGHTLY FORAMINIFERAL.
715-843 CM	INTERCALATION OF SILTY LUTITE LAYERS. (1) MODERATE YELLOWISH BROWN (10YR 5/4) [715-720, 722-745, 794-810, 827-837 CM] (2) LIGHT YELLOWISH BROWN (10YR 6/4) [745-755 CM, 770-794 CM] (3) YELLOWISH GRAY (5Y 7/2) [720-722, 755-760, 837-843 CM] (4) LIGHT GRAY (2.5 Y 7/2) [760-770 CM AT 792 CM] 810-825 CM COCCOLITH OOZE AND LUTITE. BLACK SILT INCLUSIONS.
843-1025CM	SILTY LUTITE, YELLOWISH GRAY (5Y 7/2) GRADES TO FORAMINIFERA SAND, PALE YELLOW (5Y 7/3) TO LIGHT OLIVE GRAY (5Y 6/2). LUTITE INCLUSIONS AND PATCHES.
1025-1040CM	COCCOLITH OOZE, WITH FORAMINIFERA CONTENT. WHITE (5Y 8/2) RELATIVELY UNIFORM WITH MOTTLE BURROWING AT BASE.
1040-1063CM	LUTITE, LIGHT GREENISH GRAY (5Y 7/1) EXTENSIVELY MOTTLE BURROWED WITH FILL FROM OVERLYING ZONE. SHARP BOTTOM CONTACT.
1063-1064CM	FORAMINIFERA SAND.

B

FIGURE 13

RA -ST - 1B - 2

SOUND SPEED (KM/SEC)

A

CSB-14

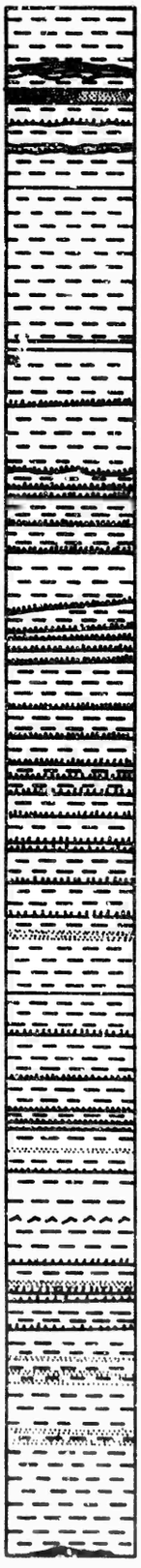

0-1120 CM LUTITE, SHOWING VARIATIONS IN COLORS AND CHARACTERIZED BY LAMINAE OF BRITTLE AND SLIGHTLY INDURATED LUTITE. LAMINAE AT 68CM, 120CM, 160-170CM, 560CM, AND 575-580CM, HAVE A SLIGHT DIATOM CONTENT WHICH GIVE THEM A FLUFFY TEXTURE.

0-35CM "RED CLAY" MOTTLE-BURROWED AT THE TOP.

35-275CM LUTITE, PREDOMINANTLY OLIVE GRAY AND DARK GRAYS IN COLOR.

275-340CM LUTITE OLIVE GRAY ALTERING TO A "RED CLAY" AT 310CM.

340-1120CM LUTITE, SIMILAR TO THAT FOUND BETWEEN 35-275CM. A FORAMINIFERA SAND AND SILT LAYER OCCURS AT 675CM.

MOTTLE BURROWING IS MODERATE THROUGHOUT.

B

FIGURE 14

RA -ST - 1B - 3
SOUND SPEED (KM/SEC)

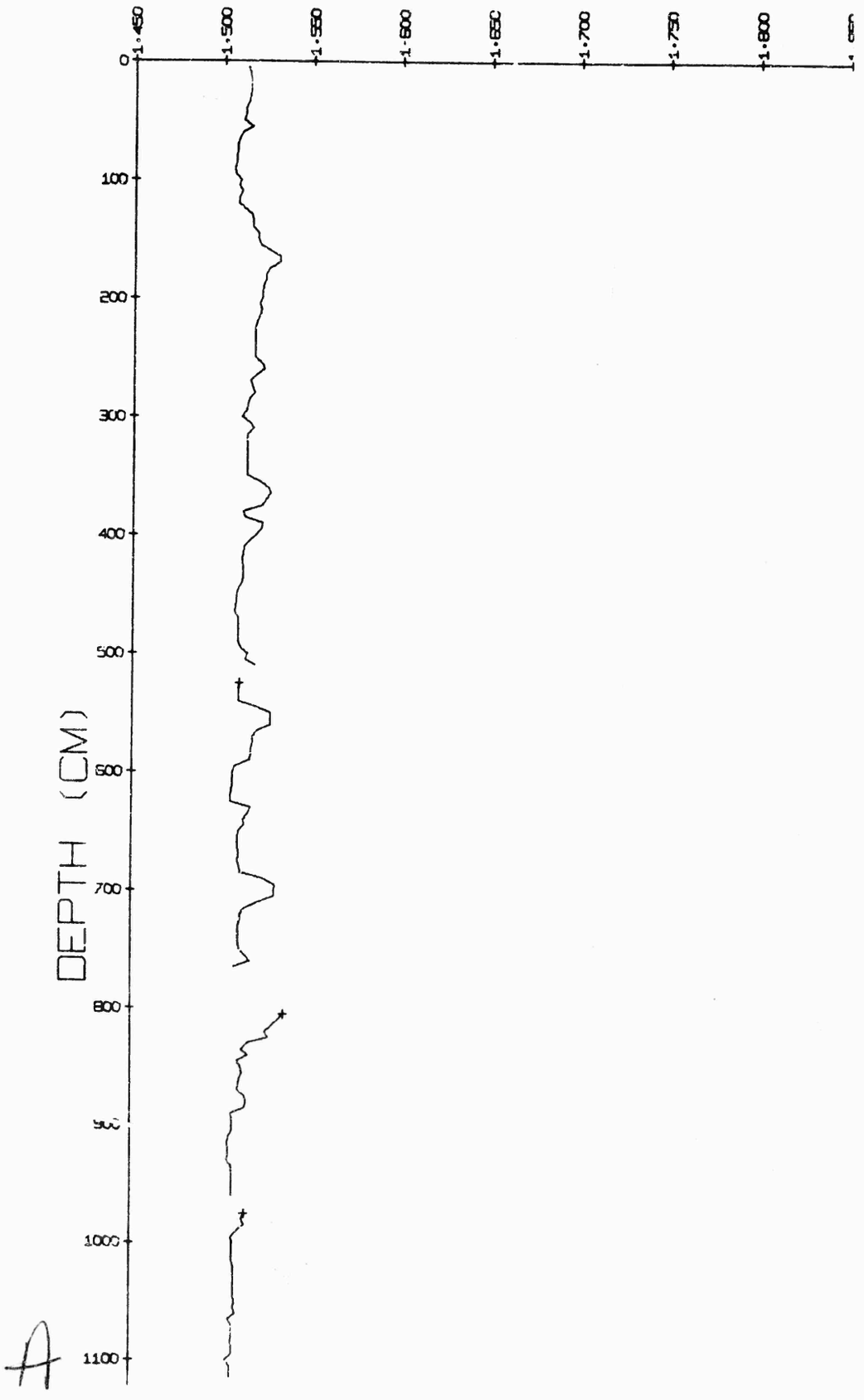

A

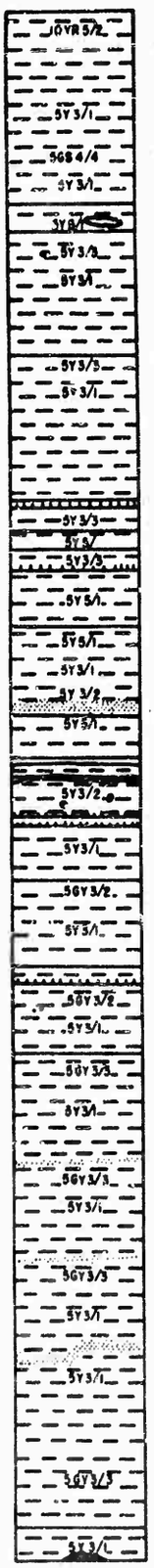

0 - 20 CM LUTITE, LIGHT BROWN (10YR 5/2), MOIST WITH SMALL PERCENTAGE OF FORAMINIFERA TESTS SEDIMENT DISTURBED AT TOP DUE TO CORING. IRREGULAR BOTTOM CONTACT.

20 - 100 CM LUTITE, OLIVE GRAY (5Y 3/1), PLASTIC AND UNIFORM IN APPEARANCE. GRADATIONAL BOTTOM CONTACT.

100 - 106 CM LUTITE, BLUISH GREEN (5GB 4/4), SLIGHTLY BRITTLE. GRADATIONAL BOTTOM CONTACT

106 - 141 CM LUTITE, OLIVE GRAY (5Y 3/1), PLASTIC, AND UNIFORM IN APPEARANCE. SHARP

141 - 161 CM LUTITE, MODERATE OLIVE GRAY (5Y 5/1), GRADING WITH DEPTH TO OLIVE GRAY (5Y 3/1) LUTITE. DIATOMS PRESENT IN MODERATE AMOUNTS. SHARP BOTTOM CONTACT.

161 - 253 CM LUTITE, DARK OLIVE, (5Y 3/3), GRADING TO MODERATE OLIVE GRAY (5Y 3/1) LUTITE AT ~ 180 CM DIATOM CONTENT GIVES SEDIMENT A FLUFFY TEXTURE. SEDIMENT BECOMES PLASTIC AND UNIFORM WITH A DECREASE IN DIATOM CONTENT WITH DEPTH. SHARP BOTTOM CONTACT.

253 - 356 CM LUTITE, DARK OLIVE (5Y 3/3), GRADING TO MODERATE OLIVE (5Y 3/1) LUTITE AT ~ 268 CM. DIATOMS PRESENT IN ABUNDANCE. RESEMBLE OVERLYING ZONE. COLOR GRADES TO MODERATE OLIVE (5Y 3/1) BELOW 268 CM. SHARP BOTTOM CONTACT.

356 - 378 CM LUTITE, DARK OLIVE (5Y 3/3), SIMILAR TO SEDIMENT OF OVERLYING ZONE. SHARP BOTTOM CONTACT.

378 - 389 CM LUTITE, GRAY (5Y 5/1). TOP 4 CM OF ZONE ARE BRITTLE AND APPEAR DRIER THAN REMAINDER OF ZONE. SHARP BOTTOM CONTACT.

389 - 445 CM LUTITE, DARK OLIVE (5Y 3/3) ALTERING TO GRAY (5Y 5/1) LUTITE AT 406 CM AND TO MODERATE GRAY AT 415 CM. SEDIMENT EXCEPT FOR COLOR IS RELATIVELY UNIFORM WITH SEMI-INDURATED LAMINA AT 406. SHARP BOTTOM CONTACT.

445 - 510 CM LUTITE, GRAY (5Y 5/1), GRADING TO MODERATE GRAY LUTITE (5Y 3/1) AT ~ 451 CM AND TO DARK OLIVE GRAY (5Y 3/2) SILTY LUTITE BETWEEN 500 AND 510 CM. SHARP BOTTOM CONTACT.

510 - 542 CM LUTITE, GRAY (5Y 5/1), SIMILAR TO THAT FOUND BETWEEN 445 CM AND 451 CM. SHARP BOTTOM CONTACT.

542 - 591 CM LUTITE, OLIVE GRAY (5Y 3/2), SLIGHTLY SILTY. MICRO BEDDING CONSISTS OF BLACK LUTITE BEDS SHOWING NO APPRECIABLE INCREASE IN SILT CONTENT. MOTTLING VERY EXTENSIVE BELOW 575 CM. COLOR GRADES WITH DEPTH TO GRAY (5Y 5/1) AND TO GRAYISH OLIVE GREEN (5GY 3/2) SHARP BOTTOM CONTACT.

591 - 825 CM SEDIMENT CONSISTS PREDOMINANTLY OF INTERCALATING LUTITE LAYERS. GENERAL PATTERN CONSISTS OF AN UPPERMOST LAYER, 5 - 15 CM IN LENGTH, OF GRAYISH OLIVE GREEN (5GY 5/2) LUTITE, SLIGHTLY BRITTLE AND INDURATED IN APPEARANCE, POSSIBLE PRIMARY ALTERATION TO CLAY MINERALS, GRADING TO A PLASTIC AND STRUCTURE-LESS MODERATE GRAYISH OLIVE (5Y 3/1) LUTITE BECOMES SLIGHTLY SILTY TOWARDS BASE ENDING WITH A SHARP BASAL CONTACT. THE MODERATE GRAYISH OLIVE LUTITE LAYERS GENERALLY RANGE BETWEEN 40 AND 50 CM IN LENGTH.

B

FIGURE 15

RA -ST - 1C - 1

SOUND SPEED (KM/SEC)

A

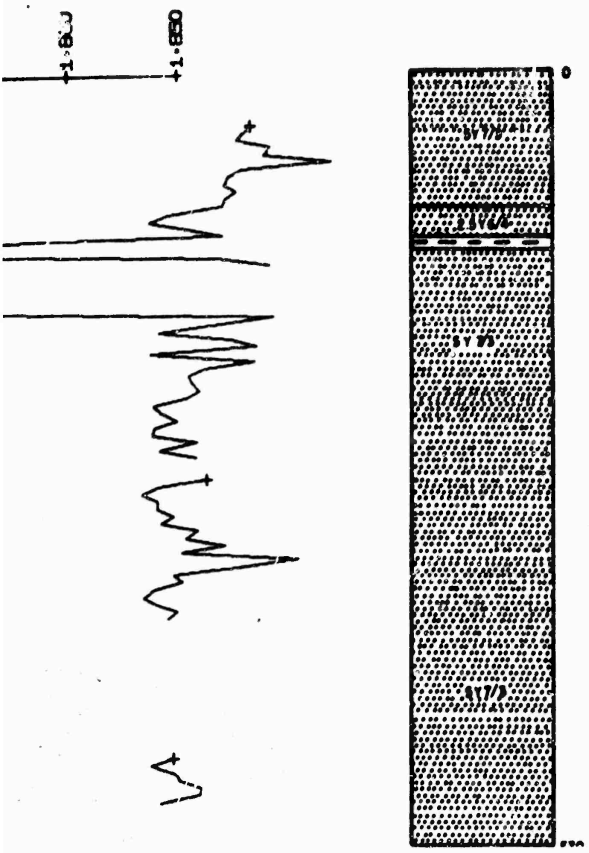

0-530 CM QUARTZITIC SAND, PALE YELLOW (5Y 7/3) CONSISTING OF MEDIUM TO FINE SIZE GRAINS, ROUNDED AND SUB-ROUNDED IN SHAPE. THE CONTINUITY OF THE LAYER IS INTERRUPTED BY A COLOR CHANGE BETWEEN BETWEEN 95-115 CM AND BY A LAYER OF FORAMINFERAL LUTITE OCCURRING BETWEEN 119-129 CM. FORAMINIFERA TESTS ARE FINE GRAIN IN SIZE AND CONSIST PREDOMINANTLY OF GLOBIGERINA AND GLOBOROTALIA SPECIES.

FIGURE 16

B

RA -ST - 1C - 2
SOUND SPEED (KM/SEC)

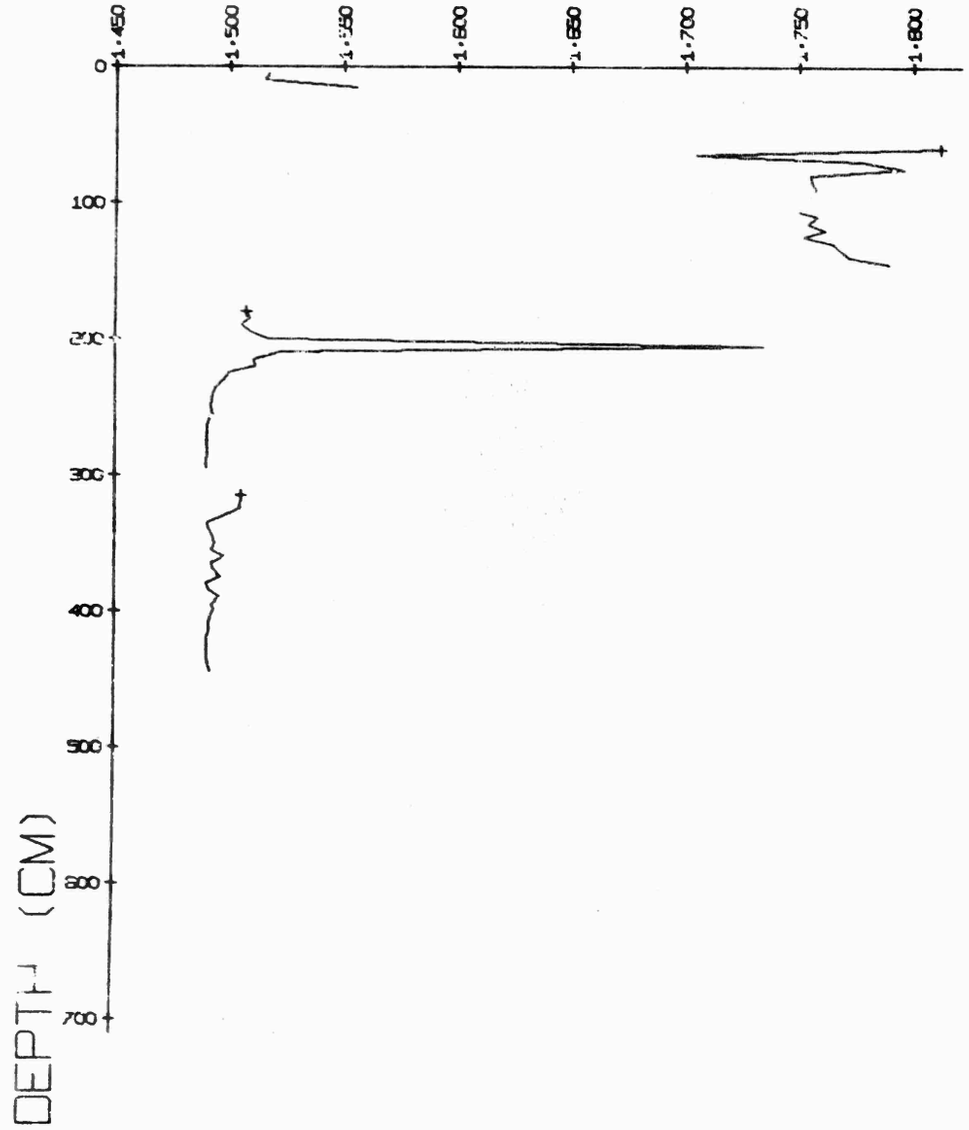

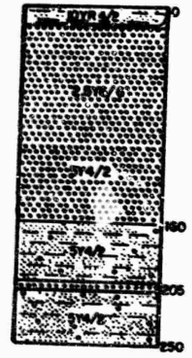

0-15 CM SAND, SILT AND LUTITE, MODERATE YELLOWISH BROWN (10 YR 4/2). COARSE FRACTION CONSISTS OF QUARTZ GRAINS, MICA FLAKES, AND A SMALL PERCENTAGE OF FORAMINIFERA TEST. SHARP IRREGULAR BOTTOM CONTACT.

15-160 CM QUARTZITIC SAND, OLIVE YELLOW ALTERING TO OLIVE GRAY QUARTZITIC SAND A 65 CM. QUARTZ GRAINS ANGULAR TO SUBANGULAR IN SHAPE. COLOR CHANGE DUE TO VARIATION IN LUTITE CONTENT. SHARP BOTTOM CONTACT.

160-230 CM SILTY LUTITE, OLIVE GRAY, WITH A VARYING PERCENTAGE OF SILT. THIS ZONE IS INTERRUPTED BY A LAYER OF OLIVE YELLOW QUARTZITIC SAND (201-209 CM) SIMILAR TO THAT FOUND AT THE TOP OF THE OVERLYING ZONE.

SEDIMENT BELOW 230 CM IS FLOW-IN.

FIGURE 17

RA -ST - 10 - 1
SOUND SPEED (KM/SEC)

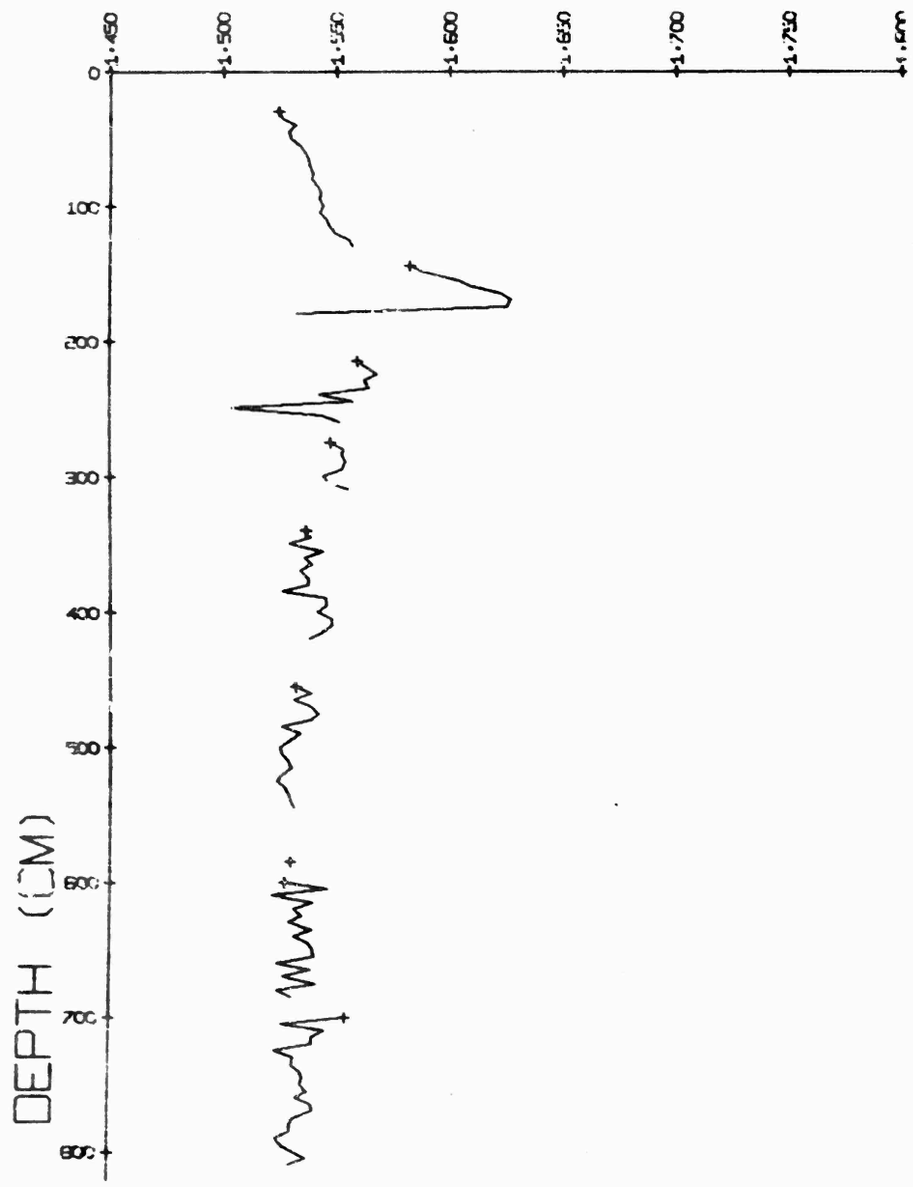

0-466 CM. FORAMINIFERA SAND, LIGHT GRAY (5Y 7/2), CONSISTING OF FINE GRAIN GLOBIGERINA SPECIES TESTS. SPONGE SPICULES AND PTEROPOD FRAGMENTS ARE PRESENTS IN SMALL AMOUNTS. TWO LAMINAE OF COCCOLITH OOZE AND FORAMINIFERA SAND BETWEEN 179-181CM AND 189-193CM ACCOUNT FOR THE ONLY BREAK IN CONTINUITY. SEDIMENT BETWEEN 320-375CM APPEARS DISTURBED PROBABLY DUE TO CORING.

FLOW-IN BEGINS BELOW 466 CM.

FIGURE 18

RA -ST - 10 - 3
SOUND SPEED (KM/SEC)

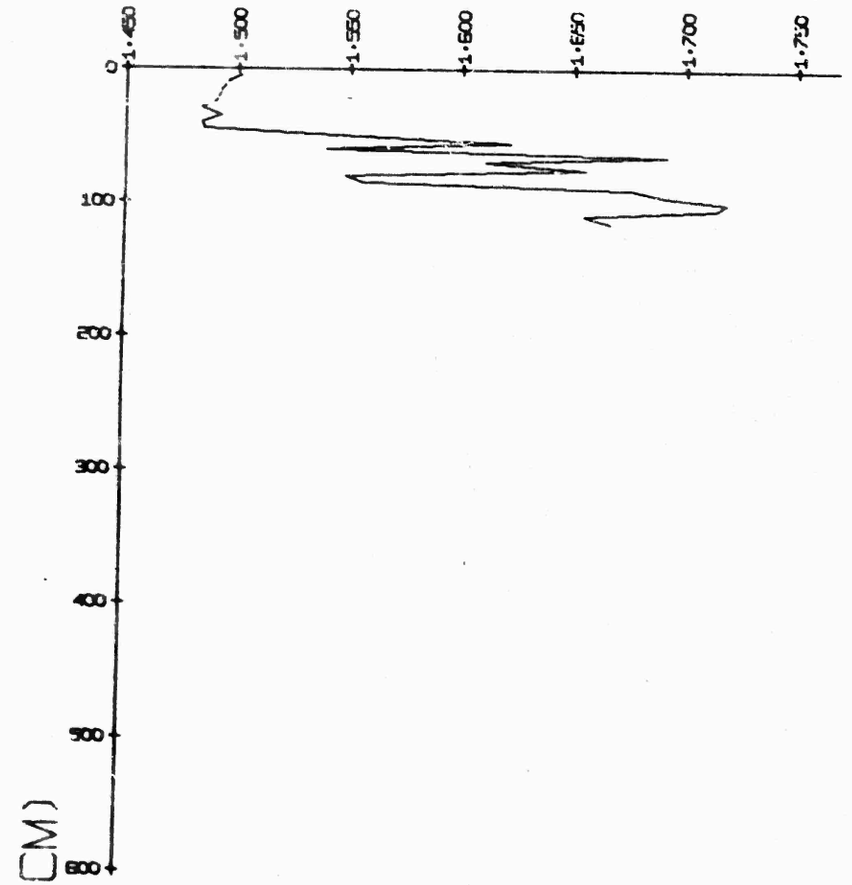

0-5 CM — SILTY LUTITE, MODERATE GRAY (10YR 6/1), SLIGHTLY DISTURBED BY CORING.

5-45 CM — FORAMINIFERAL LUTITE, YELLOWISH BROWN (10YR 5/4) SHARP BOTTOM CONTACT

45-90CM — SILT, OLIVE GREEN (5GY 3/2) CONSISTING OF MICA FLAKES. SHARP BOTTOM CONTACT.

90-125 CM — SILT, OLIVE GRAY (5Y 5/2) BECOMING SANDY BETWEEN 65 AND 100CM. BOTTOM 10 CM OF SEDIMENT SHOW A SLIGHT INCREASE IN LUTITE CONTENT. COARSE FRACTION CONSISTS PREDOMINANTLY OF MICA FLAKES.

FIGURE 19

PART IV

AREA ST VOLUME 2

SOUND VELOCITY PROFILES

by

Eleanor Weininger, E.T. Miller, and R.A. Wehnau

VOLUME 2, PART IV

TABLE OF CONTENTS

LIST OF FIGURES

LIST OF TABLES

I - INTRODUCTION

Volume 2, Part IV summarizes sound velocity measurements, ray path computations, and the associated propagation anomaly obtained on Contract N62306-2020 with the U. S. Naval Oceanographic Office. Data were gathered during May, June, July, August, and September, 1967 on cruises by the R/V Ruth Ann and R/V Santa Maria while in transit from Bermuda to Singapore. Stations were occupied in the North and South Atlantic and Indian Oceans. Sound velocity profiles in Figures 1-13 were recorded using methods described in Volume 7, Area 15 (May, 1969). Data presented in Tables 1-13 were calculated by digital computer to make refraction corrections for the associated acoustic stations. Required information was bottom angle, slant range, and propagation anomaly as a function of horizontal range. Positions of these stations are shown in Volume 1 of this report (Friedberg, 1968). A comparison between sound velocity lowerings and corresponding hydrographic casts is made in Part V of this volume (Rodriguez, 1968).

II - METHOD OF ANALYSIS

Sound velocimeter records were analyzed to calculate the effect of refraction on certain factors which describe the acoustic properties of the oceans. Specifically these factors were bottom angle, propagation anomaly, range and travel time along a ray path.

As a first approximation, propagation of sound in the ocean can be assumed as a straight line. Sound propagated along such a path would suffer a $1/r^2$ or spherical spreading loss where r is distance from the source. In reality, refraction causes the path a sound ray travels to be curved due to continuing variation in velocity along the path. This curvature causes bottom angle to differ from a straight ray solution and spreading loss to deviate from the $1/r^2$ spherical loss. The difference between non-linear spreading loss for a curved ray and the $1/r^2$ spherical loss is called the propagation anomaly.

A method has been described (Frank, et al., page 51 ff., 1946) for calculating the propagation anomaly along a given ray path. This method utilizes the theory of constant velocity gradients and assumes the ocean can be divided into layers with constant gradients. Inherent in this method is the ability to calculate other factors of value. These include slant range and bottom angle. In addition, travel times are calculated using formulas derived from the theory of constant velocity gradients (Slotnick, 1959). These methods are especially suitable for calculations utilizing digital computers. Originally, calculations of bottom angle and propagation anomaly were performed using a program provided by Woods Hole Oceanographic Institute. Presently, the calculations are done by Alpine using a modification of the WHOI program giving an expanded data output.

Figures 1-13 present profiles made during sound velocimeter lowerings. Since a constant velocity gradient would be a straight line on these graphs, the profile is approximated by a series of straight lines to best fit the sound velocity trace. The end-point X and Y pen deflection values of these lines are the inputs to the computer program, where they are converted into depth and sound velocity. This is done by the program using conversion constants determined from manufacturer's equipment specifications and from calibrations done at sea (May, 1969). Accuracy of these calibrations and specifications determines the accuracy of the data.

III - SOUND VELOCITY PROFILES

Graphs presented with this section are reproductions of original sound velocity profiles taken aboard the R/V Ruth Ann during cruises 1A, 1B, 1C, and 1D. The method by which these profiles were taken is described in Area 15, Volume 7, (May, 1969). The number of the sound velocity profile corresponds to the number of the acoustic station occupied at the same position.

An overlay grid has been prepared using manufacturer's specifications and equipment calibrations for each profile. These profiles are presented in Figures 1-13. In each case the down trace has been used for analysis.

The depth excursion of the two pens has been offset to prevent them from hitting one another as the two curves cross. Depth scale is correct for the velocity curve.

The offset is equal to 25 meters in depth for Figures 1, 3, and 4; 30 meters for Figures 5, 6, and 7; 35 meters for Figures 8 and 9; 45 meters for Figure 2; 50 meters for Figures 10 and 13; and 60 meters for Figures 11 and 12.

IV - CALCULATED DATA

Tables 1-13 present calculated results for the sound velocimeter profiles.

Velocities and depths of each layer are calculated by the program from input pen deflection values and conversion factors. These are the input data to the main calculation section.

Sound velocities at shot and phone depth are calculated by linear interpolation between limits of the layer in which they fall. Station bottom depth is the mean of depth observed over the shot run. Sound velocity at station bottom depth is calculated by one of three methods. If station bottom depth is less than maximum depth of the profile, sound velocity is found by linear interpolation. If station bottom depth is only slightly greater than the maximum profile depth, then sound velocity is found by extrapolation using the gradient in the deepest layer. If station depth is much greater than maximum profile depth, sound velocity is calculated by solving an equation in velocity versus depth. This equation is defined by plotting pressure (depth) versus sound velocity for the bottom of each sound velocity profile. For a given area of the ocean, and for depths greater than approximately 1500 meters, the points fall close to a straight line. Thus a linear equation can be found which relates velocity and depth. During these cruises many oceanographic provinces were sampled and the only two points which did not satisfy a single equation were found where the bottom temperature was about 0.5° C with a consequently different bottom velocity. The above plot is also used to check changes in sensitivities of the instrument and to check log book data. Datum points in error will be found to deviate sharply from the straight line equation.

The following quantities are calculated in the main section of the program. Total depth is twice the station bottom depth minus shot and phone depths. Beginning angle is the angle the tangent to curved ray path makes with the horizontal at the start of the curved ray path. Slant angle is the angle the straight line approximation to the curved ray path makes with the horizontal at the beginning of propagation. Bottom angle is the angle the tangent to the curved ray path makes with the horizontal at the point where it strikes bottom. Horizontal range is the horizontal distance in kiloyards between shot and hydrophone. Slant range is the straight path distance in kiloyards from shot to bottom to the hydrophone. Propagation anomaly is the difference between curved ray non-linear spreading loss and straight line spherical loss in decibels. Travel time is the time it takes a pulse to propagate along the curved ray path from shot to phone.

V - REFERENCES

Frank, P.B., Bergman, P.G., and Yaspan, A. 1946. Ray Acoustics, Physics of Sound in the Sea, Part 1: Transmission. Research Analysis Group. Committee on Undersea Warfare, National Research Council.

Friedberg, J. 1968. Area ST, Volume 1, Part I, Summary report and bottom reflection loss. Prepared by Alpine Geophysical Associates, Inc. U.S. Naval Oceanographic Office, SP-97-ST-1-I. (Conf.)

May, M., Wehnau, R.A., Griffiths, K. and Mowat, A. 1969. Area 15, Volume 7. Ship operations, measurements at sea and data analysis procedures. Prepared by Alpine Geophysical Associates, Inc. U.S. Naval Oceanographic Office, SP-97-15-7.

Rodriguez, M. 1968. Area ST, Volume 2, Part V. Core, sound velocimeter, hydrographic and bottom photographic stations-Hydrographic stations. Prepared by Alpine Geophysical Associates, Inc. U.S. Naval Oceanographic Office, SP-97-ST-2-V.

Slotnick, M.M. 1959. Lessons in Seismic Computing. Society of Exploration Geophysicists.

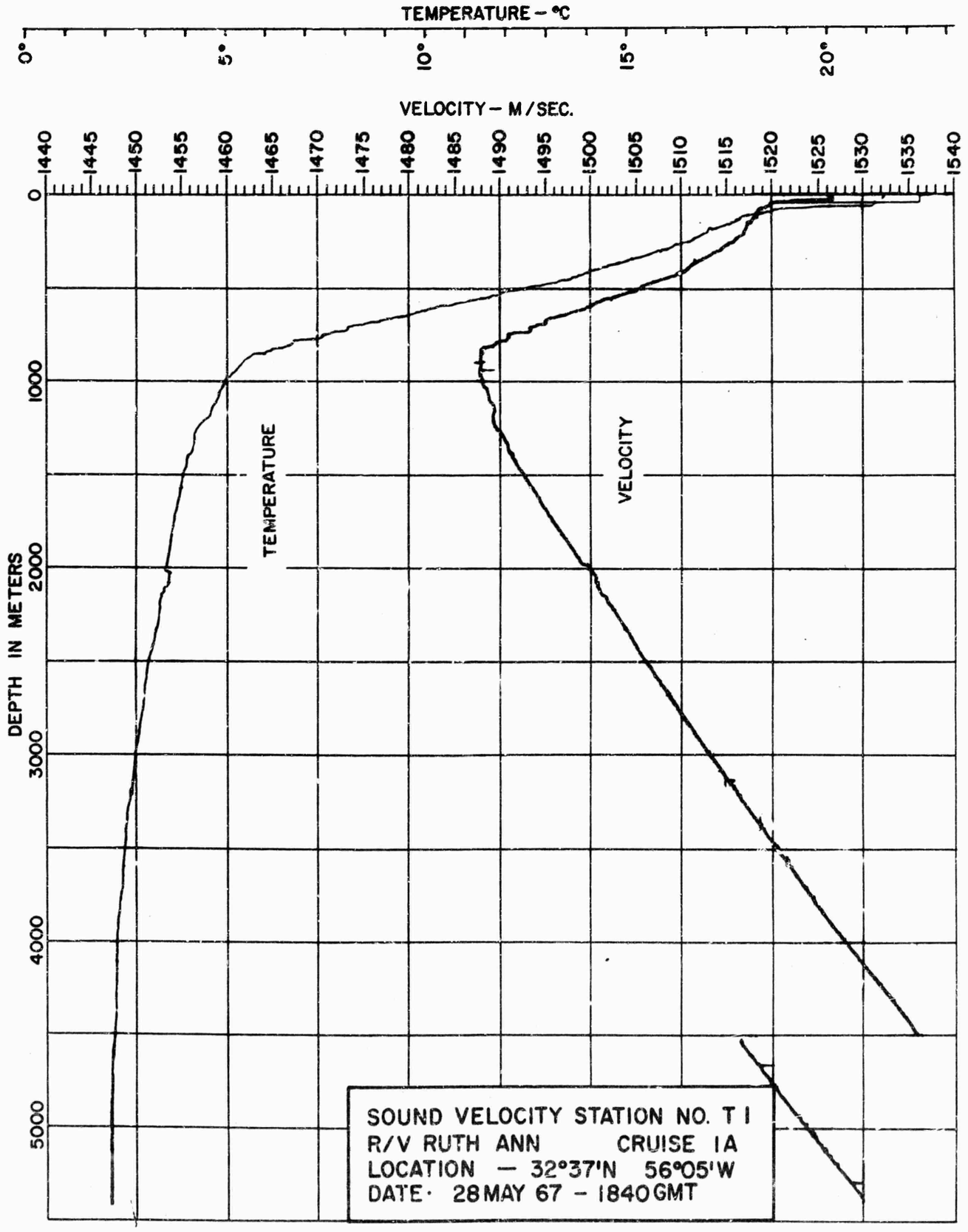
TEMPERATURE – °C
0°
5°
10°
15°
20°
VELOCITY – M/SEC.
1440
1445
1450
1455
1460
1465
1470
1475
1480
1485
1490
1495
1500
1505
1510
1515
1520
1525
1530
1535
1540
DEPTH IN METERS
0
1000
2000
3000
4000
5000
TEMPERATURE
VELOCITY
SOUND VELOCITY STATION NO. T I
R/V RUTH ANN CRUISE IA
LOCATION – 32°37'N 56°05'W
DATE· 28 MAY 67 – 1840 GMT

FIGURE I

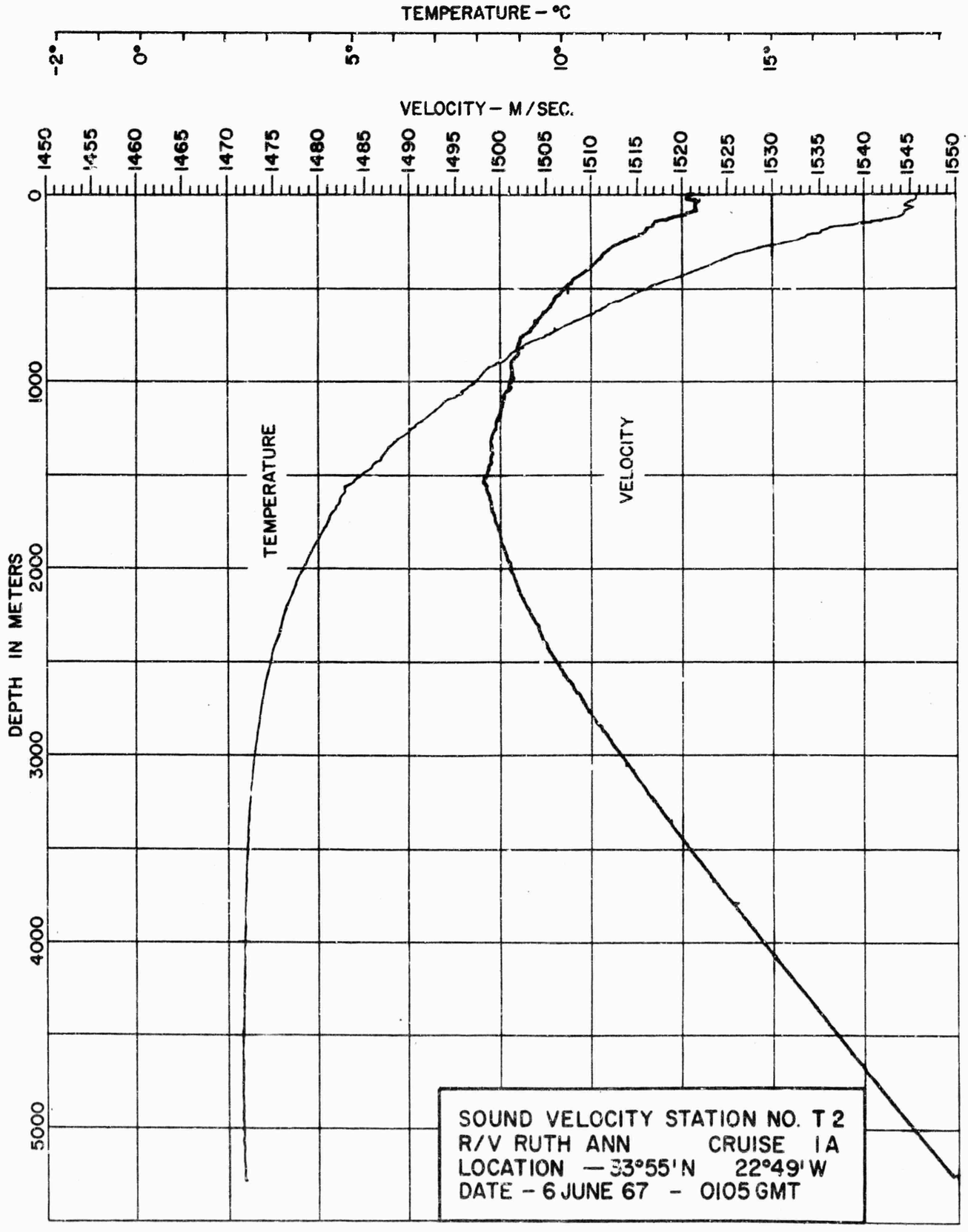
TEMPERATURE – °C
-2°
0°
5°
10°
15°
VELOCITY – M/SEC.
1450
1455
1460
1465
1470
1475
1480
1485
1490
1495
1500
1505
1510
1515
1520
1525
1530
1535
1540
1545
1550
DEPTH IN METERS
0
1000
2000
3000
4000
5000
TEMPERATURE
VELOCITY
SOUND VELOCITY STATION NO. T 2
R/V RUTH ANN CRUISE 1A
LOCATION – 33°55'N 22°49'W
DATE – 6 JUNE 67 – 0105 GMT

FIGURE 2

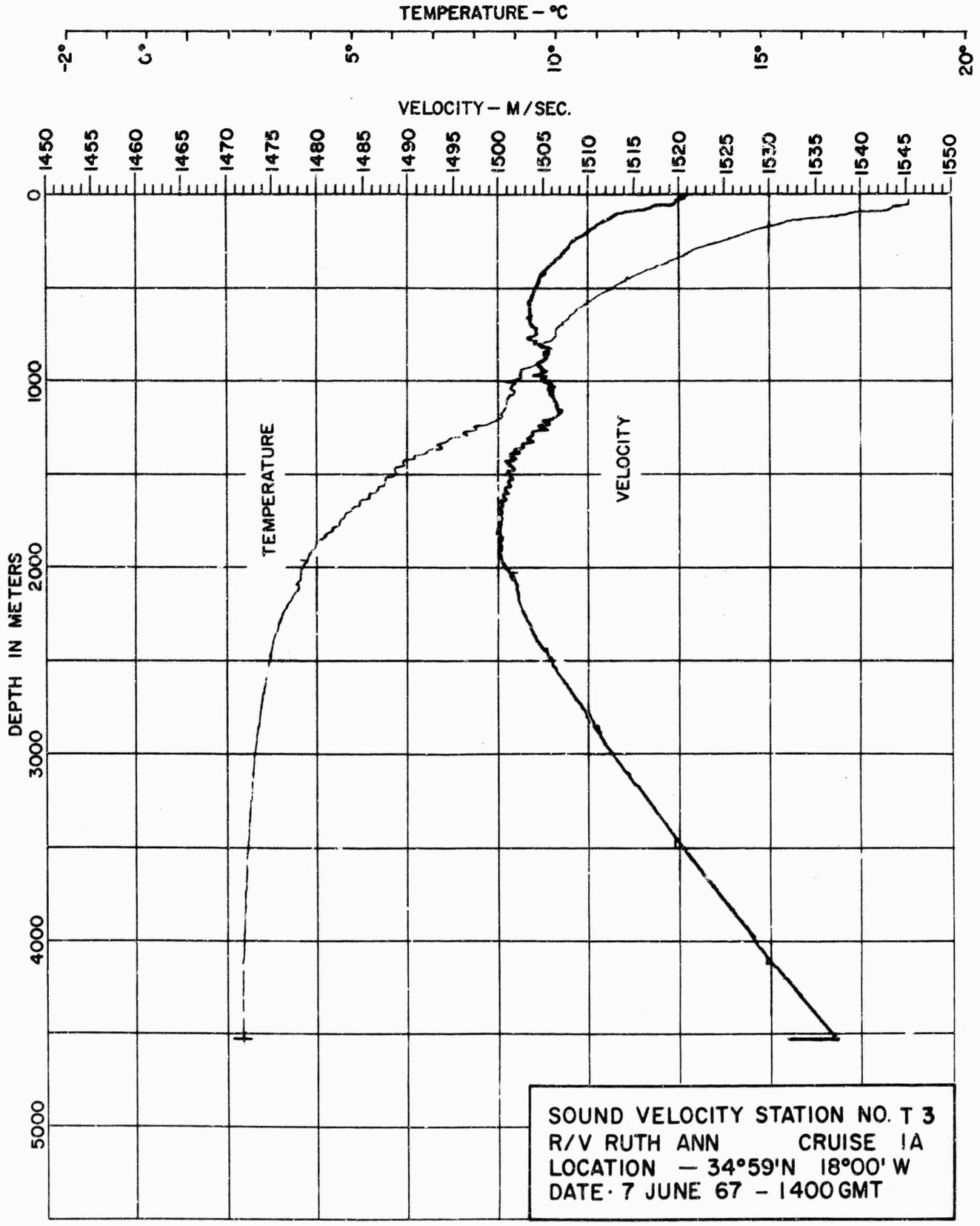
TEMPERATURE – °C
-2°
0°
5°
10°
15°
20°
VELOCITY – M/SEC.
1450
1455
1460
1465
1470
1475
1480
1485
1490
1495
1500
1505
1510
1515
1520
1525
1530
1535
1540
1545
1550
DEPTH IN METERS
0
1000
2000
3000
4000
5000
TEMPERATURE
VELOCITY
SOUND VELOCITY STATION NO. T 3
R/V RUTH ANN CRUISE 1A
LOCATION – 34°59'N 18°00' W
DATE · 7 JUNE 67 – 1400 GMT

FIGURE 3

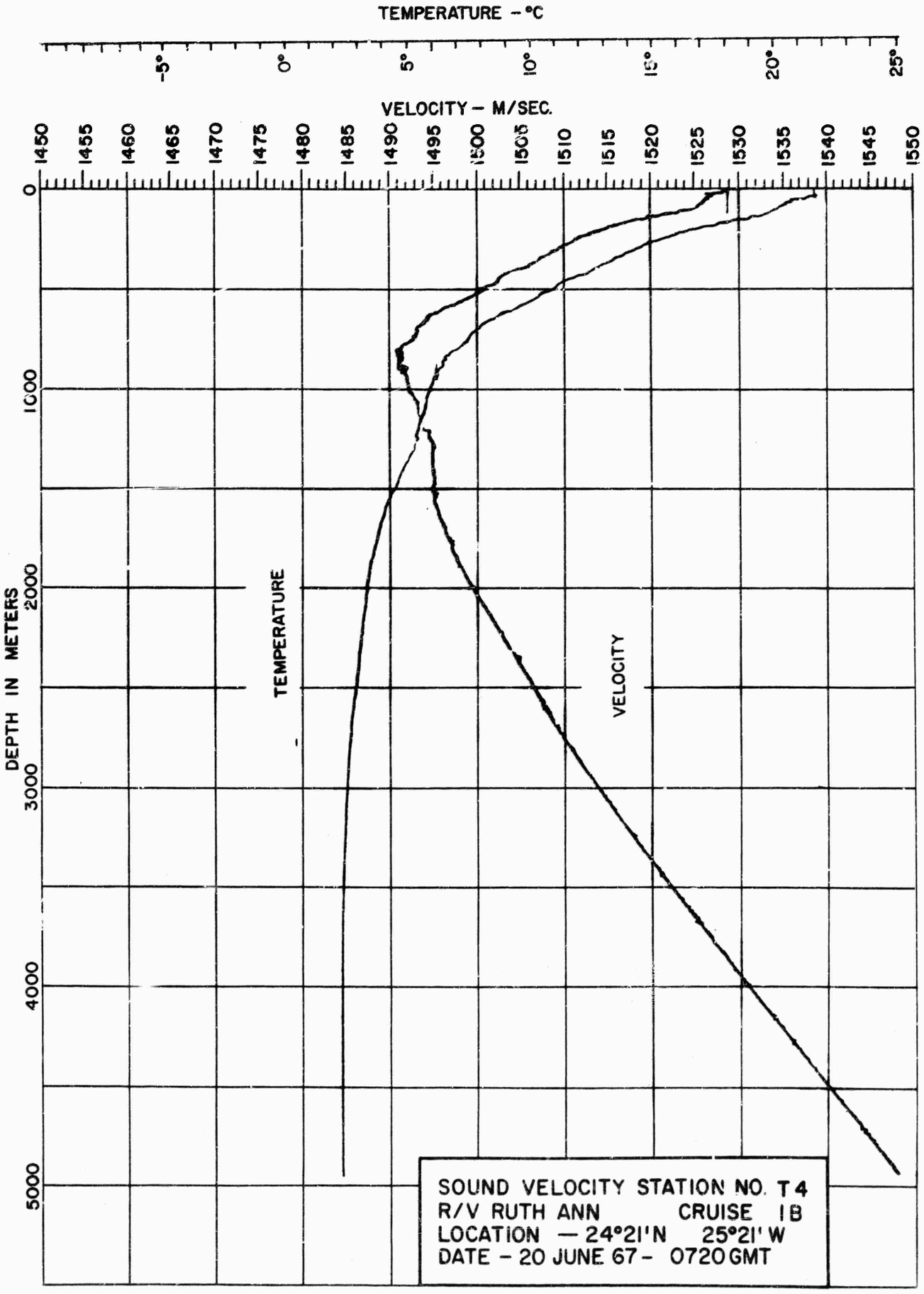
TEMPERATURE - °C
-5°
0°
5°
10°
15°
20°
25°
VELOCITY - M/SEC.
1450
1455
1460
1465
1470
1475
1480
1485
1490
1495
1500
1505
1510
1515
1520
1525
1530
1535
1540
1545
1550
DEPTH IN METERS
0
1000
2000
3000
4000
5000
TEMPERATURE
VELOCITY
SOUND VELOCITY STATION NO. T4
R/V RUTH ANN CRUISE 1B
LOCATION — 24°21'N 25°21' W
DATE - 20 JUNE 67 - 0720 GMT

FIGURE 4

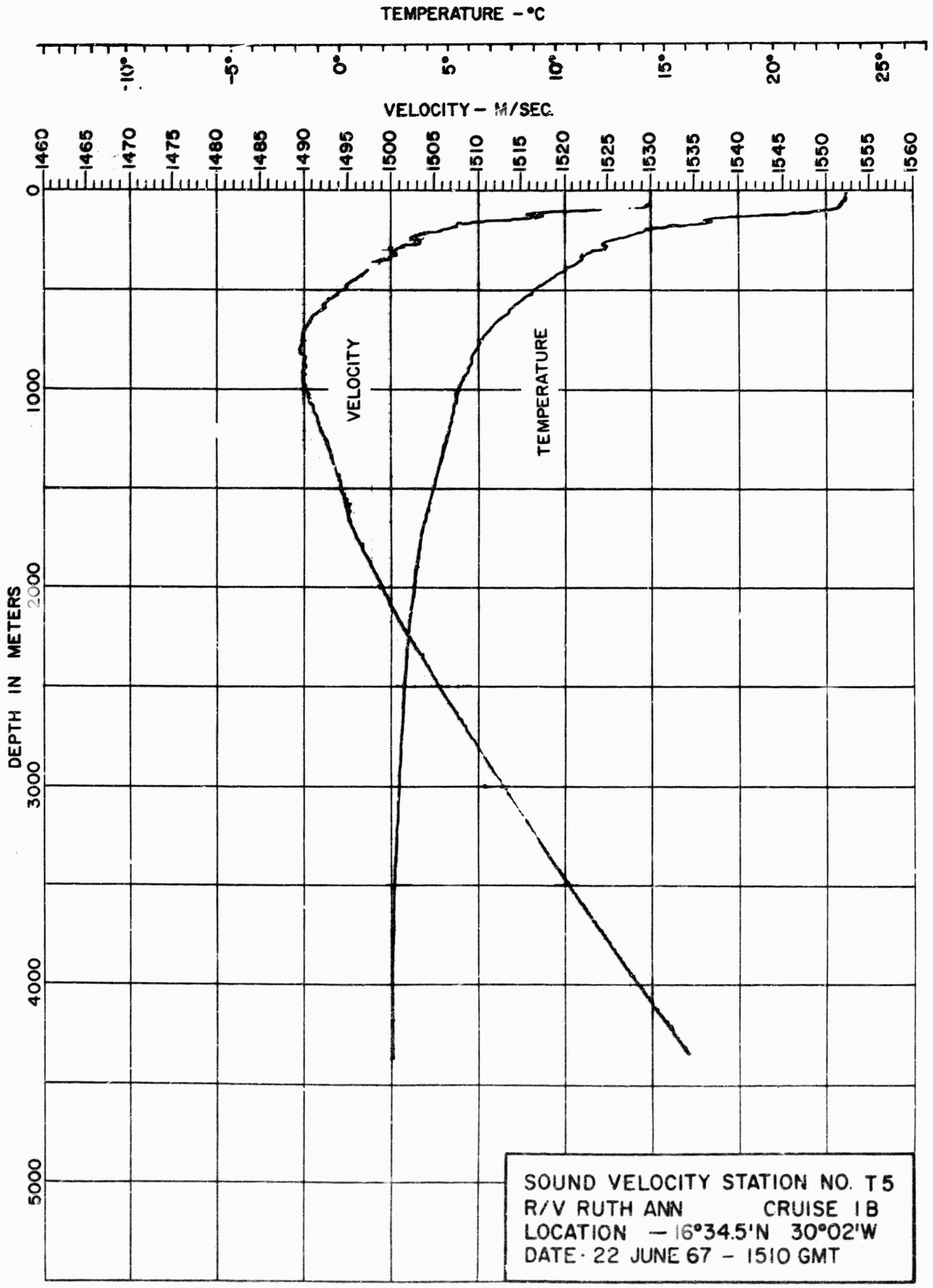
TEMPERATURE - °C
-10°
-5°
0°
5°
10°
15°
20°
25°
VELOCITY - M/SEC.
1460
1465
1470
1475
1480
1485
1490
1495
1500
1505
1510
1515
1520
1525
1530
1535
1540
1545
1550
1555
1560
DEPTH IN METERS
0
1000
2000
3000
4000
5000
VELOCITY
TEMPERATURE
SOUND VELOCITY STATION NO. T5
R/V RUTH ANN CRUISE 1B
LOCATION — 16°34.5'N 30°02'W
DATE · 22 JUNE 67 - 1510 GMT

FIGURE 5

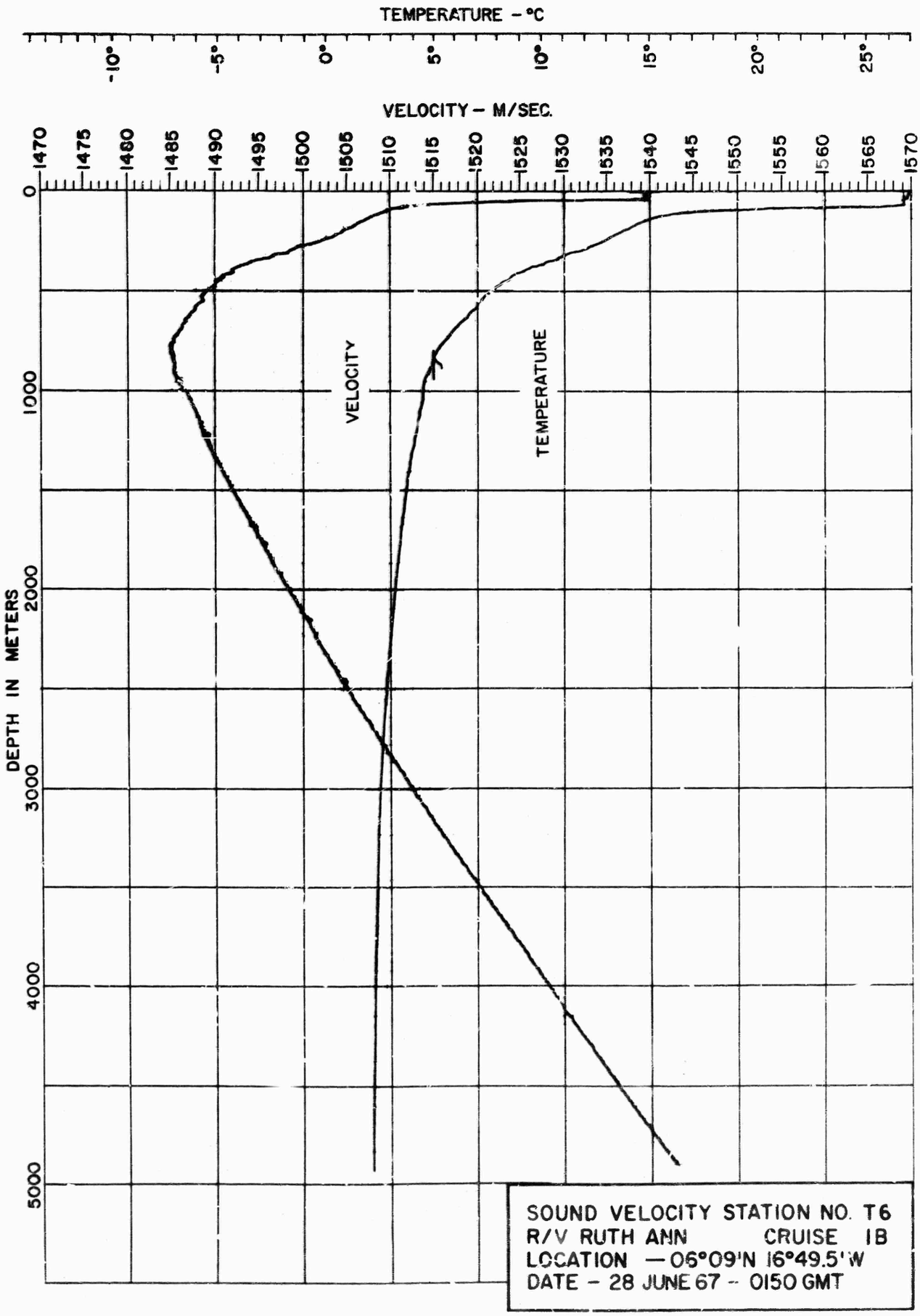
TEMPERATURE - °C
-10°
-5°
0°
5°
10°
15°
20°
25°
VELOCITY - M/SEC.
1470
1475
1480
1485
1490
1495
1500
1505
1510
1515
1520
1525
1530
1535
1540
1545
1550
1555
1560
1565
1570
DEPTH IN METERS
0
1000
2000
3000
4000
5000
VELOCITY
TEMPERATURE
SOUND VELOCITY STATION NO. T6
R/V RUTH ANN CRUISE 1B
LOCATION — 06°09'N 16°49.5'W
DATE - 28 JUNE 67 - 0150 GMT

FIGURE 6

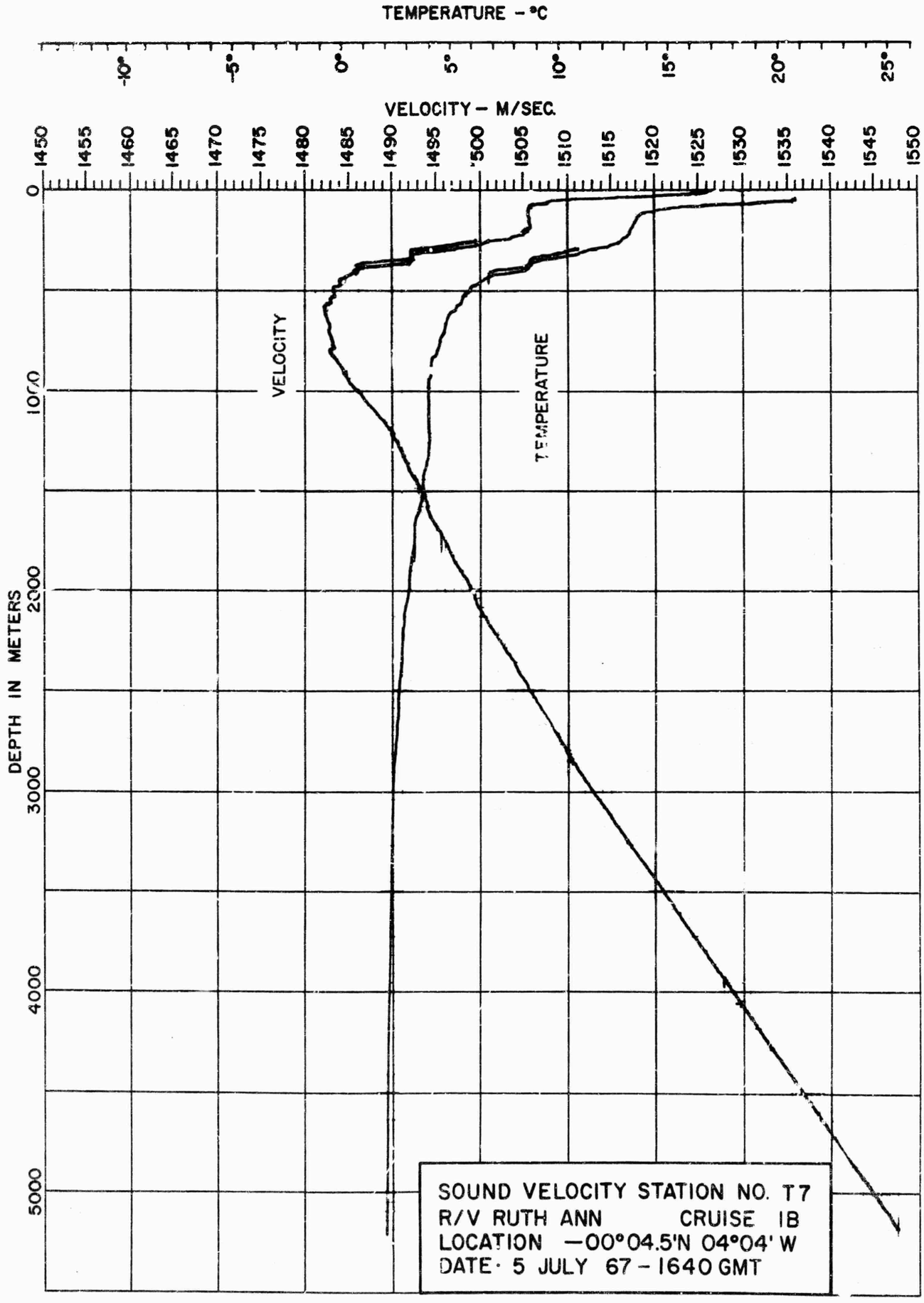
TEMPERATURE - °C
-10°
-5°
0°
5°
10°
15°
20°
25°
VELOCITY - M/SEC.
1450
1455
1460
1465
1470
1475
1480
1485
1490
1495
1500
1505
1510
1515
1520
1525
1530
1535
1540
1545
1550
DEPTH IN METERS
0
1000
2000
3000
4000
5000
VELOCITY
TEMPERATURE
SOUND VELOCITY STATION NO. T7
R/V RUTH ANN CRUISE 1B
LOCATION —00°04.5'N 04°04' W
DATE· 5 JULY 67 - 1640 GMT

FIGURE 7

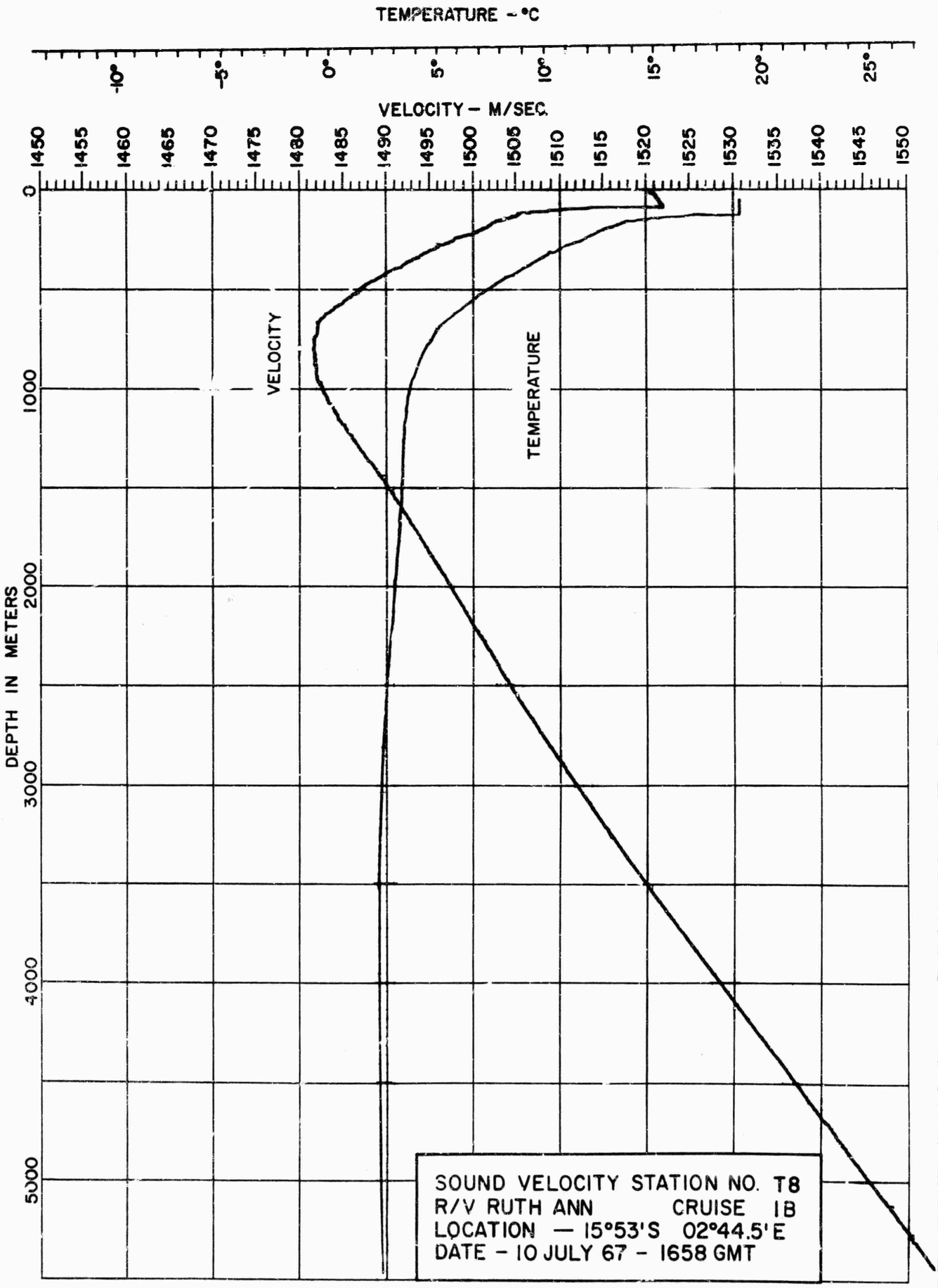
TEMPERATURE - °C
-10°
-5°
0°
5°
10°
15°
20°
25°
VELOCITY - M/SEC.
1450
1455
1460
1465
1470
1475
1480
1485
1490
1495
1500
1505
1510
1515
1520
1525
1530
1535
1540
1545
1550
DEPTH IN METERS
0
1000
2000
3000
4000
5000
VELOCITY
TEMPERATURE
SOUND VELOCITY STATION NO. T8
R/V RUTH ANN CRUISE 1B
LOCATION — 15°53'S 02°44.5'E
DATE - 10 JULY 67 - 1658 GMT

FIGURE 8

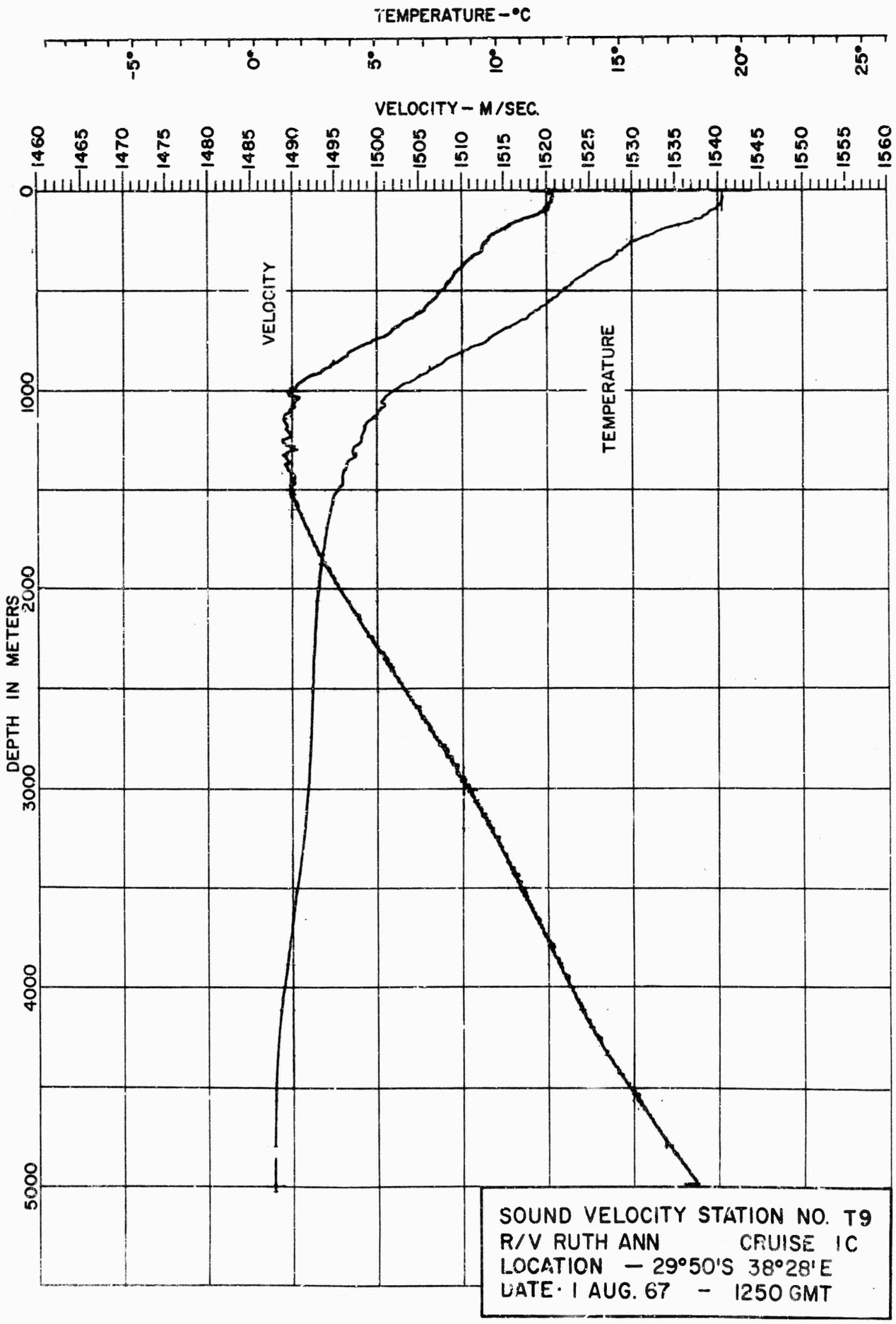
TEMPERATURE – °C
-5°
0°
5°
10°
15°
20°
25°
VELOCITY – M/SEC.
1460
1465
1470
1475
1480
1485
1490
1495
1500
1505
1510
1515
1520
1525
1530
1535
1540
1545
1550
1555
1560
DEPTH IN METERS
0
1000
2000
3000
4000
5000
VELOCITY
TEMPERATURE
SOUND VELOCITY STATION NO. T9
R/V RUTH ANN CRUISE 1C
LOCATION – 29°50'S 38°28'E
DATE· 1 AUG. 67 – 1250 GMT

FIGURE 9

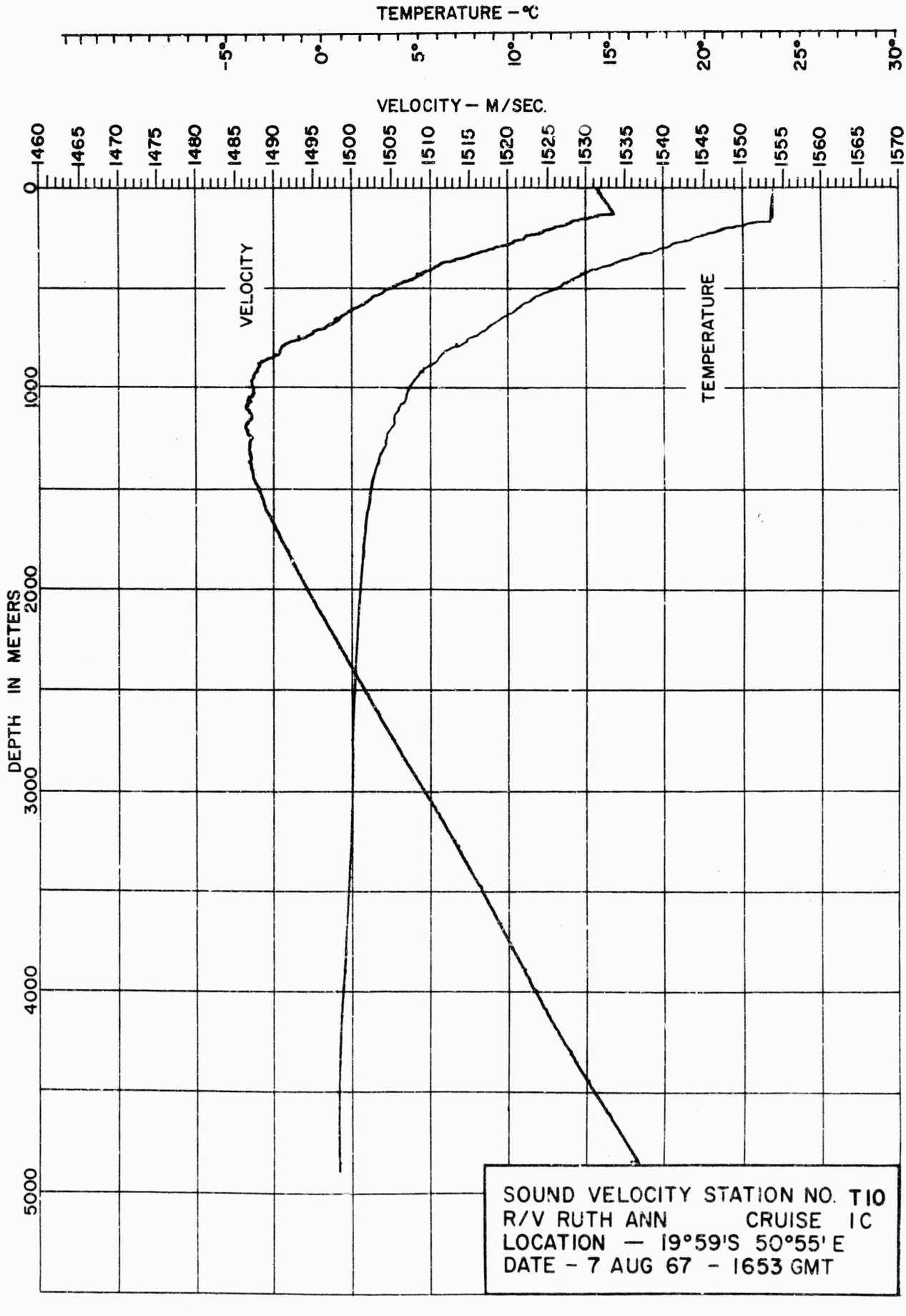
TEMPERATURE – °C
-5°
0°
5°
10°
15°
20°
25°
30°
VELOCITY – M/SEC.
1460
1465
1470
1475
1480
1485
1490
1495
1500
1505
1510
1515
1520
1525
1530
1535
1540
1545
1550
1555
1560
1565
1570
VELOCITY
TEMPERATURE
DEPTH IN METERS
0
1000
2000
3000
4000
5000
SOUND VELOCITY STATION NO. T10
R/V RUTH ANN CRUISE 1C
LOCATION — 19°59'S 50°55'E
DATE – 7 AUG 67 – 1653 GMT

FIGURE 10

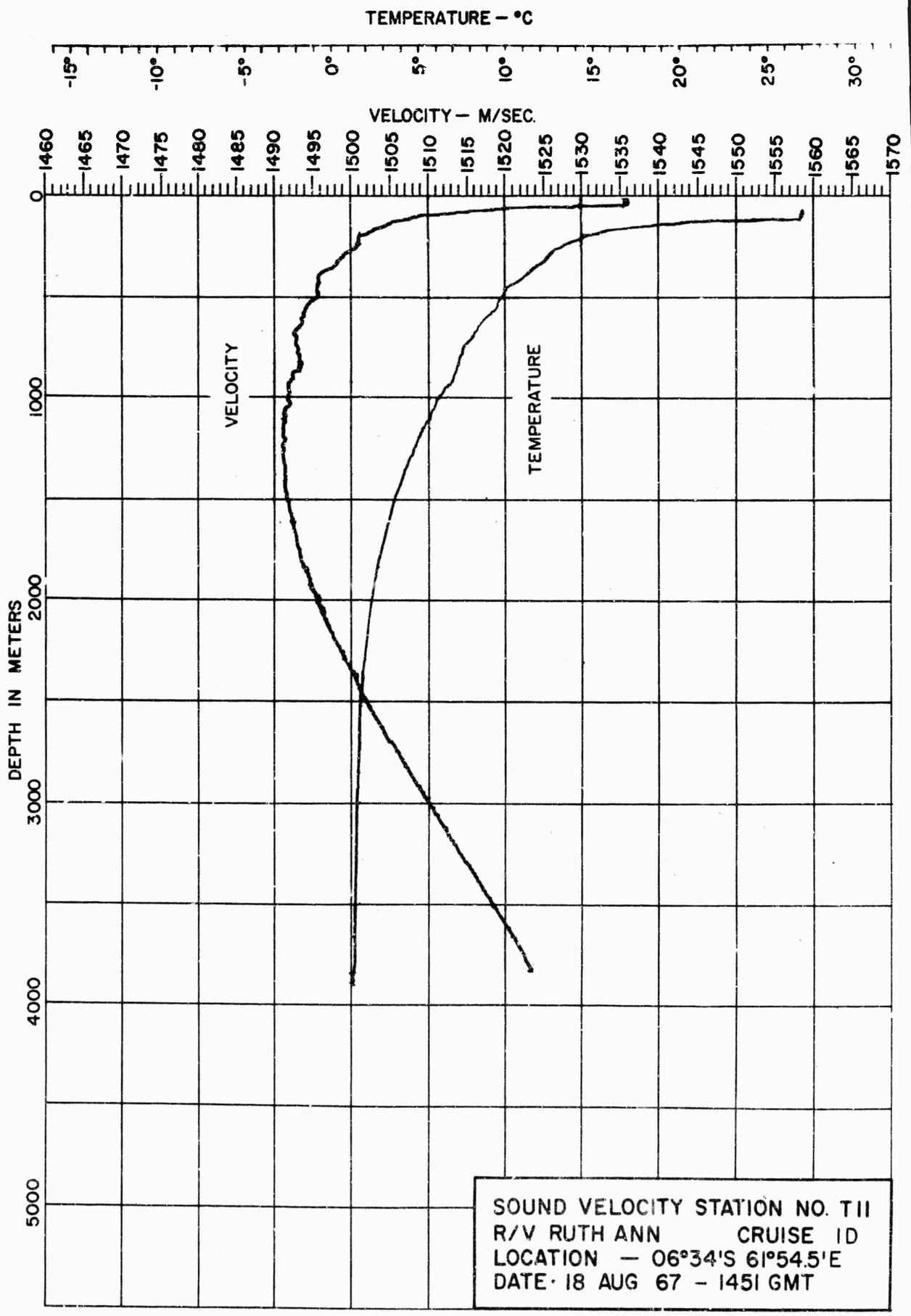
TEMPERATURE – °C
-15°
-10°
-5°
0°
5°
10°
15°
20°
25°
30°
VELOCITY – M/SEC.
1460
1465
1470
1475
1480
1485
1490
1495
1500
1505
1510
1515
1520
1525
1530
1535
1540
1545
1550
1555
1560
1565
1570
DEPTH IN METERS
0
1000
2000
3000
4000
5000
VELOCITY
TEMPERATURE
SOUND VELOCITY STATION NO. T11
R/V RUTH ANN CRUISE ID
LOCATION – 06°34'S 61°54.5'E
DATE· 18 AUG 67 – 1451 GMT

FIGURE 11

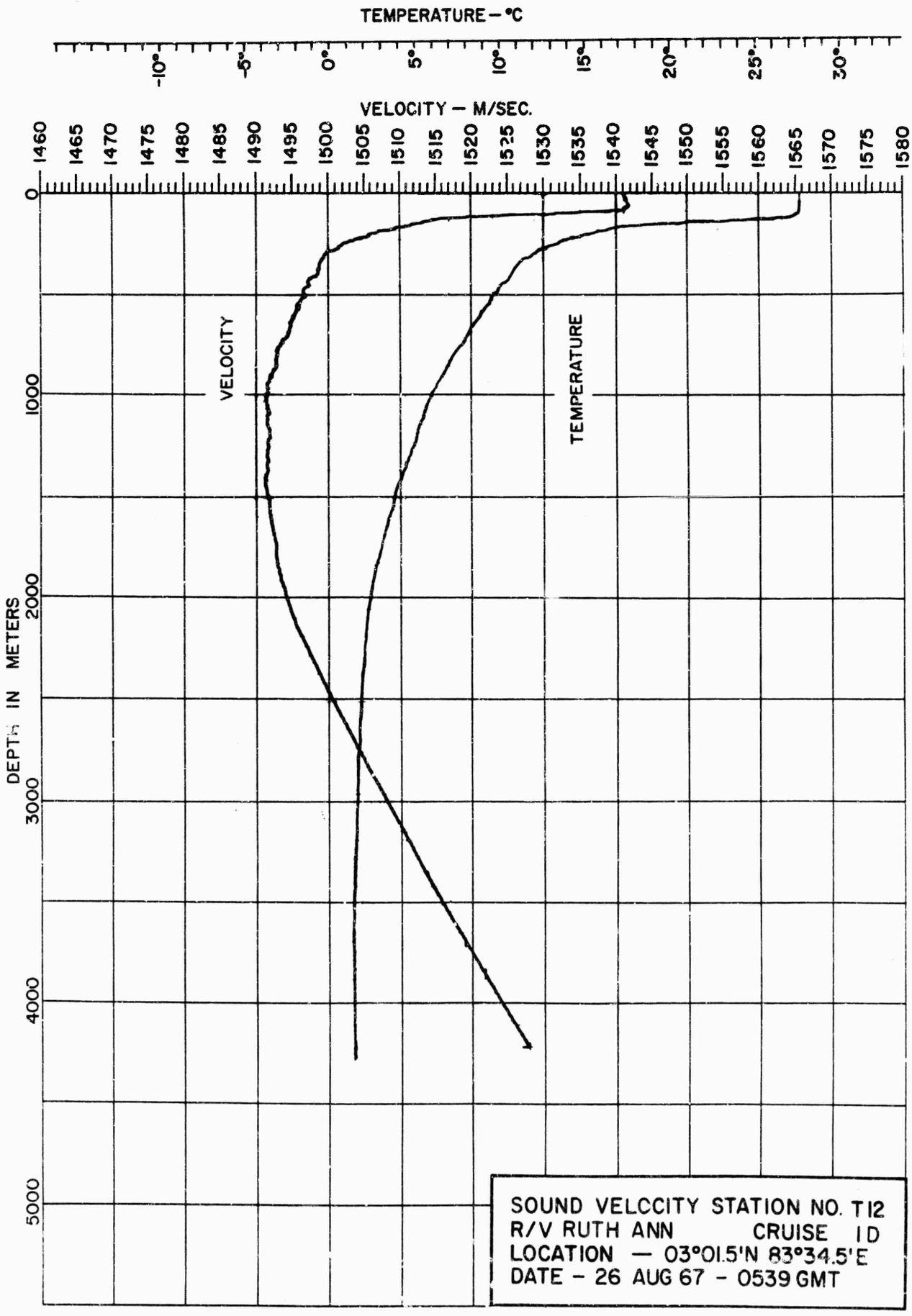
TEMPERATURE – °C
-10°
-5°
0°
5°
10°
15°
20°
25°
30°
VELOCITY – M/SEC.
1460
1465
1470
1475
1480
1485
1490
1495
1500
1505
1510
1515
1520
1525
1530
1535
1540
1545
1550
1555
1560
1565
1570
1575
1580
DEPTH IN METERS
0
1000
2000
3000
4000
5000
VELOCITY
TEMPERATURE
SOUND VELOCITY STATION NO. T12
R/V RUTH ANN CRUISE ID
LOCATION – 03°01.5'N 83°34.5'E
DATE – 26 AUG 67 – 0539 GMT

FIGURE 12

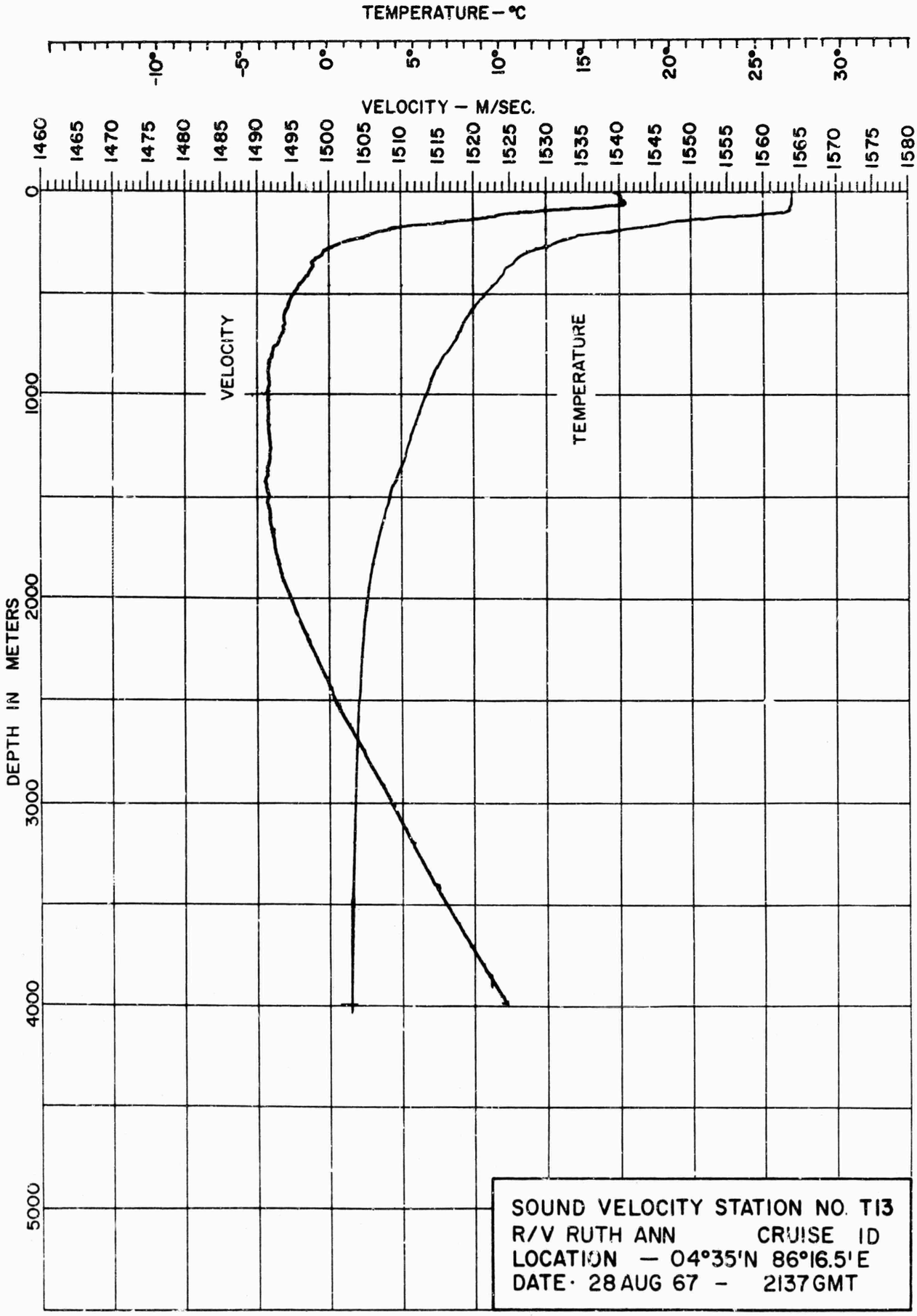
TEMPERATURE – °C
-10°
-5°
0°
5°
10°
15°
20°
25°
30°
VELOCITY – M/SEC.
1460
1465
1470
1475
1480
1485
1490
1495
1500
1505
1510
1515
1520
1525
1530
1535
1540
1545
1550
1555
1560
1565
1570
1575
1580
DEPTH IN METERS
0
1000
2000
3000
4000
5000
VELOCITY
TEMPERATURE
SOUND VELOCITY STATION NO. T13
R/V RUTH ANN CRUISE ID
LOCATION – 04°35'N 86°16.5'E
DATE· 28 AUG 67 – 2137 GMT

FIGURE 13

VELOCIMETER STATION 1, CRUISE 1A

INPUT DATA

Depths (Meters)

Water	Shot	Phone
5511.0	244.0	208.0

Layer		VELOCITY Km/Sec	DEPTH Kms	VELOCITY Ft/Sec	DEPTH Yds
1		1.5265	0.0000	5008.3	0.0
2		1.5202	0.0300	4987.6	32.9
3		1.5184	0.0681	4981.7	74.5
4	Phone	1.5170	0.2080	4976.9	227.5
5		1.5169	0.2145	4976.7	234.7
6	Shot	1.5159	0.2439	4973.4	266.9
7		1.5106	0.4010	4956.0	438.6
8		1.4879	0.8120	4881.8	888.3
9		1.4878	0.9644	4881.1	1055.0
10		1.4892	1.2030	4885.9	1316.0
11		1.4914	1.4035	4893.2	1535.4
12		1.5087	2.7007	4949.8	2954.6
13		1.5253	3.8235	5004.2	4182.9
14		1.5500	5.3834	5085.2	5889.4
	Bottom (Interp.)	1.5535	5.5109	5096.8	6029.0

CALCULATED DATA

TOTAL DEPTH = 2H-DS-DH = 10.569 kms = 11.563 kyds.

Angle (Degrees) Beginning	Slant	Bottom	Horizontal Range Kyds	Slant Range Kyds	Prop. Anomaly (db)	Travel Time (Secs)
12.632	10.038	0.163	65.322	66.337	15.08	39.912
12.829	10.857	2.264	60.291	61.390	4.80	36.953
13.026	11.304	3.210	57.845	58.990	3.67	35.516
13.224	11.681	3.946	55.930	57.113	3.04	34.391
13.421	12.020	4.573	54.307	55.524	2.60	33.439
14.160	13.121	6.453	49.606	50.936	1.67	30.686
15.149	14.398	8.432	45.041	46.502	1.07	28.023
16.139	15.573	10.129	41.490	43.072	0.73	25.961
17.131	16.692	11.667	38.561	40.257	0.53	24.268
18.123	17.778	13.103	36.062	37.871	0.39	22.832
20.110	19.889	15.777	31.962	33.989	0.22	20.495
25.086	25.010	21.854	24.786	27.351	0.06	16.497
30.069	30.048	27.515	19.989	23.093	0.01	13.930
35.057	35.057	32.977	16.479	20.131	0.00	12.144
40.047	40.058	38.326	13.752	17.967	-0.00	10.840
45.040	45.057	43.602	11.540	16.337	-0.00	9.856
50.033	50.050	48.832	9.685	15.083	-0.01	9.100
60.023	60.037	59.200	6.666	13.347	-0.01	8.053
70.014	70.025	69.496	4.203	12.303	-0.01	7.423
80.007	80.013	79.756	2.036	11.741	-0.01	7.084

VELOCIMETER STATION 2, CRUISE 1A

INPUT DATA

Depths (Meters)

Water	Shot	Phone
5325.0	244.0	255.0

Layer		VELOCITY Km/Sec	DEPTH Kms	VELOCITY Ft/Sec	DEPTH Yds
1		1.5209	0.0000	4989.8	0.0
2		1.5216	0.0360	4992.1	39.4
3		1.5216	0.0822	4992.3	89.9
4	Shot	1.5144	0.2439	4968.4	266.9
5	Phone	1.5139	0.2549	4966.8	278.9
6		1.5122	0.2907	4961.5	318.0
7		1.5021	0.7739	4928.3	846.6
8		1.4981	1.5558	4915.0	1702.1
9		1.5046	2.3939	4936.4	2619.0
10		1.5163	3.2460	4974.8	3551.2
11		1.5494	5.2651	5083.5	5760.0
	Bottom (Interp.)	1.5504	5.3249	5086.7	5825.5

CALCULATED DATA

TOTAL DEPTH = 2H-DS-DH = 10.151 kms = 11.105 kyds.

Angle (Degrees) Beginning	Slant	Bottom	Horizontal Range Kyds	Slant Range Kyds	Prop. Anomaly (db)	Travel Time (Secs)
12.380	9.105	0.163	69.290	70.174	16.99	42.187
12.580	10.154	2.257	62.002	62.988	5.72	37.891
12.780	10.663	3.201	58.981	60.017	4.33	36.112
12.980	11.074	3.934	56.735	57.812	3.55	34.791
13.180	11.437	4.560	54.888	56.000	3.03	33.705
14.000	12.687	6.590	49.326	50.561	1.88	30.442
15.000	13.986	8.537	44.583	45.946	1.24	27.670
16.000	15.178	10.217	40.934	42.413	0.89	25.547
17.000	16.313	11.743	37.943	39.535	0.67	23.816
18.000	17.413	13.170	35.408	37.109	0.52	22.356
20.000	19.550	15.833	31.272	33.185	0.34	19.995
25.000	24.726	21.893	24.114	26.549	0.15	16.000
30.000	29.809	27.546	19.383	22.338	0.08	13.464
35.000	34.857	33.002	15.944	19.430	0.05	11.711
40.000	39.888	38.345	13.287	17.316	0.04	10.438
45.000	44.911	43.619	11.139	15.729	0.03	9.481
50.000	49.927	48.845	9.342	14.512	0.02	8.748
60.000	59.951	59.209	6.424	12.829	0.01	7.733
70.000	69.969	69.502	4.048	11.820	0.01	7.125
80.000	79.986	79.759	1.960	11.276	0.01	6.798

VELOCIMETER STATION 3, CRUISE 1A

INPUT DATA

Depths (Meters)

Water	Shot	Phone
4358.0	244.0	188.0

Layer		VELOCITY Km/Sec	DEPTH Kms	VELOCITY Ft/Sec	DEPTH Yds
1		1.5206	0.0000	4988.9	0.0
2		1.5121	0.1283	4961.1	140.3
3	Phone	1.5103	0.1879	4955.0	205.6
4	Shot	1.5085	0.2439	4949.3	266.9
5		1.5082	0.2546	4948.2	278.5
6		1.5048	0.4310	4937.0	471.5
7		1.5035	0.5834	4932.8	638.2
8		1.5035	0.6877	4933.0	752.3
9		1.5066	1.1548	4943.1	1263.4
10		1.5013	1.4255	4925.5	1559.5
11		1.5000	1.9187	4921.3	2099.1
12		1.5043	2.3919	4935.4	2616.8
13		1.5212	3.5548	4990.8	3889.0
	Bottom	1.5345	4.3579	5034.6	4767.6
14	(Interp.)	1.5374	4.5272	5043.9	4952.8

CALCULATED DATA

TOTAL DEPTH = 2H-DS-DH = 8.284 kms = 9.062 kyds.

Angle (Degrees) Beginning	Slant	Bottom	Horizontal Range Kyds	Slant Range Kyds	Prop. Anomaly (db)	Travel Time (Secs)
10.567	7.986	0.142	64.592	65.224	16.05	39.403
10.760	8.861	2.046	58.126	58.829	4.89	35.553
10.954	9.298	2.904	55.351	56.088	3.59	33.902
11.147	9.657	3.572	53.256	54.022	2.88	32.656
11.341	9.977	4.143	51.515	52.306	2.41	31.621
12.307	11.322	6.347	45.261	46.160	1.29	27.912
13.283	12.505	8.096	40.861	41.854	0.83	25.311
14.263	13.617	9.635	37.411	38.493	0.58	23.281
15.245	14.694	11.052	34.559	35.728	0.43	21.610
16.229	15.750	12.389	32.132	33.386	0.33	20.194
17.215	16.791	13.669	30.033	31.371	0.26	18.976
18.202	17.822	14.907	28.188	29.609	0.21	17.911
20.181	19.865	17.293	25.082	26.669	0.14	16.134
25.141	24.922	22.945	19.503	21.506	0.06	13.011
30.114	29.946	28.364	15.730	18.154	0.04	10.984
35.094	34.966	33.662	12.958	15.813	0.02	9.567
40.078	39.972	38.889	10.810	14.107	0.01	8.535
45.066	44.978	44.071	9.069	12.821	0.01	7.757
50.055	49.982	49.222	7.609	11.833	0.00	7.160
60.038	59.991	59.466	5.234	10.465	0.00	6.332
70.024	70.006	69.664	3.297	9.643	-0.00	5.835
80.011	79.978	79.837	1.601	9.203	0.01	5.568

VELOCIMETER STATION 4, CRUISE 1B

INPUT DATA

Depths (Meters)

Water	Shot	Phone
5250.0	244.0	171.0

Layer		VELOCITY Km/Sec	DEPTH Kms	VELOCITY Ft/Sec	DEPTH Yds
1		1.5288	0.0000	5015.7	0.0
2		1.5257	0.0830	5005.5	90.8
3	Phone	1.5175	0.1710	4978.7	187.0
4		1.5133	0.2165	4964.8	236.9
5	Shot	1.5120	0.2439	4960.7	266.9
6		1.4945	0.6317	4903.1	691.1
7		1.4907	0.8302	4890.9	908.3
8		1.4947	1.2743	4903.9	1394.1
9		1.4950	1.5324	4905.1	1676.4
10		1.4976	1.8573	4913.4	2031.9
11		1.5149	3.1009	4970.3	3392.4
12		1.5479	4.9493	5078.4	5414.5
	Bottom (Interp.)	1.5492	5.2500	5082.6	5743.5

CALCULATED DATA

TOTAL DEPTH = 2H-DS-DH = 10.085 kms = 11.032 kyds.

Angle (Degrees) Beginning	Slant	Bottom	Horizontal Range Kyds	Slant Range Kyds	Prop. Anomaly (db)	Travel Time (Secs)
12.571	7.193	0.158	87.418	88.111	21.45	52.891
12.755	9.144	2.184	68.542	69.425	8.07	41.756
12.940	9.872	3.098	63.398	64.351	5.96	38.724
13.125	10.403	3.809	60.093	61.098	4.79	36.778
13.311	10.843	4.415	57.601	58.648	4.00	35.311
13.866	11.899	5.902	52.356	53.505	2.66	32.229
14.806	13.319	7.887	46.602	47.890	1.61	28.858
15.752	14.558	9.571	42.482	43.891	1.08	26.455
16.705	15.711	11.092	39.220	40.742	0.77	24.562
17.663	16.816	12.510	36.504	38.134	0.57	22.993
18.625	17.891	13.856	34.176	35.913	0.43	21.656
20.560	19.986	16.403	30.335	32.279	0.26	19.468
25.439	25.080	22.299	23.573	26.027	0.09	15.701
30.356	30.102	27.859	19.030	21.997	0.03	13.272
35.294	35.103	33.254	15.696	19.186	0.01	11.576
40.245	40.095	38.553	13.104	17.130	-0.00	10.336
45.206	45.085	43.791	11.000	15.579	-0.00	9.401
50.173	50.074	48.989	9.233	14.386	-0.00	8.681
60.119	60.053	59.307	6.356	12.732	-0.01	7.683
70.075	70.033	69.564	4.008	11.738	-0.01	7.083
80.036	80.011	79.789	1.943	11.202	-0.00	6.760

VELOCIMETER STATION 5, CRUISE 1B

INPUT DATA

Depths (Meters)

Water	Shot	Phone
4897.0	244.0	136.0

Layer		VELOCITY Km/Sec	DEPTH Kms	VELOCITY Ft/Sec	DEPTH Yds
1		1.5323	0.0000	5027.3	0.0
2		1.5323	0.0505	5027.3	55.2
3	Phone	1.5174	0.1360	4978.3	148.7
4		1.5033	0.2165	4932.1	236.9
5	Shot	1.5025	0.2439	4929.5	266.9
6		1.4901	0.6786	4888.9	742.4
7		1.4897	0.9855	4887.7	1078.1
8		1.4950	1.6443	4904.8	1798.9
9		1.4997	2.0865	4920.3	2282.7
10		1.5127	3.0107	4962.9	3293.7
11		1.5339	4.3590	5032.4	4768.8
	Bottom (Interp.)	1.5433	4.8970	5063.3	5357.3

CALCULATED DATA

TOTAL DEPTH = 2H-DS-DH = 9.413 kms = 10.298 kyds.

Angle (Degrees) Beginning	Slant	Bottom	Horizontal Range Kyds	Slant Range Kyds	Prop. Anomaly (db)	Travel Time (Secs)
13.203	9.023	0.153	64.850	65.663	16.59	39.541
13.362	9.956	2.078	58.669	59.566	5.55	35.981
13.522	10.415	2.949	56.030	56.969	4.18	34.420
13.683	10.788	3.626	54.048	55.020	3.42	33.247
13.845	11.118	4.206	52.404	53.406	2.91	32.276
14.403	12.083	5.809	48.108	49.198	1.90	29.741
15.241	13.301	7.683	43.562	44.763	1.19	27.068
16.097	14.418	9.292	40.058	41.361	0.81	25.015
16.968	15.483	10.755	37.177	38.577	0.58	23.335
17.853	16.520	12.125	34.722	36.217	0.42	21.910
18.748	17.540	13.431	32.584	34.173	0.32	20.675
19.653	18.547	14.690	30.695	32.376	0.24	19.589
21.488	20.543	17.108	27.481	29.348	0.14	17.759
26.177	25.488	22.809	21.602	23.932	0.03	14.484
30.958	30.423	28.257	17.537	20.338	-0.00	12.310
35.793	35.362	33.576	14.511	17.794	-0.02	10.771
40.664	40.310	38.818	12.139	15.919	-0.03	9.636
45.558	45.265	44.012	10.203	14.497	-0.03	8.776
50.469	50.223	49.173	8.573	13.400	-0.03	8.112
60.323	60.159	59.433	5.907	11.873	-0.04	7.187
70.204	70.095	69.643	3.729	10.953	-0.03	6.630
80.098	80.046	79.827	1.807	10.456	-0.03	6.329

VELOCIMETER STATION 6, CRUISE 1B

INPUT DATA

Depths (Meters)

Water	Shot	Phone
4921.0	244.0	158.0

Layer		VELOCITY Km/Sec	DEPTH Kms	VELOCITY Ft/Sec	DEPTH Yds
1		1.5393	0.0000	5050.3	0.0
2		1.5399	0.0451	5052.2	49.3
3		1.5112	0.0902	4958.2	98.7
4	Phone	1.5073	0.1579	4945.1	172.8
5	Shot	1.5022	0.2439	4928.6	266.9
6		1.4899	0.4548	4888.0	497.6
7		1.4846	0.7797	4871.5	853.0
8		1.4858	0.9638	4874.6	1054.4
9		1.4889	1.2562	4884.8	1374.3
10		1.5127	3.0432	4963.0	3329.2
11		1.5432	4.9204	5063.1	5382.9
	Bottom (Interp.)	1.5437	4.9210	5064.6	5383.5

CALCULATED DATA

TOTAL DEPTH = 2H-DS-DH = 9.440 kms = 10.327 kyds.

Angle (Degrees) Beginning	Slant	Bottom	Horizontal Range Kyds	Slant Range Kyds	Prop. Anomaly (db)	Travel Time (Secs)
13.311	9.571	0.163	61.242	62.106	8.68	37.522
13.498	10.244	2.266	57.140	58.066	5.46	35.095
13.686	10.717	3.213	54.562	55.531	4.38	33.570
13.874	11.117	3.949	52.553	53.558	3.71	32.382
14.062	11.475	4.577	50.870	51.908	3.24	31.389
14.748	12.597	6.411	46.210	47.350	2.21	28.642
15.699	13.922	8.400	41.661	42.922	1.51	25.971
16.655	15.131	10.102	38.191	39.563	1.11	23.943
17.615	16.278	11.644	35.365	36.842	0.86	22.300
18.580	17.387	13.083	32.978	34.558	0.68	20.919
20.520	19.538	15.760	29.101	30.879	0.46	18.696
25.407	24.729	21.842	22.422	24.686	0.22	14.950
30.330	29.817	27.506	18.019	20.769	0.12	12.579
35.272	34.866	32.970	14.822	18.065	0.08	10.942
40.227	39.897	38.320	12.352	16.100	0.05	9.752
45.191	44.919	43.597	10.356	14.625	0.04	8.859
50.160	49.935	48.827	8.685	13.494	0.03	8.174
60.110	59.957	59.197	5.972	11.930	0.02	7.226
70.069	69.973	69.495	3.764	10.991	0.01	6.658
80.033	79.988	79.755	1.823	10.487	0.01	6.352

VELOCIMETER STATION 7, CRUISE 1B

INPUT DATA

Depths (Meters)

Water	Shot	Phone
5110.0	244.0	409.0

Layer		VELOCITY Km/Sec	DEPTH Kms	VELOCITY Ft/Sec	DEPTH Yds
1		1.5257	0.0000	5005.5	0.0
2		1.5055	0.0631	4939.3	69.1
3		1.5052	0.2057	4938.5	225.1
4	Shot	1.4996	0.2439	4920.1	266.9
5		1.4920	0.2960	4895.2	323.8
6		1.4918	0.3501	4894.4	383.0
7		1.4859	0.3880	4875.0	424.5
8	Phone	1.4852	0.4089	4872.6	447.4
9		1.4839	0.4440	4868.6	485.7
10		1.4821	0.5739	4862.5	627.9
11		1.4828	0.8014	4864.8	876.7
12		1.4896	1.1967	4887.1	1309.2
13		1.4938	1.6064	4901.0	1757.4
14		1.5099	2.8194	4953.7	3084.4
	Bottom	1.5462	5.1099	5072.8	5590.3
15	(Interp.)	1.5474	5.1893	5076.9	5677.1

CALCULATED DATA

TOTAL DEPTH = 2H-DS-DH = 9.566 kms = 10.466 kyds.

Angle (Degrees) Beginning	Slant	Bottom	Horizontal Range Kyds	Slant Range Kyds	Prop. Anomaly (db)	Travel Time (secs)
14.091	8.998	0.176	66.092	66.915	18.61	40.358
14.291	10.171	2.413	58.336	59.268	7.33	35.774
14.491	10.743	3.420	55.162	56.146	5.89	33.900
14.691	11.205	4.201	52.831	53.858	5.07	32.525
14.891	11.612	4.867	50.933	51.997	4.50	31.407
15.000	11.816	5.195	50.027	51.111	4.25	30.874
16.000	13.433	7.657	43.820	45.053	2.89	27.227
17.000	14.810	9.608	39.583	40.943	2.21	24.750
18.000	16.078	11.315	36.313	37.791	1.78	22.850
19.000	17.281	12.877	33.641	35.232	1.48	21.305
20.000	18.442	14.339	31.384	33.083	1.26	20.008
25.000	23.934	20.864	23.580	25.798	0.68	15.608
30.000	29.193	26.761	18.731	21.457	0.43	12.983
35.000	34.360	32.374	15.308	18.544	0.30	11.221
40.000	39.478	37.832	12.706	16.461	0.22	9.962
45.000	44.570	43.193	10.624	14.913	0.17	9.025
50.000	49.643	48.491	8.893	13.734	0.14	8.312
60.000	59.758	58.968	6.101	12.115	0.09	7.332
70.000	69.849	69.351	3.840	11.148	0.07	6.747
80.000	79.926	79.586	1.859	10.630	0.06	6.433

VELOCIMETER STATION 8, CRUISE 1B

INPUT DATA

Depths (Meters)

Water	Shot	Phone
5484.0	244.0	134.0

Layer		VELOCITY Km/Sec	DEPTH Kms	VELOCITY Ft/Sec	DEPTH Yds
1		1.5204	0.0000	4988.2	0.0
2		1.5218	0.0884	4992.7	96.7
3		1.5052	0.1173	4938.5	128.3
4	Phone	1.5044	0.1340	4935.8	146.5
5	Shot	1.4991	0.2439	4918.3	266.9
6		1.4874	0.4835	4879.9	531.1
7		1.4819	0.6696	4861.9	732.6
8		1.4817	0.8519	4861.4	932.0
9		1.4820	0.9692	4862.2	1060.3
10		1.5136	3.1425	4965.8	3437.9
11		1.5529	5.4547	5094.8	5967.4
	Bottom (Interp.)	1.5530	5.4840	5095.3	5999.4

CALCULATED DATA

TOTAL DEPTH = 2H-DS-DH = 10.590 kms = 11.585 kyds.

Angle (Degrees) Beginning	Slant	Bottom	Horizontal Range Kyds	Slant Range Kyds	Prop. Anomaly (db)	Travel Time (Secs)
15.148	9.097	0.176	72.349	73.270	22.05	44.102
15.337	10.751	2.438	61.015	62.105	7.20	37.433
15.527	11.356	3.455	57.681	58.833	5.56	35.474
15.717	11.832	4.245	55.297	56.497	4.67	34.074
15.907	12.245	4.917	53.380	54.623	4.07	32.949
16.694	13.646	7.101	47.720	49.106	2.73	29.636
17.652	15.062	9.172	43.049	44.580	1.96	26.914
18.615	16.343	10.949	39.507	41.171	1.51	24.862
19.581	17.549	12.557	36.633	38.422	1.21	23.206
20.551	18.708	14.054	34.211	36.119	1.00	21.819
21.523	19.836	15.473	32.116	34.141	0.84	20.626
22.497	20.940	16.833	30.275	32.416	0.72	19.585
23.474	22.029	18.147	28.632	30.888	0.62	18.664
25.432	24.167	20.674	25.817	28.298	0.48	17.101
30.350	29.392	26.617	20.567	23.606	0.29	14.268
35.289	34.527	32.260	16.839	20.440	0.20	12.356
40.241	39.621	37.739	13.993	18.167	0.14	10.983
45.202	44.692	43.116	11.710	16.472	0.11	9.959
50.170	49.743	48.427	9.810	15.180	0.09	9.178
60.117	59.825	58.924	6.735	13.401	0.06	8.102
70.073	69.897	69.324	4.240	12.337	0.05	7.459
80.035	79.952	79.673	2.052	11.765	0.04	7.114

VELOCIMETER STATION 9, CRUISE 1C

INPUT DATA

Depths (Meters)

Water	Shot	Phone
4943.0	244.0	216.0

Layer		VELOCITY Km/Sec	DEPTH Kms	VELOCITY Ft/Sec	DEPTH Yds
1		1.5203	0.0000	4987.8	0.0
2		1.5202	0.0902	4987.4	98.7
3	Phone	1.5144	0.2159	4968.6	236.3
4		1.5133	0.2400	4965.0	262.6
5	Shot	1.5132	0.2439	4964.7	266.9
6		1.5051	0.5992	4938.2	655.5
7		1.4898	1.0071	4887.9	1101.8
8		1.4893	1.1894	4886.4	1301.3
9		1.4900	1.4963	4888.3	1637.0
10		1.4934	1.8501	4899.8	2024.0
11		1.5107	3.0450	4956.6	3331.2
12		1.5249	4.2128	5002.9	4608.8
	Bottom	1.5366	4.9429	5041.2	5407.6
13	(Interp.)	1.5375	5.0052	5044.5	5475.7

CALCULATED DATA

TOTAL DEPTH = 2H-DS-DH = 9.426 kms = 10.312 kyds.

Angle (Degrees) Beginning	Slant	Bottom	Horizontal Range Kyds	Slant Range Kyds	Prop. Anomaly (db)	Travel Time (Secs)
9.998	8.428	0.148	69.591	70.351	15.36	42.537
10.193	9.292	1.998	63.024	63.862	4.39	38.631
10.388	9.722	2.837	60.183	61.060	3.09	36.943
10.583	10.075	3.490	58.033	58.942	2.38	35.666
10.778	10.389	4.049	56.244	57.182	1.92	34.604
11.229	11.031	5.138	52.894	53.889	1.26	32.617
12.209	12.249	7.044	47.496	48.603	0.58	29.424
13.193	13.359	8.653	43.421	44.629	0.27	27.023
14.179	14.419	10.106	40.106	41.411	0.10	25.077
15.166	15.452	11.463	37.305	38.704	0.01	23.440
16.156	16.468	12.756	34.884	36.376	-0.04	22.032
17.146	17.474	14.001	32.757	34.341	-0.08	20.801
18.137	18.473	15.211	30.866	32.543	-0.10	19.713
20.123	20.460	17.554	27.638	29.499	-0.12	17.870
25.096	25.405	23.138	21.712	24.036	-0.11	14.562
30.077	30.347	28.515	17.613	20.410	-0.09	12.366
35.064	35.296	33.785	14.566	17.846	-0.08	10.813
40.053	40.253	38.990	12.179	15.958	-0.06	9.669
45.044	45.214	44.155	10.235	14.529	-0.05	8.804
50.037	50.182	49.293	8.596	13.425	-0.05	8.135
60.025	60.127	59.515	5.923	11.892	-0.04	7.206
70.016	70.078	69.694	3.737	10.968	-0.03	6.646
80.007	80.033	79.852	1.812	10.470	-0.02	6.344

VELOCIMETER STATION 10, CRUISE 1C

INPUT DATA

Depths (Meters)

Water	Shot	Phone
4795.0	244.0	199.0

Layer		VELOCITY Km/Sec	DEPTH Kms	VELOCITY Ft/Sec	DEPTH Yds
1		1.5317	0.0000	5025.2	0.0
2		1.5335	0.1191	5031.3	130.3
3	Phone	1.5270	0.1990	5009.9	217.7
4	Shot	1.5233	0.2439	4997.9	266.9
5		1.5091	0.4187	4951.1	458.1
6		1.4880	0.8682	4882.0	949.8
7		1.4872	0.9584	4879.4	1048.5
8		1.4865	1.1786	4877.1	1289.4
9		1.4869	1.3699	4878.4	1498.7
10		1 4924	1.8573	4896.3	2031.9
11		1.5138	3.2778	4966.6	3586.0
12		1.5234	4.0016	4998.2	4377.8
	Bottom	1.5359	4.7950	5038.9	5245.7
13	(Interp.)	1.5368	4.8536	5041.9	5309.8

CALCULATED DATA

TOTAL DEPTH = 2H-DS-DH = 9.147 kms = 10.006 kyds.

Angle (Degrees) Beginning	Slant	Bottom	Horizontal Range Kyds	Slant Range Kyds	Prop. Anomaly (db)	Travel Time (Secs)
7.320	8.354	0.125	68.139	68.870	12.88	41.468
7.489	9.050	1.589	62.824	63.616	2.17	38.505
7.659	9.393	2.262	60.485	61.307	0.90	37.114
7.830	9.675	2.790	58.695	59.542	0.24	36.050
8.003	9.925	3.246	57.187	58.056	-0.17	35.153
8.043	9.980	3.344	56.867	57.741	-0.25	34.963
8.926	11.028	5.122	51.342	52.308	-1.07	31.684
9.830	11.963	6.581	47.226	48.274	-1.29	29.247
10.752	12.860	7.898	43.830	44.957	-1.32	27.242
11.686	13.744	9.135	40.912	42.118	-1.29	25.525
12.631	14.624	10.322	38.350	39.634	-1.22	24.022
13.583	15.506	11.473	36.068	37.431	-1.14	22.689
15.505	17.283	13.706	32.160	33.681	-0.99	20.418
20.374	21.825	19.067	24.986	26.916	-0.69	16.321
25.293	26.486	24.278	20.082	22.437	-0.50	13.606
30.237	31.229	29.419	16.503	19.300	-0.38	11.705
35.196	36.029	34.523	13.758	17.012	-0.30	10.317
40.163	40.867	39.602	11.565	15.293	-0.24	9.275
45.137	45.733	44.667	9.753	13.973	-0.20	8.475
50.115	50.618	49.720	8.214	12.946	-0.18	7.852
60.079	60.428	59.808	5.678	11.505	-0.14	6.978
70.050	70.273	69.879	3.588	10.630	-0.12	6.448
80.024	80.131	79.941	1.740	10.157	-0.11	6.160

VELOCIMETER STATION 11, CRUISE 1D

INPUT DATA

Depths (Meters)

Water	Shot	Phone
4000.0	244.0	145.0

Layer		VELOCITY Km/Sec	DEPTH Kms	VELOCITY Ft/Sec	DEPTH Yds
1		1.5353	0.0000	5037.1	0.0
2		1.5358	0.0397	5038.9	43.4
3		1.5088	0.0920	4950.3	100.7
4	Phone	1.5044	0.1450	4935.6	158.6
5		1.5011	0.1841	4924.8	201.4
6	Shot	1.5008	0.2439	4923.8	266.9
7		1.5007	0.2490	4923.8	272.5
8		1.4956	0.3934	4906.9	430.4
9		1.4956	0.4891	4906.8	535.1
10		1.4925	0.6714	4896.7	734.5
11		1.4934	0.8447	4899 7	924.1
12		1.4913	1.0811	4892.9	1182.8
13		1.4914	1.4494	4893.2	1585.6
14		1.4938	1.8338	4900.9	2006.2
15		1.5013	2.4493	4925.5	2679.6
16		1.5237	3.8374	4999.1	4198.1
	Bottom (Interp.)	1.5284	4.0000	5014.5	4376.0

CALCULATED DATA

TOTAL DEPTH = 2H-DS-DH = 7.611 kms = 8.326 kyds.

Angle (Degrees) Beginning	Slant	Bottom	Horizontal Range Kyds	Slant Range Kyds	Prop. Anomaly (db)	Travel Time (Secs)
10.909	8.681	0.142	54.532	55.184	14.56	33.512
11.096	9.391	2.043	50.341	51.025	4.13	31.006
11.283	9.776	2.899	48.323	49.035	3.03	29.801
11.470	10.102	3.566	46.730	47.466	2.45	28.850
11.658	10.400	4.137	45.363	46.121	2.05	28.034
11.683	10.439	4.209	45.193	45.954	2.01	27.933
12.628	11.719	6.400	40.138	40.992	1.08	24.922
13.580	12.864	8.138	36.458	37.397	0.68	22.739
14.539	13.950	9.670	33.518	34.537	0.46	21.003
15.503	15.004	11.082	31.063	32.160	0.32	19.558
16.471	16.039	12.416	28.961	30.134	0.23	18.327
17.442	17.065	13.693	27.123	28.373	0.17	17.257
18.417	18.082	14.929	25.501	26.826	0.13	16.317
20.373	20.098	17.312	22.754	24.230	0.07	14.738
25.292	25.106	22.959	17.769	19.623	0.02	11.937
30.236	30.105	28.375	14.360	16.600	0.00	10.098
35.195	35.085	33.671	11.853	14.485	-0.00	8.812
40.163	40.075	38.896	9.896	12.933	-0.00	7.868
45.136	45.070	44.077	8.306	11.760	-0.00	7.155
50.114	50.058	49.227	6.972	10.860	-0.00	6.607
60.079	60.054	59.470	4.796	9.609	-0.01	5.846
70.049	70.023	69.666	3.026	8.859	-0.00	5.390
80.026	80.018	79.838	1.465	8.454	-0.01	5.143

VELOCIMETER STATION 12, CRUISE 1D

INPUT DATA

Depths (Meters)

Water	Shot	Phone
4233.0	244.0	102.0

Layer		VELOCITY Km/Sec	DEPTH Km	VELOCITY Ft/Sec	DEPTH Yds
1		1.5413	0.0000	5056.9	0.0
2		1.5420	0.0559	5059.1	61.2
3		1.5408	0.0866	5055.3	94.7
4	Phone	1.5318	0.1019	5025.7	111.5
5		1.5143	0.1317	4968.2	144.1
6	Shot	1.5030	0.2439	4931.3	266.9
7		1.5000	0.2743	4921.3	300.1
8		1.4930	0.7978	4898.5	872.8
9		1.4917	1.0432	4894.1	1141.3
10		1.4918	1.5071	4894.4	1648.8
11		1.4938	1.9169	4901.0	2097.0
12		1.4964	2.1876	4909.5	2393.2
13		1.5135	3.3681	4965.7	3684.7
14		1.5278	4.2273	5012.6	4624.6
	Bottom (Interp.)	1.5279	4.2329	5013.0	4630.9

CALCULATED DATA

TOTAL DEPTH = 2H-DS-DH = 8.120 kms = 8.883 kyds.

Angle (Degrees) Beginning	Slant	Bottom	Horizontal Range Kyds	Slant Range Kyds	Prop. Anomaly (db)	Travel Time (Secs)
11.121	9.991	4.077	50.422	51.198	-19.69	31.102
11.123	9.996	4.082	50.398	51.174	-13.87	31.087
11.128	10.006	4.097	50.345	51.123	-11.48	31.056
11.137	10.022	4.121	50.264	51.043	-9.96	31.008
11.149	10.043	4.155	50.157	50.937	-8.86	30.944
11.165	10.069	4.198	50.023	50.806	-8.00	30.864
11.297	10.276	4.541	48.996	49.794	-5.41	30.251
11.514	10.594	5.060	47.491	48.315	-4.08	29.354
11.810	11.002	5.709	45.691	46.547	-3.28	28.282
12.180	11.479	6.448	43.743	44.636	-2.74	27.123
14.913	14.596	10.791	34.111	35.249	-1.45	21.426
18.596	18.447	15.532	26.629	28.072	-0.92	17.066
22.772	22.697	20.394	21.238	23.021	-0.63	13.997
27.216	27.172	25.309	17.305	19.452	-0.47	11.828
31.814	31.782	30.250	14.336	16.865	-0.37	10.255
36.508	36.492	35.206	12.008	14.937	-0.31	9.083
41.265	41.252	40.172	10.128	13.472	-0.27	8.192
46.066	46.064	45.144	8.559	12.335	-0.24	7.501
50.897	50.891	50.121	7.221	11.448	-0.21	6.961
60.619	60.623	60.083	5.000	10.194	-0.19	6.199
70.391	70.373	70.052	3.167	9.431	-0.16	5.735
80.189	80.163	80.025	1.540	9.015	-0.14	5.482

VELOCIMETER STATION 13, CRUISE 1D

INPUT DATA

Depths (Meters)

Water	Shot	Phone
4050.0	244.0	195.0

Layer		VELOCITY Km/Sec	DEPTH Kms	VELOCITY Ft/Sec	DEPTH Yds
1		1.5397	0.0000	5051.4	0.0
2		1.5409	0.0631	5055.5	69.1
3		1.5088	0.1786	4950.1	195.4
4	Phone	1.5073	0.1949	4945.4	213.3
5	Shot	1.5030	0.2439	4931.0	266.9
6		1.5001	0.2761	4921.6	302.1
7		1.4978	0.3447	4914.2	377.1
8		1.4942	0.5703	4902.3	623.9
9		1.4916	0.8302	4893.9	908.3
10		1.4915	1.0162	4893.4	1111.7
11		1.4911	1.4331	4892.2	1567.8
12		1.4936	1.9060	4900.2	2085.2
13		1.5014	2.5522	4925.9	2792.1
14		1.5244	4.0089	5001.5	4385.7
	Bottom (Interp.)	1.5251	4.0499	5003.6	4430.6

CALCULATED DATA

TOTAL DEPTH = 2H-DS-DH = 7.661 kms = 8.381 kyds.

Angle (Degrees) Beginning	Slant	Bottom	Horizontal Range Kyds	Slant Range Kyds	Prop. Anomaly (db)	Travel Time (Secs)
8.751	7.737	0.142	61.685	62.252	15.43	37.825
8.951	8.580	1.894	55.545	56.174	4.53	34.146
9.151	8.998	2.690	52.923	53.582	3.20	32.575
9.351	9.340	3.311	50.956	51.640	2.48	31.398
9.551	9.643	3.844	49.322	50.029	2.00	30.421
10.000	10.250	4.859	46.346	47.098	1.33	28.643
11.000	11.430	6.692	41.453	42.292	0.63	25.725
12.000	12.509	8.244	37.775	38.694	0.32	23.539
13.000	13.545	9.652	34.789	35.784	0.15	21.771
14.000	14.556	10.971	32.276	33.346	0.06	20.289
15.000	15.556	12.231	30.106	31.251	0.00	19.015
20.000	20.489	18.055	22.428	23.943	-0.06	14.571
25.000	25.411	23.511	17.641	19.530	-0.06	11.886
30.000	30.344	28.809	14.317	16.589	-0.04	10.097
35.000	35.290	34.024	11.841	14.507	-0.03	8.829
40.000	40.246	39.189	9.901	12.972	-0.03	7.895
45.000	45.209	44.321	8.320	11.809	-0.02	7.188
50.000	50.177	49.431	6.988	10.912	-0.01	6.642
60.000	60.122	59.609	4.814	9.665	-0.01	5.883
70.000	70.071	69.754	3.038	8.914	-0.00	5.426
80.000	80.037	79.881	1.472	8.509	-0.00	5.179

PART V

AREA ST VOLUME 2

HYDROGRAPHIC STATION DATA

by

M. H. Rodriguez, Jr.

VOLUME 2, PART V

TABLE OF CONTENTS

LIST OF TABLES

LIST OF FIGURES

I - INTRODUCTION

This report covers the six hydrographic stations completed by R/V RUTH ANN in Area ST during Cruises 1A, 1C and 1D for the period of 24 May 1967 to 31 August 1967. Salinities and temperatures obtained at these hydrographic stations are used to determine values of sound velocity throughout the water column which are compared to corresponding data obtained at these same stations by sound velocimeter lowerings. Comparisons are also made between the measured properties during the cruises and those recorded previously in the same regions by other sources.

II - DISCUSSION

A - Station locations

The first hydrographic station occupied during Cruise 1A was Station 1, located in the North Atlantic, approximately 550 nautical miles east of Bermuda (Figure 1). Depth was found to be 5510 meters. A shallow cast to 1510 meters was made, but due to a pre-trip of the lowest two bottles and a large wire angle the deepest sampling point reached was 591 meters.

The next two stations occupied were Stations 9 and 10 in the Southwestern Indian Ocean on Cruise 1C - Capetown to Diego-Suarez (Figure 1). Deepest sampling depths obtained were 3724 meters and 3701 meters respectively.

Stations 11, 12 and 13 in the Northern Indian Ocean were occupied by the RUTH ANN during Cruise 1D (Figure 1), Station 11 being positioned south of the Arabian Sea and Stations 12 and 13 along the southern edge of the Bay of Bengal. Deepest sampling depths were 3865, 4010 and 3982 meters respectively.

B - Hydrographic Data Reduction Procedure

Aboard ship, temperatures were corrected, thermometric depths determined, and salinities measured (Industrial Instruments, Inc. portable induction salinometer - model RS-7B). Sound velocities were later calculated utilizing the depth, temperature and salinity of each sample as entries in Wilson's Tables (Wilson, 1962). Table I lists each sample by station location and depth, provides temperature and salinity measurements, and shows the calculated sound velocity in meters per second.

C - Comparison of Hydrographic and Sound Velocimeter Data

Hydrocasts and velocimeter lowerings in every case were at the same approximate locations, and never more than three or four miles apart. Table II compares sound velocities derived from hydrographic data and those obtained by the velocimeter. (It is noted that differences range from -2.9 to 3.2 meters/second).

Table II shows that sound velocity values from hydrographic data above the sound velocity minimum are slightly higher (approximately 1.0 meters/second) than those sound velocities from velocimeter lowerings. Likewise, it shows that sound velocity values from data below the minimum are slightly lower than those from velocimeter lowerings (approximately 1.0 meters/second). This, as other investigators (Carlson et al., 1966) have shown, is caused by the inability of the sound velocimeter's pressure sensor to reach ambient temperature instantaneously. However, the small deviation is considered relatively unimportant because sound velocities from both sources seem to be enough in agreement to provide accurate data for all stations. Figures 2A to 2F show the profiles and trends for hydrographic sound velocities for all stations.

D - Temperature-Salinity Plot Analysis

The temperature-salinity plots (Figures 3A through 3F) provide means for checking the validity of the data received from each cast. By comparing the results obtained with previous knowledge of water mass properties, we can ascertain whether irregularities or erroneous values exist in the hydrographic data collected.

Surface temperatures taken at Station 1 during May 1967 agreed with those of other sources. For the same locality, Sverdrup, et al., 1942, places the winter surface temperature range at 19-20°C and the summer surface temperature range at 26-27°C. The measured value of 21.89°C lies within these limits and is explained by the spring warming trend. For salinity, the measured 36.48°/$_{oo}$ value as opposed to the summer surface salinity range of 36.5-36.7°/$_{oo}$ (Sverdrup, et al., 1942) may be explained by increased precipitation and lower sea surface evaporation during spring. From 120 to 591 meters depth the temperature-salinity plot (Figure 3A) coincides closely with that of North Atlantic Central Water (Sverdrup, et al., 1942).

Surface temperatures taken at Stations 9 and 10 in August 1967, during the austral winter, were also found to be in close agreement with those of other sources. At Station 9 the average winter temperature range of 19-20°C and salinities of 35.4-35.6°/$_{oo}$ (Fairbridge, R.W., 1966) are close to the measured values of 19.43°C and 35.49°/$_{oo}$. Station 10, farther north, at which surface values of 24.07°C and 34.85°/$_{oo}$ were measured, were 1°C higher and 0.2°/$_{oo}$ lower, respectively, than the average range of previous investigations (Fairbridge, 1966). Below the surface, both

stations show temperature-salinity values (Figures 3B and 3C) lying midway between those for Antarctic Intermediate and Subantarctic Water. This may indicate mixing of these masses along the coast of East Africa. From 2319 to 3724 meters the salinities for Station 9 were 0.5°/$_{oo}$ higher than the mean value of Circumpolar Water known to exist here (Fairbridge, 1966). An error in the salinity determination may account for this fault. Corrected salinities lower hydrographic sound velocity values by 0.7 meters/second. The temperature-salinity plot for Station 10 (Figure 3C) agrees closely with those previously recorded for Circumpolar Water below 2300 meters.

The temperature-salinity plots for Stations 11, 12, and 13 (Figures 3D, 3E and 3F) illustrate the relatively narrow range of salinities characteristically found in the Northern Indian Ocean (Sverdrup, et al., 1942). Each station is within 0.5°C of the average August surface temperature for the same location values recorded by other authorities (Fairbridge, 1966). Surface salinities for Stations 12 and 13 match closely with those found by previous investigators at these localities, but Station 11 with a measured salinity of 34.88°/$_{oo}$ is definitely below the local average of 35.5°/$_{oo}$ reported by Fairbridge, 1966. This discrepancy may be due to an intense rainfall which fell during the cast. Seas at this time were only one foot in height, so vertical mixing of rain water in the order of 1 meter below the surface was possible. (1.7 cm of rain added to 1 meter of water at 35.5°/$_{oo}$ can lower the salinity to 34.9°/$_{oo}$).

Surface salinity measurements for the three stations decrease in value and a strong halocline develops at approximately 100 to 200 meters (Figures 3D, 3E and 3F). This effect is caused by the high river discharge

into the Bay of Bengal, forming a surface lens of diluted sea water in the northern part of the bay. This lens spreads southward and increases in salinity as it flows and mixes into the Northern Indian Ocean. As the three stations are progressively nearer to the Bay of Bengal, this decreasing salinity trend and halocline formation becomes evident. Below 200 meters all three temperature-salinity plots coincide closely with those recorded previously for Indian Ocean Equatorial Water. At 587 meters, Station 11 temperature-salinity values (Figure 3D) exhibit the properties of Antarctic Intermediate Water, graduating downward to agree closely with those of deep Circumpolar Water. Temperature-salinity values for Stations 12 and 13 (Figures 3E and 3F) agree with those of the Equatorial Water envelope until they merge with the Antarctic Intermediate and finally with the Circumpolar Water below 1500 meters. All three stations exhibit properties of Circumpolar Water at their deepest points.

An interesting anomaly is observed in the 783 meter sample of Station 11; it exhibits a notably higher salinity (Figure 3D) than those samples taken above and below this depth. This may be explained by the presence of intermediate depth intrusions of Red Sea Water traced in the Northwest Indian Ocean by the 1920-1922 Dana and the 1929-1930 Snellius Expeditions (Sverdrup, et al., 1942). This anomaly is recorded as a 1.2 meters/second rise in sound velocity in the velocimeter profile (Figure 2D) between 700 and 880 meters of depth.

III - REFERENCES

Bowditch, N., 1962 (corrected Reprint). American Practical Navigator. U. S. Naval Oceanographic Office, Washington, D.C., H. O. Pub 9: 1524 pp.

Carlson, Q., and Merrifield, R., 1966. Sound velocity system in use aboard oceanographic research ships of the Naval Oceanographic Office. U. S. Navy Jour. of Underwater Acoustics, 16: (4) 665-676.

Encyclopedia of Oceanography 1966. R.W. Fairbridge, (Editor). Reinhold Publishing Corp., New York: 1021 pp.

Sverdrup, H.U., Johnson, M.W., and Fleming, R.H., 1942. The Oceans, Prentice-Hall, New York: 1087 pp.

Wilson, W.D., 1962. Tables of Sound Speed in Sea Water. Oceanographic Analysis Div., Marine Sci. Dept., U. S. Naval Oceanographic Office SP-58 (Supplement to H. O. Pub 614).

TABLE I

Location and Results of Hydrographic Stations

R/V Ruth Ann, Area ST

Cruise	Station	Latitude	Longitude	Depth (m)	Temp. (°C)	Sal. (0/00)	Sound Velocity (m/sec)
1-A	1	32°37'N	056°05'W	3	21.89	36.482	1528.8
				22	19.73	36.424	1523.4
				41	18.66	36.425	1520.9
				60	18.33	36.425	1520.1
				80	18.07	36.425	1519.7
				91	17.95	36.423	1519.5
				120	17.73	36.420	1519.2
				179	-----	36.345	------
				237	16.33	36.229	1517.1
				357	14.82	35.970	1513.9
				472	13.08	35.706	1509.7
				591	10.96	35.397	1504.0
				*	14.36	35.897	------
				*	10.12	35.306	------
1-C	9	29°50'S	038°28'E	1	19.43	35.490	1521.2
				26	19.38	35.485	1521.4
				50	19.32	35.482	1521.6
				100	18.74	35.493	1521.9
				149	17.28	35.511	1517.5
				199	16.43	35.513	1515.7
				298	15.27	35.452	1513.7
				397	13.87	35.326	1510.7
				497	12.74	35.180	1508.3
				597	11.50	35.057	1505.7
				797	9.11	34.729	1500.0
				997	6.42	34.545	1492.8
				1121	5.09	34.465	1488.4
				1346	4.19	34.569	1489.4
				1827	2.91	34.689	1492.4
				2319	2.54	34.776	1499.3
				2722	2.30	34.806	1505.3
				3223	1.98	34.790	1512.6
				3724	1.47	34.762	1519.1
				4726	-----	34.700	------
1-C	10	19°59'S	050°55'E	1	24.07	34.853	1532.4
				22	24.02	34.850	1532.6
				42	24.02	34.850	1533.1
				89	24.00	34.939	1533.8
				135	22.54	35.134	1531.3
				179	20.80	35.290	1527.8

* - pretrip

TABLE I (continued)

Cruise	Station	Latitude	Longitude	Depth (m)	Temp. (°C)	Sal. (0/00)	Sound Velocity (m/sec)
1-C	10	19°59'S	050°55'E	269	17.79	35.513	1521.0
				361	14.98	35.441	1513.8
				449	13.00	35.247	1508.6
				541	11.25	35.007	1503.9
				722	8.55	34.681	1496.6
				902	6.24	34.489	1490.3
				1128	4.75	34.568	1488.2
				1353	3.27	34.602	1485.8
				1809	2.79	34.699	1491.5
				2272	2.19	34.727	1496.8
				2736	1.90	34.729	1503.6
				3223	1.71	34.726	1511.2
				3701	1.44	34.719	1518.4
1-D	11	06°34'S	061°54.5'E	0	25.82	34.883	1536.5
				98	15.31	35.076	1510.2
				196	12.72	35.078	1503.3
				391	10.07	34.893	1496.7
				587	8.58	34.838	1494.4
				685	7.78	34.787	1492.1
				783	7.50	34.847	1493.5
				1300	4.82	34.768	1491.7
				1531	3.95	34.771	1492.0
				1991	2.89	34.759	1495.3
				2473	2.12	34.736	1500.3
				2930	1.80	34.730	1506.3
				3415	1.67	34.733	1514.1
				3865	1.59	34.725	1521.9
1-D	12	03°01.5'N	083°34.5'E	0	28.42	34.649	1542.1
				42	28.37	34.647	1542.7
				63	28.28	34.667	1543.0
				84	26.56	34.928	1539.7
				127	17.02	35.024	1515.8
				170	15.07	35.115	1510.6
				253	12.58	35.102	1503.7
				340	11.13	35.049	1500.3
				517	9.56	35.030	1497.3
				696	8.22	35.001	1495.1
				878	7.12	34.961	1494.1
				1158	5.68	34.885	1492.7
				2175	2.39	34.760	1496.1
				2621	2.10	34.733	1502.2
				3072	1.66	34.724	1508.2
				3540	1.50	34.717	1515.6
				4010	1.46	34.715	1523.7
				4477	1.43	-----	------

TABLE I (continued)

Cruise	Station	Latitude	Longitude	Depth (m)	Temp. (°C)	Sal. (0/00)	Sound Velocity (m/sec)
1-D	13	04°35'N	086°16.5'E	0	27.86	34.115	1540.4
				48	27.75	34.600	1541.5
				97	21.44	34.634	1527.2
				146	16.39	34.621	1513.7
				195	13.57	34.995	1506.0
				244	12.12	35.038	1502.0
				293	11.26	35.043	1499.8
				343	10.58	35.038	1498.3
				392	10.15	35.035	1497.3
				590	8.76	35.004	1495.5
				789	7.53	34.960	1493.9
				989	6.33	34.917	1492.6
				1475	4.36	34.846	1492.8
				1971	2.76	34.769	1494.2
				2478	2.08	34.736	1500.0
				2978	1.74	34.724	1506.7
				3482	1.46	34.718	1514.7
				3982	1.41	34.714	1523.3

TABLE II

Comparison of Hydrographic and Sound Velocimeter Sound Velocities

Station	Depth (m)	Sound Velocity (m/s) Hydrographic	Velocimeter	Difference
1	3	1528.8	1526.2	2.6
	22	1523.4	1524.0	-0.6
	41	1520.9	1520.9	0.0
	60	1520.1	1519.6	0.5
	80	1519.7	1519.3	0.4
	91	1519.5	1519.5	0.0
	120	1519.2	1518.3	0.9
	237	1517.1	1515.9	1.2
	357	1513.9	1511.6	2.3
	472	1509.7	1508.0	1.7
	591	1504.0	1501.0	3.0
	Average of Absolute Values of Differences . . .			1.20
9	1	1521.2	1520.4	0.8
	26	1521.4	1520.8	0.6
	50	1521.6	1520.6	1.0
	100	1521.9	1520.2	1.7
	149	1517.5	1517.3	0.2
	199	1515.7	1515.0	0.7
	298	1513.7	1512.7	1.0
	397	1510.7	1509.7	1.0
	497	1508.3	1508.3	0.0
	597	1505.7	1505.8	-0.1
	797	1500.0	1496.8	3.2
	997	1492.8	1490.0	2.8
	1121	1489.4	1489.1	0.3
	1346	1489.4	1489.4	0.0
	1827	1492.4	1492.8	-0.4
	2319	1499.3	1500.2	-0.9
	2722	1505.3	1506.8	-1.5
	3223	1512.6	1513.6	-1.0
	3724	1519.1	1519.5	-0.4
	Average of Absolute Values of Differences . . .			0.93
10	1	1532.4	1531.4	1.0
	22	1532.6	1531.6	1.0
	42	1533.1	1532.1	1.0
	89	1533.8	1532.8	1.0
	135	1531.3	1531.3	0.0
	179	1527.8	1527.7	0.1
	269	1521.0	1519.7	1.3
	361	1513.8	1513.8	0.0
	449	1508.6	1508.4	0.2
	541	1503.9	1503.7	0.2

TABLE II (continued)

Station	Depth (m)	Sound Velocity (m/s) Hydrographic	Velocimeter	Difference
10	722	1496.6	1494.8	1.8
	902	1490.3	1488.1	2.2
	1128	1488.2	1487.1	1.1
	1353	1485.8	1486.9	-1.1
	1809	1491.5	1491.9	-0.4
	2272	1496.8	1498.0	-1.2
	2736	1503.6	1504.7	-1.1
	3223	1511.2	1512.8	-1.6
	3701	1518.4	1519.1	-0.7
	Average of Absolute Values of Differences . . . 0.89			
11	0	1536.5	1535.8	0.7
	98	1510.2	1510.2	0.0
	196	1503.3	1501.8	1.5
	391	1496.7	1495.9	0.8
	587	1494.4	1493.9	0.5
	685	1492.1	1492.5	-0.4
	783	1493.5	1493.3	0.2
	1300	1491.7	1491.5	0.2
	1531	1492.0	1491.8	0.2
	1991	1495.3	1495.4	-0.1
	2473	1500.3	1501.2	-0.9
	2930	1506.3	1508.9	-2.6
	3415	1514.1	1517.0	-2.9
	3865	1521.9	1523.9	-2.0
	Average of Absolute Values of Differences . . . 0.93			
12	0	1542.1	1541.0	1.1
	42	1542.7	1541.6	1.1
	63	1543.0	1541.9	1.1
	84	1539.7	1538.6	1.1
	127	1515.8	1514.9	0.9
	170	1510.6	1510.6	0.0
	253	1503.7	1502.7	1.0
	340	1500.3	1499.2	1.1
	517	1497.3	1496.4	0.9
	696	1495.1	1495.3	-0.2
	878	1494.1	1493.1	1.0
	1158	1492.7	1491.8	0.9
	2175	1496.1	1496.1	0.0
	2621	1502.2	1502.2	0.0
	3072	1508.2	1509.2	-1.0
	3540	1515.6	1517.1	-1.5
	4010	1523.7	1524.2	-0.5
	Average of Absolute Values of Differences . . . 0.79			

TABLE II (continued)

Station	Depth (m)	Sound Velocity (m/s) Hydrographic	Velocimeter	Difference
13	0	1540.4	1539.7	0.7
	48	1541.5	1540.8	0.7
	97	1527.2	1527.2	0.0
	146	1513.7	1513.9	-0.2
	195	1506.0	1506.6	-0.6
	244	1502.0	1500.9	1.1
	293	1499.8	1499.1	0.7
	343	1498.3	1497.6	0.7
	392	1497.3	1497.4	-0.1
	590	1495.5	1494.0	1.5
	789	1493.9	1492.2	1.7
	989	1492.6	1491.5	1.1
	1475	1492.8	1491.8	1.0
	1971	1494.2	1494.2	0.0
	2478	1500.0	1500.5	-0.5
	2978	1506.7	1508.0	-1.3
	3482	1514.7	1515.3	-0.6
	3982	1523.3	1523.6	-0.3

Average of Absolute Values of Differences . . . 0.71

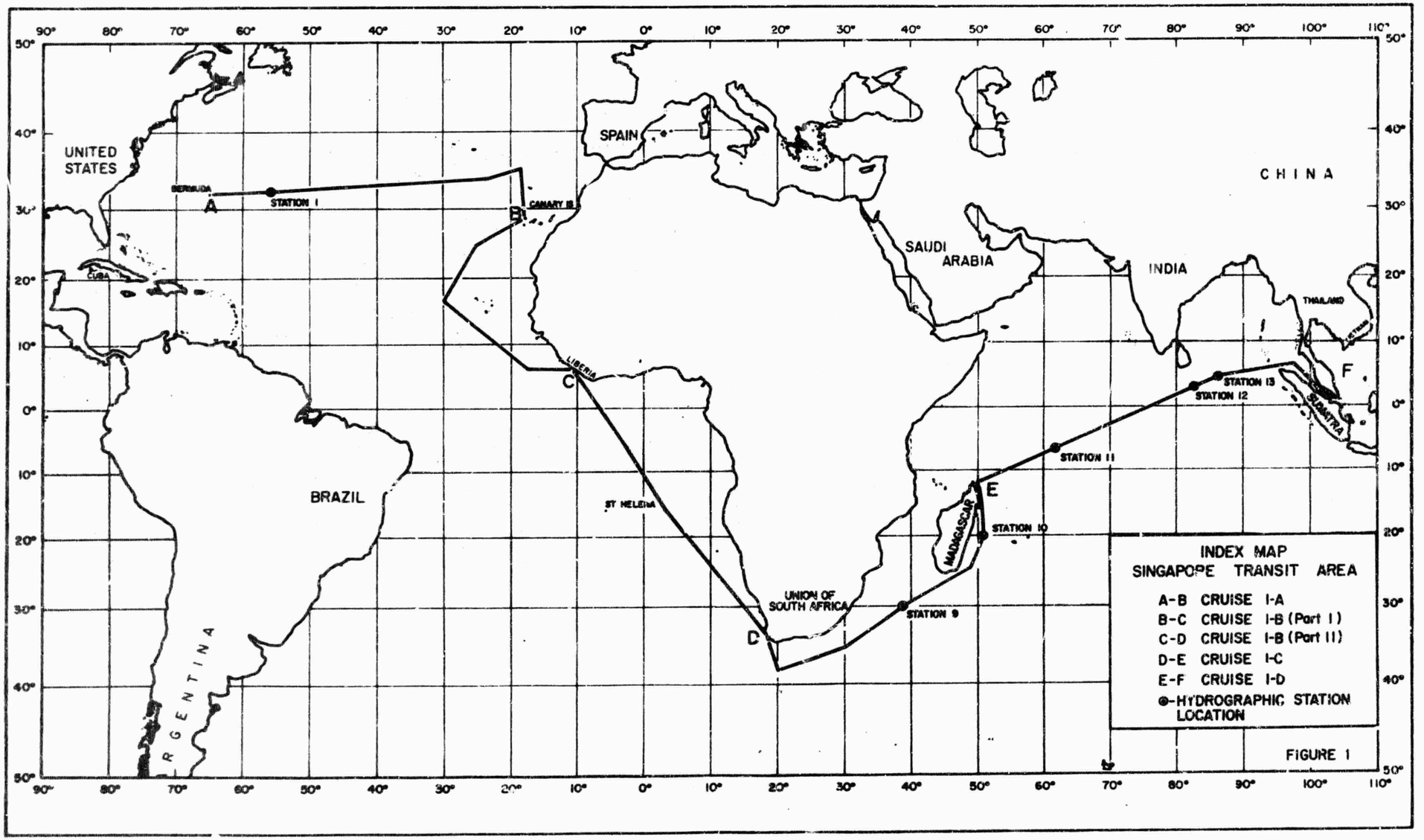
UNITED STATES
BERMUDA
A
STATION 1
B
CANARY IS
SPAIN
CHINA
SAUDI ARABIA
INDIA
CUBA
THAILAND
VIETNAM
LIBERIA
C
F
STATION 13
STATION 12
SUMATRA
STATION 11
BRAZIL
ST HELENA
E
MADAGASCAR
STATION 10
UNION OF SOUTH AFRICA
STATION 9
D
ARGENTINA
INDEX MAP
SINGAPORE TRANSIT AREA
A-B CRUISE I-A
B-C CRUISE I-B (Part I)
C-D CRUISE I-B (Part II)
D-E CRUISE I-C
E-F CRUISE I-D
⊕-HYDROGRAPHIC STATION LOCATION

FIGURE 1

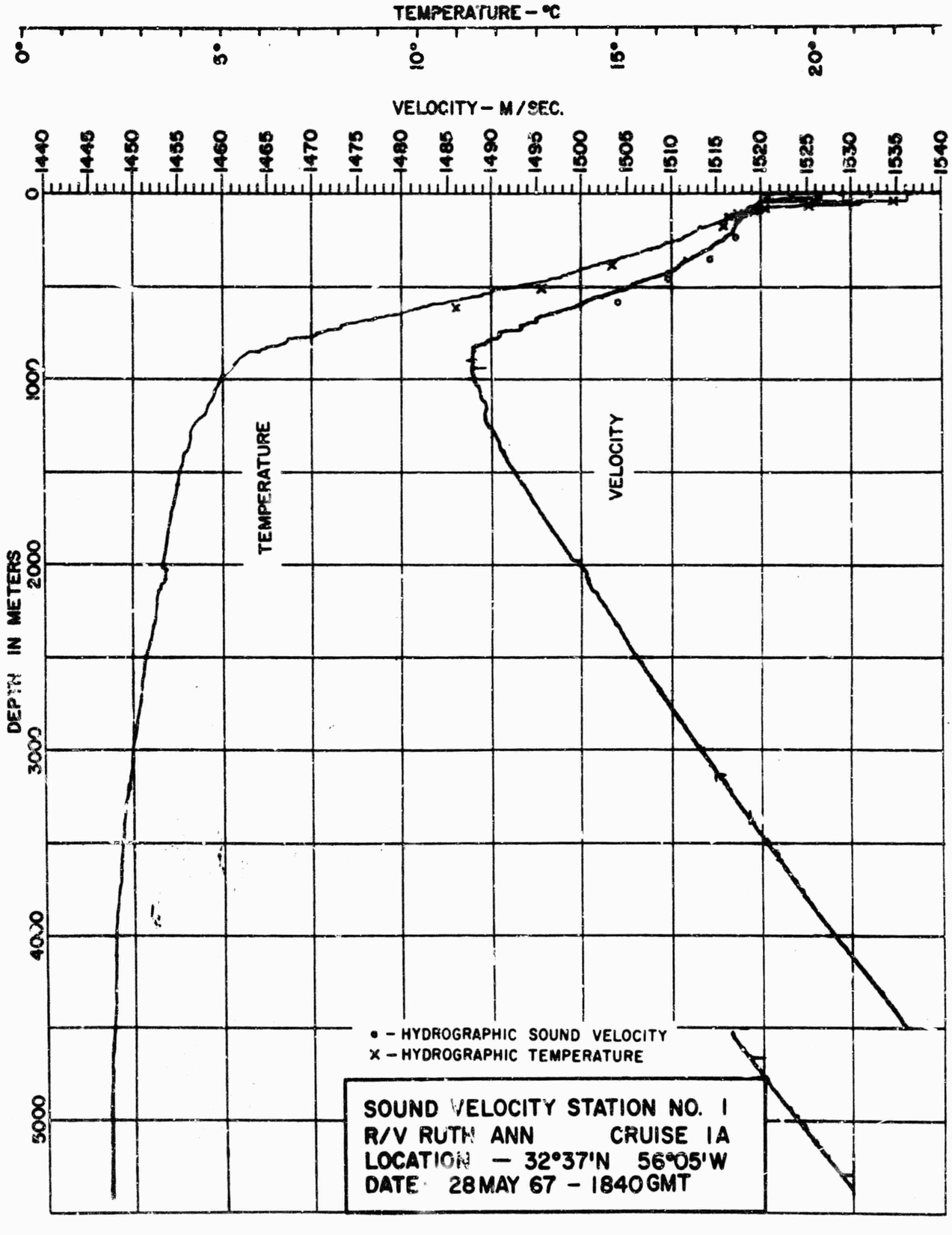
TEMPERATURE – °C
0°
5°
10°
15°
20°
VELOCITY – M/SEC.
1440
1445
1450
1455
1460
1465
1470
1475
1480
1485
1490
1495
1500
1505
1510
1515
1520
1525
1530
1535
1540
DEPTH IN METERS
0
1000
2000
3000
4000
5000
TEMPERATURE
VELOCITY
• – HYDROGRAPHIC SOUND VELOCITY
× – HYDROGRAPHIC TEMPERATURE
SOUND VELOCITY STATION NO. 1
R/V RUTH ANN CRUISE 1A
LOCATION – 32°37'N 56°05'W
DATE 28 MAY 67 – 1840 GMT

FIGURE 2A

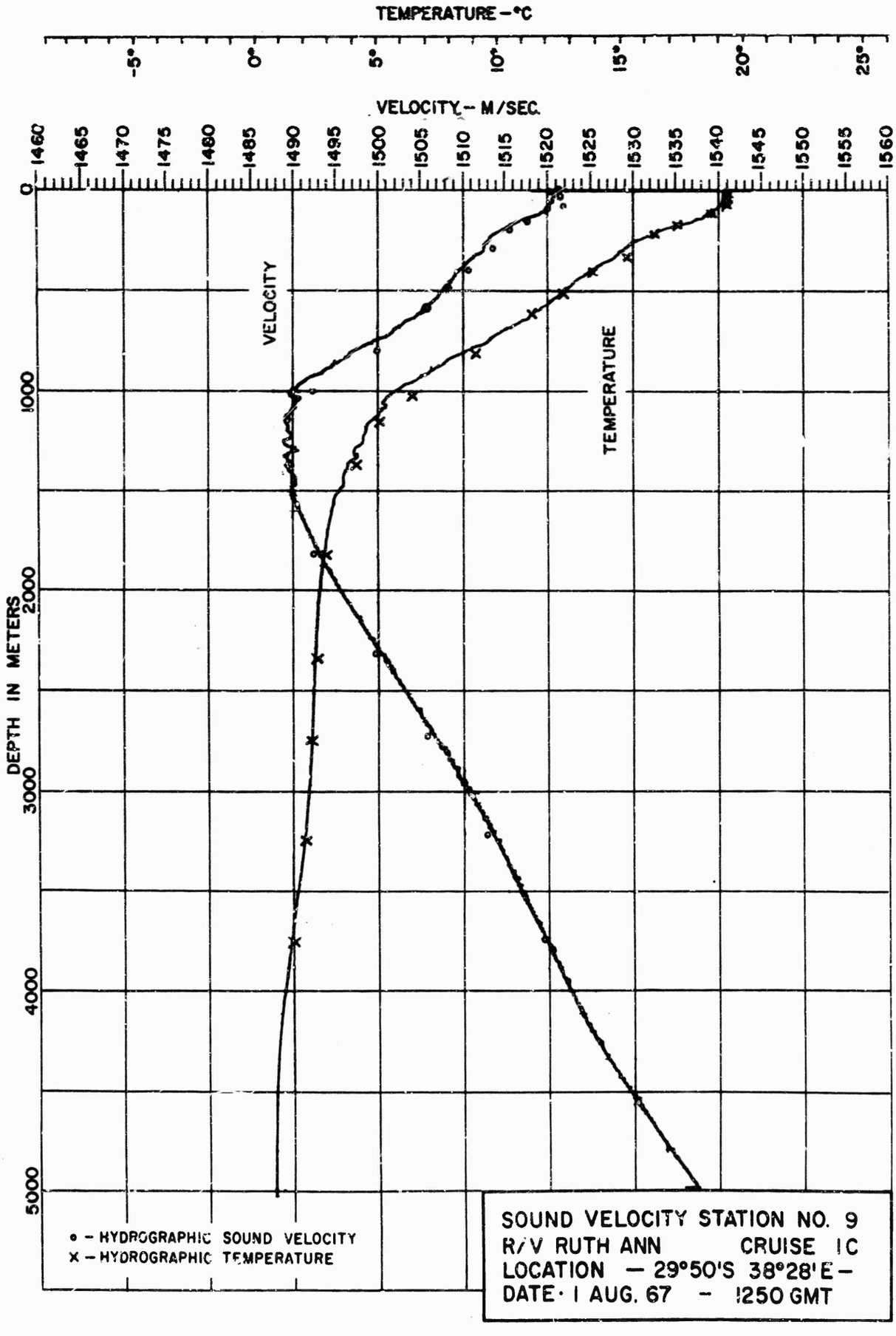
TEMPERATURE – °C
-5°
0°
5°
10°
15°
20°
25°
VELOCITY – M/SEC.
1460
1465
1470
1475
1480
1485
1490
1495
1500
1505
1510
1515
1520
1525
1530
1535
1540
1545
1550
1555
1560
DEPTH IN METERS
0
1000
2000
3000
4000
5000
VELOCITY
TEMPERATURE
• – HYDROGRAPHIC SOUND VELOCITY
× – HYDROGRAPHIC TEMPERATURE
SOUND VELOCITY STATION NO. 9
R/V RUTH ANN CRUISE IC
LOCATION – 29°50'S 38°28'E –
DATE · 1 AUG. 67 – 1250 GMT

FIGURE 2B

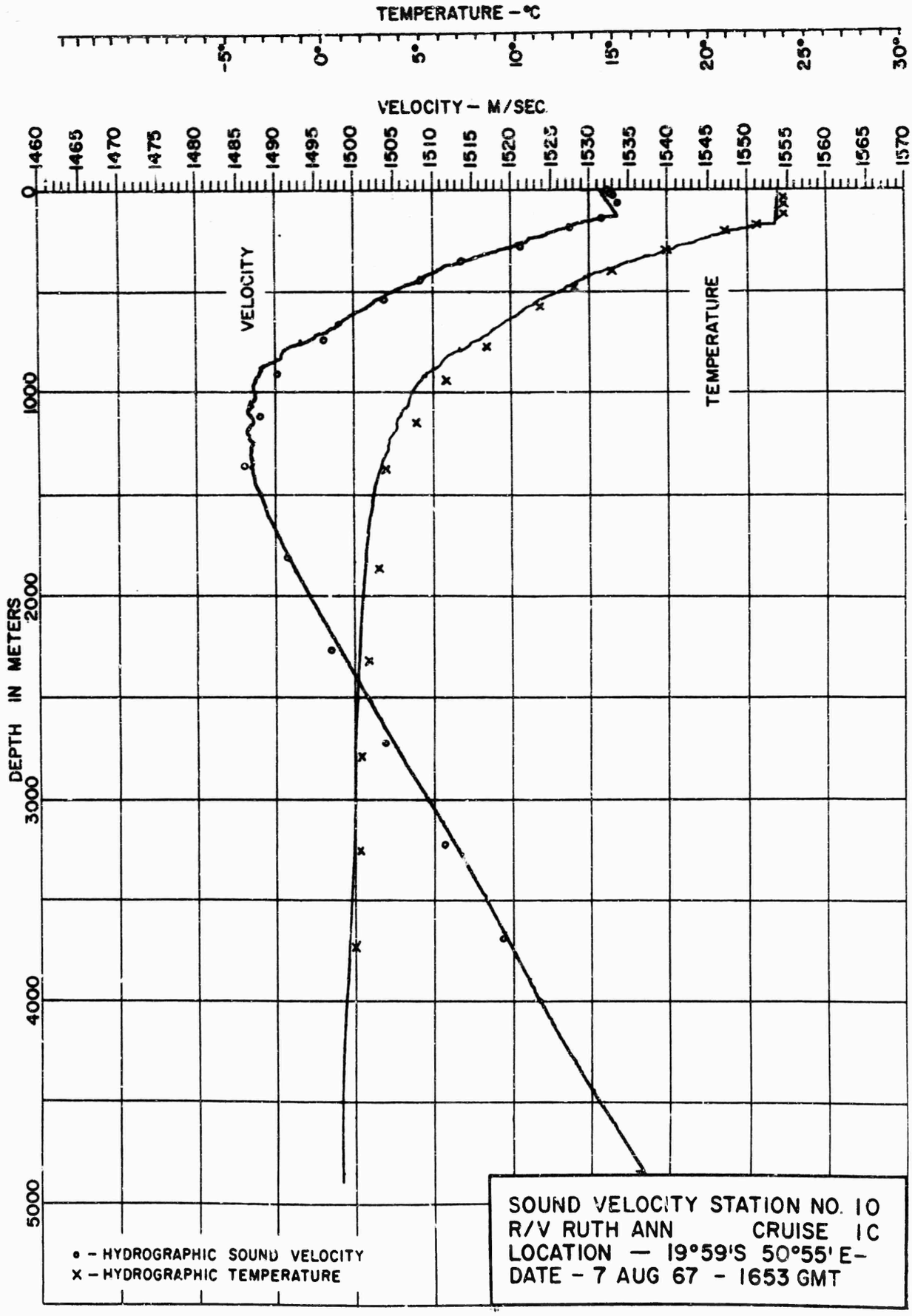
TEMPERATURE – °C
-5°
0°
5°
10°
15°
20°
25°
30°
VELOCITY – M/SEC.
1460
1465
1470
1475
1480
1485
1490
1495
1500
1505
1510
1515
1520
1525
1530
1535
1540
1545
1550
1555
1560
1565
1570
VELOCITY
TEMPERATURE
DEPTH IN METERS
0
1000
2000
3000
4000
5000
• – HYDROGRAPHIC SOUND VELOCITY
× – HYDROGRAPHIC TEMPERATURE
SOUND VELOCITY STATION NO. 10
R/V RUTH ANN CRUISE 1C
LOCATION — 19°59'S 50°55' E-
DATE – 7 AUG 67 – 1653 GMT

FIGURE 2C

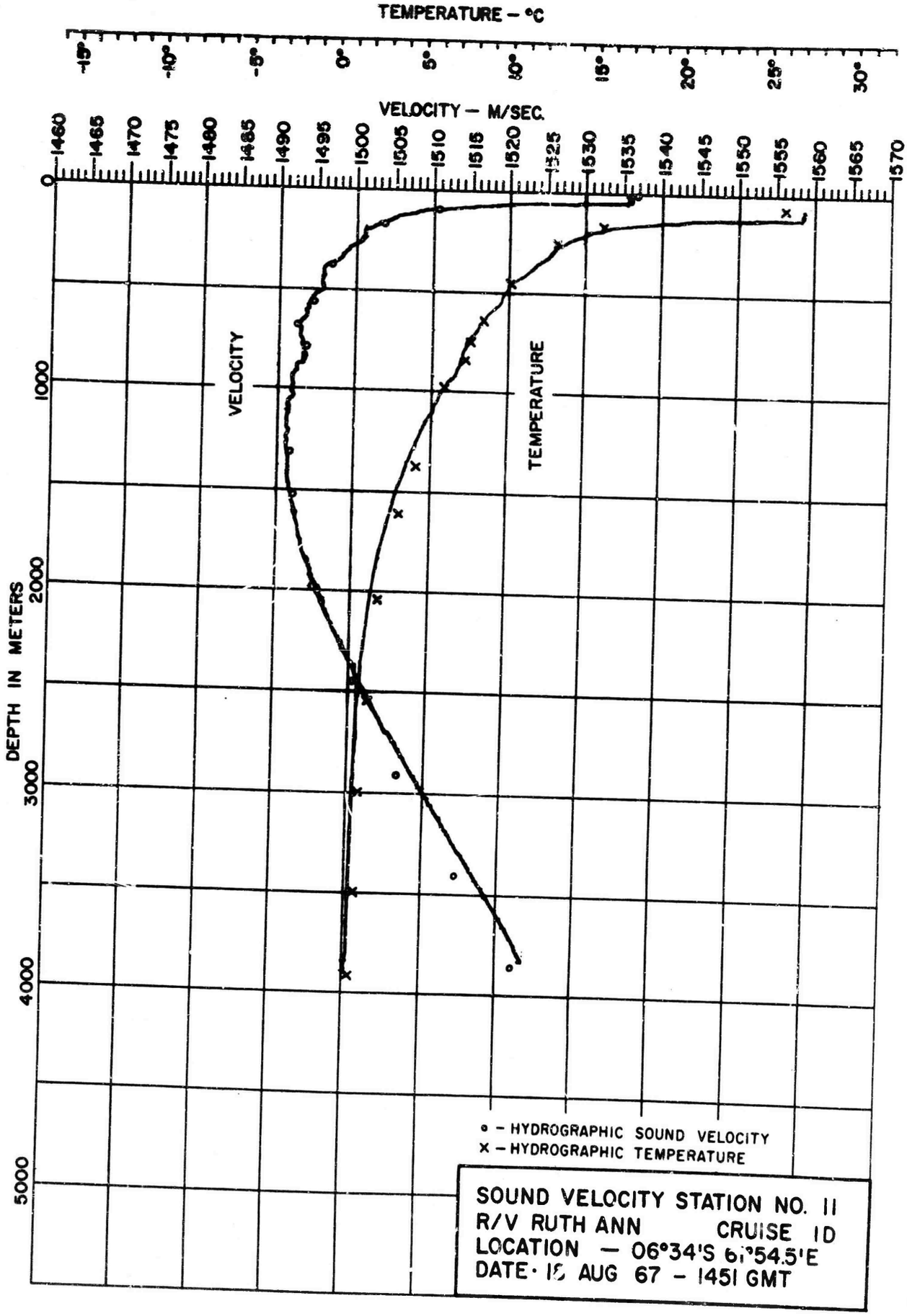
TEMPERATURE – °C
-15° -10° -5° 0° 5° 10° 15° 20° 25° 30°
VELOCITY – M/SEC.
1460 1465 1470 1475 1480 1485 1490 1495 1500 1505 1510 1515 1520 1525 1530 1535 1540 1545 1550 1555 1560 1565 1570
0
1000
2000
3000
4000
5000
DEPTH IN METERS
VELOCITY
TEMPERATURE
o – HYDROGRAPHIC SOUND VELOCITY
x – HYDROGRAPHIC TEMPERATURE
SOUND VELOCITY STATION NO. 11
R/V RUTH ANN CRUISE ID
LOCATION – 06°34'S 61°54.5'E
DATE· 18 AUG 67 – 1451 GMT

FIGURE 20

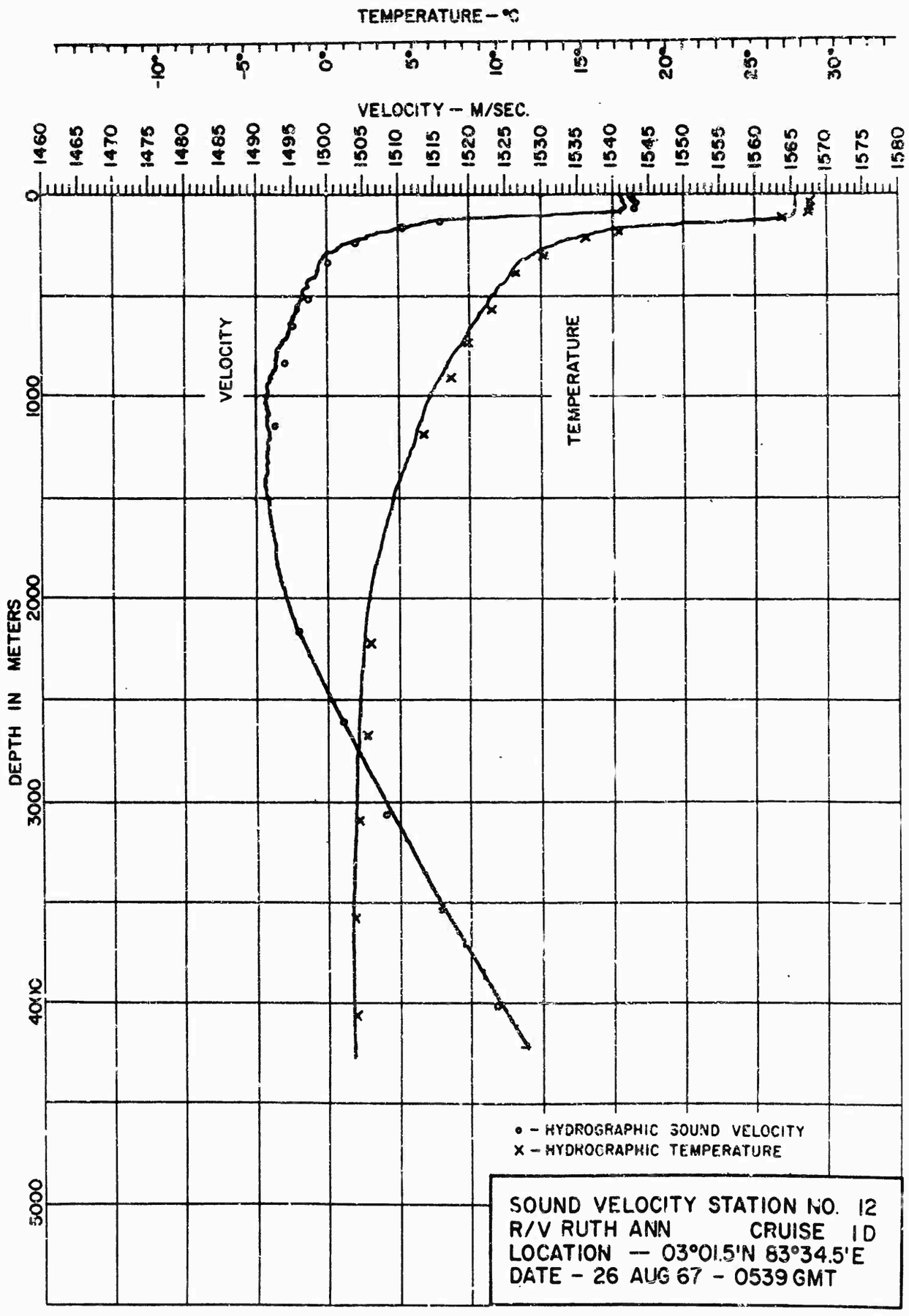
TEMPERATURE – °C
-10°
-5°
0°
5°
10°
15°
20°
25°
30°
VELOCITY – M/SEC.
1460
1465
1470
1475
1480
1485
1490
1495
1500
1505
1510
1515
1520
1525
1530
1535
1540
1545
1550
1555
1560
1565
1570
1575
1580
DEPTH IN METERS
0
1000
2000
3000
4000
5000
VELOCITY
TEMPERATURE
• – HYDROGRAPHIC SOUND VELOCITY
× – HYDROGRAPHIC TEMPERATURE
SOUND VELOCITY STATION NO. 12
R/V RUTH ANN CRUISE 1D
LOCATION – 03°01.5'N 83°34.5'E
DATE – 26 AUG 67 – 0539 GMT

FIGURE 2E

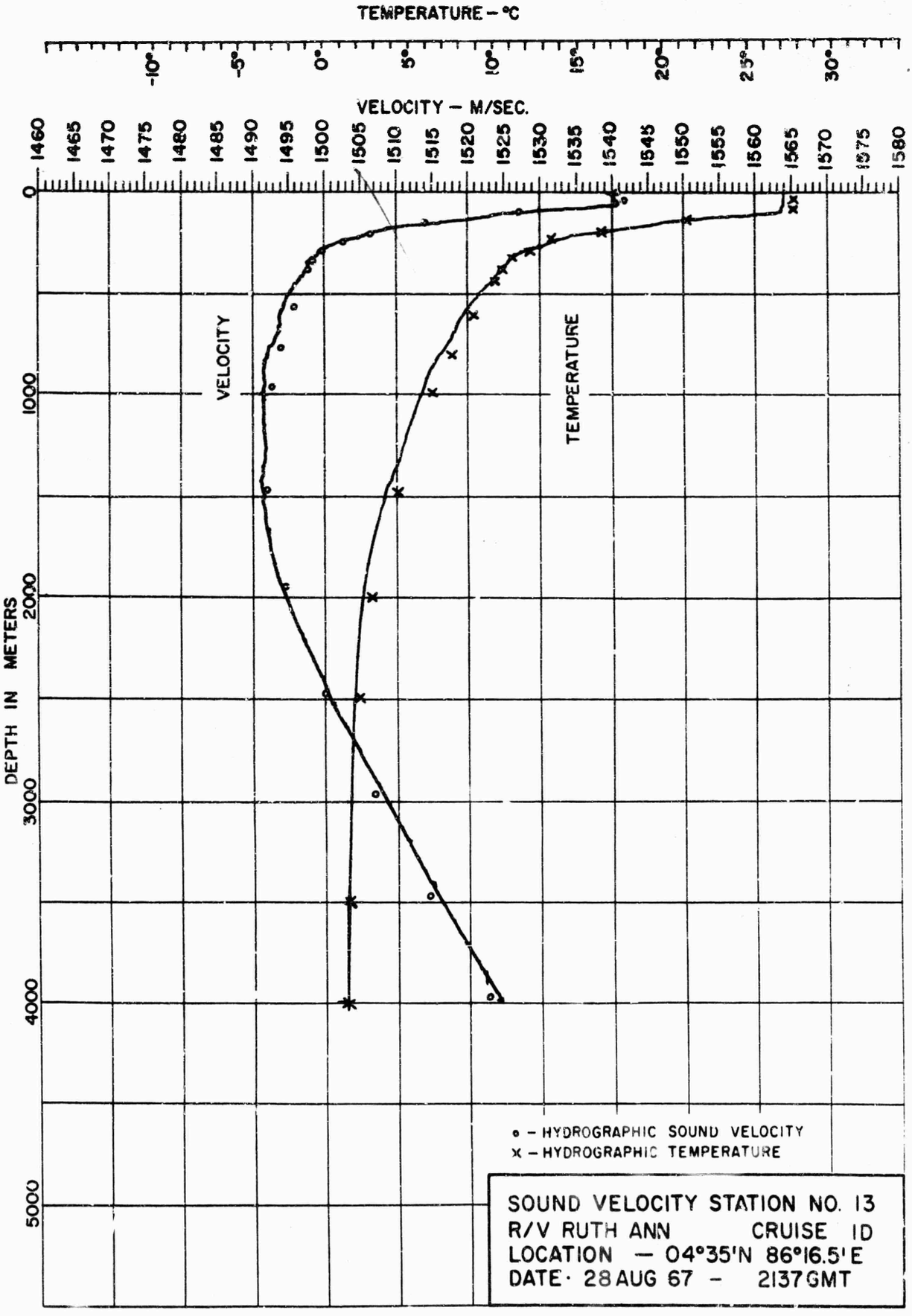
TEMPERATURE – °C
-10°
-5°
0°
5°
10°
15°
20°
25°
30°
VELOCITY – M/SEC.
1460
1465
1470
1475
1480
1485
1490
1495
1500
1505
1510
1515
1520
1525
1530
1535
1540
1545
1550
1555
1560
1565
1570
1575
1580
DEPTH IN METERS
0
1000
2000
3000
4000
5000
VELOCITY
TEMPERATURE
o – HYDROGRAPHIC SOUND VELOCITY
x – HYDROGRAPHIC TEMPERATURE
SOUND VELOCITY STATION NO. 13
R/V RUTH ANN CRUISE ID
LOCATION – 04°35'N 86°16.5'E
DATE· 28 AUG 67 – 2137 GMT

FIGURE 2F

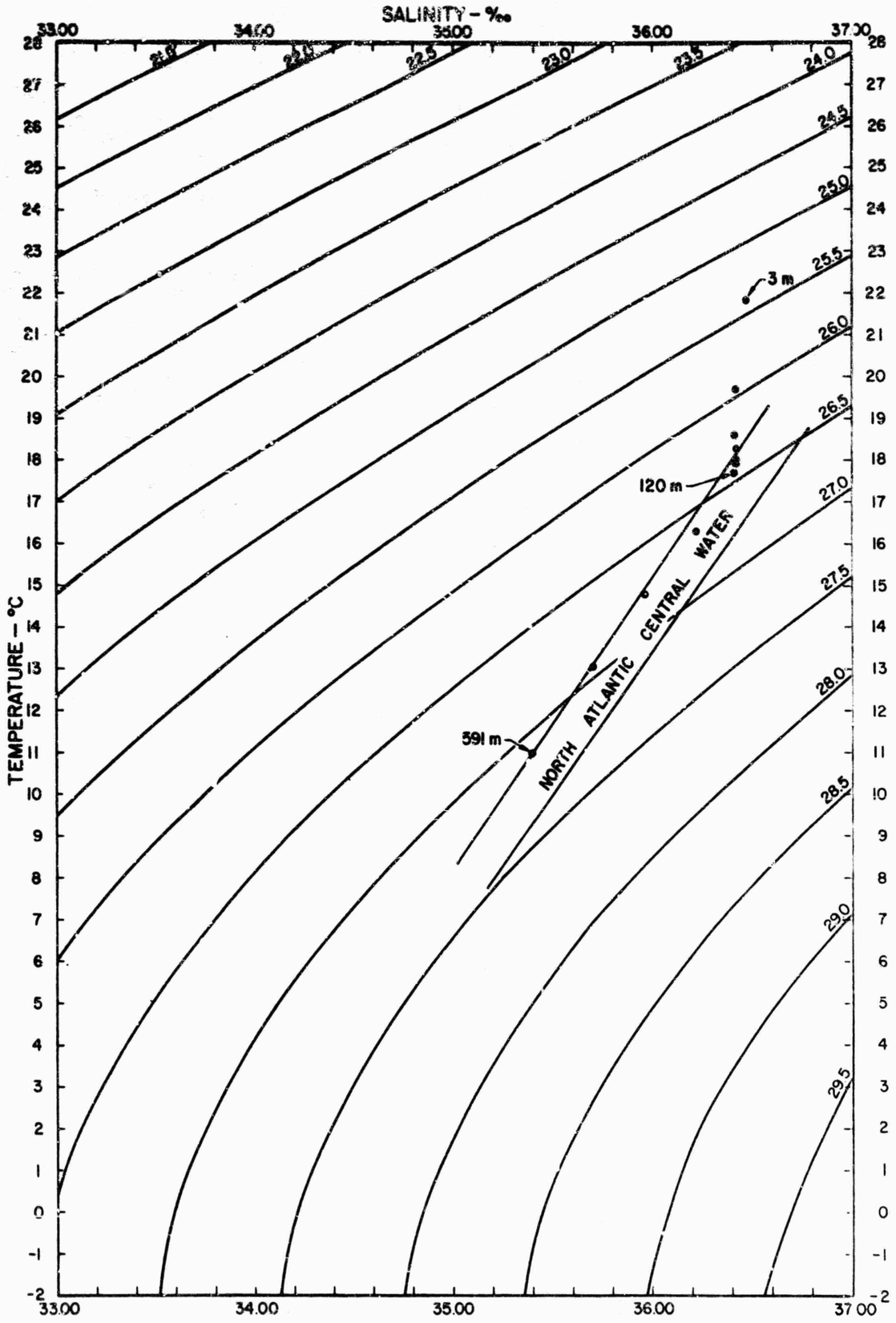

FIGURE 3A
TEMPERATURE - SALINIT. PLOT
R/V RUTH ANN AREA ST
CRUISE 1A STATION 1

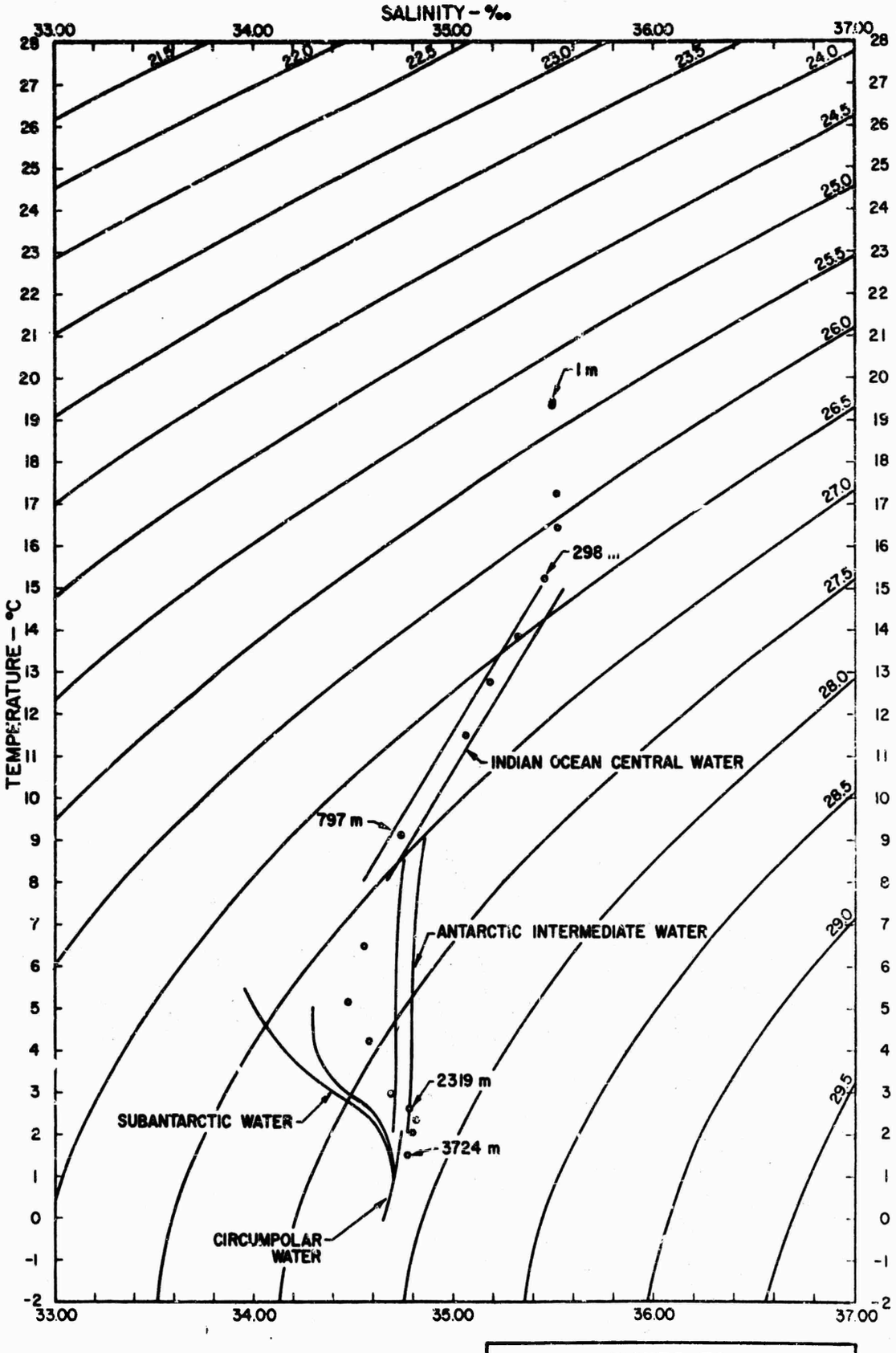

FIGURE 3B
TEMPERATURE - SALINITY PLOT
R/V RUTH ANN AREA ST
CRUISE 1C STATION 9

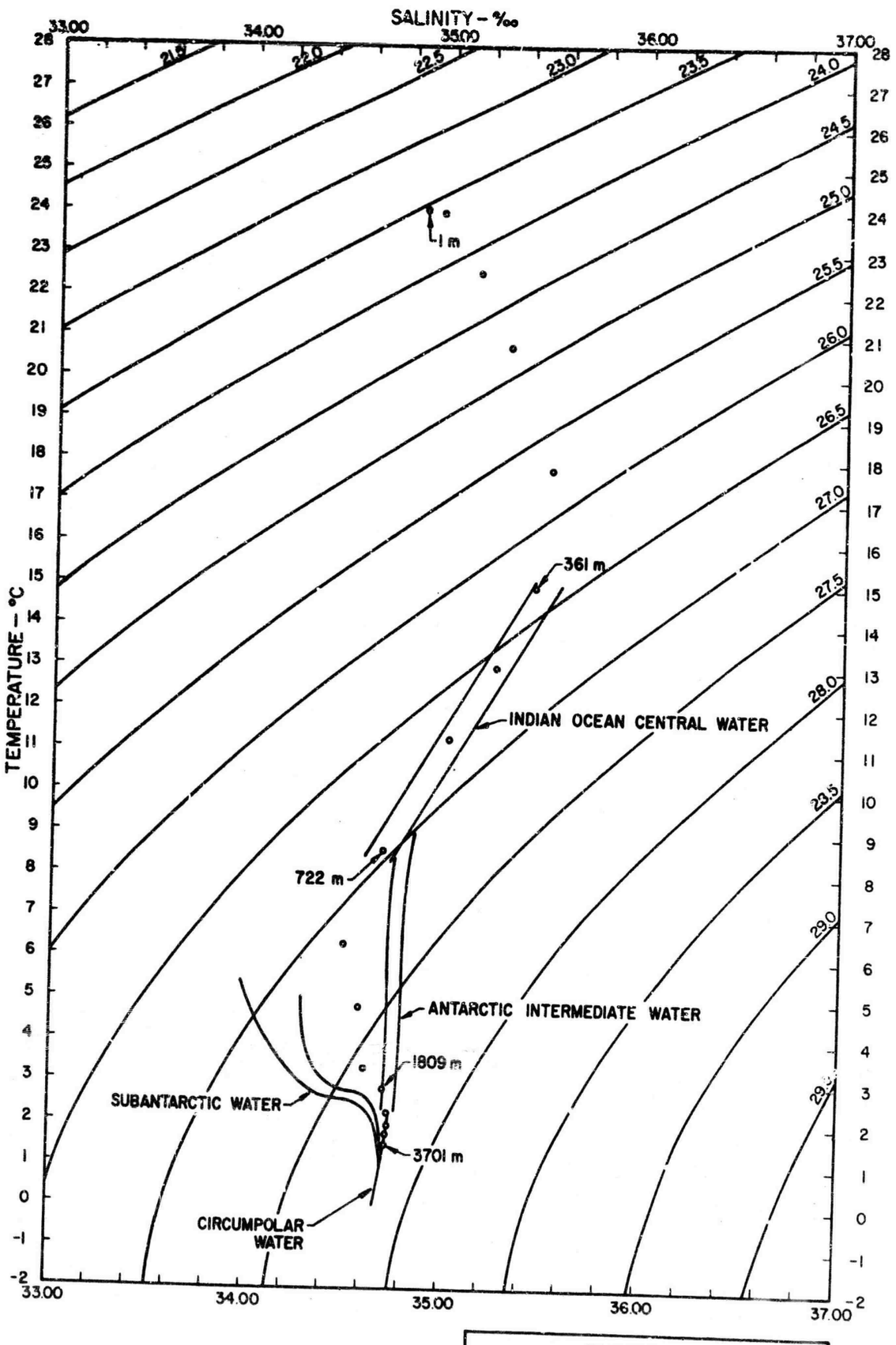

FIGURE 3C
TEMPERATURE - SALINITY PLOT
R/V RUTH ANN AREA ST
CRUISE 1C STATION 10

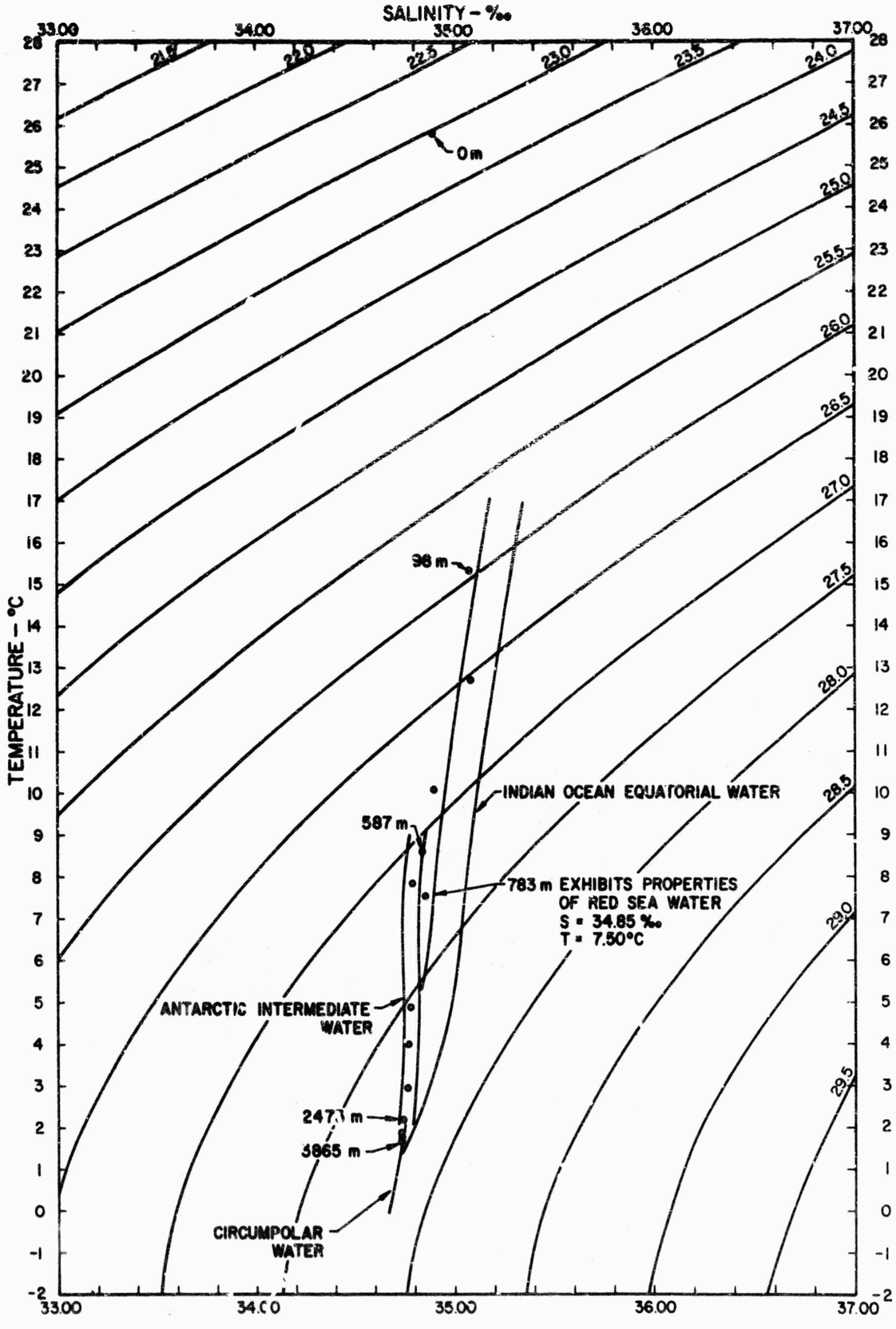

FIGURE 3D
TEMPERATURE - SALINITY PLOT
R/V RUTH ANN AREA ST
CRUISE ID STATION 11

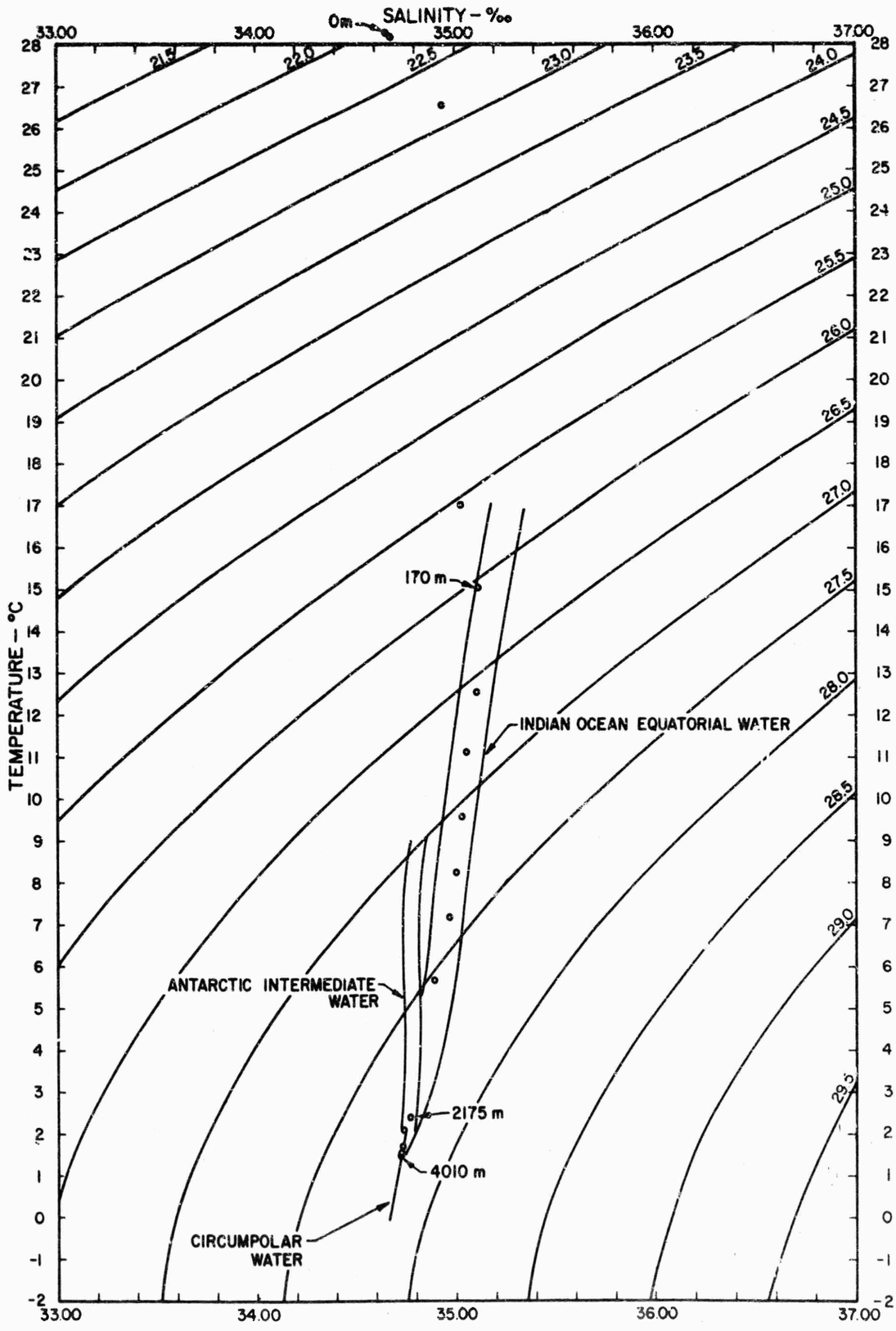

FIGURE 3E
TEMPERATURE - SALINITY PLOT
R/V RUTH ANN AREA ST
CRUISE ID STATION 12

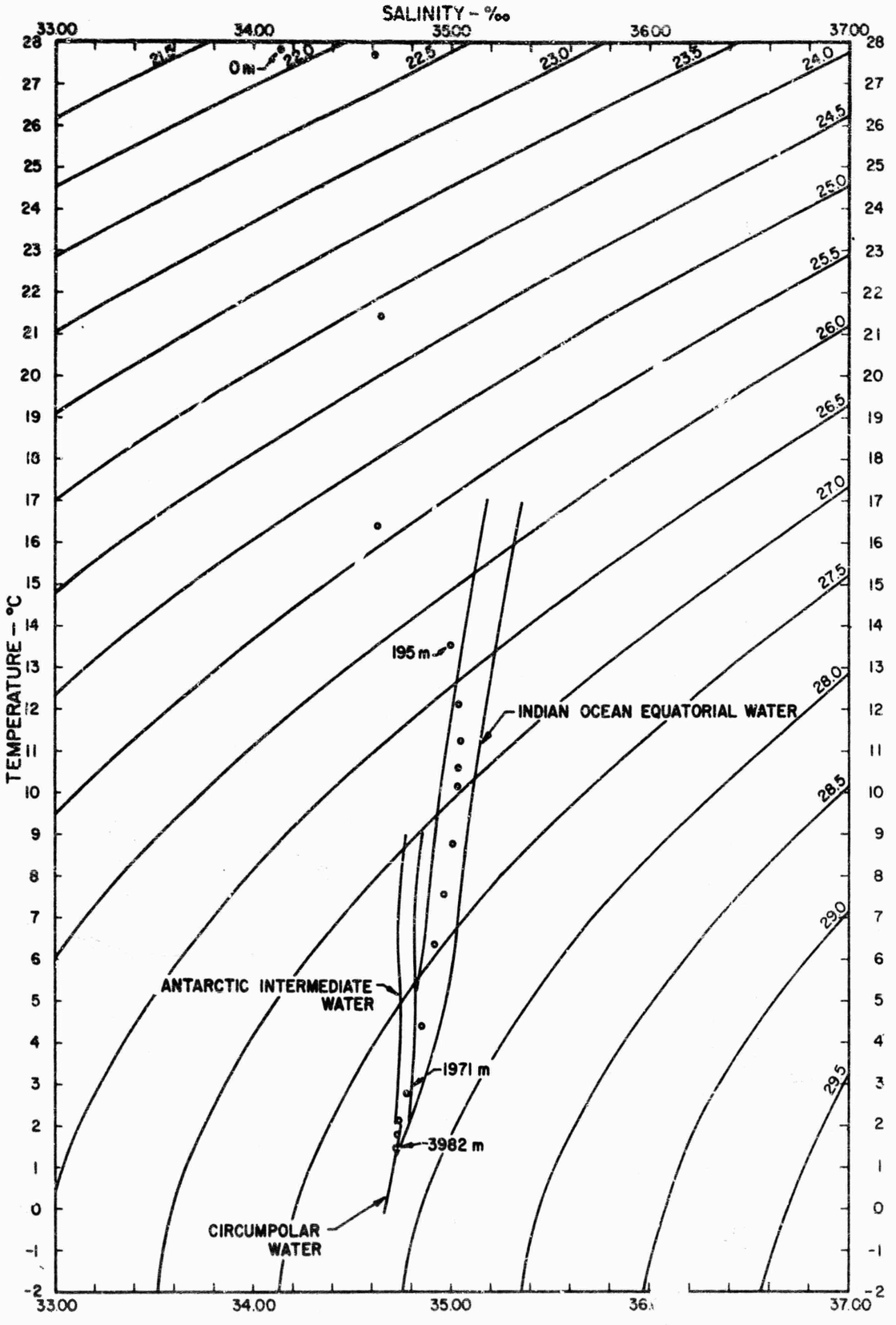

FIGURE 3F
TEMPERATURE - SALINITY PLOT
R/V RUTH ANN AREA ST
CRUISE ID STATION 13

UNCLASSIFIED
Security Classification

DOCUMENT CONTROL DATA - R&D
(Security classification of title, body of abstract and indexing annotation must be entered when the overall report is classified)

1. ORIGINATING ACTIVITY (Corporate author)	2a. REPORT SECURITY CLASSIFICATION
ALPINE GEOPHYSICAL ASSOCIATES, INC. 65 OAK STREET, NORWOOD, NEW JERSEY 07648	UNCLASSIFIED 2b. GROUP [redacted]

3. REPORT TITLE

AREA ST VOLUME 2 - "SUMMARY REPORT OF GEOPHYSICAL INFORMATION"

4. DESCRIPTIVE NOTES *(Type of report and inclusive dates)*

Final Report

5. AUTHOR(S) *(Last name, first name, initial)*

Henry, J.A.; Halpin, D.L.; Lair, C. and Sanko, P; Weininger, E., Miller, E.T., and Wehnau, R.A.; Rodriguez, Jr., M. H.

6. REPORT DATE	7a. TOTAL NO. OF PAGES	7b. NO. OF REFS
August, 1968	246	82

8a. CONTRACT OR GRANT NO.	9a. ORIGINATOR'S REPORT NUMBER(S)
b. PROJECT NO. N 62306-2020	SP 97-ST-2
c.	9b. OTHER REPORT NO(S) *(Any other numbers that may be assigned this report)*
d.	

10. AVAILABILITY/LIMITATION NOTICES This document is subject to special export controls and each transmittal to goreign governments or foreign nationals may be made only with prior approval of Naval Oceanographic Office, Code 4300, Washington, D.C. 20390.

11. SUPPLEMENTARY NOTES	12. SPONSORING MILITARY ACTIVITY
	U.S. Naval Oceanographic Office Washington, D.C. 20390

13. ABSTRACT

This volume summarizes the results of geophysical and acoustic measurements made by the R/V SANTA MARIA and R/V RUTH ANN during the transit cruises from Bermuda to Singapore from 24 May to 4 September, 1967.

Part I contains the bathymetric and subbottom profiling, and physiographic provinces descriptions.

Part II contains the magnetic intensity survey, the delineation of the magnetic province boundaries and their relation to the physiographic provinces.

An analysis of cores from 7 Stations is given in Part III. Photographs from 5 camera stations are also shown.

Part IV summarizes sound velocity measurements, ray path computations, and the associated propagation anomaly obtained during the transit.

The data from 6 hydrographic stations are presented in Part V. Salinities and temperatures obtained are used to determine values of sound velocity which are compared to corresponding data obtained at the same stations by sound velocimeter lowerings.

DD FORM 1 JAN 64 1473

UNCLASSIFIED
Security Classification

14. KEY WORDS	LINK A		LINK B		LINK C	
	ROLE	WT	ROLE	WT	ROLE	WT
Marine Geophysical Survey Program 65-67						

INSTRUCTIONS

1. ORIGINATING ACTIVITY: Enter the name and address of the contractor, subcontractor, grantee, Department of Defense activity or other organization *(corporate author)* issuing the report.

2a. REPORT SECURITY CLASSIFICATION: Enter the overall security classification of the report. Indicate whether "Restricted Data" is included. Marking is to be in accordance with appropriate security regulations.

2b. GROUP: Automatic downgrading is specified in DoD Directive 5200.10 and Armed Forces Industrial Manual. Enter the group number. Also, when applicable, show that optional markings have been used for Group 3 and Group 4 as authorized.

3. REPORT TITLE: Enter the complete report title in all capital letters. Titles in all cases should be unclassified. If a meaningful title cannot be selected without classification, show title classification in all capitals in parenthesis immediately following the title.

4. DESCRIPTIVE NOTES: If appropriate, enter the type of report, e.g., interim, progress, summary, annual, or final. Give the inclusive dates when a specific reporting period is covered.

5. AUTHOR(S): Enter the name(s) of author(s) as shown on or in the report. Enter last name, first name, middle initial. If military, show rank and branch of service. The name of the principal author is an absolute minimum requirement.

6. REPORT DATE: Enter the date of the report as day, month, year, or month, year. If more than one date appears on the report, use date of publication.

7a. TOTAL NUMBER OF PAGES: The total page count should follow normal pagination procedures, i.e., enter the number of pages containing information.

7b. NUMBER OF REFERENCES: Enter the total number of references cited in the report.

8a. CONTRACT OR GRANT NUMBER: If appropriate, enter the applicable number of the contract or grant under which the report was written.

8b, 8c, & 8d. PROJECT NUMBER: Enter the appropriate military department identification, such as project number, subproject number, system numbers, task number, etc.

9a. ORIGINATOR'S REPORT NUMBER(S): Enter the official report number by which the document will be identified and controlled by the originating activity. This number must be unique to this report.

9b. OTHER REPORT NUMBER(S): If the report has been assigned any other report numbers *(either by the originator or by the sponsor)*, also enter this number(s).

10. AVAILABILITY/LIMITATION NOTICES: Enter any limitations on further dissemination of the report, other than those imposed by security classification, using standard statements such as:

(1) "Qualified requesters may obtain copies of this report from DDC."

(2) "Foreign announcement and dissemination of this report by DDC is not authorized."

(3) "U. S. Government agencies may obtain copies of this report directly from DDC. Other qualified DDC users shall request through _____."

(4) "U. S. military agencies may obtain copies of this report directly from DDC. Other qualified users shall request through _____."

(5) "All distribution of this report is controlled. Qualified DDC users shall request through _____."

If the report has been furnished to the Office of Technical Services, Department of Commerce, for sale to the public, indicate this fact and enter the price, if known.

11. SUPPLEMENTARY NOTES: Use for additional explanatory notes.

12. SPONSORING MILITARY ACTIVITY: Enter the name of the departmental project office or laboratory sponsoring *(paying for)* the research and development. Include address.

13. ABSTRACT: Enter an abstract giving a brief and factual summary of the document indicative of the report, even though it may also appear elsewhere in the body of the technical report. If additional space is required, a continuation sheet shall be attached.

It is highly desirable that the abstract of classified reports be unclassified. Each paragraph of the abstract shall end with an indication of the military security classification of the information in the paragraph, represented as *(TS)*, *(S)*, *(C)*, or *(U)*.

There is no limitation on the length of the abstract. However, the suggested length is from 150 to 225 words.

14. KEY WORDS: Key words are technically meaningful terms or short phrases that characterize a report and may be used as index entries for cataloging the report. Key words must be selected so that no security classification is required. Identifiers, such as equipment model designation, trade name, military project code name, geographic location, may be used as key words but will be followed by an indication of technical context. The assignment of links, roles, and weights is optional.